DUAL OSTEOGENIC AND ANGIOGENIC GROWTH FACTOR DELIVERY AS A TREATMENT FOR SEGMENTAL BONE DEFECTS

A Thesis
Presented to
The Academic Faculty

by

Megan Elizabeth Oest

In Partial Fulfillment
of the Requirements for the Degree
Doctorate of Philosophy in Bioengineering

Georgia Institute of Technology
August 2007

DUAL OSTEOGENIC AND ANGIOGENIC GROWTH FACTOR DELIVERY AS A TREATMENT FOR SEGMENTAL BONE DEFECTS

Approved by:

Dr. Robert E. Guldberg, Advisor
School of Mechanical Engineering
Georgia Institute of Technology

Dr. David J. Mooney
Department of Engineering and Applied Sciences
Harvard University

Dr. Ravi Bellamkonda
Department of Biomedical Engineering
Georgia Institute of Technology

Dr. W. Robert Taylor
School of Medicine, Department of Biomedical Engineering
Emory University

Dr. Andrés García
School of Mechanical Engineering
Georgia Institute of Technology

Date Approved: 06.05.2007

To the sweethearts who are always there
for the little stars that have tumbled – been pushed maybe.
You are lights in the dark.

ACKNOWLEDGEMENTS

There are a great many lessons I have learned in my time at Georgia Tech. To enumerate a few… First, engineering is awesome. Second, Persistence pays off. Trust yourself – common sense, previous experience, intuition, and a little bit of inner faith will guide you. And finally, women must put in twice the work and do twice as well at the same job in order to be considered equals to their male counterparts. Fortunately, this is not often overly difficult.

I have the great fortune of having received assistance and encouragement from a large community of supporters, personal and professional. To each individual mentioned here, and to the many that are not, I extend my sincerest thanks and best wishes.

First and foremost I must thank my advisor, Dr. Robert Guldberg. Without him, none of this work would have been possible. I truly appreciate the many ways in which he has looked out for my best interests – both challenging and supporting me. Dr. Guldberg, thank you for your infinite patience in the development of this model and for your insistence that I learn to be an independent researcher. Thank you for those countless hours of surgery. I think we've spent more time staring at each other across the operating room table than you've ever spent with another student! Your persistence and advice have been invaluable. But one question remains – where are you ever going to find another feminist vegetarian to fill my shoes?

To my thesis committee, Dr. Andrés García, Dr. David Mooney, Dr. W. Robert Taylor, and Dr. Ravi Bellamkonda, I extend my heartfelt thanks for your input into this work and insistence on high quality research. Dr. García, thank you for your insistence on high standards. Thank you for always balancing your constructive criticisms with praise, kind words, and encouragement – you can't possibly know how thankful I am for those gentle reminders that I *would* survive this process. Thank you for reminding me that I am *not* a "moron". To Dr. Mooney I offer great thanks for the collaboration that initiated the bulk of the work in this thesis. Your availability and positive input are truly appreciated and have been invaluable. Dr. Taylor, thank you for your expertise in the world of all things vascular. Your accessibility and genuinely kind nature have always been appreciated. Dr. Bellamkonda, I truly appreciate your input and interest in the project. Your persistence in fully understanding and continued input into the project is much appreciated.

Additionally, I must thank the members of the Guldberg, Levenston, and García labs. A more caring, friendly, and supportive group of people could not possibly be found. From donating their time to endless hours of surgery to providing a shoulder to lean on, they have contributed in countless ways and devoted their time to assisting me even when their own projects were more than demanding enough. The easygoing, spirited nature of this research microcosm is something I will miss terribly. Srinidhi Nagaraja – my brother in all things subcontinental – I will miss our meetings over vindaloo, hummus, and ben-gay balls. Thank you for knowing the importance of "Moms". And always, always, thank you for always believing that somewhere inside this shell of a body, happy laughing Megan has always existed. Galen Robertson, thank you for being my constant cheerleader and the best of listeners. Even in your absence from the lab, you continue to remind me that personal growth is a lifelong journey. Craig Duvall, of the infamous "Duvall et al.", I can't thank you enough for developing that perfusion

technique. Watch out for those hamdogs. Chris Gemmiti, a fantasatic office mate, thank you for your late-night companionship and job-seeking advice. I truly appreciate your kind, paternal nature. Mela Johnson, Yash Kolambkar, and Eric Deutsch, my endless thanks for the hours upon hours you spent assisting me in surgery. Mela, your choice in scrubs has literally brightened so many of my days (go Unis!). I wish you the best of luck in your continued studies. Keep your sense of humor intact, and you'll make it through. Alex Peister, thank you for your vast knowledge in all things stem cell related, for getting up at the crack of dawn for surgery (without your Coke), and for your expertise and experience. Your smile is always a welcome sight. Angela Lin, Queen of the micro-CT, I cannot thank you enough for your vast knowledge and infinite patience with all things micro-CT related. (Angela, um, my rat is *in* the viva-CT…) You have been a rock for the Guldberg lab. To you I send my heartfelt thanks for your constant kindness, genuine nature, and for being the coolest person I know. Take care of those knees!

There have been three angels in my lab life. Few people are as lucky to meet one of these people in their professional life, and I have had the good graces to work with three. First and foremost, I must thank Dr. Angel Duty for her guidance, personal and professional, through my first three years in the lab and continued friendship. You are a constant inspiration to me, and a reminder of all things good that exist within each of us. Dr. Natasha Case, thank you for serving as a sounding board, a shoulder to cry on, and being the best of listeners. You are a model of perseverance. Angel and Natasha, you will never know how much it means to me to have shared those years with you. I miss you terribly. Ken Dupont, a genuinely kind soul, thank you for your literally endless hours in surgery, and for completing most of the mechanical testing in this thesis (Grrr…. Giants!). Your devotion, compassion, kindness, caring, and involvement mean the world to me. I can only hope that I have been as helpful and kind to you as you have been to me. I extend my best wishes for your continued success in the Guldberg lab and beyond.

Outside of the lab, there are many who contributed their expertise to this project. Thanks to Dr. Laura O'Farrell and Cherry Forkey of the IBB Physiological Research Lab for providing the animal husbandry. I must especially thank Dr. Laura O'Farrell for the time she devoted to perfecting the rat vascular perfusion technique and her unflagging support of both me and this model. Tracey Couse, thank you for your histological expertise, encouragement, and genuine interest in the project. We miss you. Aqua Asberry, you are a coverslipping machine! I extend my thanks to Jim McEntee of JM Machining and Dennis Brown of GTRI for their precision machining of the rat fixation plates, and to John Graham and the Mechanical Engineering machine shop for other parts that were custom machined for the surgical and imaging procedures.

I must also acknowledge the funding support for this research. Personal funding for was provided in the form of the National Science Foundation Graduate Research Fellowship and Georgia Tech President's Fellowship. Initial work for the development of the model was supported by Aderans Research. The bulk of the research was supported by the National Institutes for Health (NIH RO1 EB003364), Georgia Tech/Emory Center for the Engineering of Living Tissues (NSF EEC-9731643) and the Georgia Tech/Emory Biomedical Technology Research Center (NIH RO1 HL62820RO1).

On a personal note, I have a great number of people to thank. At Georgia Tech, I must specifically thank the Oregon posse – Adam Higgins, John Wilson and honorary member Chris Wilson. Without these people, I would not be where I am today. Their

commiseration, constant encouragement, and insistence on believing in me will never be forgotten. Thank you for surrounding me with your love. From the Levenston lab, I must thank John Connelly and Ashley Palmer for their encouragement, whackiness, and the initiation of Mary-oke escapades. I couldn't ask for better people or closer friends to have shared this journey with (and hopefully many journeys to come). Thanks to Lori Lowder for being the ever-persistent histology helper and fellow believer in "it's never going to work, we're never going to graduate", even when we both knew it would work out. Lori, you have a heart of gold and sarcasm that could whip a dirt devil into shape. Thanks to Janna Kay Mouw, Stacy Marie Imler, and Kathryn Brodkin for giving me a family in Georgia when I started here all alone. You have been cheerleaders, advisors, friends, and family to me. Thank you for being your unique, loving selves, and for welcoming me into your fold. Mike Robertson, thanks for two great years, but even more so, thank you for inadvertently showing me my own strength. I know now how well I can stand alone on my own two feet. ESB the band, y'all have been so awesome to me. I've never rocked so hard in my life. I will miss our Tuesday nights and the ESBian escapades. And I promise to buy a microphone…

To my family, my unending thanks and love is extended. You are my true heroes. I am ever indebted to my parents, Jane and Allen Oest, for ALWAYS believing in me and doing everything in their power to facilitate the achievement of my goals, large and small. You have always believed that I could be anything I wanted and do anything I put my mind to. Your faith in me is eternal, even when I doubted myself. From skydiving to rat surgery to simply making it out of bed in the morning, you have always been there cheering me on and facilitating my accomplishments. You have provided me with every tool within their means to make this work possible. You have taught me the strength of family and the truth that, although love may be all you need, sometimes a box of animal crackers just might help. This thesis is as much yours as it is mine. Thank you for teaching me love, thank you for allowing me to learn life.

Mom, Mum, Momma Duck, thank you for the millions of phone calls, making sure I was taking care of myself, learning to love a cat, and even helping in tissue culture and surgery. Thank you for reminding me that *we cannot discover new oceans without the courage to lose sight of the shore.* I can't begin to tell you how I love and appreciate you.

Dadzos, Poppa Bear, Daddy, and fellow Beaver Believer, thank you for believing in me, for waxing my car, taking care of me, removing cockroaches, and always being there for me. Thanks for making a special trip to ensure that rat surgery would go well. Thank you, thank you. I can only hope that you know the depth and breadth of my love and appreciation for you.

To Julie Oest, my sister: darling Josephine, thank you for, above all else, teaching me to *ROAR!* You have constantly pushed me to wear my antlers, put those high-heeled boots on, and stand proud. You are the great keeper of secrets, the best personal shopper on the planet, an amazing chef, engineer, pioneer, initiator of Starch Fest, and my best friend. A portrait of graciousness, you have always shown me the way when I've felt lost or unsure. Jules, you've taught me to trust myself and leap forward, eyes wide open. I'll never forget how you also once reminded me that now and then, my rats might benefit from a pep talk. Thank you for being your amazing self, and for sharing that self with me. I am truly honored. Your open ears, empathy, and wisdom beyond your years are

treasures I genuinely appreciate. You are my best friend, confidante, and the pulse of my heart. *A cuishle mo chroi.* I love you beyond all words.

Paul Laufer, my brother, thank you for reminding me to laugh, and for giving the best hugs. I am overjoyed to have you as my family. I can only hope that you know how you are in my heart and my wishes for all good things. For the endless hours of my complaints that you have endured, and for giving of the precious few moments you've had with your wife to calm my nerves, I am forever in your debt. You have my love and thanks always.

To Marney and Shah Malik, I must extend my great thanks for reminding me of the power, the strength, of the family. You are my second parents and I dearly love you. Thank you for being strong for me when I couldn't be strong for myself. Wherever would I be without a doting Auntie and a Whacky Paki? Kirin Jamison and Amara Malik, my sisters, my blood, thank you for being my cheerleaders. From career advice to yet another game of Pictionary, you have always been there for me. I treasure you. I love you. Sam Jamison, my first brother, thank you for supporting me and welcoming me into your life. Your rational logic and strength of spirit are such precious qualities. We all hold you so dear to our hearts. Grandma Mary Battin, thank you for continuing the matriarchy. ☺ You have been a model of courage, strength, and triumph over adversity. Your interest in my research and unending support have been invaluable throughout the Ph.D. process. Thank you for being one of those pioneers who broke trail that my path might be less arduous. I can only hope that I can follow in your footsteps and join the ranks of our strong women. To my grandparents, Cliff and Shirley Oest, many thanks for the care packages, support, and love. It's a blessing to know that someone is always thinking of you, as you have always put me in the front of your thoughts. Grandpa, you have been a model of strength and gentleness. Grammy, I can only hope that when I reach your age I will possess the some of the grace and courage that you do.

In that vein, I must thank the women who have gone before me. Eliza Styles, Ella Battin, and Mary Battin, thank you for being role models. Thank you for being family. Thank you for kicking butt in your own generation. I hope my life will prove me worthy of joining your ranks. Of my superhero collective, I must acknowledge the women that have broken trail that I might follow more easily in their footsteps: Merit Ptah (2700 BCE, the first woman in science known by name, and quite possibly, the first physician in history); Hildegard of Bingen (1136 CE, botanist, geologist, and more); Marie Curie (1903, first woman in France to complete her doctorate, discoverer of radium and polonium); Gloria Steinem (1972, feminist and founder of the Women's Action Alliance); Amelia Earhart (1928, the first woman to fly across the Atlantic and attempt to circumnavigate the globe); Rosalind Franklin (1951, crystallographer and physical chemist who made significant contributions to, among other things, the determination of the structure of DNA); Maud Menten (1912, enzyme kineticist and histochemist, contributor to the famed Michaelis-Menten equation and first person to electrophoretically separate proteins); Dorothy Mary Crowfoot Hodgkin (1937, founder of protein crystallography, Nobel prize winner, and pacifist); Lady Mary Wortley Montagu (1718, brought the practice of smallpox inoculation to Europe); Sofia Kovalevskaia (1884, first prominent female Russian mathematician, third woman to become a professor in Europe); Ellen Swallow Richards (1884, ecofeminist, environmental and industrial chemist); Barbara McClintock (1927, cytogeneticist and

pioneer of the technique used to visualize chromosomes); Florence Nightingale (1851, pioneer of modern nursing and notable statistician); Rosalyn Sussman Yalow (1977 Nobel prize co-winner, medical physicist and developer of the radioimmunoassay technique); S. Jocelyn Bell Burnell (1943, astrophysicist and Friend); and Elizabeth Blackwell (1821, first woman to practice medicine with a degree in the United States). And of course, Myra Ellen Amos, my kindred spirit in words and vehicle for the voice of the Divinely Complex; *"Most people would rather be sheep and have company than stand out with their antlers on."* Thank you Tori, thank you Josephine – let us all put our antlers on, stand up, and *ROAR!* I have had the great fortune of living and working in a community that is learning to accept women as equals. In a society where sexism is still an ugly demon rearing its head in our faces, my experience at Georgia Tech has enveloped me in an awesome group of women and exceptional men. In my community of peers I have felt heard, accepted, equal, and appreciated.

I must thank Dr. Michelle Bothwell and Dr. Joe McGuire for propelling me into the world of academia. Without your support and encouragement, I would never have attempted a Ph.D. Your knowledge, advice, and love mean so much to me. Thank you for being the best advisors a student could have, mentors for life, and some of the best friends I've known.

And finally, to Mr. Modoc E. Oest, you know all I have to say without hearing a word. You remind me that the light is within each of us, that life is love, that love is the spirit, that the spirit is the divine, and that this divine spirited love is all that matters. Thank you for finding me, for choosing me, and for loving me. At my lowest, you have given me a reason to continue (kibble time!). At my best, you have surrounded me with your love and playful antics. And everywhere in between, you have been there for me.

TOWANDA!

A prayer for the wild at heart, kept in cages.

TABLE OF CONTENTS

LIST OF TABLES

LIST OF FIGURES

LIST OF SYMBOLS AND ABBREVIATIONS

2-D	two-dimensional
3-D	three-dimensional
α-MEM	α-modified eagle's medium
ACS	absorbable collagen sponge
ALP	alkaline phosphatase
BMP	bone morphogenetic protein
BMP-2	bone morphogenetic protein-2
BMP-4	bone morphogenetic protein-4
BMP-7	bone morphogenetic protein-7
BMP-9	bone morphogenetic protein-9
BMSC	bone marrow stromal cell
BV	bone volume
BVF	bone volume fraction
caALK2	constitutively active ALK2
DBM	demineralized bone matrix
DNA	deoxyribonucleic acid
FDA	food and drug administration
HA	hydroxyapatite
hDBM	human demineralized bone matrix
HIF-1α	hypoxia-inducible factor-1α
micro-CT	micro-computed tomography
MSC	mesenchymal stem cell
PCL	polycaprolactone

PEG	polyethylene glycol
PLDL	poly(L-lactide-co-D,L-lactide)
PLGA	poly(lactic-co-glycolic acid)
PRP	platelet-rich plasma
RANKL	receptor activator of nuclear factor κB ligand
TCP	tricalcium phosphate
TGF-β1	transforming growth factor-β1
TGF-b3	transforming growth factor-β3
TGF-β3	transforming growth factor-β3
VEGF	vascular endothelial growth factor
VOI	volume of interest

SUMMARY

The complex process of critically-sized load-bearing bone defect healing is poorly understood. The interplay between revascularization of the injured tissue and regeneration of a functional bone structure is critical to survival of the limb. The central goal for this dissertation is to establish a novel *in vivo* model of segmental bone defect repair and to assess the ability of tissue-engineered scaffolds using a growth factor co-delivery strategy to heal these defects.

Traditional assessment of large bone defect healing has relied entirely on radiography and histology/histomorphometry. The animal model designed in this thesis enables the investigator to use *in vivo* X-ray and quantitative micro-CT imaging of the defect to assess mineralized matrix deposition, and to easily free the defect from the stabilization device for mechanical testing of samples *post-mortem*. Additionally, a hindlimb vascular perfusion procedure was developed to facilitate micro-CT quantification of vascular structures within the defect.

These methodologies were applied to assess functional bone repair resulting from co-delivery of osteogenic (BMP-2), chondrogenic (TGF-β3), and angiogenic (VEGF) growth factors. The dose-dependence effects of and interactions between these growth factors were assessed using micro-CT and mechanical testing methods. There was a dose-dependent response to co-delivery of BMP-2/TGF-β3 in terms of mineralized matrix deposition and restoration of mechanical properties. An additive interaction was determined between the two growth factors.

Delivery of VEGF alone did not result in a dose-dependent beneficial effect on bone formation or revascularization of the defect. Modification of the implanted porous polymer structural scaffolds to contain a macroscopic cored center and 10% ceramic component enhanced revascularization of the defects. Co-delivery of VEGF with BMП–2/TGF–β3 did not incur any benefit over delivery of only BMP-2/TGF-β3.

In conclusion, this work has yielded a novel, reproducible and robust small animal model of osseous nonunion and quantified the ability of low dose sustained release growth factor co-delivery to enhance functional bone repair.

CHAPTER 1

INTRODUCTION

1.1 Motivation

Localized bone loss due to trauma or disease is a significant cause for loss of patient quality of life and contributes to patient disability. In optimal situations, bone is recognized for its unique capability to regenerate without scar formation – given adequate vascularity, presence of vascular and osteoinductive growth factors, presence of osteoprogenitor cells, and mechanical stability. Of the roughly six million fractures that occur in the United States annually, 5-10% require clinical intervention in the form of a graft [BORRELLI 2003]. One must also account for other bone defects that require intervening therapy, such as those due to congenital malformations, disease, osteosarcoma, metabolic bone disorders, and soft tissue damage (spinal fusions).

Although autografting (removal of morselized host tissue from a remote site – typically the iliac crest) is the gold standard treatment, this procedure is limited by lack of available donor material, an inability to obtain a structural graft, and considerable donor site morbidity. Thus, the allograft is the popular and facile solution to the problem of significant bone loss. Allografts are structural segments of bone that are removed from donor cadavers and then processed to devitalize the tissue and reduce the possibility for transfer of disease-causing agents. Despite their ready availability and ease of use, allografts are subject to a high rate of re-fracture within a relatively short time period (2 years) post-engraftment [LUCARELLI 2005, WHEELER 2005, ITO 2005]. This re-

fracture incidence is due in large part to a lack of graft integration into the remaining host bone [ENNEKING 2001, ITO 2005, WHEELER 2005]. Lack of porosity within the allograft inhibits revascularization and revitalization of the allograft tissue, resulting in a propensity to accumulate microdamage that may ultimately lead to catastrophic graft failure (25% clinical failure rate) or contribute to the 30-60% complication rate associated with allografts [LUCARELLI 2005, WHEELER 2005]. Complications frequently result in treatment of defect non-unions or delayed unions, often necessitating revision surgery and significantly impacting patient quality of life.

In response to the shortcomings of the standard clinical treatments, a variety of experimental (tissue-engineered) strategies have been developed as potential treatments for large bone defects. In general, these strategies rely on a combination of a biological agent and a carrier for the agent. The biological agents are typically cells, bioactive extracellular matrix, growth factors, or gene delivery systems. The carrier materials may or may not have mechanical integrity, and may intrinsically carry bioactive factors, as is the case with active demineralized bone matrix (DBM). The driving hypothesis behind these treatment strategies is that augmenting the body's natural healing processes will stimulate the surrounding tissue to produce viable bone within the framework of the defect.

Three crucial factors in bone formation are the presence of osteoprogenitors, proper mechanical stimulation, and the availability of a proximal vascular supply. Osteoprogenitors may be delivered as part of the tissue engineering therapy or recruited from local reservoirs of these cells, such as the periosteum and bone marrow. Mechanical signals may take many forms. In osseous defect healing, the typical concern is provision

of adequate stability to the defect site to prevent atrophic nonunion. Although dynamic mechanical stimulation is known to be osteogenic at certain levels in healthy bone and at certain stages of bone development, too much mechanical freedom can be detrimental in cases of bone defect repair. Excessive micromotion in the fracture or defect site produces a situation in which healing does not progress beyond the formation of a soft tissue callus. This lack of mineralization may be partially due to disruption of vascular structure formation by micromotion. Bone formation is tightly linked to the availability of a vascular supply. Without close proximity to a blood supply (< 0.1 mm), osteocytes do not survive and new bone cannot form or existing bone remodel [SAADEH 2000]. Vascular invasion is critical for the conversion of cartilage to bone in endochondral ossification processes, including growth plate maturation and long bone healing, as well as for medullary fracture callus formation [CARLEVARO 2000, GERBER 1999]. Despite this knowledge of the critical relationship between the two tissue types, there are little data correlating the formation of mineralized tissue with the invasion or maturation of a vascular supply (angiogenesis and arteriogenesis, respectively) in fracture or defect models.

One emerging strategy used in the treatment of bone defects is growth factor therapy. Use of BMP-2 on an absorbable collagen sponge has recently been approved by the FDA for use in spinal fusions. Further investigations are assessing the efficacy of this treatment in augmenting open tibial shaft fracture repair. The effects of growth factors on biological systems are varied, complex, and not completely characterized. However, the potency of growth factors such as BMP-2 and VEGF has inspired many pre-clinical investigations into their potential as agents for bone regeneration and targets for tumor

therapy. Although less widely known, TGF-β3 is under investigation as a treatment to reduce scarring in lacerations. Not only are the effects of growth factors important, but the delivery mechanism as well. Many of these proteins have a short active half-life, making the problem of sustained delivery difficult to address. Relying on a burst-release bolus dose of growth factors often requires that a large total amount of protein be delivered. This may be due to rapid diffusion of the protein away from the site of delivery and/or an inability to preserve the protein in its bioactive form. Delivery of growth factor that is exclusively tethered to the implant is not always beneficial, as there may be insufficient quantities of diffusible protein to stimulate adjacent cells to proliferate and migrate into the implant. In natural physiologic healing processes, a variety of biochemical cues act in concert. Exploiting natural interactions between two or more growth factors may more closely mimic the natural healing process and stimulate a greater response to the delivered bioactive molecules than independent delivery of any individual molecule would achieve. The effects of growth factor co-delivery, however, are largely unknown. One interesting potential application for growth factor co-delivery is the problem of regenerating vascularized bone in large osseous defects.

Characterization and modulation of vascular invasion and mineralized matrix formation has implications for the treatment of large or challenged osseous defects. Nonunion of bony defects may occur as a result of defect size, infection, micromotion, patient health, age, or co-morbidity with other diseases, and often results in loss of limb functionality. In these situations, clinical intervention is necessitated. Accelerating vascularized bony union using a tissue-engineering approach could provide a viable and

lasting treatment for a variety of bone defects, including challenged fractures, segmental defects, cranial-maxillofacial defects, and spinal fusions.

1.2 Goal and Central Hypothesis

The long-term goal of this work is to develop tissue engineering strategies to elevate and accelerate functional bone repair in patients with clinically challenging defects. *The overall objective of this thesis is to evaluate the effects of co-delivered growth factors on functional bone repair using a robust small animal bone defect model and quantitative evaluation of vascular ingrowth, bone formation, and functional integration.* This objective will be addressed by establishing a critically-sized rat femoral defect model, quantifying mineralized tissues and vascular invasion within the defect sites, and examining the effects that delivery of scaffolds with osteogenic, chondroinductive, and angiogenic growth factors have on functional repair. The effects of scaffold macroarchitecture on mineralization and vascularization will be addressed as well.

The central hypothesis is that by exploiting the interaction effects between growth factors, osseous repair tissue can be generated more quickly and with greater functionality than can be achieved using a single growth factor delivery at the same dose. Here, interactions between osteoinductive, chondroinductive, and angiogenic growth factors are investigated.

1.3 Specific Aims

The following three specific aims are outlined in order to test the central hypothesis:

Specific Aim #1: Develop a critically-sized segmental femoral defect model in rats and test the ability of an oriented polymer scaffold to promote vascularized bone repair.

While the segmental femoral defect model itself is not novel, the development of a stable defect that is critically-sized due to the size of the defect rather than compounding factors such as micromotion is new. Stabilization hardware amenable to mechanical testing and radiography is also novel. Many groups have employed the segmental defect model, but the majority have used a sub-critical defect size, where reported spontaneous healing rates of untreated defects range from 10-50%. The fixation devices typically used to stabilize the femoral defects are simplistic and sometimes fail to provide support to the defect, resulting in collapse of the defect space. Additionally, the typical design involves a plate that directly abuts the defect, precluding tissue infiltration from that region of the implant periphery. Although perhaps more akin to clinical defect fixation, hardware that directly contacts the defect site may limit tissue interaction with the implant.

A review of the literature regarding bone defects indicates that experimental treatments rely on a variety of scaffolds or delivery vehicles. One type is a ceramic or cement. Although one such ceramic, hydroxyapatite/tricalcium phosphate (HA/TCP) is naturally found in bone, the brittleness of such scaffolds frequently leads to fracture *in vivo* [BRUDER 1998 JBJS]. Ceramic or cement scaffolds are limited by a lack of

porosity as well as a lack of pore interconnectivity – two factors crucial to the invasion of new mineralized matrix and invading vascularity. The second type of scaffold is non-structural. These scaffolds are typically hydrogels or absorbable collagen sponges, providing no mechanical integrity to the healing defect. One advantage of these scaffolds is that they are easily manipulated to conform to the defect site. These non-structural implants may provide biologically active factors, but lack the integrity needed to promote early weight bearing of the limb. The use of an absorbable polymeric scaffold with structural integrity has not been widely investigated for use in large load-bearing defect repair.

Relying on a single scaffold type makes it difficult to achieve both structural integrity and controlled release of bioactive factors in a model of clinical repair. Use of a two-phase implant gives the researcher an opportunity to focus on both mechanical stability of the implant and the release of bioactive agents. In the interest of accomplishing both tasks, we have selected a composite system of a structural polymer scaffold and hydrogel. The polymer scaffold selected for use here is poly(L-lactide-co-D,L-lactide) (PLDL) with an oriented macroporosity and random microporosity. It is hoped that the orientation of the longitudinal macropores would create channels to enhance the directionality of bone repair in the femoral defect model. The hydrogel chosen for co-delivery with the PLDL scaffold is alginate. It is hypothesized that the similarities in structure between alginate and heparin allows proteins with heparin binding domains to interact with alginate hydrogels, permitting sustained release of the molecules as the alginate matrix degrades. Use of a sustained-release system could potentially enable researchers to produce results similar to high-dose fast-release systems

while utilizing a lower total dose of protein. The work in this thesis evaluates the use of such a scaffold, including its ability to deliver biologic factors and promote healing of critically-sized segmental defects in varying geometries and compositions.

The *hypothesis* is that an 8 mm femoral defect will not heal spontaneously in rats and that scaffold treatment will enhance mineralization within the defect site as compared to non-treatment of the defects but not restore full functionality. The outcomes of this Specific Aim I are discussed in Chapter 3.

Specific Aim #2: Evaluate the ability of co-delivered TGF-β3 and BMP-2 to promote mineralization within the defect site.

Previous work by Simmons et al. has shown a synergistic interaction between TGF-β3 and BMP-2 in the presence of bone marrow stromal cells in a mouse ectopic model of osteogenesis. This treatment has not been tested in an orthotopic model [SIMMONS 2004]. Typical growth factor treatments have relied on high, supraphysiologic doses of growth factor to induce osteogenesis. This approach is often successful due to the sheer quantity of protein delivered. The use of dual growth factor delivery, particularly a therapy based on positive growth factor interactions, may have potential for clinical application in lowering the total dose of protein needed to achieve the same results. Optimization of growth factor delivery may enable investigators to more efficiently utilize the potential of bioactive factors.

The *hypothesis* is that functional repair of segmental bone defects will be improved by co-delivery of TGF-β3 and BMP-2 in a dose-dependent manner, and that

the growth factors will interact to enhance the repair response. The outcomes of Specific Aim II are discussed in Chapter 4.

Specific Aim #3: Test the effects of co-delivering angiogenic and osteogenic growth factors on early scaffold vascularization and subsequent segmental defect repair.

The processes of vascular invasion and mineralized matrix formation are tightly linked in all aspects of bone formation and repair (endochondral ossification, intramembranous ossification, fracture repair, osteocyte and osteoblast survival). Mature bony tissue is organized discretely around vascular structures. One of the frequent causes of atrophic nonunion is disruption of the developing vascular supply, either by excessive mechanical motion or disease. Recent literature publications indicate that the co-delivery of osteogenic and vascular-associated factors (such as mesenchymal stem cells and endothelial cells) interact to more rapidly and thoroughly heal bony defects [HUANG 2005 JBMR, KAIGLER 2006].

The *hypothesis* is that delivery of VEGF will enhance vascular invasion into the defect site in a dose-dependent manner and that co-delivery of both angiogenic and osteogenic/chondrogenic growth factors will produce interaction effects that enhance the quantity and functionality of mineralized repair tissue within segmental defects as compared to delivery of osteogenic/chondrogenic growth factors alone. Secondarily, it is hypothesized that scaffold macroarchitecture will affect the quantity of mineral formed within the defect and the ability of the host body to vascularized the defect site. The outcomes of Specific Aim III are discussed in Chapter 5.

This work is *innovative* because of: the use of *in vivo* micro-CT to accomplish repeated sequential images of defects over time, the combined approach of quantifying bone and vasculature, the use of co-delivered growth factors in an orthotopic site, and the evaluation of the dose-dependent effects of these co-delivered growth factors on healing. Additionally, the development of a robust, reproducible small animal model compatible with quantitative imaging strategies both *in vivo* and *in vitro* is novel.

1.4 Significance

The limitations of traditional bone repair strategies have motivated the development and clinical application of tissue-engineered bone repair strategies. Primarily, these strategies have relied on the use of a singular protein (BMP-2) delivered in a non-structural, absorbable biological matrix (absorbable bovine collagen sponge). BMP-2-based therapies have been approved by the FDA for use only at high doses of protein (1.5 mg/ml) [SWIONTKOWSKI 2006, BURKUS 2002]. The development of a lower-dose growth-factor based strategy would potentially make this therapeutic method more accessible to large bone defect applications, while still employing a minimally involved process for preparation of the implant. Additionally, treatment of large defects would be benefit from the use of a delivery scaffold with structural integrity – this would create the potential for earlier weight-bearing and/or load-sharing between support or fixation device and the implant.

One of the limitations of cell-based tissue-engineered therapies for bone regeneration is the lack of a viable nutrient supply to the interior of the construct. A vascular supply is essential to cell survival; formation, maintenance, and remodeling of

osseous tissue require the presence of a vascular supply. Vascularization must precede or coincide with formation of mineralized matrix in order to produce a viable tissue. This work seeks to develop a challenging critically-sized segmental bone defect model, to use this model to explore the relationship between angiogenesis and osteogenesis within the framework of tissue regeneration, and to investigate the ability of growth factor combinations to promote both angiogenesis and osteogenesis within the defect site thereby producing functional repair tissue.

This work is *significant* because it quantifies these two processes in a challenging orthotopic model and promotes understanding of the necessary components to the generation of an efficacious tissue-engineered construct for osseous defect repair. It assesses the ability of sustained growth factor co-delivery to accelerate bone repair and revascularization of a critically-sized segmental defect over delivery of a scaffold alone. This project provides an improved knowledge base regarding the link between early vascularization and subsequent functional bone repair. This work has produced the following outcomes: 1) established a rigorous and reproducible small animal model 2) combined the animal model with quantitative measures for assessing functional repair of segmental bone defects 3) employed novel *in vivo* and *in vitro* imaging techniques 4) determined the interactions between and dose-dependent effects of co-delivering an osteoinductive and chondrogenic growth factor combination and 5) evaluated the vascular and osteogenic responses to delivery and co-delivery of an angiogenic growth factor alone and in combination with the osteogenic growth factor combination.

CHAPTER 2

LITERATURE REVIEW

2.1 Bone Structure and Function

Bone develops from three main lineages; the craniofacial skeleton develops from the neural crest, the axial skeleton derives itself from the sclerotome of the somite masses of the mesoderm (somite masses form in symmetrical pairs, arranged alongside the neural tube of the embryo, derived from the mesodermal tissue), and the appendicular skeleton is derived from the portion of the mesoderm that also contributes to formation of limb buds. Spinal patterning is determined by the regular arrangement of the somite masses. As the somite masses mature they produce sclerotomal cells, which migrate to surround the spinal cord, forming the bony vertebrae.

There are two processes by which bone develops – endochondral ossification and intramembranous ossification. Endochondral ossification is the process by which long bones develop and grow. It is also the process by which simple fractures heal. Using long bone development as an example, a primary matrix of cartilage is laid down by chondrocytes in the general pattern of the limb. The diaphyseal region of the bone mineralizes, forming a primary ossification center. Secondary ossification centers form at either end of the long bone, and develop into growth plates.

The endochondral ossification process in growth plates is patterned into several zones, representative of the overall process that occurs during fracture healing as well. First is the resting zone, where chondrocytes maintain normal morphology and are

relatively senescent. Second is the proliferative zone, where chondrocytes are proliferating and arranging themselves into columnar formations. This is followed by the pre-hypertrophic and then hypertrophic zones, in which chondrocytes grow in size and deposit a dense pericellular matrix. In the following zone, the chondrocytes die off and chondroclasts move in, disassembling the cartilaginous matrix to some extent. As the chondroclasts move in, vascular structures develop within the semi-cartilaginous zone, bringing osteoblasts into the tissue. Osteoblasts, or bone forming cells, then deposit mineralized matrix, resulting in the formation of calcified cartilage – a collagenous structure containing immature hydroxyapatite crystals. As the tissue around the osteoblasts becomes more dense and remodeled by osteoclast and osteoblast activity, it begins to resemble mature bone, and the osteoblasts become embedded in the mineralized matrix, maturing into osteocytes.

In osteoid, or immature bone, the collagen fibrils are random and unorganized, and the hydroxyapatite crystal density is less than that of mature bone. As osteoid is remodeled into mature bone via the coupled process of bone resorption and deposition, the collagen fibrils align together in distinct units and hydroxyapatite crystal deposition becomes regular and organized. The osteocytes embedded in bone and osteoid are the mature, mechanosensitive bone cells responsible for the signaling required to maintain healthy bone structure.

Intramembranous bone formation occurs as a direct result of the condensation of the mesenchyme. Progenitor cells contained within the mesenchymal tissue that patterns the flat bones of the body, such as the craniofacial skeleton, differentiate directly into

osteoblasts and osteocytes. Bone forms through appositional deposition of mineralized matrix by these differentiated progenitor cells.

A highly organized tissue, bone is characterized by two distinct microstructures: cortical and trabecular bone. The dense cortical bone makes up structures such as the shafts of long bones, and laminates the surfaces of spongy trabecular bone. Cortical bone is composed of osteons – concentric rings of mineralized collagenous matrix embedded with osteocytes organized around a common Haversian canal. The Haversian canal is a vacuous space in the bone inhabited by a single vascular structure. The osteocytes inhabit lacunae within the Haversian system, and are connected by Volkmann's canals and tiny canaliculi that permit vascular ingrowth (Volkmann's canals) and fluid flow and growth of cellular processes (canaliculi) between the osteocytes and their lacunae. Bundling together osteons, the interior and exterior surfaces of the hollow cortical bone are covered by membranes. The endosteum, or inner membrane that abuts the marrow in the cavity of bones, and periosteum, or outer membrane covering the bony surface, provide a vascular supply and residence for bone progenitor cells. The periosteum is dense with osteoblastic precursor cells that are able to rapidly mobilize for repair of damaged bone.

Trabecular bone, also known as spongy bone, is the other type of microstructure. It is composed of a combination of plate and rod-like elements. Each trabecular strut is composed of multiple trabecular packets – areas of bone that were formed at the same time as a result of local formation or remodeling. Like cortical bone, trabecular bone is composed of organized collagen fibrils and hydroxyapatite crystals. The osteocytes within trabecular bone are also connected by canaliculi. Spongy bone is typically found within flat bones and at the epiphyses and metaphyses of long bones. The plate to rod

ratio of trabecular bone, as well as the orientation of the trabecular structures, is modulated by the mechanical demands at that specific anatomical site. Trabecular bone also plays a significant role as a load distributor in the body, cushioning the mechanical stresses placed on the joints and skeleton by activity.

Not only does the skeletal system serve as a structural tissue in the body, it also helps to keep the body biochemically balanced. Bone serves as a repository for minerals such as calcium, phosphorous, and magnesium. Bone provides exchangeable calcium for the body, a mechanism by which the body maintains its ionic homeostasis. Approximately 99% of the body's calcium is stored in bones. Calcium provides structural integrity to the skeleton in the form of hydroxyapatite crystals. Hydroxyapatite crystals in bone also contain 85% of the body's phosphorous. Magnesium, an ion that serves to link hydroxyapatite crystals to the fibrillar collagen network of bone, is 54% contained in bony tissue. Bone also contains sodium in the hydroxyapatite crystals, and plays a role in the maintenance of this ion as well. Bone composition is typically 60-75% mineral by weight, the balance being mostly organic extracellular matrix (mostly type I collagen) and fluid. Hematopoiesis is another critical function of bone. Marrow contained within the confines of the cortical bone provides the body with a constant supply of red and white blood cells, as well as a repository of mesenchymal progenitor cells, able to differentiate into multiple cell lineages.

Bone development, maintenance, and remodeling are processes driven by the mechanical forces applied to the tissue. Bone is a dynamic tissue, capable of organizing itself to best suit the mechanical environment to which it is exposed. Julian Wolff is traditionally credited with the theory that the architecture and function of bone are

inextricably linked, postulated in 1892. Galileo, however, had made similar observations in the 17th century, suggesting that the shape of a bone was related to its mechanical strength. In the 20th century, H.M. Frost proposed the mechanostat theory: strain magnitude thresholds can predict bone's adaptive response. The mechanostat theory hypothesizes that in situations of disuse (bedrest, microgravity, paralysis, etc.) bone deteriorates, while normal physiologic use maintains the mechanical integrity of bone. Slight overloading can cause a shift favoring modeling over remodeling of bone, resulting in increased mechanical properties and quantity of mineralized tissue. Thus, both the physiologic and mechanical environments are critical to bone development and adaptation. Bone is in a constant state of damage and remodeling. Disrupting the balance of these two processes leads to diseases such as osteoporosis (increased bone remodeling and decreased bone modeling) and osteopetrosis (increased bone formation with no remodeling). The signaling system that correlates the activity of osteoblasts and osteoclasts is complex and unclear, but the intricate balance of both processes is critical to normal skeletal maintenance.

2.2 Angiogenesis and Bone Formation and Repair

The formation and maintenance of bone is tightly linked to the presence of a vascular supply. Osteoblasts and osteocytes must be within 0.1 mm of a vascular structure to survive and function. In fact the microstructural unit of cortical bone, the osteon, is organized around a vascular structure. Formation rates of trabecular bone have been found to have a positive correlation with blood vessel area [BAROU 2002].

Vascularity and bone are tightly linked in the processes of endochondral ossification, callus formation, metastatic invasion, and bone regeneration [BAROU 2002].

There are two vascular growth processes responsible for promoting new bone formation and repair of bone defects: angiogenesis and arteriogenesis. Angiogenesis is the process by which new blood vessels sprout from existing vascular structures. Various proteins work in concert to increase vascular permeability within an existing vessel wall. Following this, a tubular structure begins to develop, branching off from the existing vessel and extending into the adjacent hypoxic environment. This involves migration of endothelial cells or recruitment of circulating endothelial progenitor cells to the hypoxic site [RABBANY 2003]. Endothelial progenitor cells can also be derived from the bone marrow, and may contribute to endothelialization of a newly forming capillary. In order to produce functional, non-leaky vessels, however, periendothelial cells, such as smooth muscle cells, must also be recruited to the growing vascular structure [CARMELIET 2000]. During this process, mural cells stabilize the newly formed vascular structure via inhibition of endothelial cell migration and proliferation.

The process of angiogenesis is followed by arteriogenesis – the maturation and enlargement of existing vessels. This process includes the development of a muscular sheath around a nascent vessel as well as increases in vessel diameter. In simple terms, angiogenesis is the process of vessel sprouting, while arteriogenesis is the process of collateral vessel growth and maturation [CARMELIET 2000]. Arteriogenesis plays a role in the maturation of bone repair tissue, where osteons develop around mature vascular structures, restoring normal morphology and functionality to the bone. The cells responsible for the maturation of these vessels are, unlike many of the cells involved in

bone repair, not derived from the bone marrow [ZIEGELHOEFFER 2004]. Rather, it appears that bone marrow-derived cells serve to provide paracrine signals to the migrating endothelial cells and pericytes, helping to create the inflammatory microenvironment that motivates angiogenic/arteriogenic processes [KINNAIRD 2004].

In the bone growth process of endochondral ossification, invasion of osteoblasts and deposition of mineralized matrix are facilitated by angiogenesis and arteriogenesis within the calcified zone of the growth plate. The newly developed vasculature permits migration of osteoblasts, osteoclasts, and progenitor cells to the site of the calcified cartilage, enabling the formation of osteoid and maturation of the woven bone into fully formed osteons. Fracture healing similarly relies on angiogenesis to facilitate callus formation and remodeling. Immediately following bony fracture, the damage to the blood vessels initiates the clotting cascade, and a haematoma develops. This haematoma is inherently angiogenic in its composition [STREET 2002]. Initially, the fracture haematoma suppresses endothelial cell proliferation and displays osteoblastic cytotoxicity, possibly by altering cell viability through a disruption in potassium channel function [STREET 2000 Clin Orthop Rel Res]. At later time points, however, the hypoxic environment and potent growth factor milieu contained within the clot encourage revascularization of the fracture site. Transplantation of fracture haematoma into a subcutaneous mouse model indicates enhanced blood vessel formation by 7 days post-implantation. This effect is mediated by vascular-associated growth factors contained within the clot, and primarily by high concentrations of VEGF, with VEGF release peaking at 5 days post-fracture [CARANO 2003]. As the haematoma condenses and vascular structures develop through the interfragmentary region, the periosteal tissue

develops an external mineralized callus via intramembranous ossification mediated by progenitor cells from the marrow cavity [YU JBMR V60, GERSTENFELD 2003]. During this process, the fracture haematoma is resorbed and the endochondral ossification process begins, forming a soft internal callus. The end result of this process is the formation of a large, mineralized fracture callus that encompasses the fracture site with large quantities of disorganized woven bone [KOKUBU 2003]. With time, the fracture callus remodels to reveal organized, mature bone in a uniquely scar-free healing process. A stable fracture environment is critical to the cooperative processes of angiogenesis and fracture healing. Environments that are unstable in either axial or shear modalities will disrupt the vascular supply and delay fracture healing and callus remodeling, altering the tissue differentiation profile [LIENAU 2005]. Unstable fractures also tend more towards healing via the endochondral ossification process than stable fractures [FERGUSEN 1999]. Stable fractures heal by both intramembranous and endochondral ossification pathways.

2.3 Bone Trauma and Clinical Repair

Bone trauma takes many forms. There are multiple modes of long bone fracture that can lead to a variety of defects, ranging from a simple transverse fracture caused by excessive tension, to a more complicated spiral fracture, caused by extreme torsional force. Extreme trauma can induce shattering of the bone such that traditional fracture reduction techniques are non-applicable. Bone loss due to traumatic injury or disease poses a challenge for orthopaedic treatment. Delayed union or nonunion are common results of traumatic bone damage in which a significant defect is created [BORRELLI

2003, WERNTZ 1996]. Such defects must be treated with a graft to promote union. Disease, such as bone tumors, can also force an osteotomy. Osteotomies of any critical size must be treated with grafts, typically an allograft, to ensure bony union and restoration of limb functionality. Osteomyelitis, or chronic bone infection, is a notoriously difficult condition to treat. Despite surgical intervention (osteotomy and/or debridement of the afflicted bones), nonunion in this case is a frequent occurrence [CHEN X 2006].

The gold standard treatment for osseous defects is the autograft. Autografts are not subject to rejection by the immune system since they are derived from the patient's own body. The use of autografts, however, is limited due to three critical factors. First, there is a lack of available material for use. The only real source for autograft material is the iliac crest of the pelvis, which provides only a small amount of tissue. Second, there is no means to obtain a structural graft from this tissue source. The iliac crest can provide only morselized bone chips without any mechanical integrity. Use of these bone chips requires containment and support from an outside device, such as a titanium chamber. Although this treatment is successful in certain specific procedures, such as spinal fusions, it is unsuitable for repair of long bone defects. Third, the use of autograft material is subject to significant donor site morbidity and chronic pain. These are factors which greatly diminish patient quality of life, defeating the purpose of the treatment.

The facile and de facto standard treatment for substantial bony defects is the allograft. Allografts are derived from processed cortical cadaver bone. The processing of the material, designed to ensure sterility and prevent disease transmission, devitalizes the tissue. The resulting graft, devoid of all living material and many of the bioactive factors

stored in viable bony matrix, is then implanted into the defect site as a structural support. Although effective to some extent, the allograft is constrained by two critical factors: Low porosity of the allograft severely limits graft revascularization and revitalization, which leads to slow remodeling of the allograft by the host body. Lack of remodeling leads to an accumulation of microdamage within the graft, a major contributor to catastrophic graft failure. Together, these factors lead to the 25% clinical failure rate and contribute to the 30-60% complication rate associated with allografts [LUCARELLI 2005, WHEELER, 2005]. Complications occur rapidly – within 1-2 years post-engraftment – and frequently result in defect non-unions or delayed unions, significantly impacting patient quality of life [ITO 2005].

One potential alternative for addressing the associated limitations of autografts and allografts is development of tissue-engineered bone graft replacements. Recently the first steps towards employing this technique have been taken with FDA approval of the Infuse spinal fusion system (Medtronic Sofamor Danek). Tissue engineering has been described as a three-fold strategy. First, there must be a matrix, substrate, delivery vehicle, or support for the delivery of the bioactive factors. Secondly, there must be a presence of bioactive factors; for example, growth factors, genes, or signaling molecules. Third, there must be a cellular component. This component may be delivered as a part of the therapy, or rely on recruitment of host cells from the treatment recipient. This tissue engineering strategy may combine biological factors as well as synthetics to create a porous, cell-friendly microenvironment that will enhance bone and vascular infiltration into the defect site. The work presented in this thesis represents one model strategy for a tissue-engineered bone replacement. We have developed a porous polymer scaffold with

mechanical integrity that can be co-delivered with biological agents to promote osseointegration of the scaffold into a bony defect site and enhance functional repair of the osseous defect.

2.4 Bone Defect Models

There are many models of osseous non-union. These include the cranial defect, mandibular defect, radial defect, tibial or fibular defect, and femoral defect. Cranial defects are relatively easy to generate, and require no fixation device. The major limitation of these defects, however, is that they have a high rate of spontaneous healing [BYERS 2006]. It is difficult to achieve a true critically-sized defect in the cranial model, although short-term studies have been able to detect differences in early mineralization between treatment groups [SAKATA 2006]. This is due primarily to the proximity of cranial bones to the dura mater, an excellent and ready source of vascularity, and the large quantity of periosteum surrounding the defect – an excellent source of osteoprogenitors. One must note that the marrow within the cranial bones also contains osteoprogenitor cells. These three sources of cells and vascularity are readily available to the defect site. The immediate formation of a haematoma within the defect site is often enough to initiate spontaneous fusion of the defect. Scaffolds implanted into this model rapidly facilitate bony healing when acting as osteoconductive structures.

Mandibular defects come in a variety of geometries. The most common is the circular defect in the ramus of the rat mandible, which is somewhat more challenging than the cranial defect [SAADEH 2001]. Implantation of non-porous scaffolds has been known to impede wound healing in this model, while untreated defects achieve

spontaneous union in 11% of samples [AROSARENA 2003, SROUJI 2005, SHAH 2003]. Like the cranial defect, the mandibular defect occurs in a flat bone formed by intramembranous ossification. Periosteal tissue surrounding the intact bone provides a reservoir of osteoprogenitor cells that may contribute to bone healing. Mandibular defects must be fairly large in order to be critically-sized, and the typical surgical model employs sub-critical defect sizes [SPECTOR 2001]. This model, like the cranial defect model, is suitable for evaluation of cranial-maxillofacial treatment strategies, but is not representative of a long bone defect. Results from these models should not be extrapolated to treatment of long bone defects, which tend to be more challenging.

Defects of the radius, ulna, or tibia are popular because the presence of the proximal load-sharing bone may negate the need for implantation of a fixation device, and the defects are partially load-bearing. A consistent size for these defects has not been agreed upon, and reports of what constitutes "critically-sized" vary widely, although ulnar defects tend to be larger than their radial counterparts (ranging from 0.5 cm to 2 cm) [SHELLER 2004, GIARDINO 2006, KOKUBO 2003, TUOMINEN 2001]. The presence of the intact ulna, radius, or fibula, however, also contributes a readily available source of osteoprogenitor cells and vascularity, via the periosteum, to the defect site. Because of this, these defects tend to be less challenging than the femoral defect model. The presence of the intact periosteum on the ulna of a 1 cm radial defect model in rabbits provides a source of osteoprogenitors that readily populate the surface of implants and contribute to partial bridging of untreated controls [GOGOLEWSKI 2000, YAMAMATO 2006]. Use of intramedullary Kirshner wires to stabilize the defect and graft seems to inhibit part of the healing response [TUOMINEN 2000]. Adding stability

in the form of a bone plate partially stabilizes the defects, but also provides a site for excess mineralization to occur on [ITOH 1998]. The use of ulnar defect models makes mechanical testing of the samples difficult, due to the presence of synostosis between the radius and the ulna, which occurs even in untreated control defects [BOSTROM 1996]. Murine tibial defects heal in the presence of an unaugmented collagen sponge [ENDO 2006]. Like radial defects, the size of tibial defects ranges considerably – 5 mm defects are employed in both rat and rabbit models; and mechanical fixation is required to achieve stabilization [ENDO 2006, KOMAKI 2006]. Tibial defects are a popular research model clinically as well as experimentally because the mode of fracture tends to be complex, requiring multiple stage clinical interventions [JONES 2006, ATTIAS 2006].

Femoral defects are perhaps the most challenging model of osteotomy available in the body. Beyond the cut ends of the defect site, there is no proximal periosteum to contribute vascularity or osteoprogenitors to the osteotomy. It is easy to achieve a critically-sized femoral defect due to the length of the bone. Stable fixation of these defects, however, is challenging. Typical fixation relies on a simple polyethylene bar that directly abuts the femur and implant, secured in place with four smooth pins. This fixation method is highly unstable, permitting excessive micromotion, and is prone to defect collapse. Additionally, the placement of the plate directly against the implant in the defect site prohibits invasion of cells from that portion of the circumference of the implant. This direct abutment of the plate against the defect site also predisposes the limb to formation of ectopic mineralized matrix along the length of the plate [KADIYALA 1997]. In the literature the typical defect length is 5 mm. This defect, however, is not

critically-sized, as the untreated 5 mm defects are prone to spontaneous healing. Published spontaneous union rates range from 10-50%. [WERNTZ 1996, NOTTEBAERT 1989] Without a truly critically-sized defect, stringent evaluation of large bone defect treatment strategies is not possible. The robust 8 mm defect in rat models is critically-sized, unlike the more commonly used 5 mm defect. Pilot work for the studies presented here included an attempt at the 5 mm defect using the standard block-and-pin fixation strategy widely employed in the literature. That pilot study was compromised by frequent collapse of the defects and spontaneous union in multiple untreated defects. Given a larger defect (8 mm) and a more stable fixation system such as the one employed in the work presented here, however, a secure, robust, and challenging defect model can be established. The stable 8 mm defect is not subject to spontaneous healing, and fits the criteria for a critically-sized defect as established by Hollinger [BRUDER JOR 1998, FEIGHAN 1995, KADIYALA 1997, LIEBERMAN 1999 JBJS, STEVENSON 1994, HOLLINGER 1990].

2.5 Experimental Treatments

Experimental treatments for large osseous defects are wide-ranging in their specific components, but consist of two fundamental elements – a delivery vehicle (scaffold) and a stimulus intended to evoke a biologic response (cells, growth factors, or genes).

Scaffolds may serve a variety of purposes. Some investigators choose to use materials with structural integrity that may provide mechanical support to the bony defect; others select materials with little to no mechanical strength, serving primarily as

delivery vehicles for biologics. The typical structural scaffold implanted into defects is hydroxyapatite/tricalcium phosphate (HA/TCP). This ceramic scaffold is composed of naturally occurring minerals in bone tissue. However, it is limited by low porosity, lack of interconnected porosity, and brittleness that predisposes it to fracture when exposed to mild loading *in vivo* [BRUDER 1998 JBJS]. Implantation of a plain HA scaffold *in vivo* does not promote union of an osseous defect, and results in formation of fibrous tissue within the defect site [BRUDER 1998 JOR, KADIYALA 1997]. The healing response to implantation of HA/TCP is not elevated by augmentation with bone marrow. The result of this treatment is minimal bone fill into the scaffolds by 8 weeks post-op. However, addition of mesenchymal stem cells (MSCs) to the HA/TCP scaffold substantially improved formation of new mineralized matrix, resulting in the formation of a periosteal callus around the implant [KADIYALA 1997]. This strategy has even been attempted clinically; in four patients ranging from 16 to 41 year of age autologous BMSCs were harvested and seeded onto porous HA blocks implanted *in vivo*. The results showed improved functionality of the affected limbs and incorporation of the graft into the host bone over the first year *in vivo*, but relied heavily on mechanical stabilization of the limb and implant [MARCACCI 2007]. Augmentation of HA scaffolds with demineralized bone matrix (DBM) enhances mineralization somewhat, but does not restore mechanical integrity. In a study involving rat femurs, samples were so brittle and grossly unstable that mechanical testing *post mortem* was impossible [FEIGHAN 1995].

DBM itself has also been delivered to segmental defects in varying formulations. In a rat model utilizing 8 mm femoral defects, human demineralized bone matrix (hDBM) was delivered in one of two carriers – hyaluronic acid or glycerol. While

delivery of the carrier alone did not encourage mineral formation, a small number of hDBM-treated groups achieved bony union (8/48) by 16 weeks post-op [OAKES 2003]. These results point to the potential osteoconductive properties of DBM, but a lack of osteoinductivity.

Although limited by a lack of mechanical integrity, a number of gel-consistency materials have been used as experimental treatments for bone regeneration. Collagen is a popular matrix due to its inherent biocompatibility. Because of its lack of bioactivity, collagen matrices must be combined with other biologically active factors in order to promote osseous union. A popular use of this delivery method is the clinically-approved delivery of bone morphogenetic protein-2 (BMP-2) in an absorbable bovine collagen sponge to produce spinal fusions. This method is also being clinically investigated as a means of accelerating open tibial shaft fracture repair [SWIONTKOWSKI 2006, BURKUS 2002]. Delivery of BMP-2 in an absorbable collagen sponge may also aid allograft incorporation into the host bone [ZABKA 2001]. The bovine collagen sponge has also been used experimentally in animal models to deliver morselized autogenous bone chips and cell culture extracts in an attempt to promote healing. The use of autogenous bone chips in a rat segmental defect model failed to heal the defect; rather, it resulted in formation of fibrous tissue [HUNT 1996]. Conversely, autogenous bone chip treatments have been used clinically to produce spinal fusions and met with success in producing radio-opaque mineralized tissue in a critically-sized canine femoral defect model [SWIONTKOWSKI 2006, KRAUS 1999]. Mechanical integrity, however, was not restored in the canine model by 16 weeks post-op.

BMPs are also a popular choice for gene therapy in a variety of delivery systems. Delivery of BMP-9 by intramuscular adenoviral injection induces ectopic mineralization *in vivo* and stimulates *in vitro* ALP production by human MSCs [LI 2003]. Direct transfer of adenoviral BMP-2 locally to a tibial fracture in an osteoporotic ovine model enhances the bending strength, callus area, and callus density over untransfected controls [EGERMANN 2006]. Thus, gene therapy has potential for application even in challenging fracture models [EGERMANN 2005]. Local injection of adenoviruses encoding BMP-2 to a stabilized lapine femoral defect of 1.3 cm significantly improved the bending strength and stiffness over treatment with adenoviral luciferase (control vector). Bony bridging of the defect was apparent in both treatment groups [BALTZER 2000]. A parallel study in a 5 mm rat femoral defect model showed enhanced mineralized matrix in BMP-2 gene-treated defects versus luciferase cDNA treated defects. However, the incidence of bony union in the BMP-2 treated defects hovered around 75%, although 50% of these defects still contained islands of cartilaginous tissue by 8 weeks post-op [BETZ 2006]. Mechanical integrity was not restored. Delaying the delivery of adenoviral BMP-2 until day 5 or 10 post-op slightly increased the incidence of bony union to 86% [BETZ 2007]. Delivery of condensed plasmid BMP-4 to murine cranial defects in PLGA enhances bone fill by 4.5 fold over delivery of a scaffold or non-condensed plasmid [HUANG 2005]. This study illustrates that the delivery method for gene-based therapies is of great importance, similar to the observations made regarding protein therapies. However, when the correct titre of virus is delivered, delivery of genes such as caALK2, VEGF, and RANKL have been shown to revitalize even cortical allografts [AWAD 2007].

Regional gene therapy for bone defects is also commonly achieved via implantation of pre-transfected cells [BALTZER 2004]. Local delivery of BMP-2-transfected BMSCs in an alginate hydrogel enhances late bone formation in a rabbit cranial defect model [CHANG 2004]. Both delivery of BMP-2-producing BMSCs and delivery of BMP-2 protein (both in guanidine-extracted DBM) produce similar results in terms of radiographically-defined bony union in an 8 mm rat femoral defect model or a 6 mm defect (BMP-2 transfected MSCs on a collagen scaffold) [LIEBERMAN 1999, TSUCHIDA 2003]. However, histomorphometric analysis showed an increase in total bone area in the gene therapy group over the protein delivery group. This increase in bone area did not correlate to an increase in mechanical though, indicating that bone quality may be more critical than bone quantity for restoration of limb functionality. Transduction of BMSCs with BMP-4 enhances mineralized tissue deposition in sub-critical rabbit femoral defects over delivery of unaltered BMSCs [SAVARINO 2007]. Delivery of the BMSCs alone enhanced tissue invasion into the defect site, but did not impact mineralization to the degree that implantation of transfected BMSCs did. Transduced mesenchymal cell lines (BMP-2/β-galactosidase) have been used *in vivo* as a type of engineered periosteum to enhance incorporation of allografts into a murine segmental defect model [XIE 2007].

Gene therapy can also be used to induce osteogenic gene expression in non-osteoblastic cells, such as fibroblasts and muscle-derived cells [KREBSBACH 2000, PHILLIPS 2006, SHEN 2004]. BMP-7 (OP-1)-producing fibroblasts have been shown to produce mineralized tissue when implanted *in vivo* (subcutaneous rat model) on Gelfoam sponges. This approach also enhances healing of murine cranial defects over delivery of

untransfected fibroblasts [KREBSBACH 2000]. Primary muscle-derived cells (preplate isolation technique) can be transfected to express BMP-4 and, upon implantation into a murine femoral defect, produce radiographically apparent union and partially restore limb functionality [SHEN 2004]. Adipose-derived MSCs modified to produce BMP-2 have also been shown to have osteoregenerative potential with results similar to those produced by high dose BMP-2 (20 μg in a 6mm rat femoral defect) [PETERSON 2005]. However, the ability of non-osteoblastic cells transfected with gene constructs, such as Runx-2, to mineralize has been shown to be highly scaffold-dependent [PHILLIPS 2006].

Cell-based therapies without genetic modification have also been investigated. In a canine parietal bone defect model, delivery of BMSCs has been shown to have osteoregeneration potential similar to delivery of autologous bone chips [UMEDA 2007, NIEDZWIEDZKI 1993]. Similar results were achieved in an ovine metatarsal defect model [VIATEAU 2007]. The reported ability of simple cellular therapies to regenerate large defects varies widely, but when the degradation properties of the delivery scaffold are adequately matched to the rate of mineralized matrix deposition, this approach can be successful [BENSAID 2005, BRUDER Clin Orthop Rel Res 1998, BRUDER JOR 1998]. Although whole bone marrow has occasionally been used in combination with ceramic scaffolds to attempt osseous defect regeneration, there is evidence supporting the hypothesis that selecting a specific population or populations of cells from the marrow cavity may be more advantageous [KADIYALA 1997]. Although autogenous bone marrow-derived cells are optimal as they do not activate the host immune system, allogeneic stem cell populations may by immunologically inert enough to successfully engraft in the recipient [LIVINGSTON 2003]. The key factor present in bone marrow

necessary to potentiate this regenerative capacity appears to be the living cells, not the inherent growth factor milieu [WERNTZ 1996].

Combining cellular therapies with growth factor or gene therapy can also accelerate the process of bone regeneration. In a rat radial defect model, addition of basic fibroblast growth factor (bFGF or FGF-2) to BMSCs accelerated deposition of bone repair tissue [LISIGNOLI 2002]. Co-delivery of condensed plasmid DNA encoding BMP-4 and VEGF with BMSCs on a PLGA scaffold significantly improved the ability of the cells to induce ectopic osteogenesis and implant vascularization [HUANG 2005]. The role of VEGF in bone defect repair models is a complex problem, and reports on the efficacy of VEGF as a treatment are varied. Delivery of high-dose VEGF (10 μg) in protein form to a stabilized but challenged (periosteal stripped) mouse fracture model stimulated an increase in the percent of the callus that was calcified [STREET 2002]. Systemic treatment with soluble VEGF receptor of animals that had received a stabilized fracture resulted in dramatic impairment of new bone formation and an overall decrease in callus mineral content [STREET 2002]. The same results were seen in a cortical bone defect model of intramembranous bone healing. In a segmental defect of the radius in rabbits, VEGF was continuously delivered via an osmotic pump over the first 7 days post-op. VEGF treatment at a dose of 250 μg stimulated significant filling of the defect site with new bone, while non-treatment resulted in a lack of bony bridging [STREET 2002]. In a murine cortical defect model, delivery of VEGF in gene form intramuscularly to the defect location resulted in a moderate increase in the bone mineral content at an early time point (2 weeks) [TARKKA 2003]. By week 4 the control group (LacZ-treated) and VEGF groups were comparable in bone mineral content and histological appearance.

VEGF gene therapy decreased the quantity of cartilage at 2 weeks post-op; it is unclear if VEGF therapy accelerated endochondral ossification or simply forced direct ossification, circumventing the cartilaginous period. In exercise-induced models of anabolic bone formation, blocking VEGF signaling attenuates the modeling response that occurs in untreated animals. Gene therapy using VEGF and RANKL enhances revascularization, resorption, and mineralization of processed cadaveric allografts in a mouse model [ITO 2005]. Similarly, co-delivery of BMP-4 and VEGF condensed plasmid DNA along with BMSCs into a subcutaneous location induced local bone formation [HUANG 2005]. Continuous delivery of VEGF or VEGF-inhibitor to a lapine tibial segmental defect, however, failed to induce an osteogenic response. Delivery of VEGF in this model did enhance vascular invasion [ECKHARDT 2003]. Delivery of 3 μg of VEGF to a 3.5 mm diameter calvarial defect enhanced defect vascularization in both irradiated and non-irradiated samples. Bony bridging was enhanced by delivery of VEGF-containing scaffolds in both groups [KAIGLER 2006]. Collectively, these studies point to the potential for a highly dose-dependent and injury-dependent efficacy of delivering VEGF for bone regeneration therapy.

The therapies described above relied largely on delivery vehicles or scaffolds with suboptimal mechanical properties. In addition to exploiting the chemoresponsive stimuli to regenerate bone, one can design a treatment strategy that incorporates the mechanosensitive nature of the tissue. Because mechanical stimulation is known to potentiate increases in bone quantity and quality, it may be advantageous to design a tissue-engineered construct that can load-share with the mechanical stabilization apparatuses. Structural polymer scaffolds can be produced with sufficient elasticity and

integrity to achieve these goals. The use of structural polymer scaffolds as treatments for large load-bearing defects, however, has not been widely investigated. For segmental defect repair in load-bearing sites, HA/TCP is the typical scaffold delivered if structural stability of the implant is a factor for consideration [BRUDER 1998 JBJS, FEIGHAN 1995, BRUDER 1998 JOR, KADIYALA 1997]. There are few instances of polymer implantation [OEST 2007, RAI 2007, CHU 2007]. However, this strategy has been explored for reconstruction of craniofacial defects [SCHANTZ 2003, ROHNER 2003, GOMEZ 2006, KAIGLER 2006]. The inert nature of the simple polymer scaffold necessitates combination with biologically active agents, such as marrow cells and/or growth factors. Incorporation of VEGF into a PLGA scaffold enhanced both angiogenesis and mineralized matrix formation in an irradiated murine calvarial defect model [KAIGLER 2006]. Polycaprolactone (PCL) has been investigated by several research groups. Combination of autologous bone marrow with a porous PCL scaffold significantly improved bony fill in a porcine orbital defect model over delivery of a naked PCL scaffold. Non-treatment of the defect resulted in fibrous tissue formation [ROHNER 2003]. Use of a lapine calvarial defect model was applied to the investigation of marrow progenitor cell- and osteoblast-seeded PCL scaffold abilities to regenerate osseous tissue. The PCL scaffolds used here were similar to those investigated by Rohner et al. The cells were seeded in a fibrin glue suspension into the PCL scaffolds with a 3 day preculture period prior to implantation. Incorporation of cells into the scaffold significantly enhanced bony fill and push-out strength within the calvarial defects (by approximately 60%). The type of cell delivered did not significantly impact bone regeneration or mechanical integrity [SCHANTZ 2003].

The results of the various treatment strategies reviewed here attest to the complex nature of the bone regeneration problem. Without a biologically active component, delivery of a bare scaffold is insufficient to induce osteogenesis *in vivo*. Although simple cell-based therapies meet with some success, their efficacy can be improved upon by co-delivery with active proteins or genetic modification. Provision of grafted cells on the scaffold is not necessary to produce an osteogenic response, as scaffold modification with gene-encoding vectors or growth factors is suitable to elicit a response from the surrounding host cells. The current limitation of these acellular therapies is largely based on the sheer quantity of vector or protein that must be delivered. Transfection rates for viral vectors remain relatively low, and many investigators may overdose the quantity of growth factor in order to induce a positive response. The work presented here rigorously evaluates the potential to efficiently generate consistent bony union in a large femoral defect model using low-dose growth factor co-delivery.

2.6 Growth Factor Selection

In order to promote vascularized bone healing within the segmental defect, three growth factors (osteogenic, chondrogenic, and angiogenic) have been selected for use in these studies.

BMP-2 (bone morphogenetic protein-2) was selected for its potent osteoinductive activity both *in vivo* and *in vitro*, and is essential for fetal skeletal development (deficient phenotypes of BMPs -2, -4, and -7 are embryonic lethal) [SCHMITT 1999]. BMPs play roles not only in calcified tissue development, but also in cartilage and skeletal connective tissue formation [WOZNEY 1998]. BMP-2 is capable of inducing progenitor

cells to adopt an osteoblastic phenotype when implanted both ectopically and orthotopically *in vivo* [RILEY 1996]. Endogenous BMP-2 is heavily implicated in fracture healing and bone induction [REDDI 1998]. The key steps in the bone induction cascade -- chemotaxis, mitosis, and differentiation -- are all promoted by BMP-2 at varying doses, although BMP production during fracture healing seems to be restricted to the initial phases of healing [REDDI 1998, EINHORN 1998]. BMP-2 is known to induce osteoblast migration *in vitro*, and is involved in the differentiation of progenitor cells derived from both bone marrow and periosteum to the osteoblastic phenotype [MAYR-WOLFHART 2002]. Chondrogenic differentiation of progenitor cells is also partially regulated by BMP-2 expression [EINHORN 1998, RILEY 1996, WOZNEY 1998]. Peak BMP-2 expression occurs during early stages of fracture healing, where the growth factor plays an important role in initiating and directing the formation of new bone by progenitor and osteoblastic cells *in vivo.*

BMP-2 is also known to play a role in the regulation of angiogenesis in both soft tissues and bone [LANGENFELD 2004]. BMPs can induce production of VEGF by osteoblastic cells and placental growth factor (PlGF) in mesenchymal cells [DECKERS 2002, MARRONY 2003]. Although osteoblastic differentiation occurs independently of VEGF production, the dual effects of BMP-2 on angiogenesis and osteogenesis suggest an important bifunctional role for the protein *in vivo.* The final connection in this circular regulation is the ability of endothelial cells to secrete BMP-2 and thereby attract osteoblasts and osteoblastic progenitor cells.

The specific osteogenic activity of BMP-2 has prompted extensive *in vivo* evaluation of the peptide for bone regeneration. Administration of BMP-2 to segmental

defect sites has been shown to promote bony union in defects at extremely high concentrations (up to 20 micrograms per defect), but not at lower concentrations (1.4 micrograms per defect) [ISOBE 1999, LEE 1994, YASKO 1992, PETERSON 2005]. BMP-2 administration has been approved for clinical use in spinal fusions, and has been extensively tested in bone defect models and ectopic implantations in a wide range of animals [WOZNEY 1998]. The proposed growth factor dose for the studies in specific aims II and III is significantly lower than the effective dose used by Yasko et al. and Peterson et al. in accordance with the hypothesis that co-delivery of BMP-2 with another protein may lower the concentration of BMP-2 required to promote union.

The growth factor selected for co-delivery with BMP-2 was TGF-β3 (transforming growth factor beta-3). TGF-βs are typically associated with chondrogenesis, but have been shown to act synergistically with BMP-2 to form mineralized matrix in an ectopic mouse model of osteogenesis, and TGF-β1 is known to synergize with BMP-7 to enhance angiogenesis [SIMMONS 2004, RAMOSHEBI 2000]. TGF-β family proteins are highly expressed during endochondral ossification and fracture healing, and serve to partially regulate the chondrogenic phenotype adopted by progenitor cells during fracture healing [LIEBERMAN 1999]. TGF-β synthesis may also be upregulated under hypoxic conditions such as those seen locally during fracture healing [BOULETREAU 2002, SAADEH 2000]. During the initial inflammatory phase reaction to bone fracture, TGF-β is released by platelets [EINHORN 1998]. TGF-β is involved in the regulation of late stage chondrocyte and osteoblast differentiation in fracture healing as well as osteoblast/osteoclast coupling and extracellular matrix production [CARANO 2003]. Delivery of TGF-β3 to an osseous defect may promote

formation of cartilaginous tissue which can be subsequently calcified and remodeled to form fully mineralized matrix. TGF-β3 expression can also increase VEGF production in osteoblastic cells, linking it to angiogenic responses [SAADEH 1999]. TGF-β family members, specifically TGF-β3, are crucial to reducing inflammation and promoting scar-free healing. TGF-β3 is under clinical investigation as an agent to promote scar-free healing of a variety of tissue defects.

VEGF (vascular endothelial growth factor) is the classic angiogenic growth factor that, at low doses, promotes formation of neovasculature both *in vivo* and *in vitro* while also acting to induce vascular permeability [PUFE 2002, DVORAK 2002]. VEGF production represents the crucial rate-limiting step in angiogenesis, inducing the proliferation, migration, and survival of endothelial cells both *in vivo* and *in vitro* [COSTA 2004]. VEGF is capable of inducing bone marrow-derived endothelial progenitor cells to enter the circulatory system and contribute to angiogenic processes *in vivo* [ASHARA 1999]. However, the vasculature formed by delivering high levels of VEGF alone has been shown to be leaky and immature in nature [McCOLL 2004]. Formation of functional, mature vascular tubes requires co-migration of pericytes and smooth muscle cells in addition to endothelial cells, emphasizing the fact that angiogenesis is a complex process regulated by multiple factors [KURZ 2000]. VEGF synthesis by endothelial and osteoblastic cells is upregulated under hypoxic conditions, such as those seen in ischemia and large tissue defects, via elevated expression of HIF-1α (hypoxia inducible factor 1-alpha), which in turn induces transcriptional activation of VEGF [BOULETREAU 2002, McCOLL 2004]. VEGF is chemotactic and mitogenic for endothelial cells (as well as osteoblasts and osteoclasts), and may also induce smooth

muscle cell migration [BUSCHMANN 2003, GERBER 1999, MAYER 2005]. The ability of the body to produce VEGF, stimulate angiogenesis, and heal wounds is known to decrease with age suggesting a potential regulatory mechanism for the observation of delayed tissue repair in elderly patients [SWIFT 1999].

VEGF, particularly slice variant 164 (murine) or 165 (human), has also been implicated in the process of bone formation by promoting angiogenesis and thereby facilitating bone and calcified cartilage remodeling [STREET 2002, PUFE 2002]. VEGF expression is increased during osteogenic differentiation, inhibiting apoptosis of osteoblasts and newly migrated endothelial cells and helping to maintain the viability of the neovasculature and osseous repair tissue [CARANO 2003, MAYER 2005]. In turn, VEGF treatment of endothelial cells increases BMP-2 expression [BOULETREAU 2002]. VEGF expression in the fracture callus recapitulates the expression of VEGF seen in long bone development, where VEGF expression is critical to promoting chondrocyte cell death and mineralization of the cartilaginous tissue [CARANO 2003, GERBER 1999]. Inhibition of VEGF may block BMP-induced angiogenesis as well as osteoblast differentiation and bone formation while addition of VEGF to segmental defects enhances bone formation [CARANO 2003, MAYER 2005]. VEGF activity in bone repair typically peaks around 5 days post-fracture and returns to basal levels by day 10 [PUFE 2002]. The ability of VEGF delivery to promote fracture healing may, however, be highly dose-dependent as there are varying reports on the efficacy of this treatment [ECKHARDT 2003, STREET 2002].

The effects of delivering these growth factors both individually and in combination were investigated in the work presented here. Traditionally growth factor

therapies have relied heavily on bulk doses of a single osteogenic peptide. The limitations of this simplistic approach are primarily found in 1) the associated cost of the treatment and 2) the potential for inducing ectopic osteogenesis or hyperossification of the treatment site. Using a more diversified therapy to treat the complex problem of functional bone regeneration may promote a more natural and controlled mechanism for healing of critically-sized defects.

2.7 Methods of Growth Factor Delivery

Non-structural scaffolds are the primary mode of growth factor delivery; hydrogels and gel-consistency polymers are popular choices. Both biologically-derived and synthetic hydrogels are commonly used in tissue engineering applications [KRETLOW 2007]. Although their consistency is more similar to that of cartilaginous tissues, hydrogels serve as effective delivery vehicles for growth factors, cells, genes, and other biologics [KASPER 2006, SIMMONS 2004]. Co-delivery of human MSCs with BMP-2 in a hyaluronic acid-based hydrogel was shown to enhance regenerative tissue formation in a rat cranial defect model over delivery of a scaffold alone, delivery of only BMP-2 on the scaffold, or delivery of only MSCs on the scaffold [KIM 2007]. The efficacy of synthetic matrices, such as PEG, is largely impacted by the degradability of the polymer and/or release and support of the biological component(s). Physical linkage of BMP-2 to a PEG (polyethylene glycol) matrix via a proteolytically degradable mechanism proved to be a suboptimal strategy for healing of murine cranial defects [RIZZI 2006, LUTOLF 2003]. It is likely that this delivery strategy was ineffective because 1) the hydrogel matrix was not easily degraded by the native host cells and 2) the

BMP-2 was not released into the surrounding tissue to chemotactically cue the surrounding cells to proliferate and/or migrate into the defect site. Use of a fibrin matrix with similarly incorporated BMP-2 also failed to regenerate cranial defects in both murine and lapine models suggesting that to some extent the BMP-2 must be soluble in order to induce osteoprogenitor cell proliferation and migration [SCHMOEKEL 2004]. In contrast, if a biodegradable hydrogel (in this case gelatin) is engineered to release BMP-2 in a controlled fashion, a large lapine ulnar osseous defect can be effectively regenerated [YAMAMOTO 2006 Tissue Eng]. *In vitro* use of anti-adhesive hydrogels (such as hyaluronic acid and PEG) has proven challenging in terms of maintaining cell viability. This observation may also partially explain the limited efficacy of these treatments *in vivo* [KIM 2007].

In addition to growth factors, complex naturally derived biologics can be employed for tissue engineering. One such example is platelet-rich plasma (PRP). Although initially investigated for use in dental and maxillofacial reconstructive applications, PRP has also recently been investigated as an agent for tissue engineering of other skeletal components [RAI 2007, ROLDAN 2004]. Augmenting gelatin hydrogels with PRP significantly improved mineralized matrix deposition in a lapine ulnar defect as compared to delivery of a naked matrix or free PRP. Formation of new bone was somewhat improved in the gelatin-PRP group as compared to a fibrin-PRP treatment group. This finding illustrates the importance of developing a proper interaction and release profile for biologically augmented matrices [HOKUGO 2005].

In addition to controlling for release of biologics, the converse aspect of controlling the retention of these factors is also important. Although extremely high doses

of free, soluble growth factor (particularly BMP-2) have occasionally shown positive results, most studies have shown that soluble growth factor is a challenging mode of delivery to use [HONG 2000]. Application of gelatin hydrogels with varying water contents and TGF-β1 to calvarial defects in a lapine model was effective only when the hydrogel was able to both prevent rapid soft tissue formation in the defect (serve as a placeholder) and retain the growth factor long enough to stimulate mineralized matrix formation [YAMAMOTO 2000 J Control Release, HONG 2000]. Chimeric natural-synthetic hydrogels are possible, although not widely used. PEGylated fibrinogen hydrogels can, similarly to gelatin hydrogels, serve as place holders to prevent rapid soft tissue invasion. When designed with a degradation rate that is roughly on par with the rate of appositional bone formation in a murine tibial defect model, the PEGylated fibrinogen hydrogel can encourage osteogenesis more effectively than if it is designed with a particularly rapid or slow degradation rate [PELED 2007]. Controlled release capsules containing BMP-2 delivered to a femoral defect site have been shown to induce bony bridging of the defect by 8 weeks post-op. In this case, a high dose of BMP-2 was used (5 mg per defect). Using PLGA particles of various sizes to deliver BMP-2, Lee et al. investigated the dose-dependent response of segmental defect healing [LEE 1994]. In terms of mechanical properties, significant differences in failure torque between defects treated with particles alone and particles augmented with BMP-2 were only seen at the highest dose (9.3 μg per defect), and not at the two lower doses (3.1 μg or 0.93 μg). High doses of BMP-7 (200 μg per 6 mm defect) delivered in a lyophilized collagen carrier can efficaciously overcome challenged (chronically infected) nonunion models when delivered concomitantly with antibiotics [CHEN X 2006]. What these studies point to is

the importance of properly managing growth factor release in order to elicit the desired biological response. Controlled and/or sustained release of proteins is a challenging problem to engineer. This situation may be further complicated by use of a two-phase system with separate components for structural support and delivery of biologics.

CHAPTER 3

Quantitative Assessment of Scaffold and Growth Factor-Mediated Repair of Critically Sized Bone Defects

3.1 Abstract

An 8 mm rat segmental defect model was used to quantitatively evaluate the ability of longitudinally-oriented poly(L-lactide-co-D,L-lactide) (PLDL) scaffolds with or without growth factors to promote bone healing. BMP-2 and TGF-β3 combined with RGD-alginate hydrogel were co-delivered to femoral defects within the polymer scaffolds at a dose previously shown to synergistically induce ectopic mineralization. A novel modular composite implant design was used to reproducibly achieve stable fixation, provide a window for longitudinal *in vivo* micro-CT monitoring of 3-D bone ingrowth, and allow torsional biomechanical testing of functional integration. A contrast agent perfusion procedure was established to enable micro-CT imaging and quantification of vascular structures within the defect site. Sequential *in vivo* micro-CT analysis showed that bone ingrowth increased significantly between 4 and 16 weeks for the scaffold-treated defects with or without growth factors, but no increase with time was observed in empty defect controls. *Post-mortem* regional micro-CT analysis revealed that the majority of the new bone formation occurred in the proximal half of the 8 mm defect. Treatment with scaffold alone improved defect stability at 16 weeks compared to non-treatment but did not achieve bone union or restoration of mechanical function. Augmentation of scaffolds with BMP-2 and TGF-β3 significantly increased bone formation at both 4 and 16 weeks compared to non-treatment but only produced bone

bridging of the defect region in 2 of 6 cases. Mineralization was observed to form first at the periphery of the scaffolds followed by more limited mineral deposition within the scaffold interior, suggesting that the cells participating in the initial healing response were primarily periosteal-derived. This study introduces a challenging segmental defect model that facilitates quantitative evaluation of strategies to repair critically-sized bone defects. Healing of the defect region was improved by implantation of structural polymeric scaffolds infused with growth factors incorporated within RGD-alginate, however, functional integration of the constructs appeared to be limited by continued presence of the slow-degrading scaffolds and perhaps suboptimal dose or delivery of osteoinductive signals.

3.2 Introduction

Large osseous defects pose a significant treatment challenge to orthopaedic surgeons and nonunion is common [BORRELLI 2003, WERNTZ 1996]. Although the gold standard treatment is autologous bone grafting, this procedure is constrained by the inability to obtain large structural grafts for transplantation and significant donor site morbidity. As a result, the clinical use of processed cadaveric allografts continues to increase [LUCARELLI 2005, WHEELER 2005]. However, allografts do not repair as quickly or completely as autografts and carry some risk of disease transmission. The destruction of live cells during tissue processing is a primary factor responsible for the loss of osteogenic properties, and the dense nature of cortical bone allografts impedes revascularization and cellular invasion from the host following implantation [ENNEKING 2001, ITO 2005, WHEELER 2005]. This limited ability to revascularize

and remodel is believed to be responsible for the 25% clinical failure rate and 30-60% complication rate associated with allograft implantation [LUCARELLI 2005, WHEELER 2005].

Tissue engineering strategies that include a porous structural scaffold with or without delivery of biological components provide a possible approach to the development of effective bone graft substitutes. The critically-sized segmental defect model can serve as a robust test bed for tissue-engineered bone regeneration strategies, even in small animals such as rats [BRAUN 1992, BRUDER 1998 Clin Orthop, CHEN 2002, LIEBERMAN 1999 JBJS, LEE 1994, OHURA 1999, WERNTZ 1996, YASKO 1992]. Although most segmental defect repair studies have focused on radiographic evaluation of healing, more quantitative measures of functional integration may provide an improved ability to benchmark different strategies for bone regeneration. In addition to biomechanical testing to quantify functional integration of bone repair constructs, *in vitro* or *in vivo* microcomputed tomography (micro-CT) imaging can be applied to quantify the ingrowth of mineralized matrix into bone defects [CASE 2003, GULDBERG 1997].

The composition and architecture of biomaterial scaffolds are important variables that strongly affect the repair response. Although ceramic scaffolds composed of hydroxyapatite or tri-calcium phosphate are by composition an attractive option, they are typically limited by brittleness, incomplete interconnectivity, and relatively low porosity. When implanted *in vivo*, ceramics may in fact sustain enough damage under repeated loading to fracture [BRUDER 1998 JBJS]. In order to achieve more desirable mechanical properties and more controllable architecture, polymeric or composite scaffolds may be

custom manufactured to meet the functional requirements at the defect site [ZEIN 2002]. However, the ability of structural polymeric scaffolds to promote the repair of large critically-sized defects – alone or in combination with bioactive factors – is not well established.

Growth factors, such as members of the bone morphogenetic protein (BMP) family, are frequently used at very high doses to treat osseous defects [YASKO 1992, SWIONTKOWSKI 2006, BURKUS 2002]. It has been shown previously, however, that delivery of two growth factors together, specifically BMP-2 and transforming growth factor β3 (TGF-β3), can result in a synergistic interaction that promotes bone formation at relatively low doses of total delivered protein in the presence of bone marrow stromal cells [SIMMONS 2004]. This work, however, was done in an ectopic mouse model of osteogenesis and the potential for co-delivered growth factors to promote functional repair in a critically-sized segmental bone defect model has not been previously investigated.

One essential element contributing to the viability of an implanted tissue-engineered construct is the development of a vascular supply to the implant that will provide nourishment and biological cues for cells migrating into or previously seeded onto the scaffold. In order to develop an efficacious tissue-engineered bone replacement, it is important to understand the process of and factors affecting vascular ingrowth into the defect site. Although traditional methods have relied on histological methods to quantify vascular structure density, recent use of micro-CT coupled with perimortem perfusion of a radio-opaque contrast agent provides a promising and more facile alternative method [DUVALL 2004]. This technique was developed and characterized in

a mouse model, and some adaptation would be required for application to a larger rodent model, such as the rat.

The goals of this study were to establish a segmental bone defect test bed model that allowed *in vivo* micro-CT analysis, to test the ability of structural polymer scaffolds to promote bone repair and restore mechanical function in the rat femur, and to establish the feasibility of a hindlimb vascular perfusion procedure. Polymeric scaffolds having longitudinally oriented porosity aligned with the direction of healing were tested with and without augmentation by low doses of co-delivered BMP-2 and TGF-β3.

3.3 Methods

3.3.1 Scaffold Production

Poly(L-lactide-co-D,L-lactide 70:30) (PLDL) cylindrical scaffolds with longitudinally oriented porosity (4 mm ϕ x 8 mm L) were created using previously described methods [LIN 2003]. Briefly, 100 micron removable fibers coated with a mixture of PLDL and the porogen azodicarbonamide were used to create oriented macroporosity, while decomposition of the porogen with the addition of heat produced random microporosity. Prior to implantation, the PLDL scaffolds were sterilized by gamma-irradiation (2.5 Mrad). The scaffolds were then wetted with 70% ethanol and rinsed in saline prior to vacuum coating with 25 μg/ml rat plasma fibronectin (F0635; Sigma-Aldrich) overnight to improve cell adhesion capability. Excess fibronectin was diluted from the scaffolds using a sterile saline rinse.

3.3.2 Addition of Growth Factor to Scaffolds

Sterile recombinant carrier-free BMP-2 and TGF-β3 (355-BM/CF and 243-B3/CF, R&D Systems, Minneapolis, MN) were reconstituted in 4 mM HCl immediately prior to use. MVG sodium alginate (Pronova Biopolymers, Norway) was gamma-irradiated at a dose of 5 Mrad to produce a short chain length alginate powder. The short chain alginate was then functionalized with a G_4RGDSP sequence at a density of 2 RGD sequences per chain using carbodiimide chemistry [SIMMONS 2004]. The RGD-alginate was sterile filtered and lyophilized. For use in the PLDL scaffold system, RGD-alginate was reconstituted to a concentration of 2%, containing either BMP-2 and TGF-β3 or no growth factor. Fibronectin-coated PLDL scaffolds were placed into cylindrical molds with a $CaCl_2$-wetted membrane on the bottom surface. A volume of 50 μl RGD-alginate containing either 200 ng BMP-2 and 20 ng TGF-β3 (growth factor-treated group) or no growth factor (scaffold only group) was pipetted into each scaffold, and a $CaCl_2$-wetted membrane was placed on top of the scaffold in the cylindrical mold. After 20 minutes, the scaffolds were removed from the molds and placed into a sterile $CaCl_2$ bath for an additional 20 minutes to allow full cross-linking of RGD-alginate within the scaffold.

3.3.3 Surgical Technique

All surgical techniques and procedures were reviewed and approved by the Institutional Animal Care and Use Committee at Georgia Institute of Technology (Protocol #A03017). The study presented here tested the effects of implanting plain or

growth factor augmented PLDL scaffolds on mineralized matrix formation and mechanical properties within an 8 mm gap defect. Female Sasco Sprague-Dawley rats (Charles River Labs, Wilmington, MA) aged 13 weeks were anesthetized using isoflurane. Taking an anterior approach, bilateral incisions were made over the length of the femurs. Each limb received a custom modular fixation plate secured directly to the femur using four miniature screws (J.I. Morris Co, Southbridge, MA). Bilateral full-thickness diaphyseal segmental defects 8 mm in length were created using a miniature oscillating saw and flushed with saline (Figure 1). Defects received one of the following three treatments: no scaffold (empty treatment group) (n = 7), a PLDL scaffold (n = 15), or a PLDL scaffold augmented with 200 ng BMP-2 and 20 ng TGF-β3 co-delivered in RGD-alginate (n = 6). Animals were given 0.05 mg/kg buprenorphine subcutaneously every 12 hours for the first 48 hours post-op. Within 2-3 days post-op, the animals resumed normal ambulation and did not show signs of pain or distress.

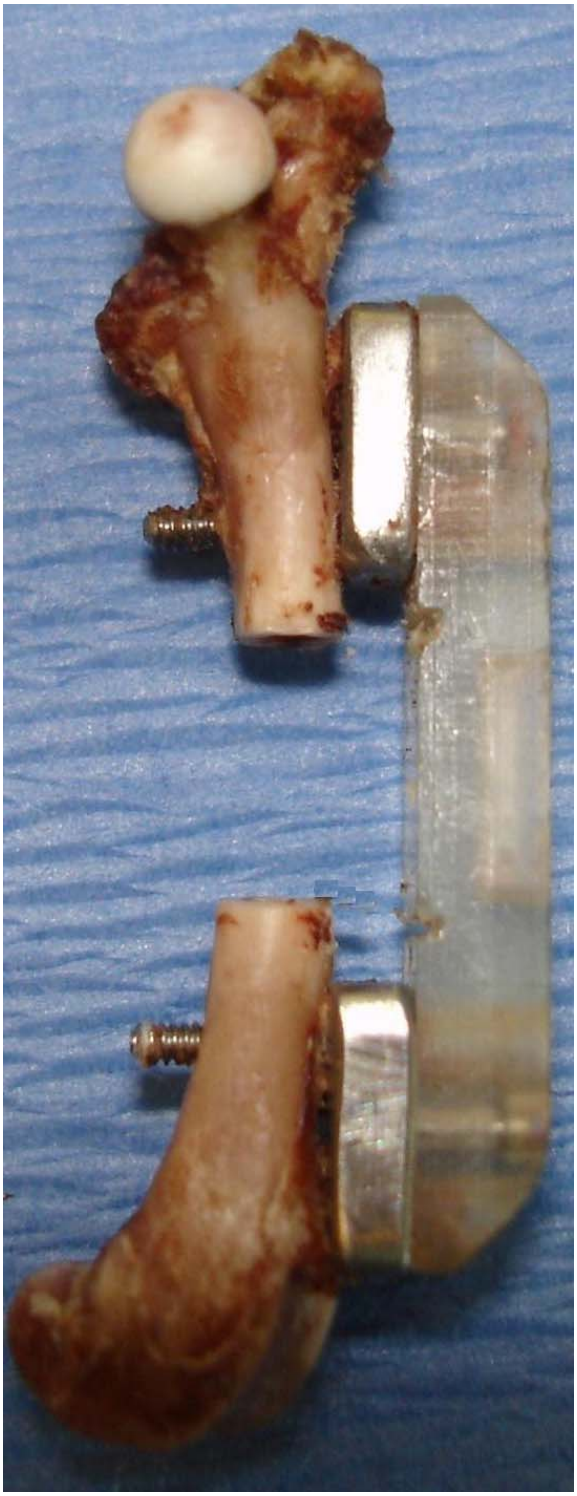

Figure 1: Rat femur with attached fixation plate assembly and 8 mm defect.

3.3.4 X-ray and Micro-CT

Two-dimensional *in vivo* digital X-rays (Faxitron MX-20 Digital; Faxitron X-ray Corporation, Wheeling, IL) were taken at five time points: 3 days post-op and 4, 8, 12, and 16 weeks post-op. These X-rays provided a qualitative assessment of healing and defect stability over time. Rates of union were assessed by two blinded observers. Union was considered to occur when a visible bridge of bone extended completely across the length of the defect site.

Quantitative 3-D analysis of bone ingrowth in 8 mm defects was performed at 4 and 16 weeks post-op using an *in vivo* micro-CT system (Viva-CT 40; Scanco Medical, Bassersdorf, Switzerland) at a 38.5 μm voxel resolution (*in vivo* scans) and 20 μm resolution (*in vitro* scans). After scanning, a constant volume of interest (VOI) centered over the defect site was selected for analysis of all samples. Two VOIs were analyzed; the *in vivo* VOI was 118 slices thick (approximately 4.6 mm thick) and centered over the defect longitudinally while the *in vitro* VOI was 400 slices thick (approximately 8 mm). A Gaussian filter (sigma = 1.2, support = 1) was used to suppress noise in the VOI prior to application of a consistent global threshold corresponding to 272 mg hydroxyapatite/cm^3. The threshold was selected manually using evaluations of ten single tomographic slices to isolate the bone tissue and preserve its morphology while excluding soft tissues and polymer scaffold. The exclusion of soft tissues and polymer using this threshold was verified by plotting a histogram of voxel attenuation versus threshold values. The selected threshold of 272 mg hydroxyapatite/cm^3 was consistently found to lie outside of the range of values corresponding to soft tissue and polymer. Applying this global threshold to the VOI, object (bone) volume and total volume were computed as

total number of voxels multiplied by voxel volume (a direct measurement that does not assume any particular microstructural morphology).

For post-mortem (*in vitro*) micro-CT imaging only, spatial analysis of the mineralized matrix was conducted. Bone formation in the proximal 4 mm of the defect was compared to that in the distal 4 mm of the defect. The amount of mineral in the core 2 mm of the scaffold was also compared to that in the edges of the scaffold and surrounding matrix (periphery). Spatial analysis wasn't done on *in vivo* images due to the small VOI. The distribution of mineral in the proximal and distal halves of the *in vivo* VOI is generally homogeneous. Additionally, the angle at which the femur must be scanned in order to permit travel of the animal's body into the bore of the Viva-CT 40 is such that core vs. periphery analysis is not possible – the long axis of the femur lies at a variable angle.

3.3.5 Mechanical Testing

After euthanasia at 16 weeks post-op, samples were harvested and wrapped in saline-soaked gauze for subsequent storage at -20°C. Prior to mechanical testing, the samples were allowed to thaw to room temperature in a saline bath before removal of the gauze. The samples were subjected to torsion using a servohydraulic mechanical testing system (858 MiniBionix II load frame; MTS, Eden Prairie, MN). The ends of the femurs were potted using Wood's Metal (033218-36; Alfa Aesar, Ward Hill, MA) and pinned through the potting blocks. The potted femurs remained wrapped in saline-soaked gauze to maintain hydration of the tissues during testing. Samples were loaded into the testing system and the bridging components of the plates were removed along with the gauze.

Samples were then tested at a rate of 3°/sec to failure. Age-matched intact femurs were also tested for comparison.

3.3.6 Vascular Perfusion

In a small 5 mm defect pilot study, vascularization within the defect region was quantified at 16 weeks post-op. Animals (n=3) were anesthetized and the abdominal aorta was catheterized for this terminal procedure. Heparin (H0777; Sigma-Aldrich) was delivered via the catheter. All blood was flushed from the hindlimbs with saline and exited through a vent in the inferior vena cava. A 10% neutral-buffered formalin wash was perfused to fix the vessel walls. After a saline rinse, the vasculature was finally filled with a radio-opaque silicone-based contrast agent (Microfil MV122; Flowtech Inc., Carver MA). The contrast agent was allowed to polymerize before the femurs were harvested and formalin fixed. Each femur was scanned *in vitro* to obtain a composite 3D image of mineralized matrix and vascularity. The samples were subsequently decalcified and micro-CT imaged again at a 20 μm voxel size to produce a 3D reconstructed image of vascular ingrowth.

3.3.7 Histology

One sample from each treatment group was selected for histological analysis. Stains used included von Kossa, Masson's trichrome, and haematoxylin and eosin.

3.3.8 Statistics

Analysis of variance was performed using a general linear model and Tukey pairwise post-hoc comparisons (Minitab). Differences between variables measured for scaffold-treated and control defects were considered significant at $p \leq 0.05$ and a trend at $p \leq 0.10$.

3.4 Results

3.4.1 Scaffold Characterization

The scaffolds produced were transversely isotropic with longitudinally oriented macropores (Figure 2). Micro-CT quantification of scaffold parameters revealed that the resulting scaffold porosity averaged 77% A previously described method involving 3-D image inversion and discrete component labeling indicated that the porosity was over 99% interconnected, verifying that porogen decomposition did not produce isolated bubbles within the polymer struts [LIN 2003]. Analysis of strut morphology showed an average thickness of 0.08 mm and spacing (i.e. pore size) of 0.38 mm. The mechanical properties of the scaffolds after irradiation included a mean elastic modulus of 63.35 ± 5.12 MPa, and mean ultimate compressive strength of 2.87 ± 0.12 MPa.

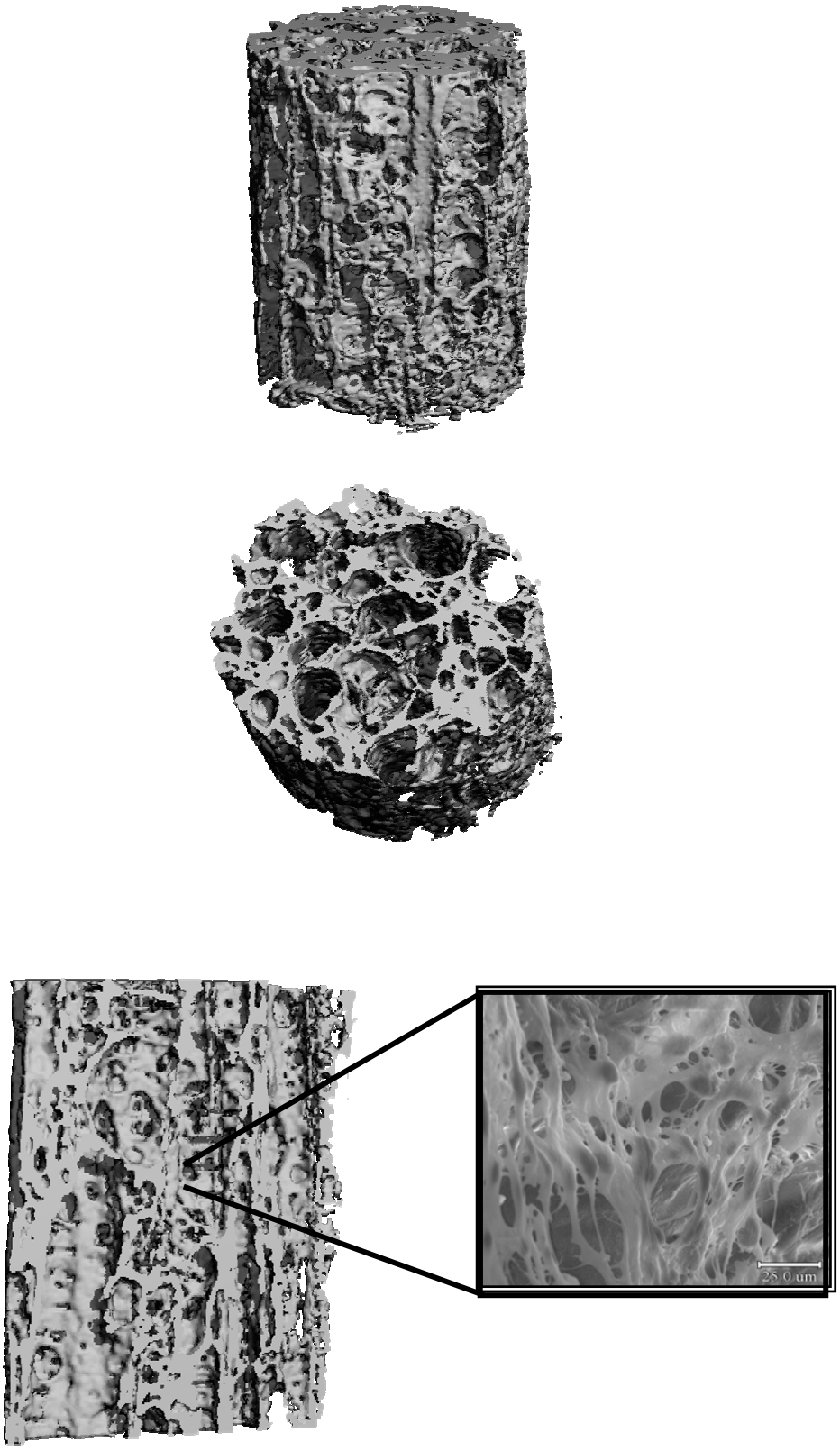

Figure 2: Micro-CT and electron microscopy images of PLDL scaffolds.

3.4.2 X-ray Imaging

Monthly Faxitron X-ray images beginning at week 4 were used to qualitatively track the progression of bone ingrowth into the defect region (Figure 3). In untreated (empty) control defects, the cut ends of the femurs were consistently rounded off with a small amount of appositional bone formation, and bridging of the defects was never observed. In contrast, X-ray images showed progressive infiltration of mineralized tissue into scaffold-treated defects over the 16 week *in vivo* implantation period. Mineral deposition typically initiated at the periosteal surface and the proximal end of the defect, forming a sheath-like structure around the ends of the scaffolds. At 16 weeks, mineralized tissue was observed to form within the scaffold pore space as well. However, PLDL treatment resulted in bridging of the defect site with mineralized tissue in only two cases. Augmentation of the scaffolds with 200 ng BMP-2 and 20 ng TGF-β3 resulted in apparently denser mineralized matrix formation within the defect site, proceeding similarly to PLDL only treated defects, with union occurring in 33% (2 of 6) samples as compared to 17% (2 of 12) for the PLDL scaffold-only group.

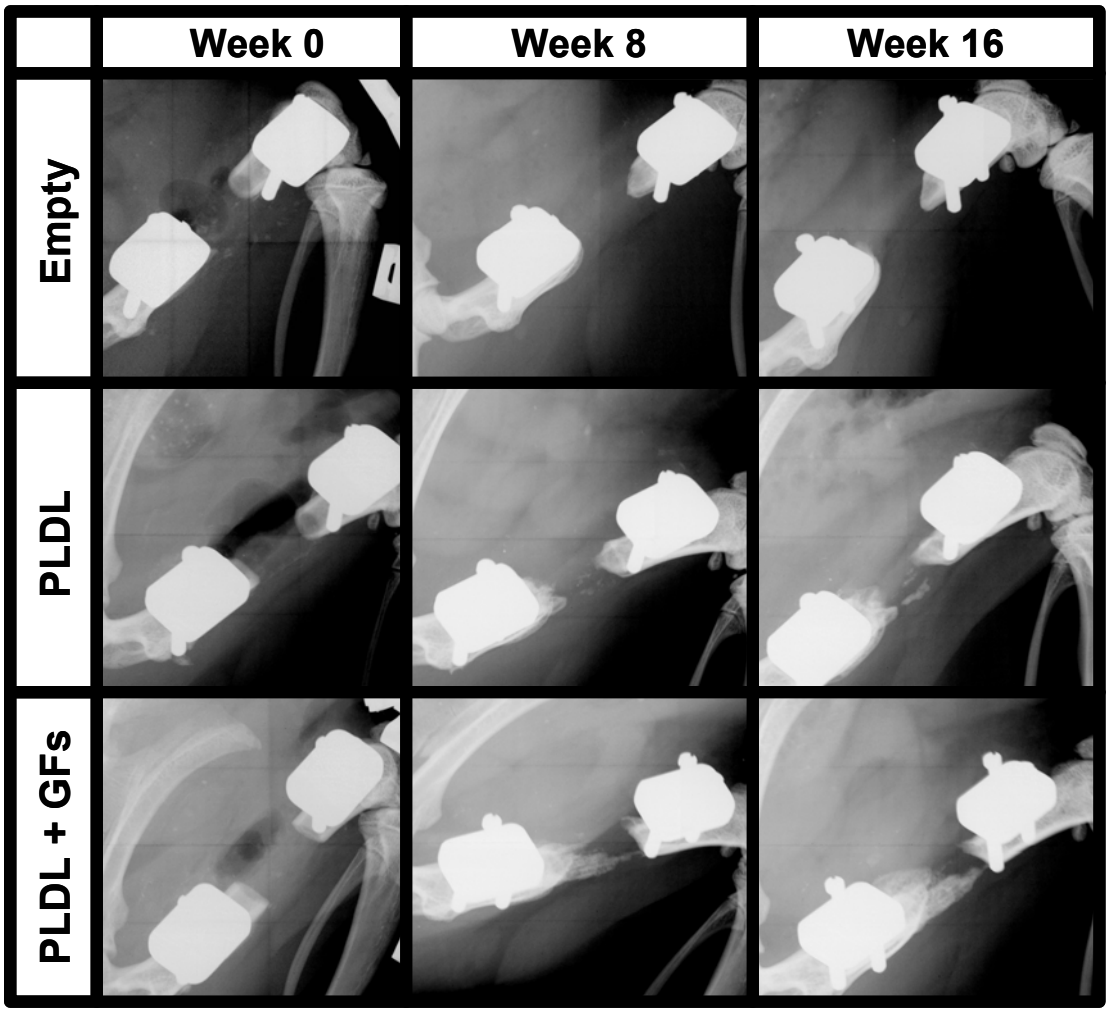

Figure 3: Digital X-ray images of femurs from each of the three treatment groups. Rates of bony union were: 2/6 for the 200/20 dose BMP-2/TGF-β3 augmented group and 2/12 for the PLDL only treated group. The empty defects never achieved union (n = 6).

3.4.3 Micro-CT Analysis

In Vivo Micro-CT Analysis of Bone Formation

In vivo micro-CT imaging permits quantitative 3-D analysis of bone ingrowth into the central region of the defect within the same animal at multiple time points. Bone volume (BV) was therefore quantified within a consistent VOI centralized in the 8 mm defect region for each group and compared at 4 and 16 weeks post-op (Figure 4). There was a significant increase in BV overall with time. Within treatment groups, defects treated with PLDL scaffolds showed a significant increase in BV from 4 to 16 weeks, as did the growth factor augmented treatment group, while there was no increase in bone volume from week 4 to week 16 in the empty defect control group. Compared to empty defects, implantation of scaffold alone did not significantly increase BV at either time point, while the scaffold plus growth factor group significantly improved repair at both 4 and 16 weeks.

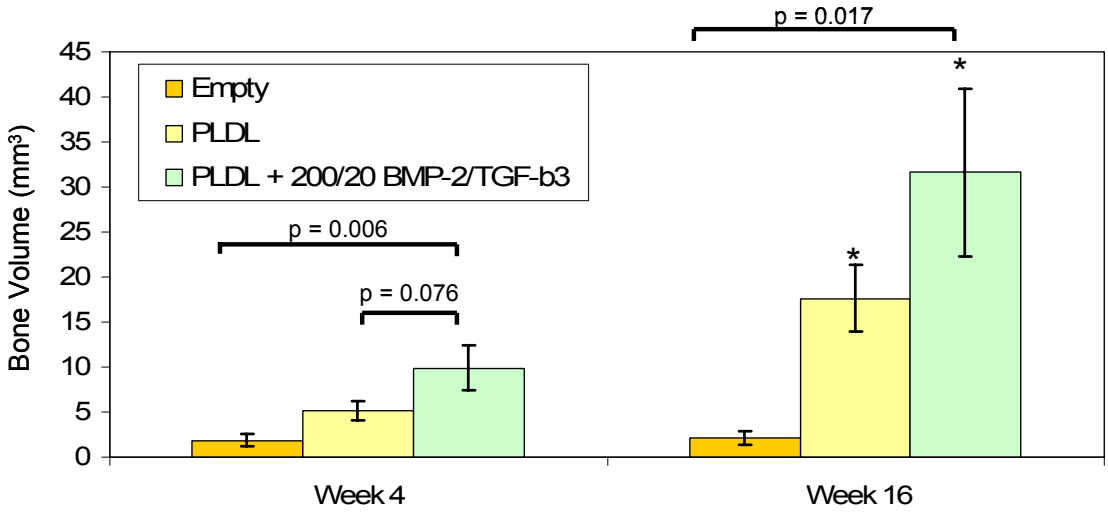

Figure 4: Average bone volumes at 4 and 16 weeks post-op for the three treatment groups. * denotes $p < 0.05$ for an increase in bone volume from 4 to 16 weeks within a treatment group ($6 \leq n \leq 15$).

In Vitro Micro-CT Analysis of Bone Formation

Micro-CT imaging done *post-mortem* and immediately prior to mechanical testing yielded similar results as were seen in the week 16 *in vivo* micro-CT calculations in terms of mature bone volume (Figures 5 and 6). The difference in bone volumes between the growth factor augmented group and the empty defects group was statistically significant ($p = 0.009$). Spatial analysis of the defect regions demonstrated that augmenting the scaffold with the 200/20 dose of BMP-2/TGF-β3 significantly improved mineralized matrix within the core of the scaffold as compared to delivery of the scaffold alone or non-treatment (empty defects) (Figure 7). The amount of bone forming within the periphery of the scaffold and the area immediately surrounding the scaffold was significantly improved in the growth factor augmented group as compared to non-treatment (Figure 7). The bone volume fraction (BVF), or percent of the VOI filled with mineralized tissue, was significantly elevated in the 200/20 dose growth factor treatment group as compared to the empty defect group for the peripheral VOI (Figure 8). Additionally, the delivery of low-dose growth factors significantly improved the formation of bone on the proximal half of the defect as compared to empty defects. Bone volume on the distal half of the defect site was not significantly impacted (Figure 9).

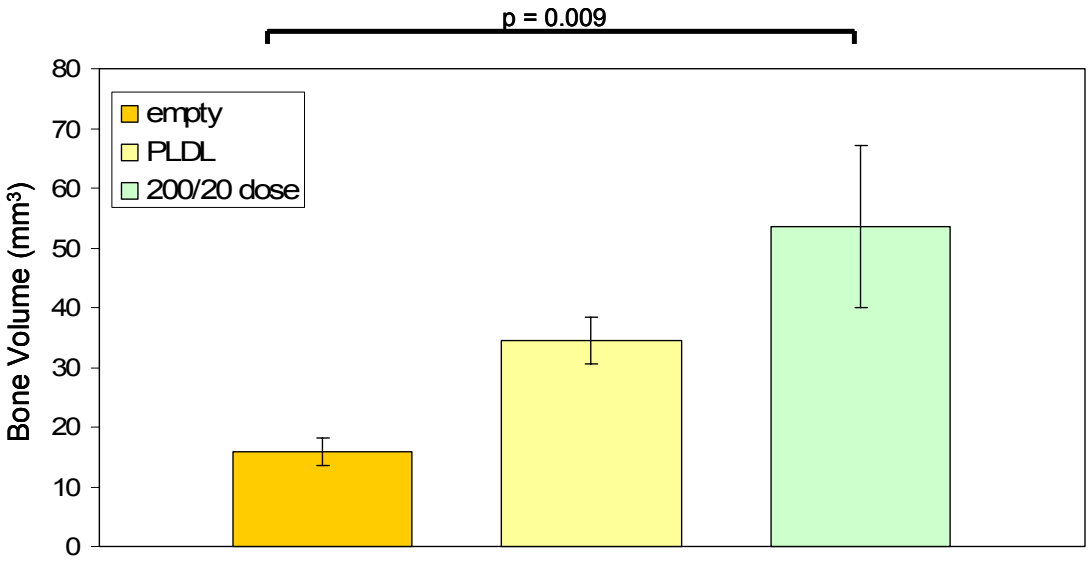

Figure 5: Post mortem bone volumes (16 weeks) for the entire defect region ($5 \leq n \leq 10$). While implantation of a plain PLDL scaffold did not significantly enhance mineral deposition over non-treatment, addition of 200 ng BMP-2 and 20 ng TGF-β3 did significantly impact bone volume ($p = 0.009$).

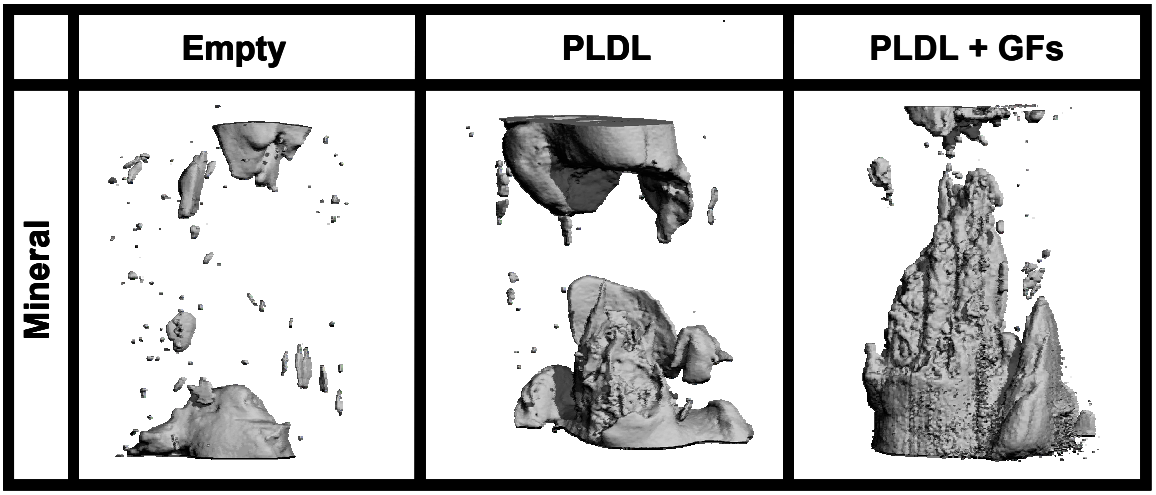

Figure 6: Micro-CT images of the defect region taken post mortem. Left, mineral in an empty defect shows only a small amount of appositional bone formation. Middle, some infiltration of mineral into the scaffold porosity is evident. Right, mineralized matrix is significantly more present in the 200/20 dose growth factor-augmented treatment.

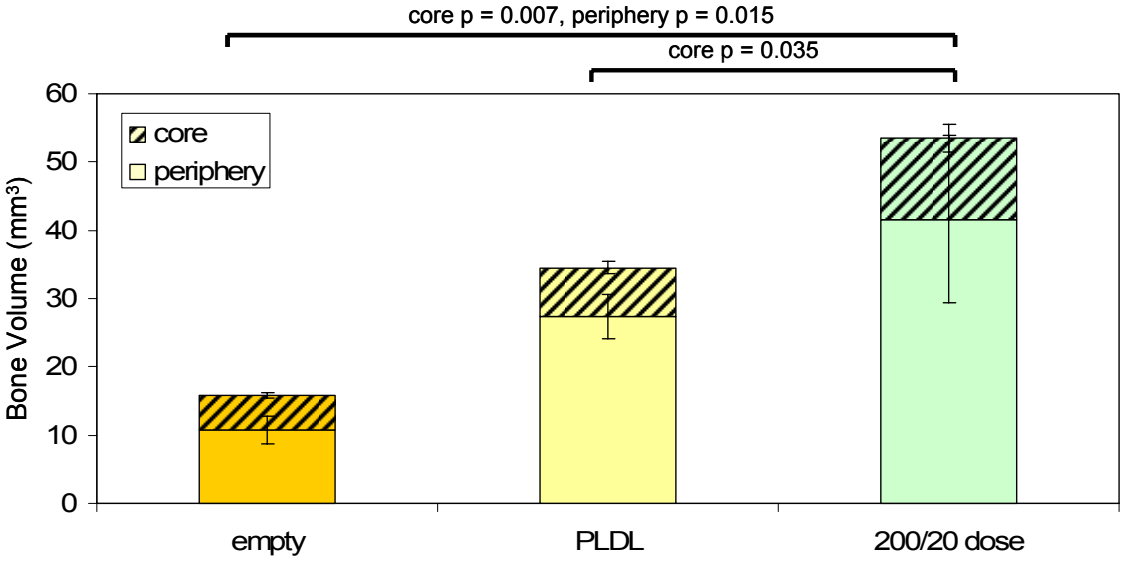

Figure 7: Spatial distribution of post mortem bone volumes ($5 \leq n \leq 10$). Volumes of interest are separated as the core (central 2 mm) and periphery (external 2 mm of scaffold and adjacent periphery) along the 8 mm length of the defect. The treatment group receiving the 200/20 dose of BMP-2/TGF-β3 had significantly improved mineral volumes in both the core and periphery as compared to empty (untreated) defects. Augmentation of the PLDL scaffold with the low dose of BMP-2/TGF-β3 significantly increased the quantity of mineral in the core of the scaffold.

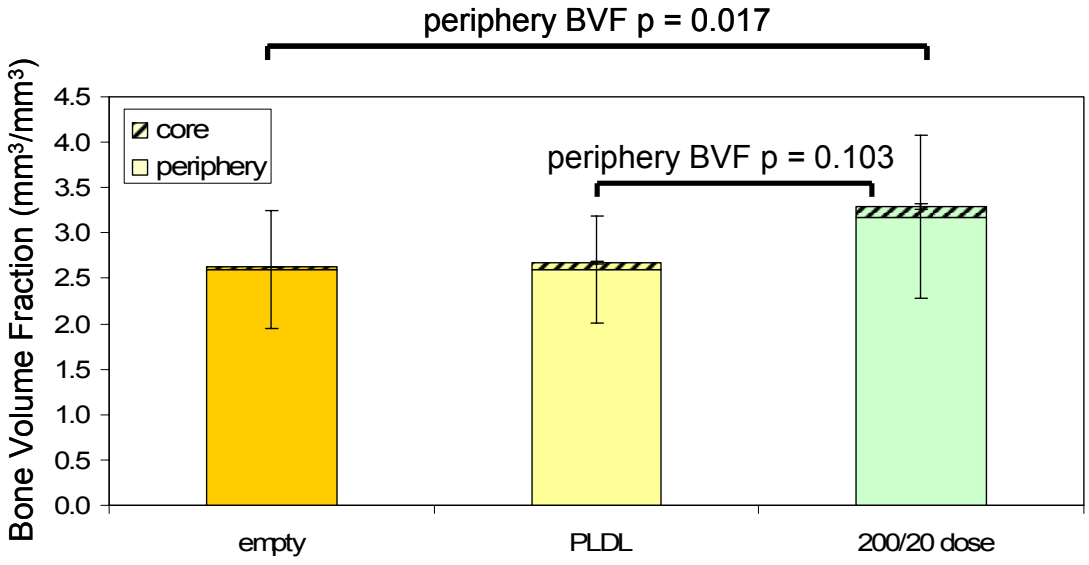

Figure 8: Spatial distribution of post mortem bone volume fractions ($5 \leq n \leq 10$). Volumes of interest are separated as the core (central 2 mm) and periphery (external 2 mm of scaffold and adjacent periphery) along the 8 mm length of the defect. The treatment group receiving the 200/20 dose of BMP-2/TGF-β3 had a significantly improved peripheral bone volume fraction as compared to the empty (untreated) group. There were no differences in core BVF between the treatment groups.

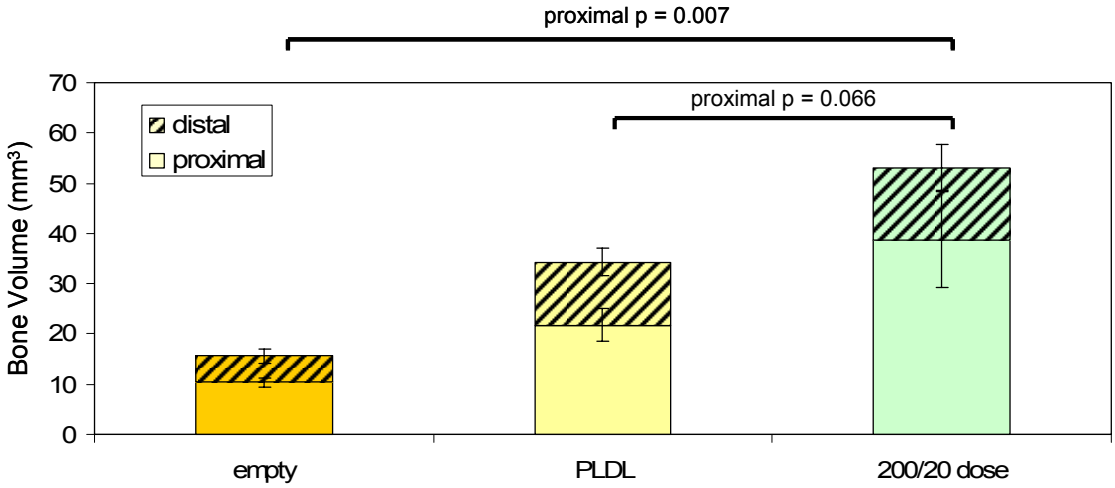

Figure 9: Spatial distribution of post mortem bone volumes along the long axis of the femur ($5 \leq n \leq 10$). There was significantly more mineral in the proximal end of the defect in the group treated with a scaffold and 200 ng BMP-2/20 ng TGF-β3 than in the empty defects.

In Vitro Micro-CT Analysis of Vascular Structures

In the 5mm defect pilot study, *in vitro* micro-CT was performed on three perfused samples before and after decalcification to isolate the vascularity and demonstrate the feasibility of the technique (Figure 10). The protocol for this perfusion technique was adopted from previously published work using a mouse model of hindlimb ischemia, and is described in Appendix D [DUVALL 2004]. Micro-CT done before decalcification gives images and quantitative information regarding the bone and vascular structures together. Imaging of samples after decalcification permits quantification of vascular structures alone (vascular volume) (Figure 11). Using a strictly defined VOI enables estimation of the bone volumes that can be obtained by subtracting the vascular volumes from the combined object volume of the bone and vasculature together. Although the small sample size precluded statistical analysis, a small elevation in vascular volume was observed in PLDL-treated defects as compared to empty defects (20.7 mm^3 for PLDL-treated defects and 16.3 mm^3 for empty defects).

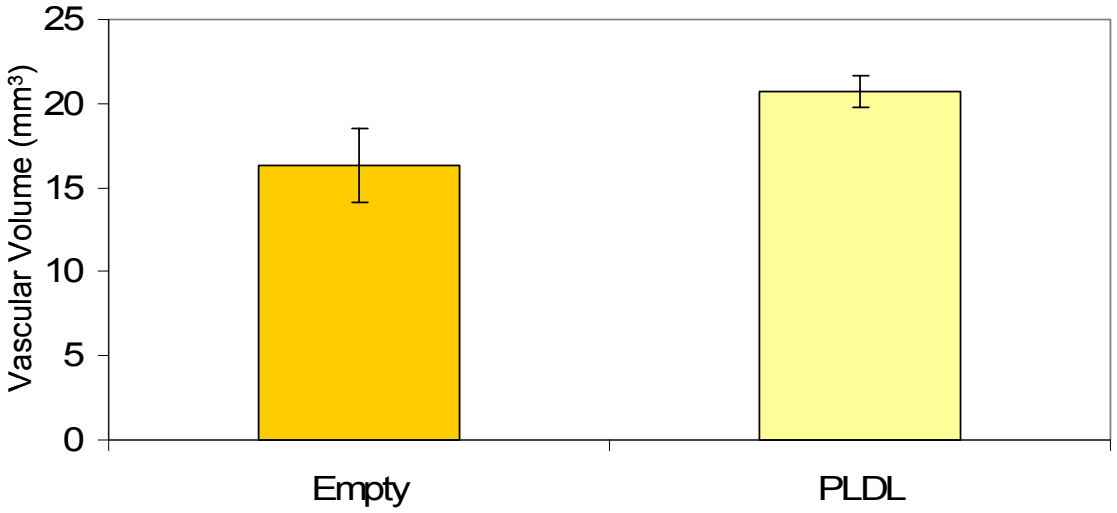

Figure 10: *In vitro* micro-CT quantification of vascular structures in decalcified samples. Statistical significance was not determined due to the small sample size (n = 3). The results served primarily to establish that perfusion of the hindlimb defect area was feasible and that the vascular volume could be quantified using micro-CT.

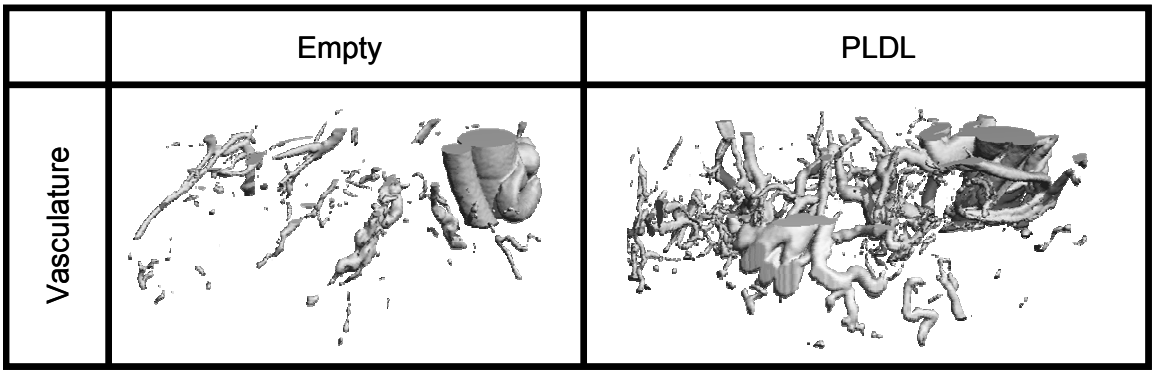

Figure 11: Images taken from i*n vitro* micro-CT quantification of vascular structures in decalcified samples. There appears to be somewhat more vasculature in the PLDL-treated defect than in the empty defect, although the sample size was not adequate to permit statistical analysis.

3.4.4 Mechanical Testing

Torsional mechanical testing was performed on samples harvested at 16 weeks post-op. Even at this late time point, empty control defects were found to have negligible resistance to torsional deformation with both strength and stiffness below the resolution of the mechanical testing system. In contrast, PLDL-treated 8 mm defects reached an average maximum torque of 0.0402 ± 0.019 N-m (Figure 12) and stiffness of 0.0003 ± 0.00019 N-m/deg (Figure 13). Although most PLDL-treated samples did not achieve bony union across the defect, sufficient integration of the scaffold into the defect site had occurred to permit torsional testing of these samples. All failures occurred at the distal scaffold-bone interface, consistent with observation of greater bone formation at the proximal end. Augmentation of the scaffolds with BMP-2 and TGF-β3 yielded a further increase in mechanical properties, however the differences in maximum torque and stiffness were not statistically significant (Figures 12 and 13, Table 1). Although scaffold and growth factor treatment resulted in an improvement in mechanical function over empty defects, maximum torque and stiffness remained approximately an order of magnitude lower than those measured for age-matched intact femurs (0.4932 N-m and 0.0457 N-m/deg, respectively).

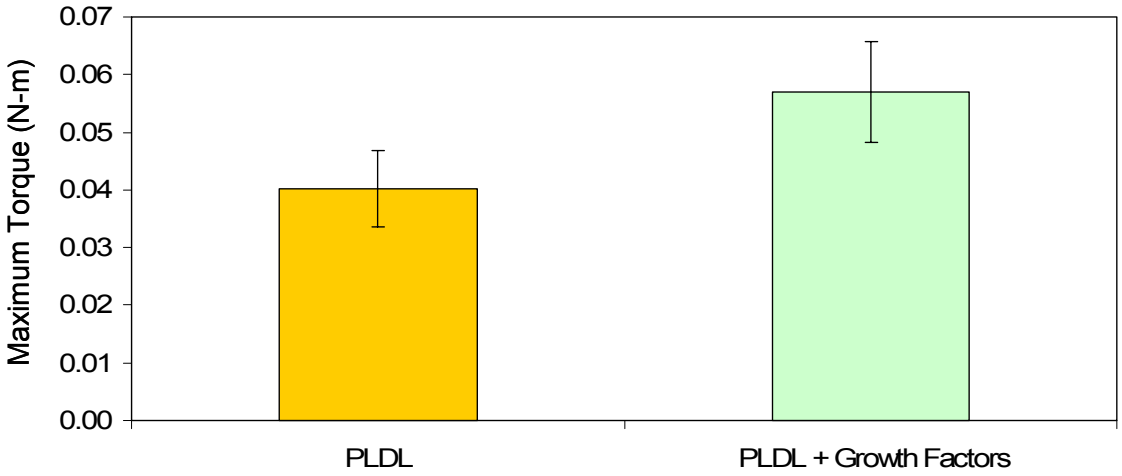

Figure 12: Average maximum torque for PLDL and 200/20 dose BMP-2/TGF-β3 augmented groups at 16 weeks ($5 \leq n \leq 10$). The difference in maximum torque between the treatment groups is not statistically significant.

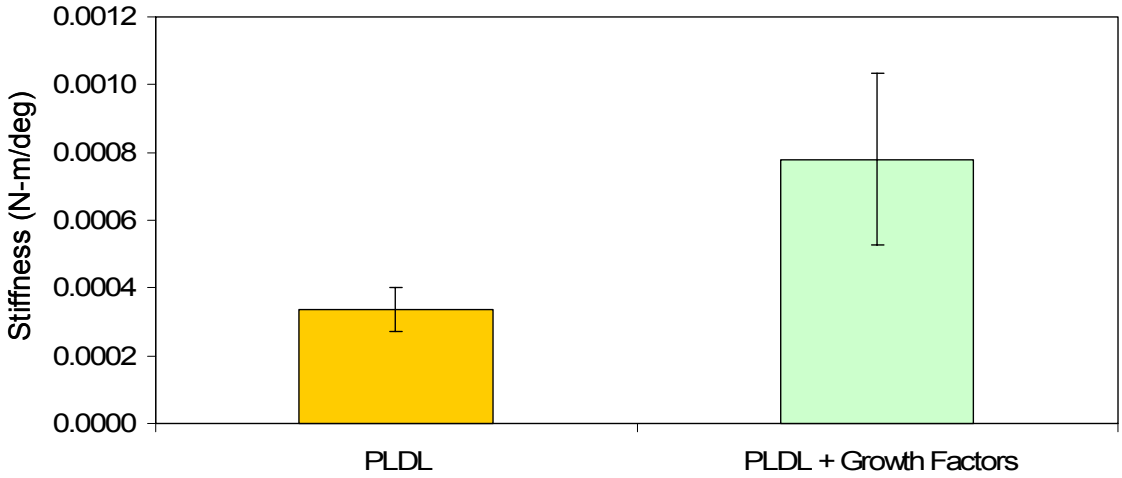

Figure 13: Average stiffness for PLDL and 200/20 dose BMP-2/TGF-β3 augmented groups at 16 weeks ($5 \leq n \leq 10$). The difference in stiffness between the two treatment groups is not statistically significant.

Table 1: Average bone volumes and mechanical properties for samples from the three treatment groups.

Sample	Average Bone Volume Week 4 (mm^3)	Average Bone Volume Week 16 (mm^3)	Average Stiffness (N-mm/deg)	Average Maximum Torque (N-mm)
Empty	1.8538 (n=7)	2.1397 (n=6)	NA	NA
PLDL	5.1639 (n=15)	17.6466 (n=12)	0.3 (n=8)	40.2 (n=8)
PLDL + 200/20 Dose Growth Factors	9.8809 (n=6)	31.6099 (n=6)	0.8 (n=5)	56.9 (n=5)

3.4.5 Histology

Staining of 8 mm defects indicated that, in empty defects, the defect site was filled by loosely organized fibrous tissue with no indication of bony bridge formation (Figure 14). PLDL-treated defects showed invasion of highly cellular tissue into the porosity of the scaffold, with limited mineralized tissue infiltration into the scaffold longitudinal macropores primarily at the proximal end of the defect (Figure 15). Consistent with the healing response to segmental bone grafts, most bone formation occurred around the periphery of the scaffold. Masson's trichrome and von Kossa staining of undecalcified sections confirmed formation of mineralized matrix along the periphery of the implanted scaffold with some bone ingrowth into the macropores, and that the empty defects were filled with fibrous tissue. Residual scaffold material was visible in PLDL-treated defects at 16 weeks post-op. The BMP-2 and TGF-β3 treatment group exhibited results similar to the scaffold only treatment group – mineralized matrix formation along the periphery of the scaffold and to a lesser extent within the porosity of the scaffold (Figure 16). There were no signs of an inflammatory reaction to the scaffold in any of the treatment groups.

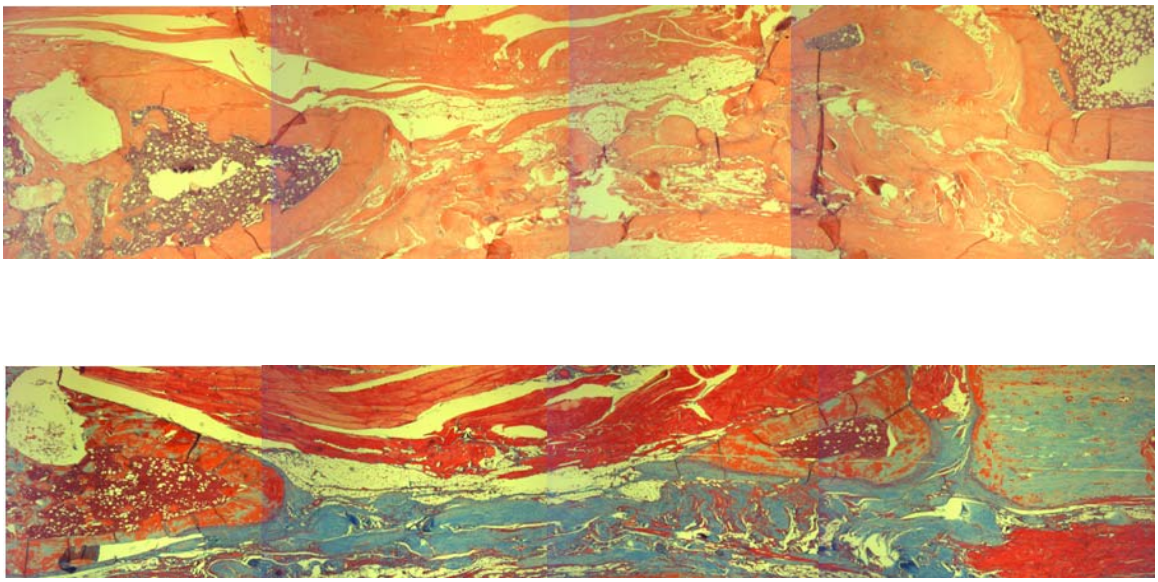

Figure 14: Histological sections taken from an empty defect; top row H&E, lower row Masson's trichrome. In H&E stains, tissue stains varying colors of pink (with mineralized matrix showing as bright pink at either end of the image) and the cell nuclei stain dark purple. In Masson's trichrome, muscle fibers stain red, bone and other collagenous tissues stain blue, and cell nuclei stain dark purple. The remains of the femur at the cutting interface can be seen as the blue squared-off structure at the right end of the image. The muscle can be seen lapsing into the defect area in the upper half of the images.

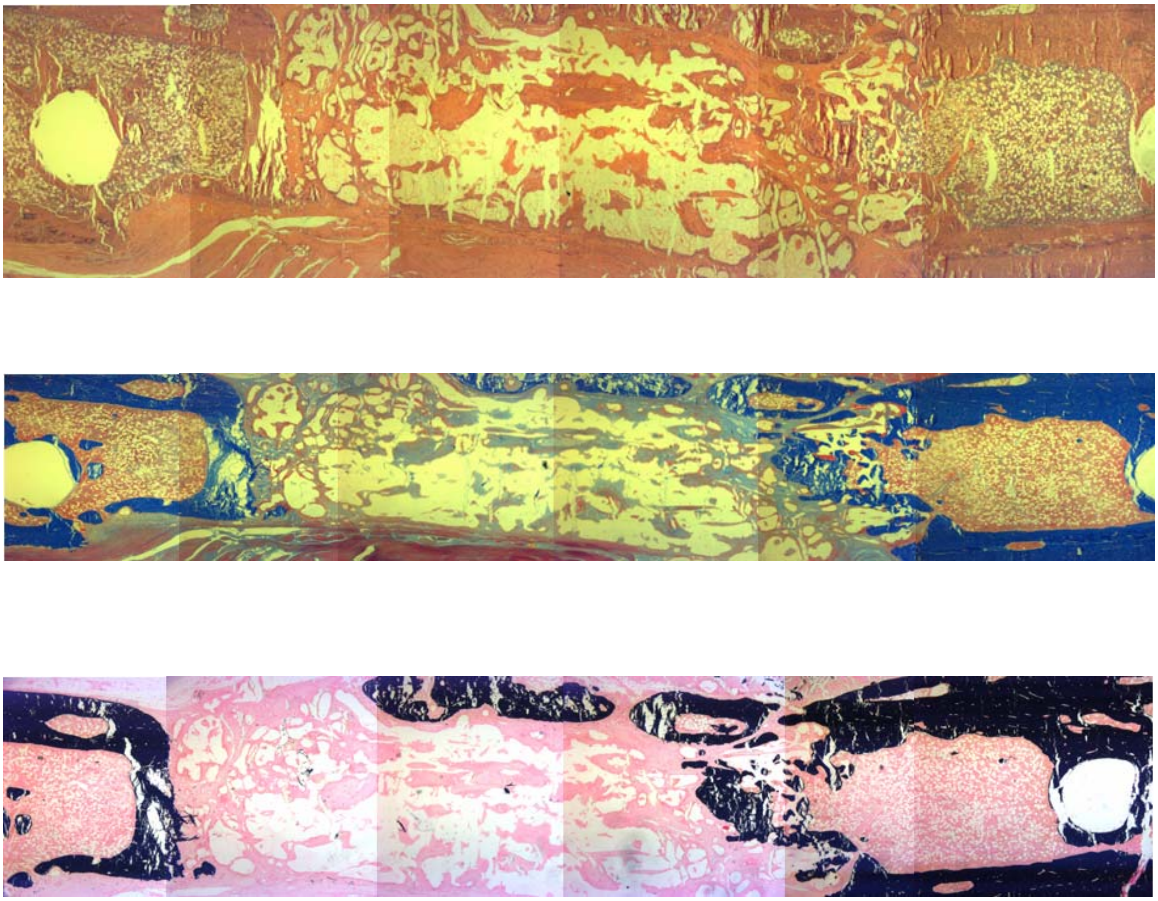

Figure 15: Histological sections taken from scaffold-treated defect; top row H&E, middle row Masson's trichrome, lower row von Kossa. In H&E stains, tissue stains varying colors of pink (with mineralized matrix showing as bright pink at either end of the image) and the cell nuclei stain dark purple. A hole remains where one of the screws for the fixation plate was placed. In Masson's trichrome, muscle fibers stain red, bone and other collagenous tissues stain blue, and cell nuclei stain dark purple. The remains of the femur at the cutting interface can be seen as jagged bright blue structures at the ends of the image. In von Kossa staining, mineral is represented by black areas with a haematoxylin counterstain. The results parallel those of Masson's trichrome.

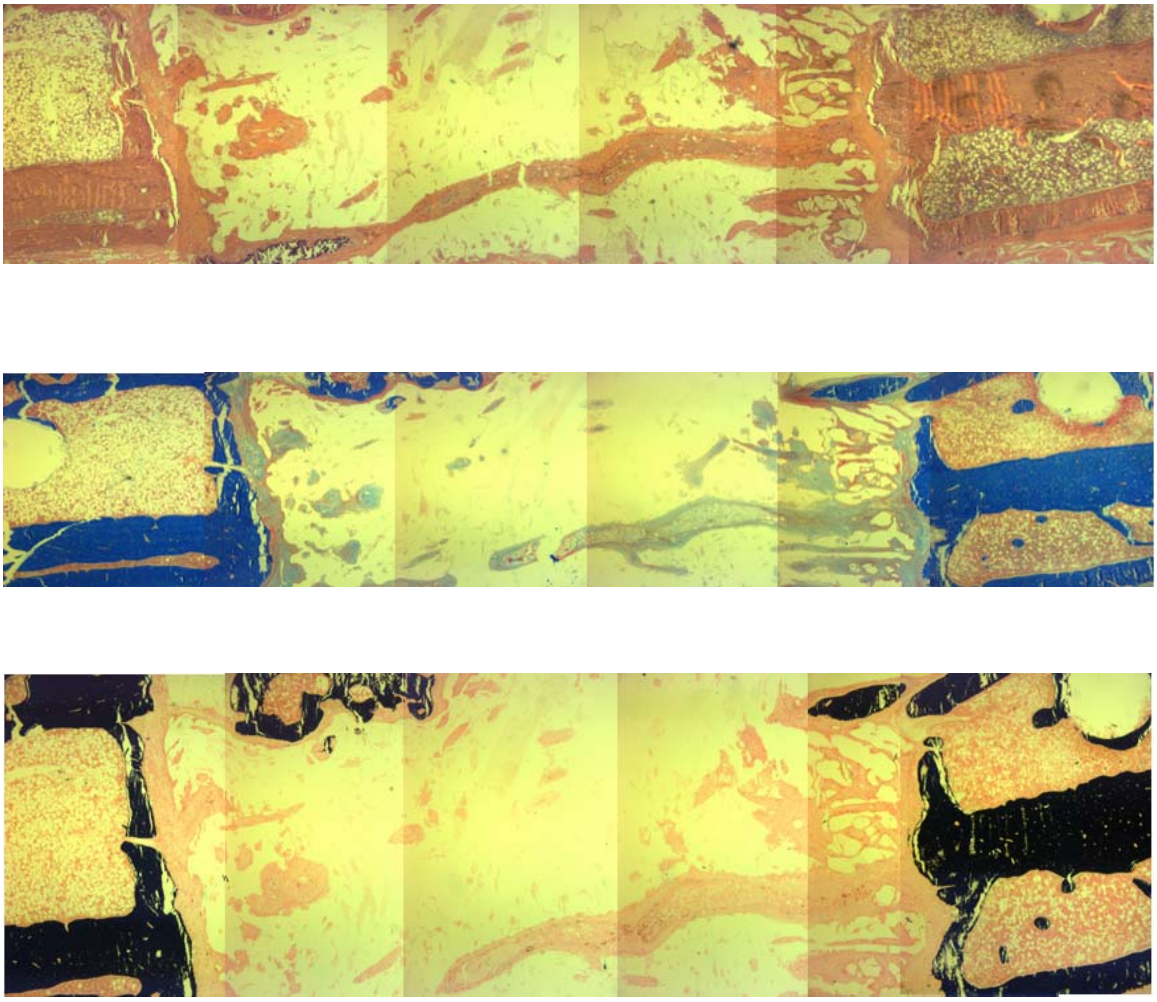

Figure 16: Histological sections taken from a defect augmented with 200 ng BMP-2 and 20 ng TGF-β3; top row H&E, middle row Masson's trichrome, lower row von Kossa. In H&E stains, tissue stains varying colors of pink (with mineralized matrix showing as bright pink at either end of the image) and the cell nuclei stain dark purple. A hole remains where one of the screws for the fixation plate was placed. In Masson's trichrome, muscle fibers stain red, bone and other collagenous tissues stain blue, and cell nuclei stain dark purple. The remains of the femur at the cutting interface can be seen at the ends of the image. Muscle tissue is not seen in this image as the scaffold has excluded it from the defect region. In von Kossa staining, mineral is represented by black areas with a haematoxylin counterstain. The results parallel those of Masson's trichrome.

3.5 Discussion

Long-term success of clinical treatments for repair of large segmental bone defects relies heavily on achieving stable union and subsequent promotion of bone remodeling. Although increasingly used clinically because of its desirable size and structural properties, processed allograft bone provides a suboptimal solution due to the lack of living cells and low porosity, resulting in a high rate of re-fractures within one to two years [ITO 2005]. In these studies, a structural polymer scaffold with oriented porosity designed to facilitate bone ingrowth was evaluated as a bone graft substitute in a critically-sized rat segmental defect model. Micro-CT based methods were established to quantify 3-D mineralized matrix ingrowth into the implanted scaffolds. These quantitative methods in combination with biomechanical evaluation of functional integration provide a robust approach to evaluate and benchmark different approaches to segmental bone repair.

The standard rat segmental defect model, originally used by Nottebaert et al., was modified to achieve highly stable fixation of a reproducible critically-sized 8 mm femoral segmental defects while permitting *in vivo* micro-CT and X-ray imaging [NOTTEBAERT 1989]. The custom modular fixation plates are designed with an offset from the bone to permit tissue infiltration from the entire periphery of the defect. The fixation plates are comprised of three components; two stainless steel anchor plates that affix directly to the bone via miniature screws and one polymer bridging plate that is secured to the stainless steel plates. This modular design provides a radiolucent window that permits *in vivo* micro-CT and X-ray imaging. The unique design also facilitated removal of the polymer bridging plate for torsional testing without causing damage to the

bone or repair tissue, as it was connected only to the anchor plates, which remained intact and fixed to the femur. The fixation plate assembly also serves as a cutting guide that enables the surgeon to create consistent and uniformly sized defects. The large size, stability, and consistency of the 8 mm defect used resulted in a highly consistent model of defect nonunion. The advantages of using a small animal model include the ability to use high-resolution *in vivo* imaging techniques and the potential to house larger sample sizes within the study than are typically used in larger animal models such as canines. Among the disadvantages is the possibility that certain processes, such as revascularization, may be less relevant and difficult to rigorously assess as the net size of the defect is significantly smaller than what can be achieved in larger animal models. In an attempt to compensate for the inherent limitations and scaling problems of a small animal model, the segmental femoral defect has been made as large as possible.

The sequential imaging strategy of multiple *in vivo* micro-CT scans for quantification of bone formation facilitated direct comparisons within the same animal at multiple time points, reducing the number of animals required and variability within treatment groups. Longitudinal scanning was done at 4 and 16 weeks post-op in 8 mm defect samples, permitting direct study of the changes in bone volume within the same sample population. Although longitudinal micro-CT scanning is very useful, repeated X-ray exposure may have an effect on the repair response. However, the size and resolution of the images produced in these studies produced an estimated local dose of 0.17 Gy per scan. This dose is well below the dosages (4 Gy or greater) that have been shown to inhibit cell proliferation and growth factor production by cells *in vitro* [DUDZIAK 2000].

Bone volume within empty defect controls was minimal and did not increase from 4 to 16 weeks, confirming that 8 mm represents a critically-sized defect in the rat. This is consistent with several previous studies that have used segmental bone defects in the rat model ranging from 5 to 8 mm [BRAUN 1992, BRUDER 1998 Clin Orthop, BRUDER 1998 JOR, CHEN 2002, FEIGHAN 1995, HOLLINGER 1990, ISOBE 1999, LIEBERMAN 1999 JBJS, NOTTEBAERT 1989, OAKES 2003, OHURA 1999, STEVENSON 1994, WERNTZ 1996, YASKO 1992]. Typically, 5 mm defects achieve a spontaneous union rate ranging from 10-50%; the 100% rate of non-union in untreated defects here suggests that the 8 mm defect is sufficient in size to achieve a critically-sized model [WERNTZ 1996, NOTTEBAERT 1989]. Bone ingrowth into PLDL scaffolds, with or without growth factors, increased significantly from 4 to 16 weeks. However, micro-CT and mechanical testing data clearly indicated that PLDL scaffold treatment was necessary, but alone was insufficient to consistently bridge the defect region and restore the functional properties of the femur. It is possible that consistent bone union could be achieved in this model by using different scaffold materials or architectures or by waiting longer than 4 months. However, in this study, Faxitron scans qualitatively suggested that although bone density continued to increase between 8 and 16 weeks, the extent of immature ingrowth was largely determined by 8 weeks. All of the defects found to be bridged by mineralized matrix at 16 weeks, for example, had a similar distribution of slightly lower density tissue ingrowth at 8 weeks. These data suggest that the presence of an appropriate scaffold template is necessary but not sufficient to restore long bone function in the 8 mm rat defect model.

These results were consistent with several previous studies that demonstrated the need for biological enhancement of porous scaffolds to repair large segmental bone defects. Bruder et al. implanted hydroxyapatite/tricalcium phosphate (HA/TCP) ceramic cylinders into defects and found healing dominated by fibrous tissue formation and minimal integration at the cut bone-scaffold interfaces. The addition of mesenchymal stem cells to the HA/TCP implants improved the bone repair response [BRUDER 1998 JOR]. Work by Feighan et al. showed that addition of demineralized bone matrix gel to HA/TCP scaffolds resulted in increased bone formation as compared to the delivery of HA/TCP alone, with neither group achieving functional union [FEIGHAN 1995]. Isobe et al. treated segmental defects with PLGA capsules containing PLGA particles with or without BMP-2 within the defect site [ISOBE 1999]. This treatment resulted in osseous union only in the BMP-2 treated groups. Overall, the evidence points to the necessary addition of a biological component to implanted scaffolds in order to promote union of large bone defects [BRUDER 1998 JOR, FEIGHAN 1995, ISOBE 1999, LIEBERMAN 1999 JBJS, LEE 1994, NOTTEBAERT 1989, OAKES 2003, OHURA 1999, STEVENSON 1994, YASKO 1992]. However, the optimal strategy for safe and effective biological enhancement of scaffolds has not yet been determined.

The addition of low dose of co-delivered growth factors (200 ng BMP-2 and 20 ng TGF-β3) to a scaffold induced greater mineralized matrix formation within the defect and a higher rate of bone bridging across the defect than non-treatment. Growth factor augmentation of the scaffold significantly improved bone volume within the core of the scaffold over core bone volumes in the other two treatment groups. Peripheral bone volume was significantly increased between the growth factor group and the empty

group, but not between the scaffold group and the growth factor group. Bone volume within the core 2 mm diameter of the scaffold was significantly enhanced by addition of BMP-2/TGF-β3 over delivery of a scaffold alone. It is possible that the scaffold provides a physical path down which marrow-derived osteoprogenitors can migrate, and that addition of physiologic doses of BMP-2 and TGF-β3 are sufficient to enhance this marrow cavity response. This suggests that even at very low doses, the growth factors are capable of encouraging more evenly-distributed mineralization than is achieved with scaffold delivery alone. Additionally, proximal bone volume was affected by treatment while distal bone volume was not. These data suggest that the periosteal response, which is the likely source for osteoprogenitors contributing to the peripheral bone volume, is stimulated by the presence of the scaffold, but that augmentation with the low dose (200 ng BMP-2 and 20 ng TGF-β3) of growth factor is insufficient to stimulate the pre-osteoblastic cells to regenerate a full mineralized callus around the implant. Anecdotally, it is known that in segmental defect models there tends to be a stronger response to treatment on the proximal end of the defect region. The reason for this is not known, although it has been hypothesized that the distal end may suffer more necrosis than the proximal end due to differences in the vascularity of the tissue. The reason for this phenomenon merits further investigation.

The growth factor augmented constructs, however, failed to consistently produce bone union across the defect and did not significantly improve torsional strength relative to the scaffold only group. Although the low dose of co-delivered growth factors tested has been shown previously to induce osteogenesis in an ectopic model, this study suggests that a higher dose of BMP-2 and TGF-β3, or some other combination of growth

factors, is required to restore function to large orthotopic defects [SIMMONS 2004]. In a challenging environment such as the segmental defect, much higher doses of growth factor have traditionally been used (9-20 μg of growth factor) [YASKO 1992, LIEBERMAN JBJS 1999]. It is possible that requirement for these extremely high doses of growth factor may be decreased through combining growth factors that demonstrate synergistic or additive interactions or by employing sustained release strategies. The need to use high doses of growth factors has been one aspect of traditional investigations that has slowed the translation of growth factor therapy into the clinical setting. If the efficacy of lower doses of growth factor can be demonstrated, it may facilitate the clinical use of growth factor therapies for bone repair.

The slow degradation rate of the PLDL scaffolds used in this study may have also impeded mineralized matrix formation into the defect region. Scaffold modifications to accelerate degradation such as the addition of ceramic particles that increase the surface area available for hydrolysis may therefore improve functional repair of segmental defects. Matching the degradation rate of the scaffold to the rate of mineralized matrix deposition is important in maintaining structural integrity of the defect while still promoting functional osseous union. Scaffold pore geometry may also play an important role. Both histological and micro-CT images showed progressive infiltration of bone into the longitudinal macropores of the scaffold, while radial ingrowth appeared to rely on scaffold degradation from the periphery inward.

Rather than relying on histological methods, quantitative analysis of vascular structures was achieved using a terminal perfusion procedure coupled with decalcification of samples and subsequent *in vitro* micro-CT imaging. The sample size

was insufficient to conduct statistical analysis, as the pilot study was done strictly to demonstrate the feasibility of the technique for use in quantifying vasculature within the implant. Decalcification substantially improved the ability to isolate and analyze 3D vascular ingrowth since segmentation of mineralized bone from perfused vasculature is difficult (in segmenting the bone out of the image, the integrity of the continuous voxels representing the vascular structures is diminished). Good agreement between micro-CT based vessel density calculations and traditional histomorphometric measurements has previously been shown [DUVALL 2004]. Combining this vascular imaging method with *in vivo* micro-CT analysis of bone ingrowth allows evaluation of 3D mineralization and vascularization within the same defects. However, a limitation of the combined *in vivo*/*in vitro* scanning technique is that the decalcification step required for vascular imaging precludes subsequent biomechanical testing.

This study established a challenging rat segmental bone defect model compatible with *in vivo* micro-CT imaging to quantify longitudinal 3-D mineralized matrix ingrowth. Healing of the defect region was improved by implantation of structural polymeric scaffolds infused with growth factors incorporated within RGD-alginate, however, functional integration of the constructs appeared to be limited by continued presence of the slow-degrading scaffolds and perhaps suboptimal dose or delivery of osteoinductive signals. Subsequent chapters will focus on quantifying dose-dependent effects of co-delivered growth factors on the ability of porous polymer scaffolds to restore function to large segmental bone defects.

CHAPTER 4

DOSE-DEPENDENT AND INTERACTION EFFECTS OF DUAL OSTEOGENIC AND CHONDROGENIC GROWTH FACTOR DELIVERY

4.1 Abstract

The delivery of bioactive proteins within porous biomaterial scaffolds represents a potential alternative treatment strategy to bone grafting. Given the complex temporal and spatial expression of multiple growth factors during bone repair, an approach involving sustained co-delivery of proteins may be advantageous. In this study, an oriented polylactide scaffold was used to provide structural support to 8 mm rat segmental bone defects and combined with RGD alginate containing BMP-2 and TGF-β3. These two growth factors have previously been shown to interact synergistically in an ectopic model of osteogenesis. A previously established critically-sized femoral defect model in rats was employed to assess the ability of these growth factor-infused constructs to bridge large bone defects and restore limb functionality. A dose-dependent increase in bone volume and mechanical properties was seen with co-delivery of the growth factors to the defect site (233% increase in bone volume, 160-200% increase in mechanical properties). The higher dose, 2000 ng BMP-2 and 200 ng TGF-β3, was more efficacious than the low dose treatment (200 ng BMP-2 and 20 ng TGF-β3), particularly at increasing bone volume at the early (4 week) time point. These data indicate that by exploiting growth factor interactions, low doses of total growth factor can successfully be used to promote bony union and improve functional integration of a bone graft substitute into a large osseous defect located at a load-bearing site.

4.2 Introduction

Bone loss due to traumatic injury, disease, or fracture complications poses a challenge for orthopaedic treatment. Issues such as open tibial shaft fractures and spinal fusions require frequent surgical intervention. Use of traditional approaches to treating these defects has frequently required secondary revision surgeries to address nonunions or pseudarthrosis at the treatment site. Delayed union and nonunion are common results of traumatic bone damage in which a significant defect is created [BORRELLI 2003, WERNTZ 1996, SWIONTKOWSKI 2006]. Although autografting is the gold standard treatment, this procedure is constrained by the lack of available donor material, an inability to obtain a structural graft, and considerable donor site morbidity. Thus, the allograft is the popular and facile solution to the problem of significant bone loss, although subject to a high rate of re-fracture and gross failure within a relatively short time period (2 years) post-engraftment [LUCARELLI 2005, WHEELER 2005, ITO 2005]. This re-fracture incidence is due in large part to a lack of graft integration into the remaining host bone [ENNEKING 2001, ITO 2005, WHEELER 2005]. Lack of porosity within the allograft inhibits revascularization and revitalization of the allograft tissue, resulting in a propensity to accumulate microdamage that may ultimately lead to catastrophic graft failure (25% clinical failure rate) or contribute to the 30-60% complication rate associated with allografts [LUCARELLI 2005, WHEELER 2005]. Complications frequently result in treatment of defect nonunions or delayed unions, often necessitating revision surgery and significantly impacting patient quality of life.

Increasingly, surgeons are turning to non-host biologics to address the limitations of allografts and the pain concomitant with use of autografts. BMP-2 – the classic

osteoinductive growth factor – has been used with general success in clinical trials to augment mechanical fixation of open tibial fractures and as a replacement for autograft tissue in spinal fusions.

The strategy of combining synthetic and biological factors to create a porous, cell-friendly microenvironment that will enhance cellular invasion, implant vitalization, and bone formation in the defect site holds promise, as evidenced by the general success of the BMP-2/absorbable collagen sponge trials [SWIONTKOWSKI 2006, BURKUS 2002]. To this end, we have developed a porous polymer scaffold with mechanical integrity that can be co-delivered with biological agents to promote osseointegration of the scaffold into a bony defect site and enhance functional repair of the osseous defect.

The 8 mm critically-sized segmental femoral rat defect model used in these studies provides a robust model of non-union in the absence of treatment. This defect model has been modified by our research group to provide several advantages over traditional fixation methods and simple radiological assessment of healing [OEST 2007]. The fixation plates in our model have been custom designed to obtain highly stable fixation of the defect and permit creation of uniform defects centrally located along the diaphysis of the femur. The plates are modular; a polymer bridging component permits *in vivo* micro-computed tomography (micro-CT) and X-ray imaging of the defect site while still allowing the researcher to remove the bridging plate without damaging the remaining bone or repair tissue for mechanical testing of samples *post-mortem*. The large size of the defect permits stringent comparison of various treatments while maintaining consistent non-union results in untreated (empty) defects. Smaller, more commonly used defects, (5 mm in length) have a spontaneous union rate of 10-50% [WERNTZ 1996,

NOTTEBAERT 1989]. Additionally, a new strategy for quantitative evaluation of the healing response has been generated for the segmental defect model [OEST 2007]. This evaluation regime consists of quantitative micro-CT determination of bone volume within the defect at two time points *in vivo*, quantitative determination of limb functionality using biomechanical testing, and the traditional and qualitative measures of radiographic assessment of union rates and histological analysis.

Growth factor treatment of large osseous defects has traditionally relied on a large dose of a single osteoinductive growth factor – typically BMP-2 [LEE 1994, YASKO 1992, LIEBERMAN 1999]. Experimental doses in murine models may be as high as 11-20 μg per defect [YASKO 1992, LIEBERMAN 1999]. Although this results in reproducible bony union of the defect as assessed by radiography, typically in 5 mm defects, the equivalent amount of protein required to treat a critical human defect is substantial. One way to reduce the quantity of protein required is to exploit interactions between growth factors. Previously, BMP-2 and TGF-β3 have been shown to interact synergistically in the presence of bone marrow stromal cells to promote mineralized matrix formation in an ectopic mouse model of osteogenesis at very low (physiologic) doses [SIMMONS 2004].

The goals of this study were to assess the interaction between BMP-2 and TGF-β3 and dose-dependent effects of the co-delivery of these growth factors in a critically-sized femoral defect model. The outcome measures were: radiographic assessment of rate of union, micro-CT measurements of bone volume within the defect, torsional testing to determine mechanical properties of the repair tissue, and histological comparison.

4.3 Methods

4.3.1 Scaffold Production

Poly-(L-co-D,L-lactide 70:30) (PLDL) cylindrical scaffolds measuring 8 mm in length and 4 mm in diameter were produced using a fiber coating and porogen decomposition technique described previously [LIN 2003]. Briefly, 100 micron fibers were coated with a mixture of PLDL and azodicarbonamide solvated in acetone. Fibers were bundled, fused together, and heat treated. During heat treatment, the azodicarbonamide decomposes from a solid to a gaseous phase, producing random interconnected micropores in the scaffold. The removal of the wires revealed oriented longitudinal macropores with approximately 77% porosity. Scaffolds were sterilized by gamma irradiation (2.5 Mrad), and coated with rat plasma fibronectin (25 μg/ml, F0635; Sigma-Aldrich) prior to seeding with growth factor.

4.3.2 Addition of Growth Factor to Scaffolds

Sterile recombinant human BMP-2 and/or TGF-β3 (355-BM/CF and 243-B3/CF, R&D Systems, Minneapolis MN) were reconstituted with sterile 0.1% rat serum albumen in 4 mM HCl immediately prior to use. Short chain length MVG sodium alginate (Pronova Biopolymers, Norway) was produced by exposing the stock alginate to a 5 Mrad dose of gamma irradiation. The short chain alginate was then functionalized with a G_4RGDSP peptide sequence at a density of 2 RGD sequences per chain via carbodiimide chemistry [SIMMONS 2004]. The RGD-functionalized alginate was sterile filtered and lyophilized for storage at -20°C. For use in the PLDL scaffolds, the alginate was

reconstituted with α-MEM to a concentration of 2%, including one of the following growth factor doses: 200 ng BMP-2 and 20 ng TGF-β3 (200/20 dose), 2000 ng BMP-2 and 200 ng TGF-β3 (2000/200 dose), 2000 ng BMP-2, 200 ng TGF-β3, or no growth factor. Scaffold only treatment groups included a scaffold that was infiltrated with RGD-alginate without growth factors. The 200/20 dose and 2000/200 dose groups were compared in one study, while the delivery of individual growth factors and dual growth factor delivery were compared in a second study at the 2000/200 dose. Fibronectin-coated PLDL scaffolds were placed into molds that served to contain the alginate solution as it infiltrated the porosity of the scaffold. Membranes wetted with $CaCl_2$ bounded the scaffold at either end, initiating crosslinking of the alginate *in situ*. After 20 minutes in the molds, the scaffolds were transferred from to a bath of $CaCl_2$ where the crosslinking process was completed. As a final step, the scaffolds were rinsed and stored in α-MEM until implantation.

4.3.3 Surgical Procedure

All surgical techniques were reviewed and approved by the Institutional Animal Care and Use Committee at Georgia Institute of Technology (Protocols A03017 and A05041). Female Sasco Sprague-Dawley rats aged 13 weeks were anesthetized using isoflurane. Bilateral anterior incisions were made over the femurs. The femurs were exposed using blunt dissection through the muscle. Custom modular fixation plates were secured directly to the bone using four miniature screws (J.I. Morris Co, Southbridge MA). Bilateral full-thickness 8 mm long diaphyseal defects were created using a miniature oscillating saw under irrigation. After flushing the defect site with sterile

saline, scaffolds with or without BMP-2 and/or TGF-β3 were press-fit securely into the defects. Incisions were closed according to anatomic layers using absorbable suture and wound clips. Animals were given 0.05 mg/kg buprenorphine every 8 hours postoperatively for the first 48 hours and 0.025 mg/kg buprenorphine every 8 hours for the following 24 hours. Within 2-3 days post-op, animals had resumed normal ambulation and did not show signs of distress or pain.

4.3.4 X-ray and Micro-CT

Digital 2-D X-rays were taken every four weeks postoperatively until the termination of the studies. Rates of union were assessed by two blinded observers, with union qualified as formation of a continuous bony bridge across any region of the defect. *In vivo* 3-D micro-CT imaging was done at 4 and 12 weeks post-op using a 38.5 μm voxel resolution (Viva-CT 40; Scanco Medical, Bassersdorf, Switzerland). A consistent central diaphyseal volume of interest (VOI) was selected for all analyses. This VOI was approximately 4.6 mm thick. A Gaussian filter (sigma = 1.2, support = 1) was used to partially suppress noise in the VOI prior to application of a global threshold. The global thresholds corresponded to densities of 206.7 and 270.3 mg hydroxyapatite/cm^3, and excluded all non-mineralized tissues and residual scaffold material, as verified by visual examination of individual 2-D slices. The lower threshold was used to assess total bone volume (mature + immature), while the upper threshold was used to quantify mature bone volume. Immature bone volume was calculated as the difference between total bone volume and mature bone volume. The upper threshold (mature bone) was determined by two methods; a histogram of the number of voxels attenuating vs the threshold was

plotted and used to select an approximate threshold value. This threshold value was then validated using visual inspection of 2-D slices. The threshold of 272 mg HA/cm^3 corresponds to the attenuation of mature cortical bone in a rat. The immature bone threshold was selected as the lowest value that could be analyzed without picking up image artifacts or distorting the bone structure.

4.3.5 Mechanical Testing

Samples were harvested at 12 weeks post-op and wrapped in saline-soaked gauze prior to storage at -20°C. For mechanical testing, samples were thawed in a bath of room-temperature saline, unwrapped, and imaged using *in vitro* micro-CT immediately prior to potting in end blocks using Wood's metal. After potting and placement of a transverse stabilizing pin through the end blocks and proximal and distal ends of the femur, the bridging component of the stabilization plate was removed. To preserve tissue hydration, samples were wrapped with saline soaked gauze during handling and placement into the testing system. Samples were then tested to failure in torsion at a rate of 3°/second using a Bose ElectroForce (ELF) system (ElectroForce 3200, Bose Corporation, Eden Prairie, MN).

4.3.6 Histology

One sample from each treatment group was selected for histological evaluation. Stains used in this evaluation included haematoxylin and eosin, Masson's trichrome, von Kossa, and safranin-O.

4.3.7 Statistics

Analysis of variance was conducted using a general linear model and Tukey pairwise post-hoc comparisons (Minitab). Differences were considered statistically significant at $p \leq 0.05$.

4.4 Results

4.4.1 X-ray Imaging

Faxitron 2-D X-ray images were taken every 4 weeks post-op to monitor defect stability and bony ingrowth. In the 200/20 dose treatment group, there was some bony fill within the defect site, extending from the cut ends of the femur. The rate of bony union for this treatment group was 29% (2/7). In the 2000/200 dose treatment group there was a 63% (10/16) incidence of bony union; no samples from the scaffold only treatment group achieved osseous union (0/9) (Figure 17).

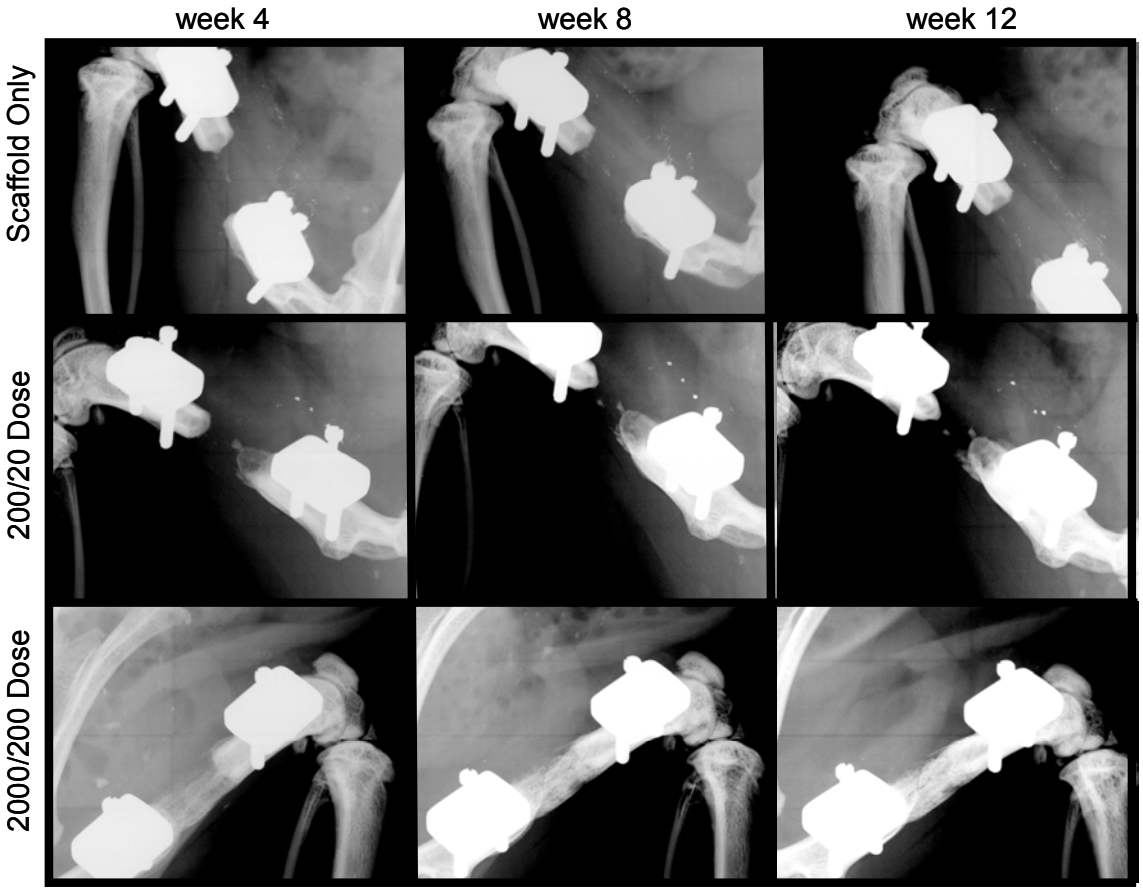

Figure 17: Digital X-rays taken of the three treatment groups at 4, 8 and 12 weeks post-op. Rates of bony union were as follows: scaffold only – 0/9; 200/20 ng dose of BMP-2/TGF-β3 – 2/7, 2000/200 ng dose of BMP-2/TGF-β3 – 10/16.

In the scaffold only and TGF-β3 only treatment groups, there was a minimal amount of bony ingrowth, with a small amount of appositional bone formation dominating the healing process. None of the samples in either of these treatment groups achieved bony union. In the BMP-2 only treatment group there was an increase in the amount of bone formation within the defects, with some samples achieving bony union (38% or 3/8). Addition of TGF-β3 to the BMP-2 further increased the rate of union (55% or 5/9) as well as increasing the amount of bony fill within the defect site (Figure 18).

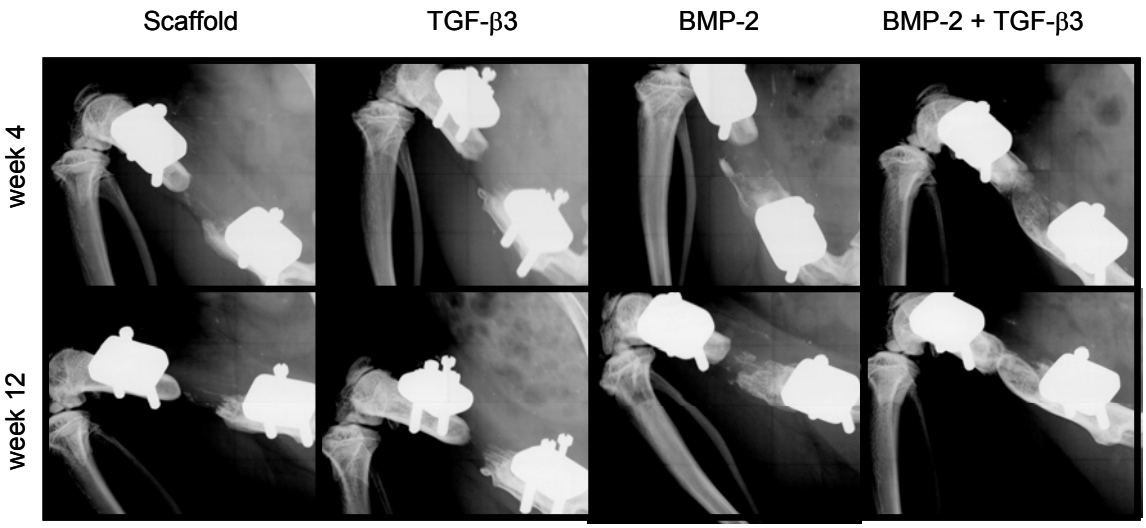

Figure 18: Digital X-rays taken of the three treatment groups at 4, 8 and 12 weeks post-op. Rates of bony union were as follows: scaffold only – 0/; 200 ng TGF-β3 only – 0/7, 2000 ng BMP-2 only – 3/8; 2000/200 co-delivery dose – 5/9.

4.4.2 Micro-CT Analysis

In vivo micro-CT analysis was conducted at 4 and 12 weeks post-op for both studies. In the dose response study, micro-CT analysis revealed a significant elevation in bone volume in the 2000/200 dose group as compared to delivery of a scaffold alone at both time points ($p < 0.001$ at week 4, $p = 0.004$ at week 12) (Figure 19). Additionally, at 4 weeks post-op the 2000/200 dose group had a significantly higher bone volume than the 200/20 dose group ($p = 0.020$). Overall, treatment and time were both significant factors ($p < 0.001$, $p < 0.001$). Bone volume did not increase significantly between 4 and 12 weeks in the scaffold only treatment group ($p = 0.053$). There was a significant increase in bone volume for the 2000/200 dose treatment group between 4 and 12 weeks ($p = 0.001$), as well as for the 200/20 dose treatment group ($p = 0.010$).

In vitro micro-CT imaging was done on samples immediately prior to mechanical testing. It should be noted that *in vitro* micro-CT analysis is a less sensitive measure of defect healing, as the bone volumes are somewhat normalized by the presence of intact host bone at the proximal and distal edges of the defect. There was a significant increase in the quantity of mature bone in the 2000/200 dose group as compared to the scaffold only group. Similarly, there was a statistically significant increase in both total bone volume and immature bone volume with the addition of the 2000/200 dose of BMP-2/TGF-β3 to the scaffold alone (Figure 20). For this group, spatial analysis of the post-mortem samples indicated a significant increase in the quantity of bone surrounding the periphery of the scaffold, but not within the core of the scaffold (Figure 21). Similarly, the bone volume fraction in the periphery was significantly increased in the 2000/200 dose group over the scaffold alone group. There was no significant difference between

the 200/20 dose and the scaffold or the 2000/200 dose and the 200/20 dose (Figure 22). Delivery of the 2000/200 BMP-2/TGF-β3 growth factor dose significantly improved the quantity of bone within the proximal half of the defect as compared to implantation of a scaffold alone, but did not impact the formation of bone on the distal aspect of the defect (Figure 23). Representative images from the *in vitro* micro-CT visually demonstrate the trends quantified using 3-D tomographic analysis (Figure 24).

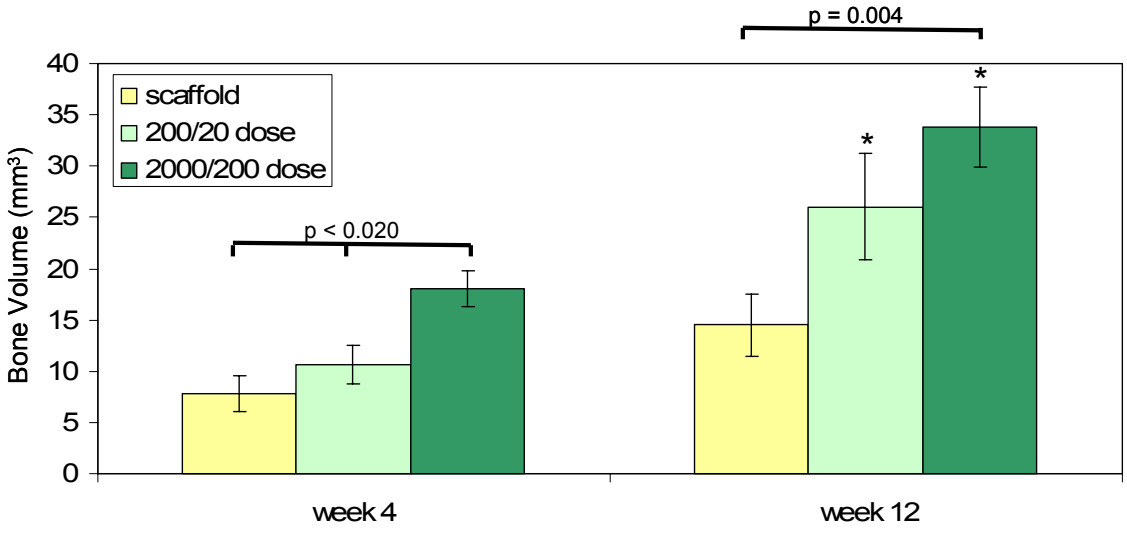

Figure 19: *In vivo* bone volume measurements taken at 4 and 12 weeks post-op ($13 \leq n \leq 17$). * denotes a significant increase in bone volume within the treatment group from 4 to 12 weeks post-op. The 2000/200 ng BMP-2/TGF-β3 treatment group had significantly improved bone volume over both the scaffold only and 200/20 ng co-delivery treatment group at 4 weeks post-op. At 12 weeks post-op, the 2000/200 dose treatment group still had significantly improved bone volume over the scaffold only treatment group.

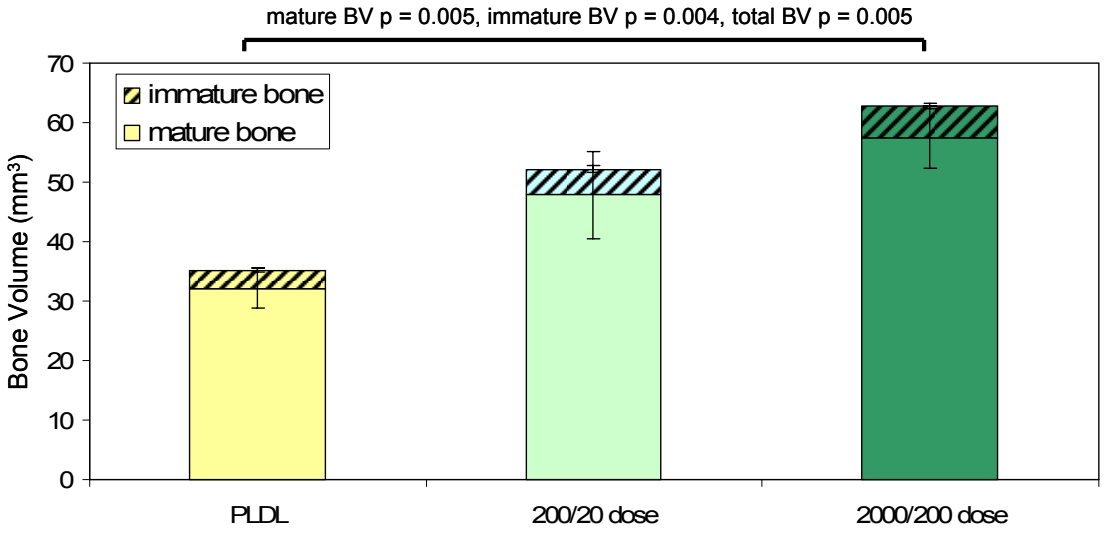

Figure 20: *In vitro* bone volume measurements taken at 12 weeks post-op ($11 \leq n \leq 14$). All three measurements – total bone volume (mature + immature), immature bone volume, and mature bone volume – were significantly greater in the 2000/200 ng co-delivery treatment group than in the scaffold only treatment group.

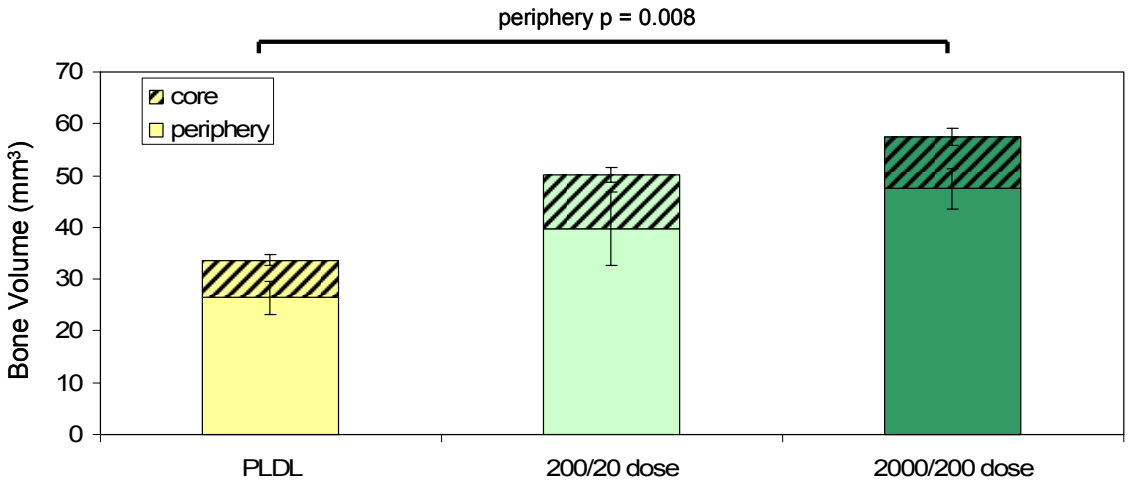

Figure 21: *In vitro* bone volume spatial distribution measurements segmented by core (central 2 mm diameter) vs. periphery (outer portion of scaffold and area around the scaffold) of the implant taken at 12 weeks post-op ($11 \leq n \leq 14$). The bone volume in the core of the scaffold was not impacted by growth factor augmentation, but the peripheral bone volume was significantly increased in the 2000/200 ng dose treatment group over delivery of a scaffold alone.

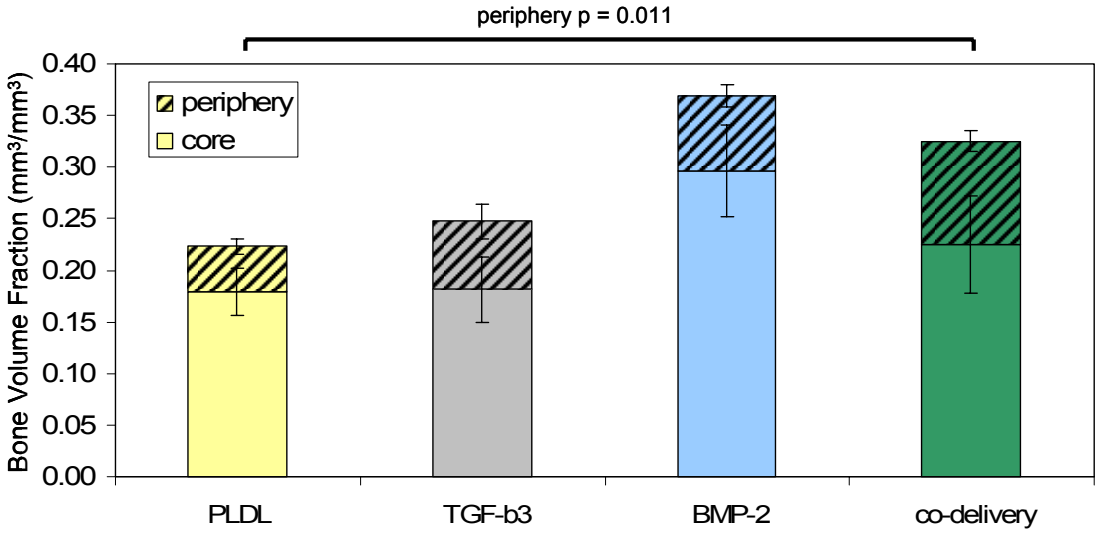

Figure 22: *In vitro* bone volume fraction spatial distribution measurements segmented by core (central 2 mm diameter) vs. periphery (outer portion of scaffold and area around the scaffold) of the implant taken at 12 weeks post-op ($11 \leq n \leq 14$). The bone volume fraction in the core of the scaffold was not impacted by growth factor augmentation, but the peripheral bone volume was significantly increased in the 2000/200 ng dose treatment group over delivery of a scaffold alone.

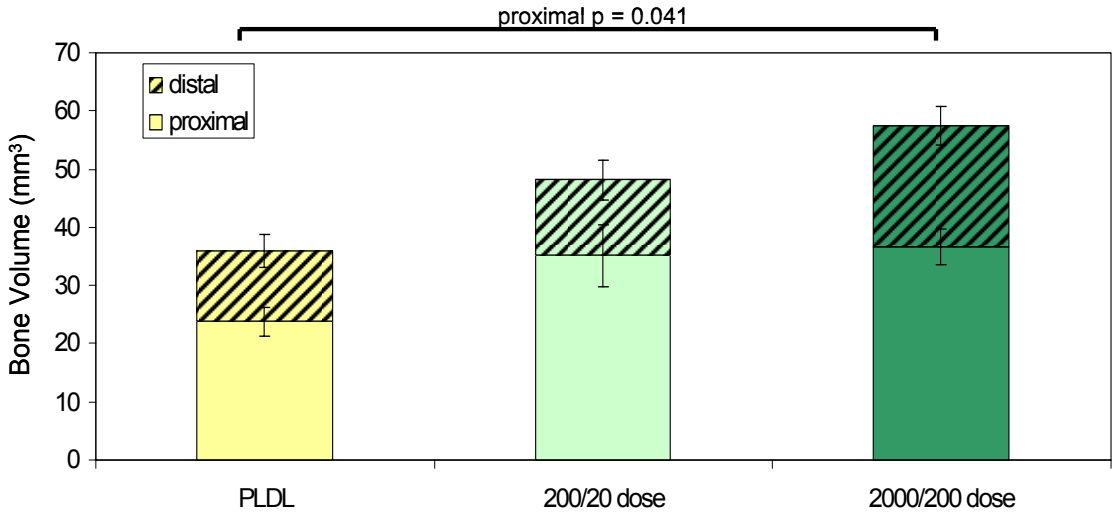

Figure 23: *In vitro* bone volume spatial distribution measurements segmented by proximal vs. distal regions of the defect taken at 12 weeks post-op. The bone volume in the proximal 4 mm of the defect was significantly increased in the group augmented with 2000 ng BMP-2 and 200 ng TGF-β3 (2000/200 dose) as compared to the PLDL (scaffold only) treatment group.

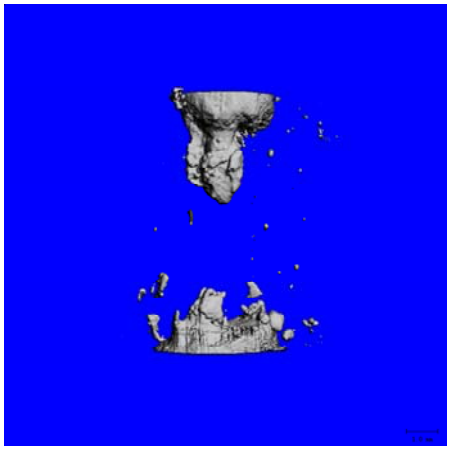

scaffold

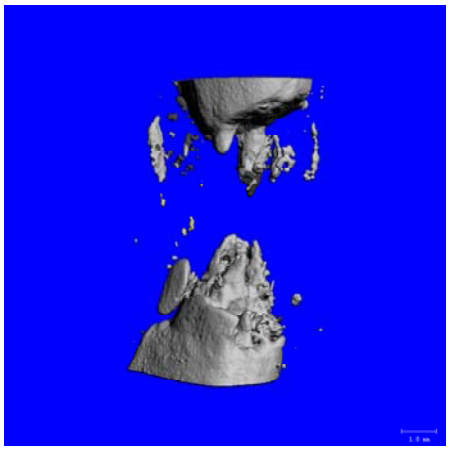

200/20 dose

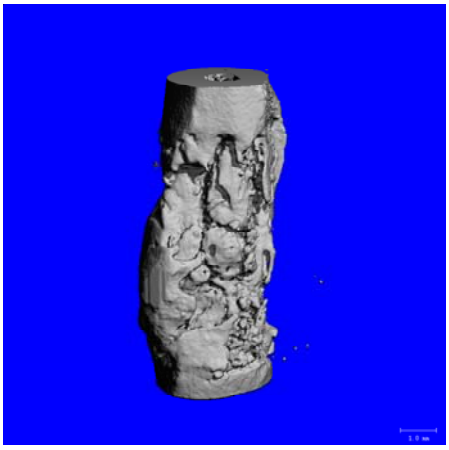

2000/200 dose

Figure 24: *In vitro* micro-CT images of the 8 mm long defect regions for three treatment groups taken post mortem at 12 weeks. The dose-dependent increase noted in quantitative micro-CT measurements is also visually discernable in the images.

In the study comparing bone volumes for dual vs. single growth factor delivery, treatment was a significant factor for both mature and immature bone volumes at 4 and 12 weeks post-op (Figures 25 and 26) . The co-delivery treatment group was the only group that experienced a significant increase in mature bone volume with time ($p < 0.050$). At week 4, there was a significant increase in immature bone volume in the co-delivery group as compared to the scaffold only group ($p = 0.034$). There were no other significant differences at week 4 in terms of mature bone volume or total bone volume. At week 12, a significant increase in both immature and mature bone volumes was quantified in the co-delivery treatment group as compared to delivery of a scaffold alone. There was a significant increase in mature bone volume and immature bone volume in the 2000/200 co-delivery group over delivery of TGF-β3 alone. Immature bone volume was significantly elevated in the BMP-2 only group as compared to the scaffold treatment group as well. Overall, treatment was a significant factor for both mature and immature bone volumes at 12 weeks post-op.

In vitro micro-CT indicated a statistically significant increase in immature, mature, and total bone volumes for the 2000/200 dose co-delivery treatment group over delivery of a scaffold alone ($p < 0.022$) (Figure 27). The proximal and peripheral bone volumes were also elevated in the co-delivery group as compared to the scaffold treatment group ($p < 0.020$) (Figures 28 and 29). Peripheral bone volume fraction was likewise significantly higher in the co-delivery treatment group than in the scaffold treatment group (Figure 30).

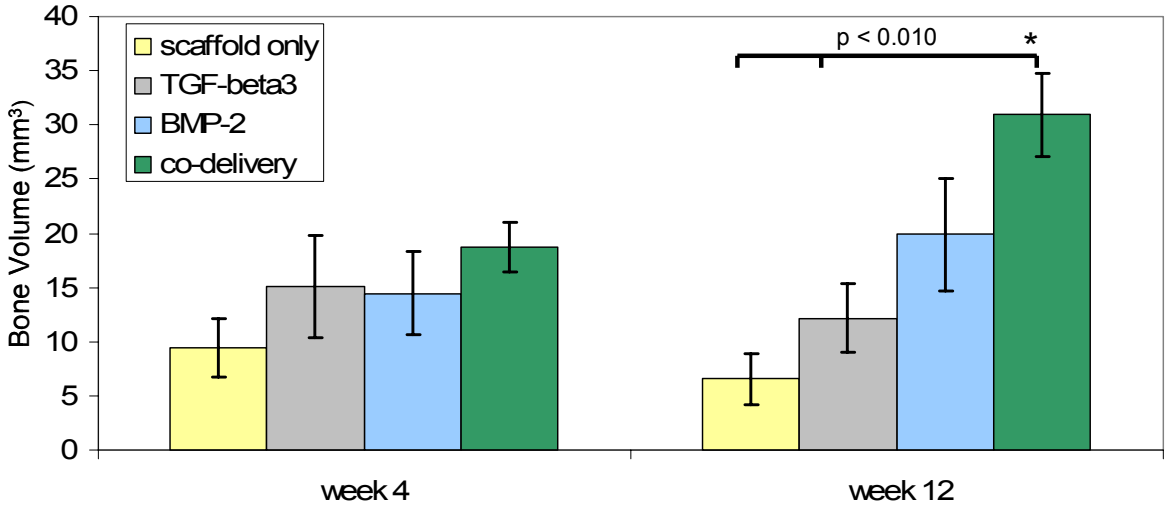

Figure 25: Mature bone volume measurements taken at 4 and 12 weeks post-op using *in vivo* micro-CT ($8 \leq n \leq 10$). The co-delivery group (2000 ng BMP-2/200 ng TGF-β3) experienced had a significantly higher bone volume at 12 weeks post-op than either the scaffold only (PLDL) or TGF-β3 only treatment groups. * denotes a significant increase in bone volume within the co-delivery treatment group with time.

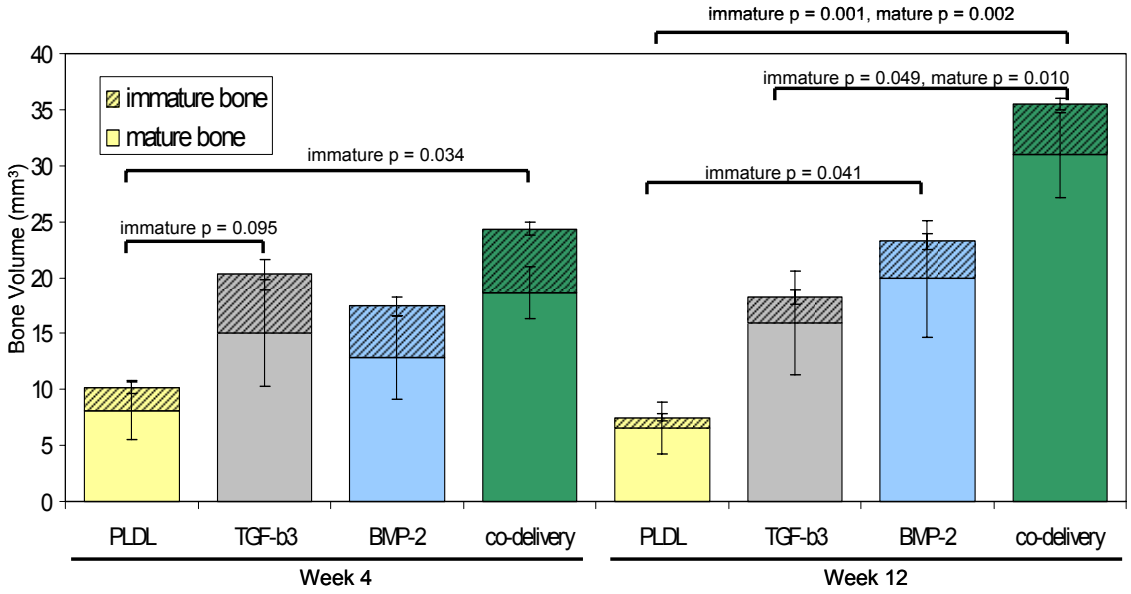

Figure 26: Mature and immature bone volume measurements taken at 4 and 12 weeks post-op using *in vivo* micro-CT ($8 \leq n \leq 10$). At 4 weeks post-op, there was a significantly greater quantity of immature bone in the co-delivery group as compared to the scaffold alone group, and a strong trend towards an increase in immature bone in the TGF-β3 treatment group over the PLDL group. At 12 weeks post-op the quantity of immature and mature bone was greater in the co-delivery group than in the scaffold or TGF-β3 alone groups. The BMP-2 only group had significantly more immature bone at 12 weeks post-op than the scaffold only group.

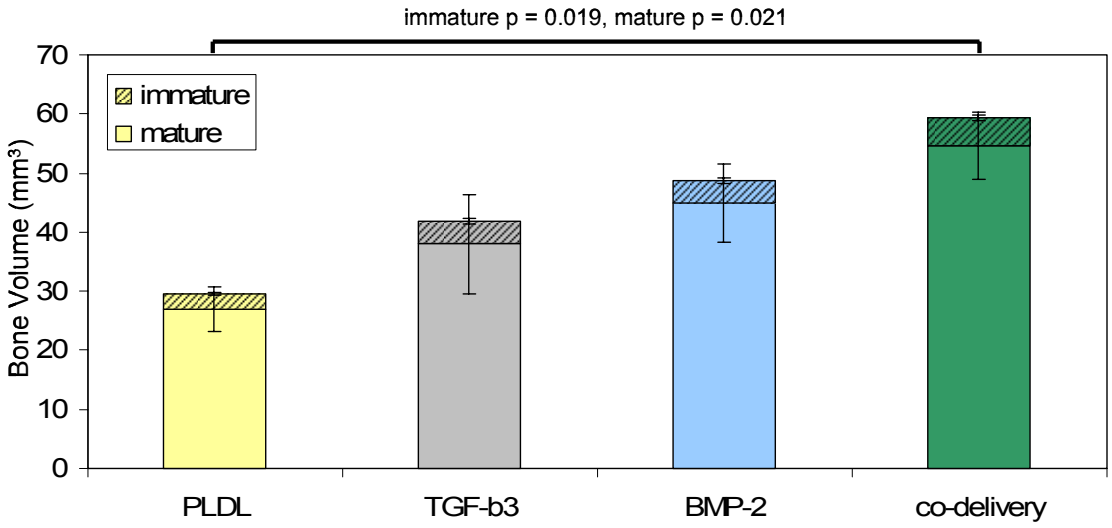

Figure 27: Mature and immature bone volume measurements taken at 12 weeks post-op using *in vitro* micro-CT ($7 \leq n \leq 8$). There is a significant increase in both immature and mature bone volumes for the co-delivery group over delivery of a scaffold alone.

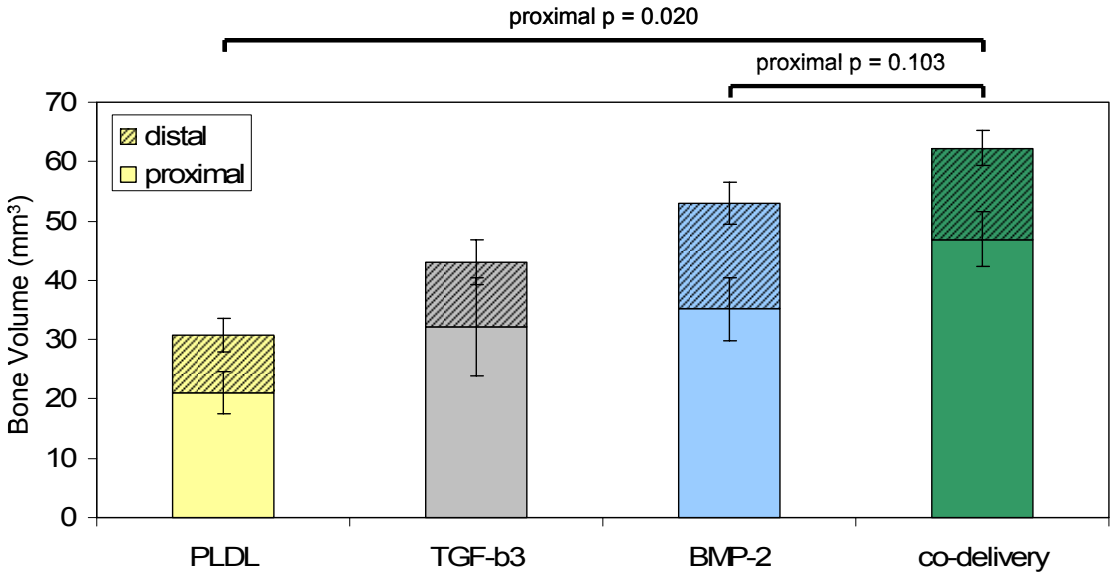

Figure 28: Proximal and distal bone volume measurements taken at 12 weeks post-op using *in vitro* micro-CT ($7 \leq n \leq 8$). The proximal bone volume in the co-delivery treatment group is significantly greater than the proximal bone volume in the PLDL (scaffold only) treatment group. There was a trend towards an increase in proximal bone volume in the co-delivery treatment group over the BMP-2 monotherapy group.

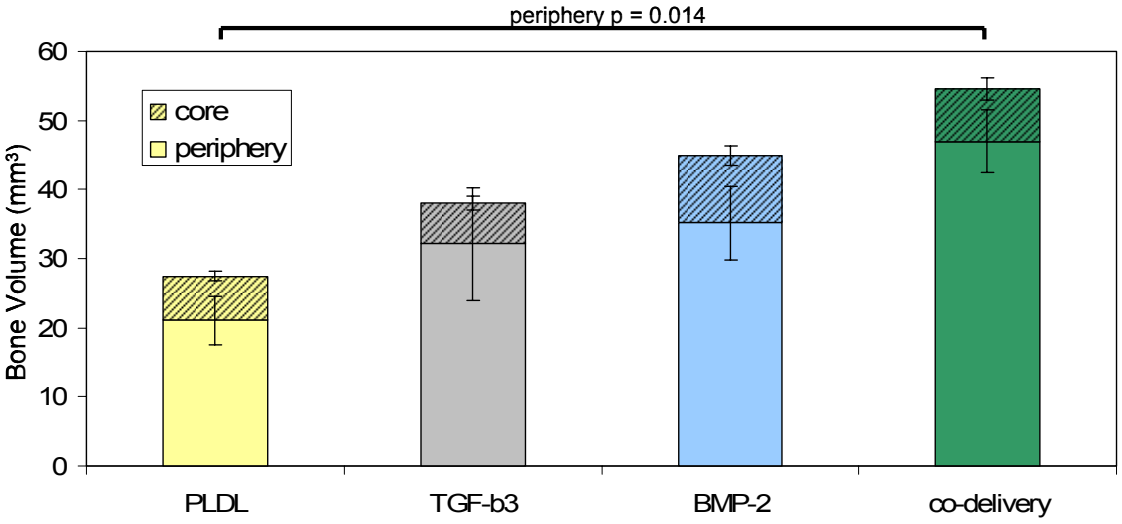

Figure 29: Core and peripheral bone volume measurements taken at 12 weeks post-op using *in vitro* micro-CT ($7 \leq n \leq 8$). Peripheral bone volume was elevated in the 2000/200 ng BMP-2/TGF-β3 co-delivery treatment group as compared to delivery of a PLDL scaffold alone.

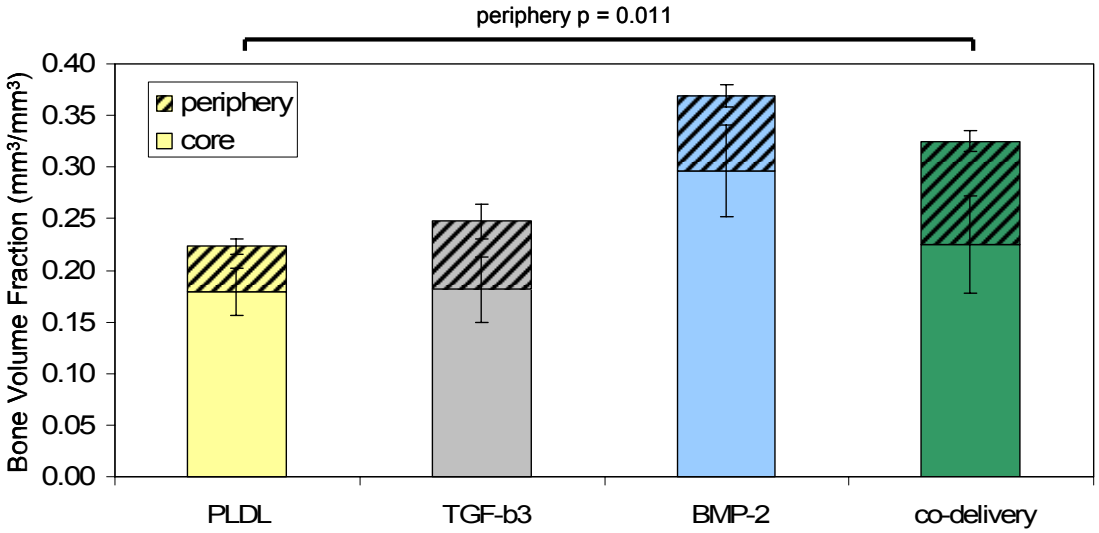

Figure 30: Core and peripheral bone volume fraction measurements taken at 12 weeks post-op using *in vitro* micro-CT ($7 \leq n \leq 8$). The peripheral bone volume fraction was increased in the co-delivery treatment group as compared to the scaffold only treatment group (PLDL). Core bone volume fraction was not impacted by treatment.

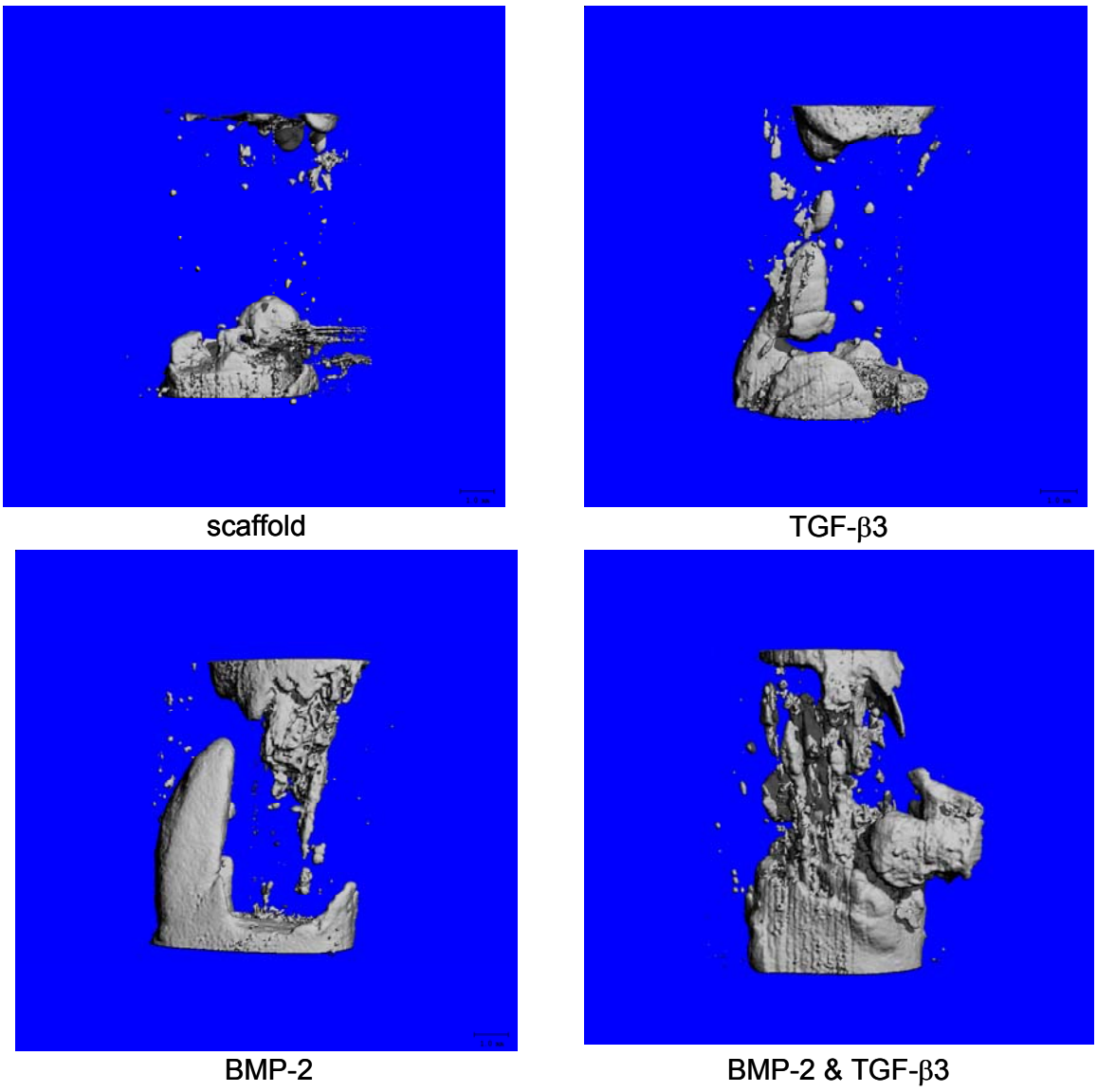

Figure 31: Post mortem micro-CT images of the full defect site average responders for four treatment groups taken from *in vitro* micro-CT. The images visually confirm the differences in treatment determined quantitatively by micro-CT.

4.4.3 Mechanical Testing

Torsional mechanical testing was done on samples harvested at 12 weeks post-op. In the dose dependence study, delivery of the 2000/200 dose of BMP-2 and TGF-β3 significantly increased stiffness over delivery of a scaffold alone ($p = 0.003$) and resulted in a nearly significant increase in the 2000/200 group over the 200/20 group ($p = 0.054$) (Figure 32). The maximum torque achieved by the 2000/200 dose treatment group was significantly greater than the maximum torque reached by the 200/20 dose group or the scaffold alone group ($p = 0.031$, $p = 0.002$ respectively) (Figure 33). Work to maximum torque was not significantly impacted by treatment ($p = 0.116$) (Figure 34).

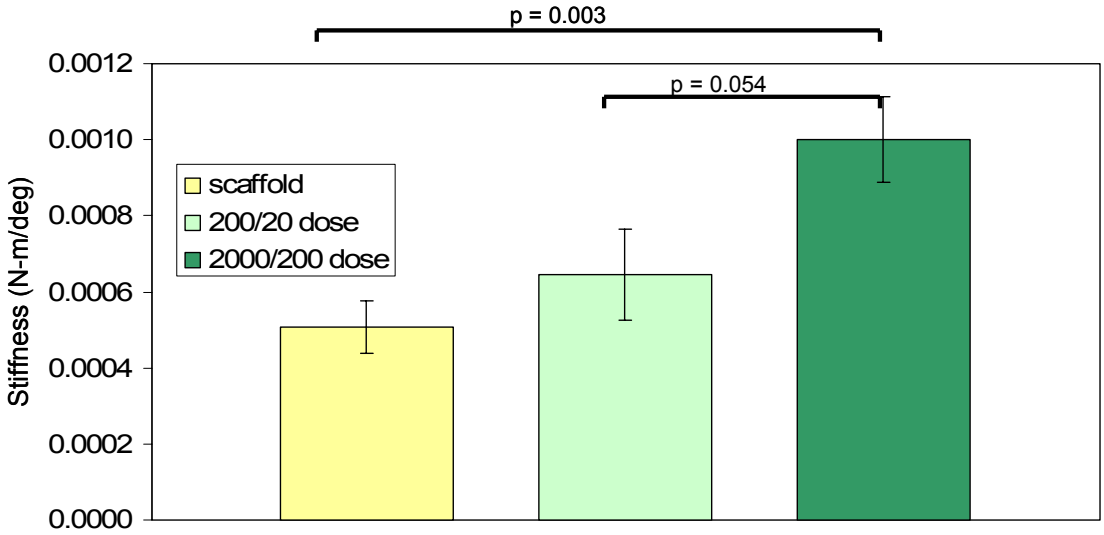

Figure 32: Average stiffness values for three treatment groups ($11 \leq n \leq 14$). Stiffness was significantly increased by the co-delivery of 2000 ng BMP-2 and 200 ng TGF-β3 to the PLDL scaffold, but not by addition of the 200/20 dose. There was a nearly significant increase in stiffness with increasing growth factor dose (2000/200 dose over 200/20 dose).

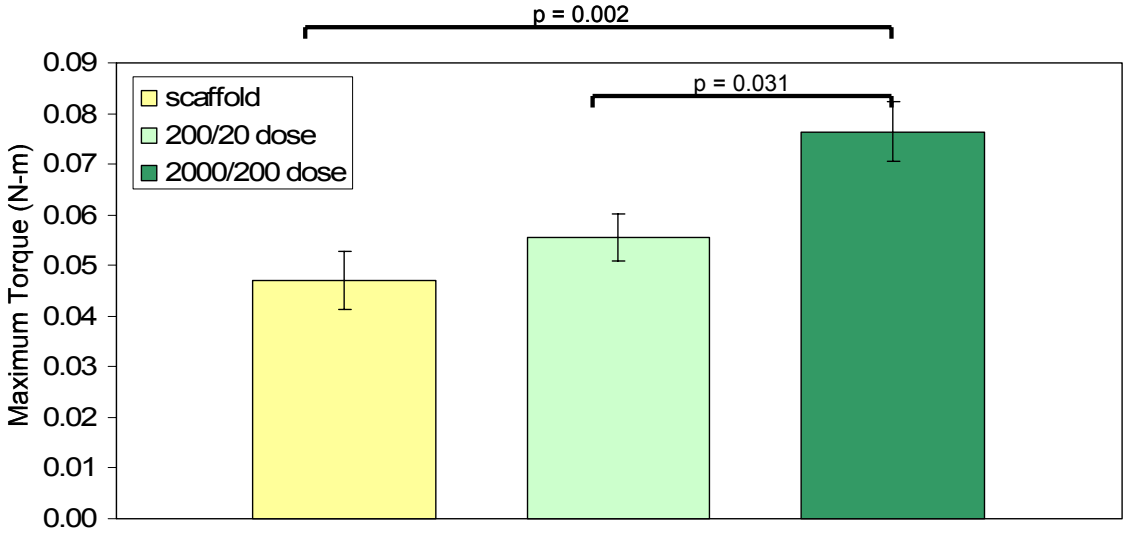

Figure 33: Average maximum torque values for three treatment groups ($11 \leq n \leq 14$). Maximum torque was significantly increased in the 2000/200 ng co-delivery treatment group as compared to both the 200/20 ng co-delivery group and the scaffold only group. Delivery of the 200/20 dose did not significantly improve maximum torque over delivery of a scaffold alone.

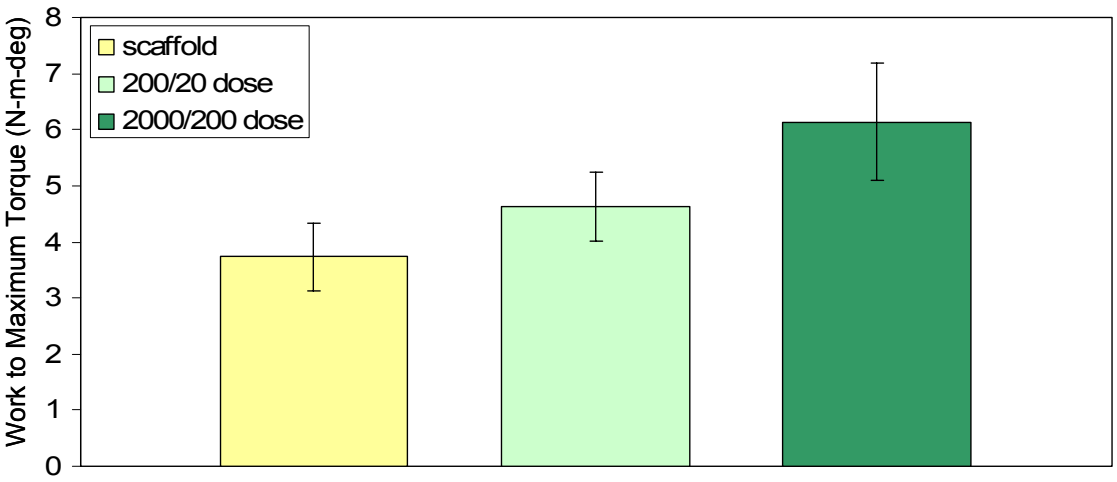

Figure 34: Average work to maximum torque values for three treatment groups ($11 \leq n \leq 14$). Treatment of the defects with either dose of growth factor (2000 ng BMP-2/200 ng TGF-β3 or 200 ng BMP-2/20 ng TGF-β3) did not impact work to maximum torque.

In the study that compared single growth factor delivery to dual growth factor delivery, treatment was a significant factor in determining stiffness ($p = 0.014$) (Figure 35). The BMP-2 and TGF-β3 co-delivery group had a significantly higher stiffness than the TGF-β3 only ($p = 0.021$) or scaffold alone ($p = 0.034$) groups. The co-delivery treatment group was not significantly different from the BMP-2 only group ($p = 0.354$), nor was the BMP-2 only group significantly different from any of the other treatment groups in terms of stiffness ($p = 0.623$ for scaffold only, $p = 0.451$ for TGF-β3). Maximum torque was also significantly affected by treatment ($p = 0.005$) (Figure 36). BMP-2 and TGF-β3 co-delivery produced an average maximum torque that was significantly greater than that achieved by the TGF-β3 ($p = 0.009$) or scaffold only ($p = 0.014$) groups. The difference in maximum torque between the co-delivery group and the BMP-2 only group was not statistically significant ($p = 0.077$). The scaffold only and TGF-β3 only treatment groups were not significantly different ($p = 0.988$) in maximum torque, and BMP-2 only treatment was not significantly different from treatment with TGF-β3 alone ($p = 0.728$) or a growth factor-free scaffold ($p = 0.878$). Calculating work to maximum torque did not reveal any statistically significant differences between treatment groups (Figure 37).

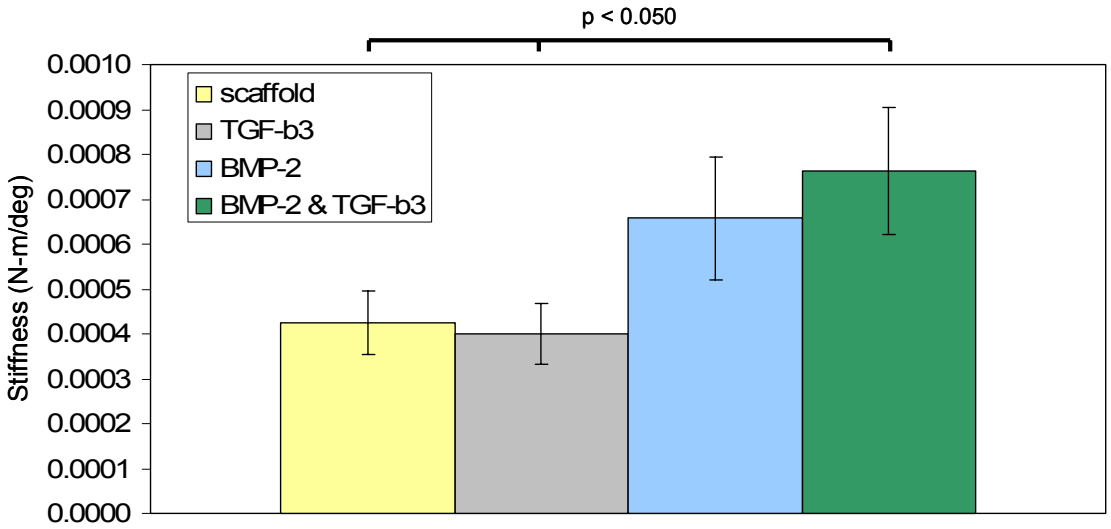

Figure 35: Average stiffness measurements taken *post mortem* at 12 weeks post-op ($6 \leq n \leq 8$). The stiffness of the BMP-2/TGF-β3 (2000/200 ng dose) co-delivery group was significantly higher than that of both the TGF-β3 monotherapy and scaffold only groups. The difference in stiffness between the BMP-2 only and co-delivery treatment groups was not significant.

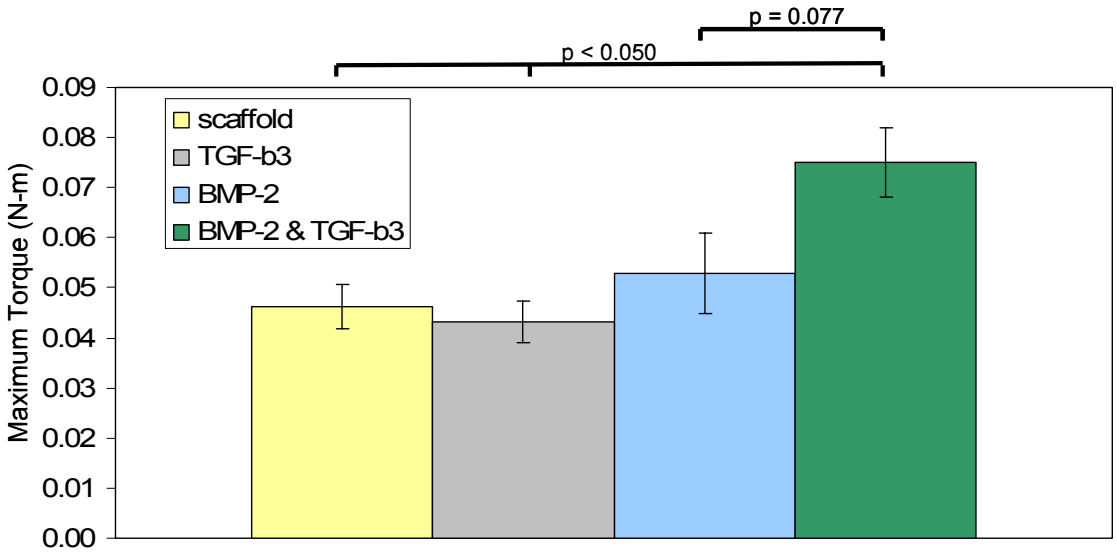

Figure 36: Average maximum torque values obtained *post mortem* at 12 weeks post-op ($6 \leq n \leq 8$). Maximum torque was significantly elevated in the BMP-2/TGF-β3 (2000/200 ng dose) co-delivery treatment group as compared to delivery of both TGF-β3 alone and a PLDL scaffold alone. There was a strong trend indicating an increase in maximum torque in the growth factor co-delivery group over delivery of BMP-2 alone.

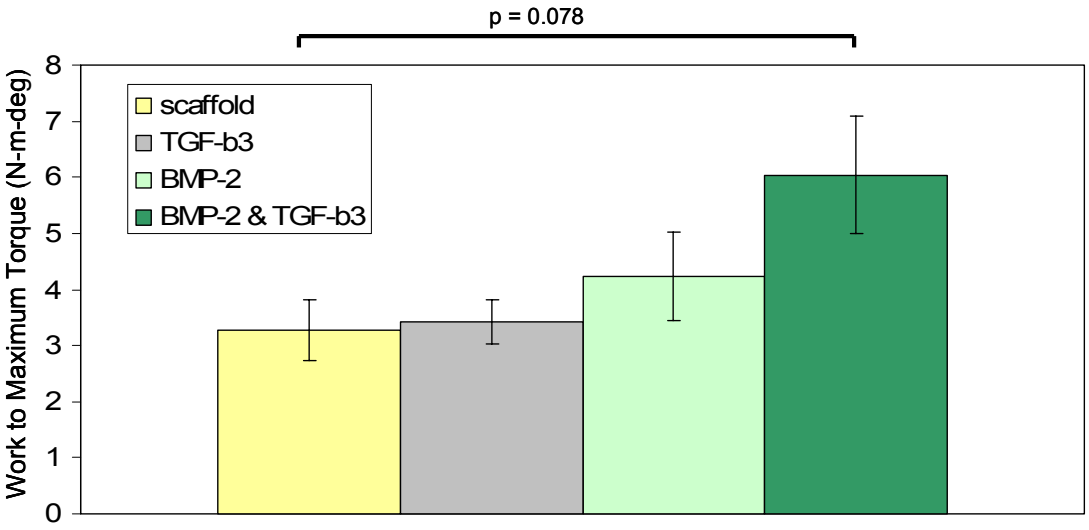

Figure 37: Average work to maximum torque ($6 \leq n \leq 8$). There was a trend towards increased work to maximum torque in the growth factor co-delivery group as compared to delivery of a scaffold alone.

4.4.4 Histology

Staining of 5 μm thick sections revealed minimal mineralized matrix formation in both the scaffold only and 200/20 dose treated samples. New bone formation was constrained to appositional deposition of mineral along the cut edges of the femur (Figure 38, Figure 39). Micro-CT analysis of these samples at the terminal time point indicated low bone volumes. In a representative sample of a defect treated with 2000 ng BMP-2, there was a substantial quantity of mineralized tissue forming within the scaffold region. Ingrowth of the mineralized matrix appeared to occur mainly along the longitudinal macropores of the scaffold (Figure 40). This sample had a bone volume of approximately 38 mm^3 by 4 weeks post-op, indicating that there is a correspondence between bone volume as measured by micro-CT and qualitative histological staining.

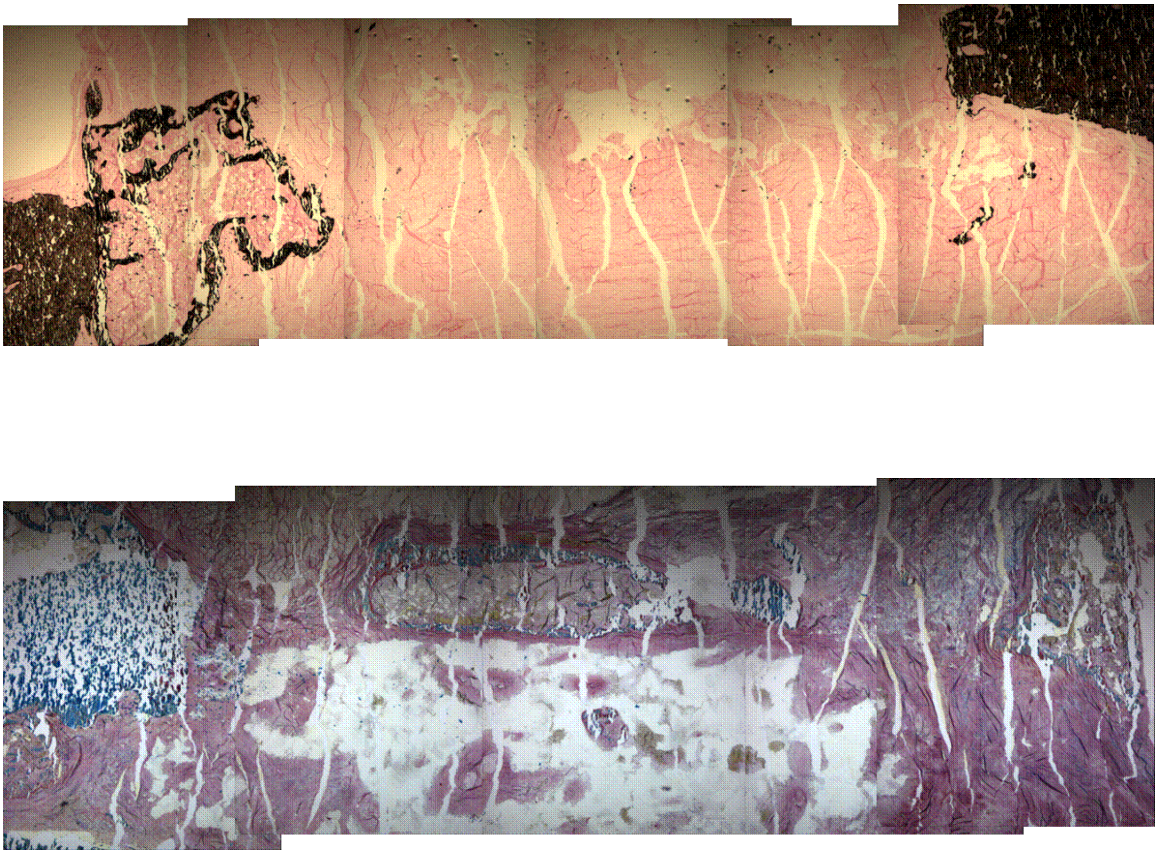

Figure 38: Histological sections taken from a sample treated with an unaugmented RGD-alginate filled PLDL scaffold. Top row, von Kossa stain; lower row, Massons' trichrome. Safranin-O staining did not reveal any cartilaginous tissue. The scaffold region is filled by primarily fibrous, unmineralized tissue.

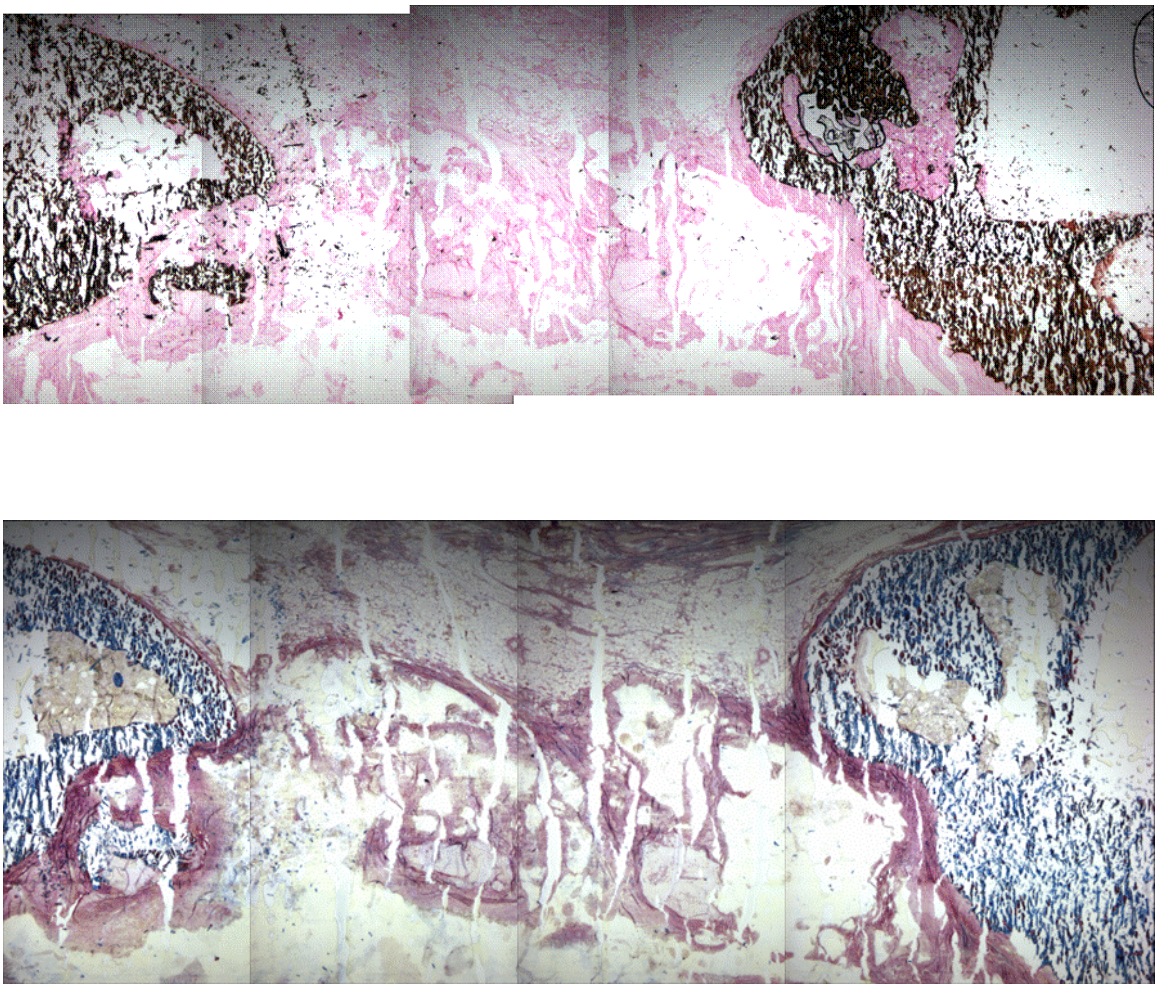

Figure 39: Histological sections taken from a sample treated with 200 ng BMP-2 and 20 ng TGF-β3. Top row, von Kossa stain; lower row, Massons' trichrome. Safranin-O staining did not reveal any cartilaginous tissue. Tissue ingrowth is constrained to appositional bone formation along the cut ends of the femur.

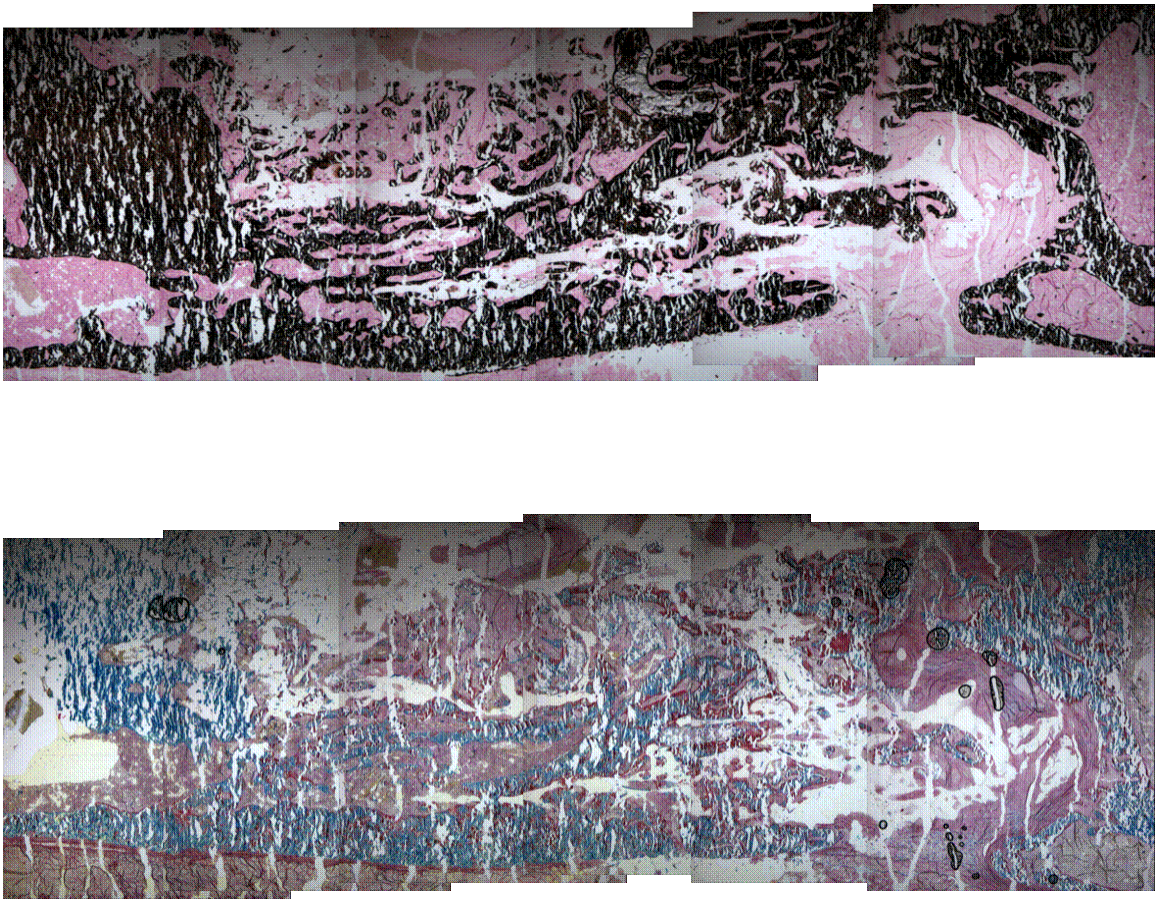

Figure 40: Histological sections taken from a sample treated with 2000 ng BMP-2. Top row, von Kossa stain; lower row, Massons' trichrome. Safranin-O staining did not reveal any cartilaginous tissue. Staining reveals formation of mineralized tissue throughout the scaffold in the defect area, with ingrowth occurring mainly through the longitudinal macropores.

4.5 Discussion

Treatments for osseous defects must achieve stable bony union, restore functionality to the limb, and promote remodeling of the repair tissue in order to regenerate normal bone anatomy, strength, and function long-term. Allografts are an easily available source of structural material with which to treat critically-sized defects, but are limited by the many associated complications that result from incomplete integration and remodeling of the graft [LUCARELLI 2005, WHEELER 1998, ITO 2005, ENNEKING 2001]. Tissue-engineering approaches, such as those employed in the work presented here, may provide a viable alternative for treatment of large osseous defects.

Here, a growth factor-based tissue-engineered bone replacement construct was generated using a structural polymer scaffold as both a mechanical support and, combined with RGD-alginate, growth factor delivery vehicle. The growth factors BMP-2 and TGF-β3 were selected based on their potent osteoinductive and chondroinductive properties. A dose-dependent increase in bone volume was noted particularly at the early (4 week) time point. Both growth factor treated groups demonstrated a significant increase in bone volume between weeks 4 and 12, while the scaffold only group did not. The delivery of the growth factors promoted accelerated and continued increases in mineralized matrix formation within the defect site over 12 weeks *in vivo*. Delivery of the 2000/200 dose of growth factor was particularly beneficial over delivery of the 200/20 dose of BMP-2/TGF-β3 in terms of promoting early mineralization within the central longitudinal region of the defect, as measured using *in vivo* micro-CT. Because increases in mineralized tissue within this volume of interest correlated to increases in stiffness and

maximum torque, it is possible that the increase in early mineralization also resulted in increased mechanical properties early in the post-operative *in vivo* period. This effect is mirrored by the dose-dependent increase in mechanical properties seen at 12 weeks post-op. In addition to increased mechanical properties and bone volume, the increase in growth factor dose also corresponded to an increase in the rate of bony union across the defect site.

It has been shown previously that BMP-2 and TGF-β3 interact synergistically to produce mineralized matrix in the presence of bone marrow stromal cells when delivered to a subcutaneous site in an ectopic mouse model of osteogenesis [SIMMONS 2004]. A synergistic interaction was not determined in these studies. It should also be noted the co-delivery of both BMP-2 and TGF-β3 resulted in an increase in the incidence of bony union as assessed by blinded observation of digital 2-D X-rays. Taken as whole, these data demonstrate a beneficial effect of low dose growth factor co-delivery as compared to single delivery of either factor alone. The lack of synergistic response may be due in part to the traumatic nature of the injury and the absence of direct cell delivery to the defect. The subcutaneous model in which this treatment strategy was first investigated is far less traumatic than the segmental defect model, and may not provoke the same acute physiologic response. This acute response may in fact be masking the full potential of the growth factors due to the active proteases, inflammation, and presence of endogenous signaling molecules. Not delivering bone marrow cells directly with the implants may also be inhibiting the full response of the treatment, as it takes some time for the native bone marrow stromal cells to invade into the defect region and be activated by the residual growth factor.

The dose-dependent response was expected, and further, it indicates that although physiologic doses of growth factor are sufficient to induce ectopic osteogenesis, moderately higher doses of growth factor are required to regenerate bone in a critically-sized orthotopic defect site. This is not an unexpected result, given that a critically-sized load-bearing osseous defect requires a far larger volume of mineral to be generated than a 50 μl hydrogel does (the implant described by Simmons et al.), and the segmental defect described here requires a greater host of biological signals and agents to act in concert in order to functionally heal the wound [SIMMONS 2004]. However, the doses used in this study were still well below the dose of single growth factor that is generally applied to promote osseous healing of segmental defects. Here, a total of 2.2 μg of growth factor delivered to the defect consistently promoted osseous union and abundant mineralized matrix formation, as compared to other studies in which doses as high as 9-20 μg of various growth factors (BMP-2, VEGF, osteogenin, and BMP-7) have been used for similarly sized or smaller defects [LEE 1994, STREET 2002, CHEN 2002, YASKO 1992, LIEBERMAN 1999, CHEN 2006]. Such supraphysiologic doses are frequently effective at promoting bony union, but produce varied results (particularly VEGF) and are often limited to experimental investigations partially because of the unknown physiologic effects of delivering such large quantities of a single protein. These high level doses of growth factor may also hold the potential to induce excessive bone formation around the defect site. On the lower end of reported dosages in this spectrum, 5 mm defects have been treated with 3 μg BMP-2, but mechanical integrity of the treated defects was not investigated [ISOBE 1999]. Additionally, a 5 mm defect in the rat femur is not critically-sized, and is subject to spontaneous union even in the absence of

treatment [WERNTZ 1996, NOTTEBAERT 1989]. There is clinical indication for use of BMP-2, as an osteoinductive agent in some applications. The current approved dose by the FDA for human clinical trial use of BMP-2 is 1.50 mg/ml in an absorbable collagen (bovine) sponge (ACS) [SWIONTKOWSKI 2006]. This dose has been approved for use in spinal fusions and evaluated for repair of open tibial fractures. The equivalent dose used in the studies presented here is 0.02 mg/ml. Here, the growth factor-laden scaffold was delivered within the defect itself. The BMP-2/ACS treatment for tibial fractures is an overlay technique in which the matrix is simply placed over the fracture site after stabilization with an intramedullary nailing technique. This difference in delivery technique may result in limited efficacy, thereby requiring a higher dose of growth factor in the tibial fracture application. The use of BMP-2 in this manner is efficacious – patients on average bear weight on the injured tibia 32 days sooner than their counterparts who do not receive the BMP-2/ACS onlay. Additionally, delivery of BMP-2 to the tibial defect decreases the need for invasive surgical revisions [SWIONTKOWSKI 2006]. BMP-2/ACS is also used as a treatment for anterior lumbar interbody fusion (spinal fusion). Although local reaming is used to prepare the vertebral endplates for insertion of a spinal fusion cage when the graft is composed of autografted bone, local reaming is not typically used when the BMP-2/ACS graft is used placed within the cage [BURKUS 2002]. Because there is no acute local injury in the BMP-2/ACS treated spinal fusions, the higher (1.5 mg/ml) dose of BMP-2 may be necessitated. In the critically-sized femoral defect model presented here, an acute injury is created, possibly priming the defect site for response to bioactive factors. This acute injury may be part of the reason that the low dose of BMP-2/TGF-β3 is efficacious.

Delivering cells, specifically mesenchymal stem cells (MSCs) and bone marrow stromal cells (BMSCs), has been extensively investigated in the context of brittle ceramic graft implantation [BRUDER 1998 JBJS, BRUDER 1998 JOR, KADIYALA 1997, TSUCHIDA 2001]. While delivery of MSCs or BMSCs to the defect site significantly improves integration of hydroxyapatite scaffolds into segmental defects in both canine and murine models, cellular treatment of defects requires substantial lead time to isolate and expand the autogenous cells before delivering them via a scaffold to the defect site. This delay in treatment may be detrimental to the healing and restoration of full functionality to the defect site as the body's natural healing responses, such as the phase that promotes angiogenesis, may have senesced by the time the defect can be treated. Use of a brittle ceramic scaffold is also not an optimal base for tissue engineered bone replacements, as fractures frequently develop in the ceramic implant as a function of time and use [BRUDER 1998 JBJS]. The use of cellular treatment in combination with an absorbable, structural polymeric scaffold as an approach to the treatment of load-bearing critically-sized defects has not been investigated to date.

In the vein of allograft treatment, use of demineralized bone matrix has been a popular alternative to treatment of segmental bone defects in animal models [BALDIK 2002, CHAKKALAKAL 1999, CHAKKALAKAL 2001, FEIGHAN 1995, GEBHART]. Demineralized bone, however, still bears the risk for potential disease transmission. Demineralized bone grafts are also unable to provide any structural support to the defect site. Providing a scaffold with structural integrity to the defect site may be important in promoting early weight-bearing – a potent stimulator of osteogenesis. In these studies, an absorbable porous synthetic scaffold was used to both deliver biologics incorporated with

a hydrogel and serve as a structural support. The approach taken here asserts two functions (delivery of biologics and mechanical support) as opposed to the single function (delivery of growth factors) of demineralized bone matrix.

Allograft treatment has been modified using gene delivery therapy to achieve somewhat better results than are seen with allograft treatment alone. Incorporation of allografted tissue typically is limited to new bone deposition along the host-graft interface, rather than formation of a complete callus. The angiogenic response is similarly constrained. Coating of allografts in murine models with BMP-2-transfected MSCs enhances the ability of the host to form a callus around the allograft [XIE 2007, LIEBERMAN 1999 JBJS]. Alternatively, a virus encoding a specific gene (such as caALK2) can be directly coated onto the allograft, also enhancing the mineralization surrounding the allograft [AWAD 2007]. However, the incorporation of the allograft is still limited by slow resorption and low porosity.

In conclusion, dual delivery of BMP-2 and TGF-β3 resulted in an increase in bony fill. Co-delivery of these growth factors at two levels indicated a dose-dependent effect on bone volume, stiffness, and maximum torque, with the 2000 ng BMP-2 and 200 ng TGF-β3 co-delivery dose being most beneficial. This dose is low compared to the doses of growth factor typically used to treat critically-sized segmental defects in animal models and the FDA approved dose of BMP-2 monotherapy for clinical human use. The approach demonstrated here serves to deliver low dose bioactive factors and may promote early functional use of the limb. The last chapter focuses on co-delivery of osteogenic and angiogenic growth factors, as well as modifications to the scaffold to better accommodate the rate of bony ingrowth.

CHAPTER 5

EFFECTS OF ANGIOGENIC GROWTH FACTOR DELIVERY AND SCAFFOLD DESIGN ON FUNCTIONAL REPAIR OF SEGMENTAL DEFECTS

5.1 Abstract

Tissue-engineering strategies provide a potential alternative to the traditional large bone defect repair strategy that incorporates a poorly-remodeling allograft. In bone formation and repair, development and maintained presence of vascular structures is critical to survival of osteoprogenitors, osteocytes, and the tissue as a whole. VEGF has been investigated primarily as an agent to induce angiogenesis in *in vivo* models, although recent reports on its ability to promote osteogenesis have been published. Here, the osteogenic and angiogenic responses to three doses of VEGF (10 ng , 100 ng, and 1000 ng) delivered to a critically-sized segmental femoral defect in rats are investigated. The effects of scaffold geometry and composition on mineralization and vascularization are also assessed. Finally, the potential for interactive effects between delivery of the osteogenic growth factor combination of 2000 ng BMP-2/200 ng TGF-β3 and 1000 ng VEGF in the segmental defect model is determined. There was no dose-dependent response to the delivery of VEGF alone in terms of either bone formation or vascular invasion into the defect site. Modifying scaffold geometry by removing a 1.5 mm longitudinal core from the central region of the scaffold and addition of 10% tricalcium phosphate (TCP) improved the rate of union of the defects, but did not significantly enhance bone volume or mechanical properties over any other scaffold design (traditional

PLDL, cored PLDL, traditional geometry PLDL/TCP). Coring of the scaffold improved vascularization within the defect site as compared to the study where no core was removed, but did not improve the lack of dose-dependent response to VEGF treatment. The presence of alginate used to deliver growth factors within the scaffold porosity did not impact revascularization within the core of the defect site. Addition of 1000 ng VEGF to the defects resulted in a significant increase in bone volume within the treatment group with time, although bone volume was not improved as compared to delivery of BMP-2/TGF-β3 or BMP-2/TGF-β3/VEGF. Addition of VEGF to BMP-2/TGF-β3 did not affect bone volume over delivery of only BMP-2/TGF-β3. *In vitro* growth factor release studies indicated that approximately 25% of the growth factor loaded (for BMP-2, TGF-β3, and VEGF) was readily released over 5 days incubation period. Extending the incubation to 21 days did not result in further growth factor release. The remaining 75% of the growth factor may have remained bound by the residual alginate matrix. This indicated that the delivery mechanism in this model system is one of extended controlled release, which may account for the lack of response seen with delivery of VEGF in terms of both revascularization and mineralization.

5.2 Introduction

The problem of regenerating bone in large osseous defects and compromised fractures is non-trivial. While mechanical stabilization and placement of a cadaveric allograft remain the standard treatments for such clinical situations, this treatment is severely compromised in its efficacy due to the low porosity of the allograft. The low porosity and lack of bioactive factors are impediments to the revascularization,

revitalization, and remodeling of the allograft. Because the allograft does not fully incorporate into the recipient body it is subject to complications within as little as 1-2 years post-operatively. The complication rate for allografting is 30-60%, with a 25% graft failure rate [ITO 2005, LUCARELLI 2005, WHEELER 2005]

Tissue engineering is emerging as a clinical therapy for large bone defects in both load-bearing and non-load-bearing applications. The simplistic strategy of combining one high-dose osteogenic growth factor (BMP-2) therapy with a biocompatible carrier (bovine absorbable collagen sponge) is now FDA-approved for clinical use in spinal fusions and under investigation for use as treatment augmentation for complex tibial shaft fractures (Infuse technology, Medtronic Sofamor Danek) [SWIONTKOWSKI 2006, BURKUS 2002]. Tissue-engineered grafts have been widely investigated in experimental animal models. There are three fundamental treatment strategies, all relying on some type of delivery vehicle, scaffold, or substrate: cell delivery, bioactive peptide delivery, and gene therapy. The treatment strategy selected for investigation here is growth factor delivery.

Design of a biocompatible scaffold that not only permits, but is conducive to, functional, vascularized bony union is a complex problem. While ceramics – both natural (coral) and manufactured (hydroxyapatite/tricalcium phosphate) – are appealing due to their near physiologic mineral content, they are inherently limited by a lack of porosity and structural brittleness that tends toward failure under loading *in vivo* [BRUDER 1998 JBJS]. Nonstructural matrices are a popular option because their morphology is conducive to use in geometrically challenging defects and they can be synthesized in nearly any composition the investigator desires [KRETLOW 2007]. Specific

modifications to polymers, such as adding metalloproteinase cleavage sites to link a growth factor to a hydrogel, can also be engineered [RIZZI 2006, LUTOLF 2003]. Biologically-derived nonstructural matrices can be either inherently inert, such as collagen, or bioactive like some formulations of demineralized bone matrix. The risk of using natural bioactive matrices, however, is that the level of their activity is prone to variability from one preparation to another. Structural polymers and polymer-ceramic hybrids have not been largely investigated to date for use in load-bearing defect sites, although some investigation into their use for intramembranous bone repair has been done [ROHNER 2003, SCHANTZ 2003].

Bone is a mechano-sensitive tissue. The structure and function of bone are tightly linked to not only the biological environment of the tissue, but the mechanical environment as well [FROST 1987]. In a feedback circuit, early load bearing (without excessive micromotion) of a fractured bone leads to more rapid bone formation and remodeling, while rapid bone formation also permits early load-bearing on the afflicted bone. Taking advantage of bone's natural response to loading, developing a tissue-engineered treatment for large or challenged osseous defects that maintains structural integrity under a load-sharing system with some type of fixation device may enhance not only the rate of bone mineral deposition, but lead to early and improved limb functionality.

Structural polymer scaffolds have not been widely used as delivery vehicles for bioactive factors, and may be suitable for treatment of large load-bearing defects [RAI 2007, OEST 2007]. Sustained delivery of growth factors from a structural scaffold requires that the growth factors be either directly incorporated into the polymer during

fabrication, or that some sort of controlled-release matrix be delivered within the scaffold porosity. The latter method is selected for use in the studies that follow. Alginate is a biocompatible hydrogel that has been shown to control the release of certain growth factors, and in the case of VEGF, actually enhance the activity of the protein [SHERIDAN 2000].

The robust model selected here to test tissue-engineered bone regeneration strategies does not heal in the absence of treatment [OEST 2007]. Three growth factors, BMP-2, TGF-β3, and VEGF were selected for delivery into the defect. In previous chapters, the dose-dependent effects of BMP-2 and TGF-β3 on bone formation have been described. VEGF is known to induce angiogenesis in a variety of *in vivo* models, including the CAM assay, retinal vascularization, and subcutaneous implantation. Its reported effects on bone formation, however, vary widely [STREET 2002, ECKHARDT 2003].

The goals of these studies were to: quantify the dose-dependent effects of VEGF delivery on bone formation and vascular invasion in a critically-sized femoral defect model, determine an optimal scaffold geometry and composition for repair of femoral defects, and investigate the potential interaction effects of co-delivering VEGF with BMP-2 and TGF-β3.

5.3 Methods

5.3.1 Scaffold Production

Structural lactic acid-based polymer scaffolds containing 10% tricalcium phosphate (PLDL/TCP) were generated using a fiber-coating porogen decomposition technique previously described [LIN 2003]. Briefly, 100 micron diameter stainless steel fibers were coated in seven sequential steps using a syringe with varying gage hypodermic needles to flow the solvated polymer and porogen onto the fibers. After coating, the wires were cut, bundled, and heat treated to fuse the bundled wires together. During a second heat treatment the porogen was decomposed from solid to gaseous phase, producing random micropores in the scaffold structure. Removal of the wires revealed longitudinal macropores in the scaffold. Scaffolds were cut to length (8 mm) and punched to size (4 mm diameter), then rinsed to remove degradation particles from the heat treatment. In some studies, a central 1.5 mm longitudinal core was removed using a biopsy punch. Sterilization was achieved by γ-irradiation at a dose of 2.5 Mrad. Prior to loading with growth factor, the scaffolds were coated for 16 hours in rat plasma fibronectin (25 μg/ml, F0635, Sigma Aldrich) using a vacuum-coating technique.

5.3.2 Addition of Growth Factors to Scaffolds

Three growth factors were selected for delivery or co-delivery: recombinant human BMP-2, TGF-β3, and recombinant rat $VEGF_{164}$ (355-BM/CF, 243-B3/CF, and 564-RV, R&D Systems, Minneapolis, MN). Growth factors were reconstituted aseptically using 0.1% rat serum albumin fraction V in 4 mM HCl immediately prior to

use. MVG sodium alginate (Pronova Biopolymers, Norway) was converted to a short chain length form by exposing the stock alginate to a 5 Mrad dose of γ-irradiation. This short chain alginate was functionalized with a G_4RGDSP (RGD motif) peptide sequence at a density of 2 sequences per chain using carbodiimide chemistry [SIMMONS 2004]. The resulting RGD-alginate was sterile filtered and lyophilized for storage at -20°C until use. The growth factor doses were chosen based on the success of previous experiments delivering BMP-2 and TGF-β3 described in Chapter 4, and values reported in the literature to induce angiogenesis and osteoblast cell migration [LEE 2003, EMAD 2006, MAYR-WOHLFHART 2002, PUFE 2002].

5.3.3 Quantification of Growth Factor Release Kinetics

Seven scaffolds were loaded with 2000 ng BMP-2, 200 ng TGF-β3, and 1000 ng VEGF each. The preparation of these scaffolds was consistent with those prepared for *in vivo* implantation. Scaffolds were maintained at 37°C for 21 days in serum-free α-MEM. Media was collected and entirely replaced to maintain sink conditions at the following time points: 20 minutes, 40 minutes, 6 hours, 12 hours, 24 hours, 2 days, 3 days, 4 days, 5 days, 6 days, 7 days, 10 days, 14 days, and 21 days. The quantity of growth factor released to the media was quantified using ELISA kits obtained from R&D Systems (Minneapolis, MN). For TGF-β3, only the active form of the growth factor is quantified by this method. Likewise, the ELISA kits quantify only the mature dimerized forms of BMP-2 and VEGF.

5.3.4 Study Designs

Multiple studies were run to determine the effects of several conditions *in vivo*.

Study 1: Dose-Dependent Effects of VEGF Delivery on Bone and Vascular Structure Formation

Two identical studies were run with two different outcome measures. One sample population went towards quantification of vascular invasion into the defect site using contrast agent-enhanced micro-CT. The second sample population was assayed by use of *in vivo* X-rays, *in vivo* and *in vitro* micro-CT, and post-mortem mechanical testing. For both studies there were four treatment groups: 0 ng VEGF (PLDL only), 10 ng VEGF, 100 ng VEGF, and 1000 ng VEGF.

Study 2: Effects of Scaffold Geometry and Composition on Bone Formation and Vascular Invasion

In the interest of improving the rate and quantity of bone deposition within the defect area and increasing the quantity of vasculature that forms within the core of the scaffold, the scaffold geometry and composition was modified. Scaffold geometry was modified by removing a 1.5 mm longitudinal core from the center of the scaffold. Composition was altered by adding 10% α-tricalcium phosphate to the polymer solution during the production process. The effects of these parameters were quantified by assessing radiographic union using digital X-rays, use of *in vivo* and *in vitro* micro-CT, and mechanical testing. In the interest of enhancing angiogenesis within the center of the scaffold, cored PLDL/TCP scaffolds were augmented with growth factor using two different techniques: fill the scaffold with growth factor in alginate then remove the core

(fill then core) or core the scaffold and then fill with growth factor in alginate (core then fill). The purpose of employing these two different loading regimes was to determine if the presence of alginate was inhibiting revascularization of the defect site.

Study 3: Addition of an Angiogenic Growth Factor to the Osteogenic Cocktail BMP-2/TGF-β3

Triple growth factor delivery (2000 ng BMP-2 + 200 ng TGF-β3 + 1000 ng VEGF) was compared to dual growth factor delivery (BMP-2 + TGF-β3), single growth factor delivery (VEGF), and delivery of a scaffold alone. For all groups, cored PLDL/TCP scaffolds filled with short chain RGD-functionalized alginate (core scaffold then fill with alginate method) were used. The efficacy of these treatments was determined using 2-D digital X-rays, 3-D quantitative micro-CT done both *in vivo* and *in vitro* to assess bone formation, *in vitro* micro-CT paired with contrast agent delivery for assessment of vascular structure formation, and torsional mechanical testing.

5.3.5 Surgical Procedure

All surgical procedures were reviewed and approved by the Institutional Animal Care and Use Committee at Georgia Institute of Technology (Protocol A05041). Female Sasco Sprague Dawley-rats aged 13 weeks were used. Anesthesia was induced and maintained using isoflurane. Bilateral incisions were made over the anterior aspect of the femurs. The femurs were exposed using blunt dissection of the muscle tissue. Custom modular fixation plates were secured directly to the bone using miniature screws. Full-thickness 8 mm long diaphyseal defects were created bilaterally using a miniature

oscillating saw cutting under irrigation. Defects were flushed with sterile saline prior to implantation of a scaffold. PLDL scaffolds with or without growth factors (all containing RGD-alginate) were press-fit into the defects. The incisions were closed according to anatomic layers using absorbable suture and wound clips. Analgesia consisted of 0.05 mg/kg buprenorphine every 8 hours postoperatively for the first 48 hours and 0.025 mg/kg buprenorphine every 8 hours for the following 24 hours. Animals resumed normal ambulation within 2-3 days post-op and did not show signs of pain or distress.

5.3.6 X-ray and Micro-CT

Digital 2-D X-rays were taken every 4 weeks postoperatively until the studies were terminated. These X-rays were used primarily to assess defect stability. *In vivo* micro-CT was done at 4 and 12 weeks post-op in all studies where bone formation was assessed. For *in vivo* micro-CT, a resolution of 38.9 microns was used (Viva-CT 40, Scanco Medical, Bassersdorf Switzerland). The VOI was 4.6 mm thick. A Gaussian filter (sigma = 1.2, support = 1) was used to partially suppress noise in the VOI prior to application of a global threshold. The global thresholds corresponded to densities of 206.7 and 270.3 mg hydroxyapatite/cm^3, and excluded all non-mineralized tissues and residual scaffold material, as verified by visual examination of individual 2-D slices. The lower threshold was used to quantify total bone volume (mature + immature), while the upper threshold was used to assess mature bone volume. Immature bone volume was calculated as the difference between total bone volume and mature bone volume. The upper threshold (mature bone) was determined by two methods; a histogram of voxels attenuating vs the threshold was plotted and used to select an approximate threshold

value. This threshold value was then validated using visual inspection of 2-D slices. The threshold of 270.3 mg HA/cm^3 corresponds to the attenuation of mature cortical bone in a rat. The immature bone threshold was selected as the lowest value that could be analyzed without picking up image artifacts or distorting the bone structure.

5.3.7 Mechanical Testing

Samples were harvested at the termination of each study (12 weeks post-op), wrapped in saline-soaked gauze and stored at -20°C. Mechanical testing was done after samples were thawed in a bath of room-temperature saline, unwrapped, and immediately scanned using *in vitro* micro-CT at a 20 μm resolution. After scanning, samples were potted in end blocks using Wood's metal and secured by placement of a transverse pin that penetrated the potting blocks and the ends of the femur. Samples were wrapped in saline-soaked gauze to preserve tissue hydration during transport and setup. Samples were then tested to failure in torsion at a rate of 3°/second using a Bose ElectroForce (ELF) system (ElectroForce 3200, Bose Corporation, Eden Prairie, MN).

5.3.8 Histology

One representative sample from each treatment group was selected for histological evaluation. Sections were taken at a 5 μm thickness and stained using Masson's trichrome, safranin-O, von Kossa, and haematoxylin and eosin.

5.3.9 Statistics

Analysis of variance was conducted using a general linear model and Tukey pairwise post-hoc comparisons (Minitab). Differences were considered statistically significant at $p \leq 0.05$.

5.4 Results

5.4.1 Quantification of Growth Factor Release Kinetics

Release of growth factors was quantified using ELISAs. The ELISA kits, purchased from R&D Systems (Minneapolis, MN), quantified only the active form of TGF-β3 and the mature forms of soluble BMP-2 and VEGF. Seven scaffolds were loaded with the triple growth factor combination delivered in RGD-alginate: 2000 ng BMP-2, 200 ng TGF-β3, and 1000 ng VEGF. They were maintained in media at 37°C for 21 days. Samples were collected at the following points in the incubation period: $CaCl_2$ bath, $CaCl_2$ + NaCl + HEPES bath, 6 hours post-seeding, 12 hours, 24 hours, 1 day, 2 days, 3 days, 4 days, 5 days, 6 days, 7 days, 10 days, 14 days and 21 days. For all three growth factors, the majority of the release took place over the first 5 days in culture (Figures 41, 42, 43). About 25% of the total growth factor delivered was released in active soluble form over 21 days *in vitro*. VEGF released somewhat more quickly than BMP-2 and TGF-β3 did, with the majority of the release occurring within the first 2 days of culture.

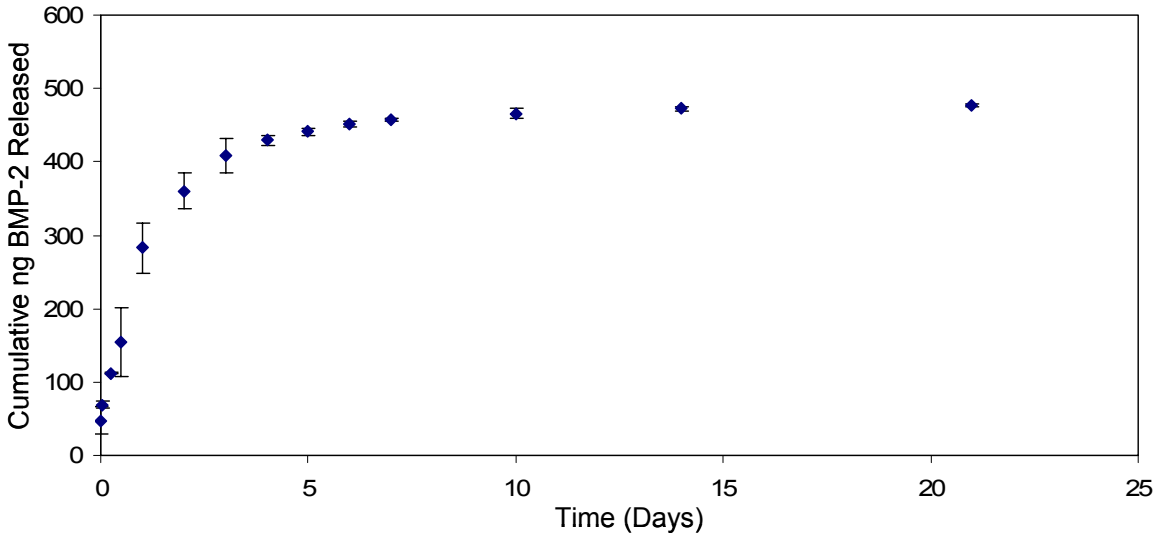

Figure 41: Cumulative quantity of soluble active BMP-2 released to media over 21 days in an *in vitro* growth factor release study as determined by an ELISA.

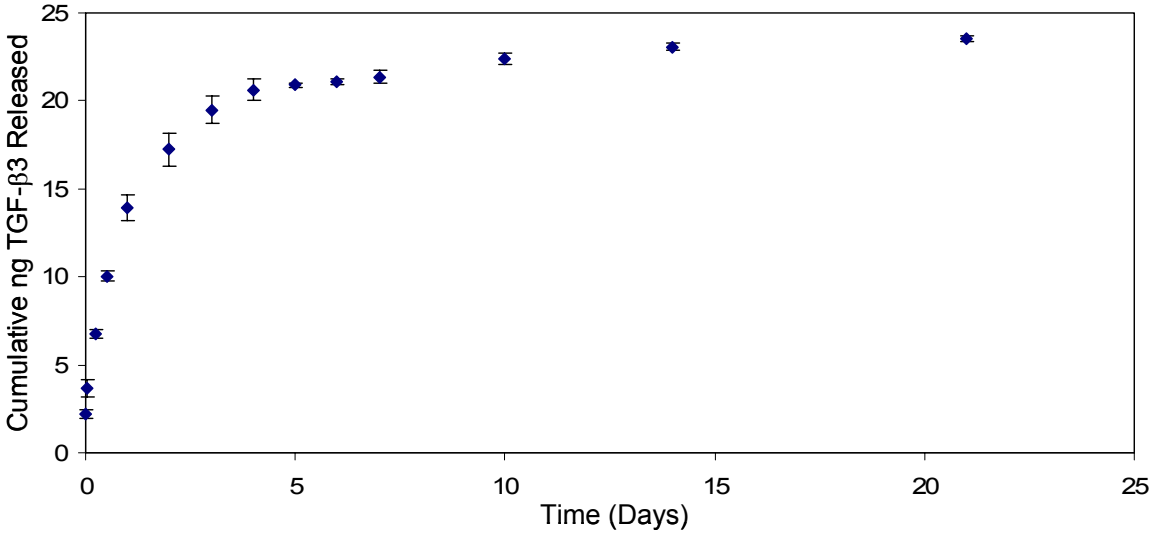

Figure 42: Cumulative quantity of soluble active TGF-β3 released to media over 21 days in an *in vitro* growth factor release study as determined by an ELISA.

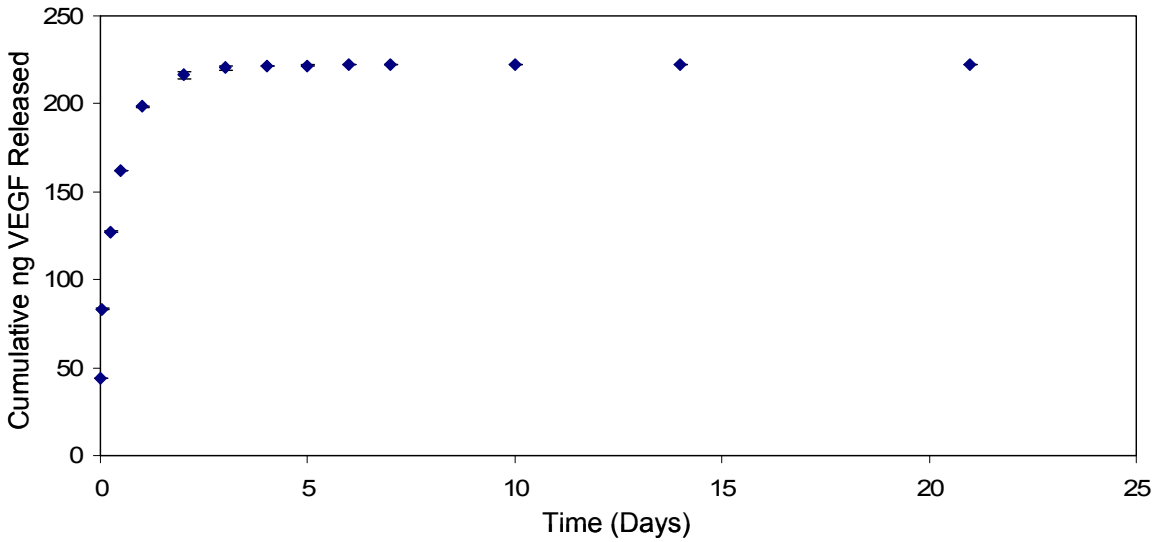

Figure 43: Cumulative quantity of soluble active VEGF released to media over 21 days in an *in vitro* growth factor release study as determined by an ELISA.

5.4.3 X-ray Imaging

Study 1: Dose-Dependent Effects of VEGF Delivery on Bone and Vascular Structure Formation

Delivery of VEGF at any of the three doses (10 ng, 100 ng, 1000 ng) did not have a marked effect on the rate of bony union (Figure 44). Osseous union was apparent in only two samples over the course of this study; one sample from the 10 ng treatment group (1/5) and one sample from the 1000 ng treatment group (1/7). For a scaffold alone, no samples achieved bony union (0/5) and likewise for the 100 ng treatment group (0/7).

Study 2: Effects of Scaffold Geometry and Composition on Bone Formation and Vascular Invasion

In this study, rates of bony union were assessed for four different scaffold designs, each delivering 2000 ng BMP-2 and 200 ng TGF-β3. In the traditional geometry PLDL treatment group, 5/7 sample united. When a 1.5 mm core was removed from the PLDL treatment group, 9/15 samples achieved bony union. Addition of 10% TCP to a traditional PLDL scaffold resulted in 3/9 samples achieving union. Coring of this PLDL/TCP scaffold containing growth factors promoted 8/8 samples to achieve bony union (Figure 45).

Study 3: Addition of an Angiogenic Growth Factor to the Osteogenic Cocktail BMP-2/TGF-β3

Addition of 1000 ng VEGF to the osteogenic growth factor mix of 2000 ng BMP-2 and 200 ng TGF-β3 did not affect the rate of bony union in cored PLDL/TCP scaffolds (Figure 46). For this study, rates of bony union were as follows: Scaffold only 2/7, 1000 ng VEGF 0/5, BMP-2/TGF-β3 11/12, BMP-2/TGF-β3/VEGF 11/12.

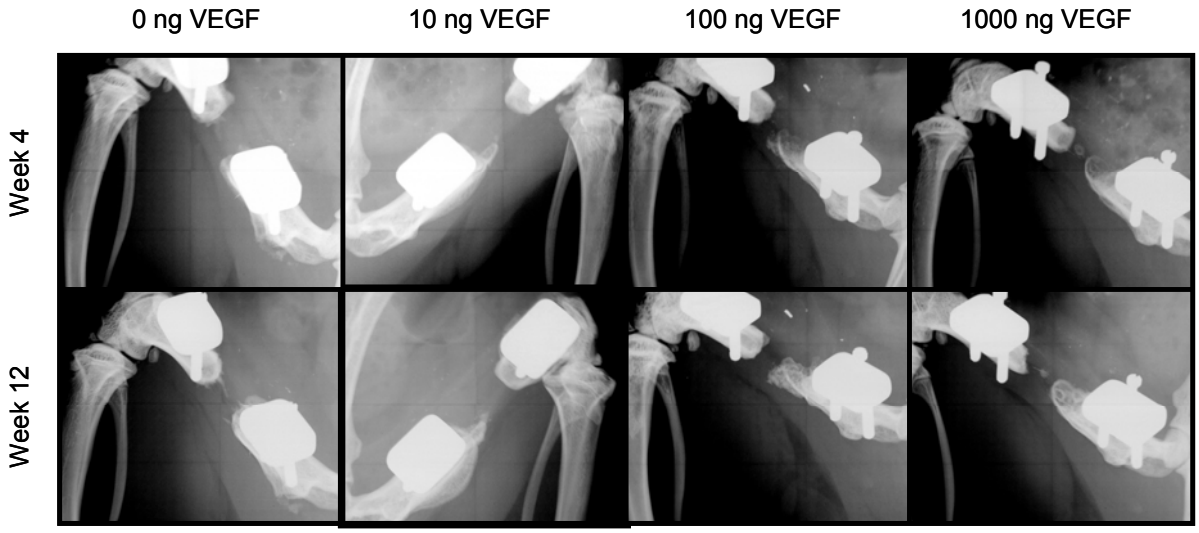

Figure 44: Digital 2-D X-rays of samples from the VEGF dose study ($5 \leq n \leq 7$). Rates of union were: 0 ng VEGF 0/5, 10 ng VEGF 1/5, 100 ng VEGF 0/7, and 1000 ng VEGF 1/7.

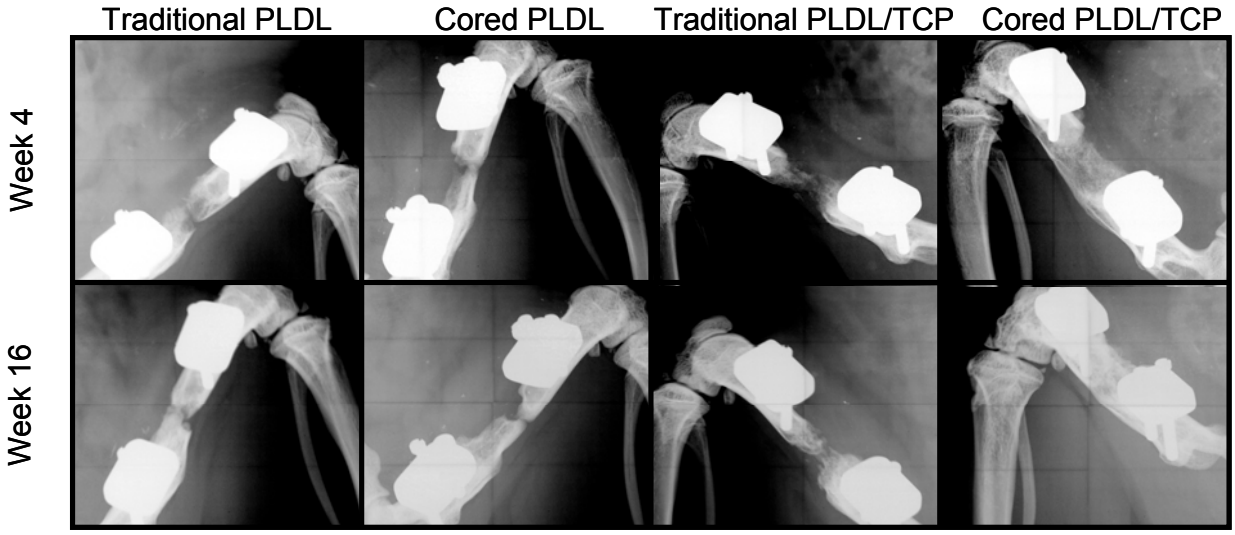

Figure 45: Digital 2-D X-rays of samples from the scaffold modification study ($7 \leq n \leq 15$). In the traditional PLDL treatment group, 5/7 samples achieved union. For cored PLDL 9/15, 3/9 traditional PLDL/TCP, and 8/8 cored PLDL/TCP samples achieved union.

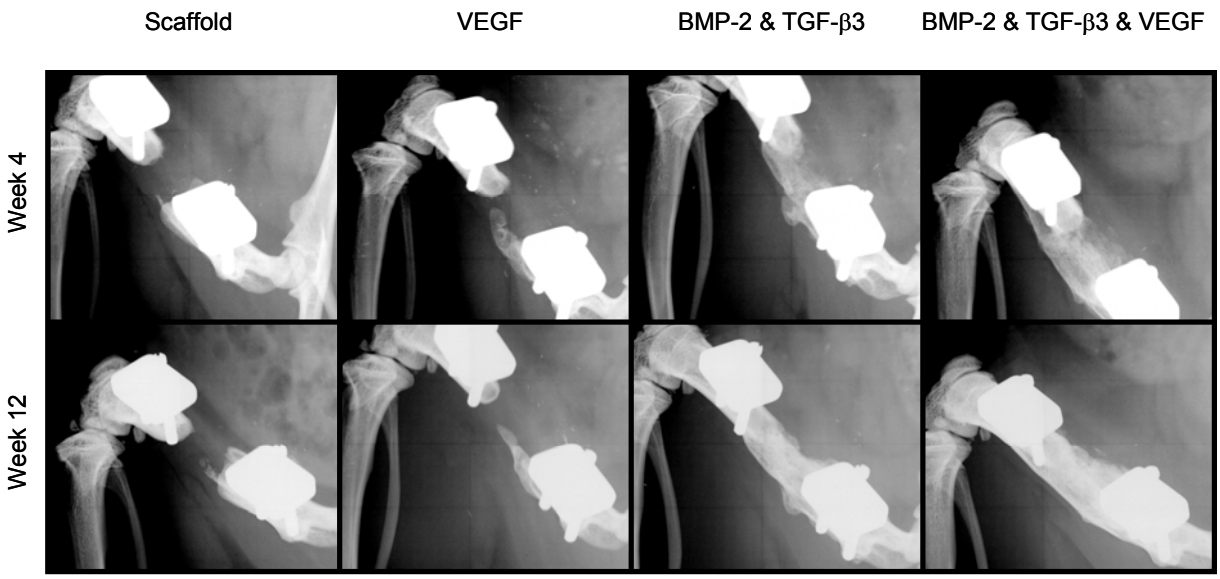

Figure 46: Digital 2-D radiographs of the samples from the triple growth factor co-delivery study ($5 \leq n \leq 12$). Of the samples that received BMP-2, TGF-β3, and VEGF 11/12 achieved union. Co-delivery of BMP-2 and TGF-β3 promoted 11/12 samples to unite. Delivery of VEGF alone did not elevate the rate of union (0/5) over that achieved by delivering a scaffold alone (2/7).

5.4.4 Micro-CT Analysis

Study 1: Dose-Dependent Effects of VEGF Delivery on Bone and Vascular Structure Formation

Quantitative *in vivo* micro-CT analysis was done at weeks 4 and 12 post-op. There were no differences in the bone volumes of these samples at either time point (Figure 47). *Post mortem* analysis at 12 weeks post-op showed results similar to the *in vivo* analysis (Figure 48). Spatial analysis of the core and peripheral VOIs as well as the proximal and distal VOIs revealed no differences (Figure 49, Figure 50, Figure 51). This *in vitro* micro-CT analysis revealed more bone on the distal end of the defect than on the proximal end. It is possible that the samples were inverted during scanning, which would explain this difference.

Combination of a contrast agent (Microfil MV122, Flowtech, Carver, MA) with micro-CT enabled quantification of the vascular structures within the defect site at 2 weeks post-op. There were no differences between VEGF treatments in any of the VOIs assessed (scaffold and periphery, periphery, scaffold, or core) (Figure 52, Figure 53).

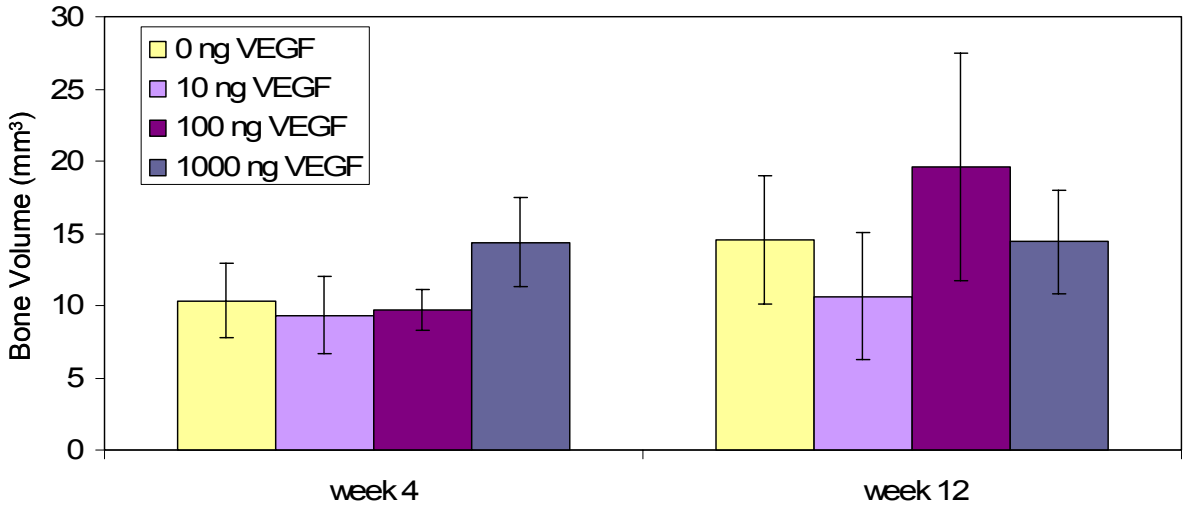

Figure 47: Bone volumes in the central 4.8 mm of the defect area as determined using *in vivo* micro-CT at weeks 4 and 12 post-op ($5 \leq n \leq 8$). There were no significant differences.

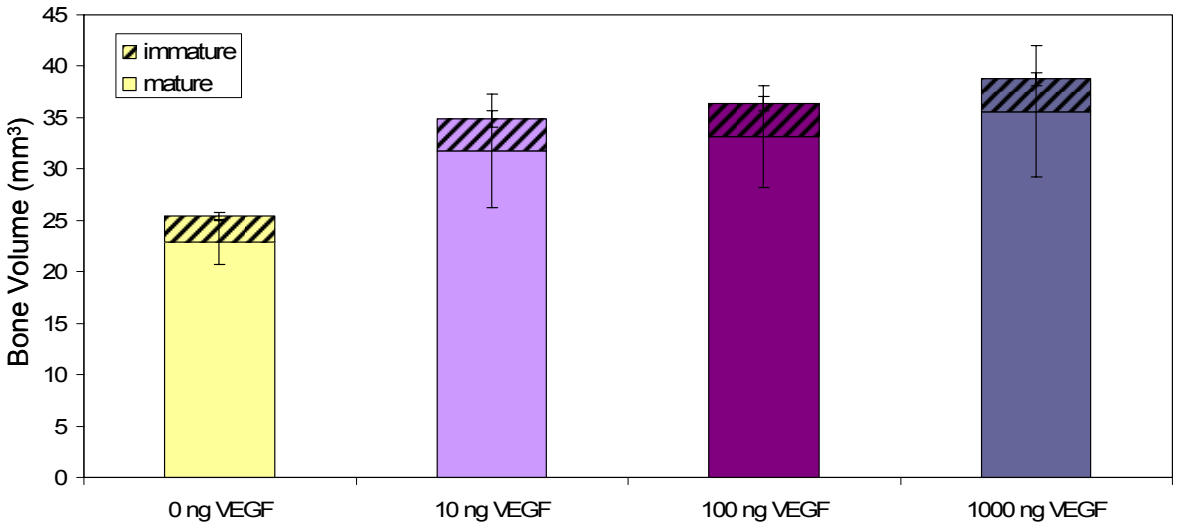

Figure 48: Bone volumes as determined using *in vitro post mortem* micro-CT at 12 weeks post-op ($4 \leq n \leq 7$). There were no significant differences for immature, mature, or total bone volumes.

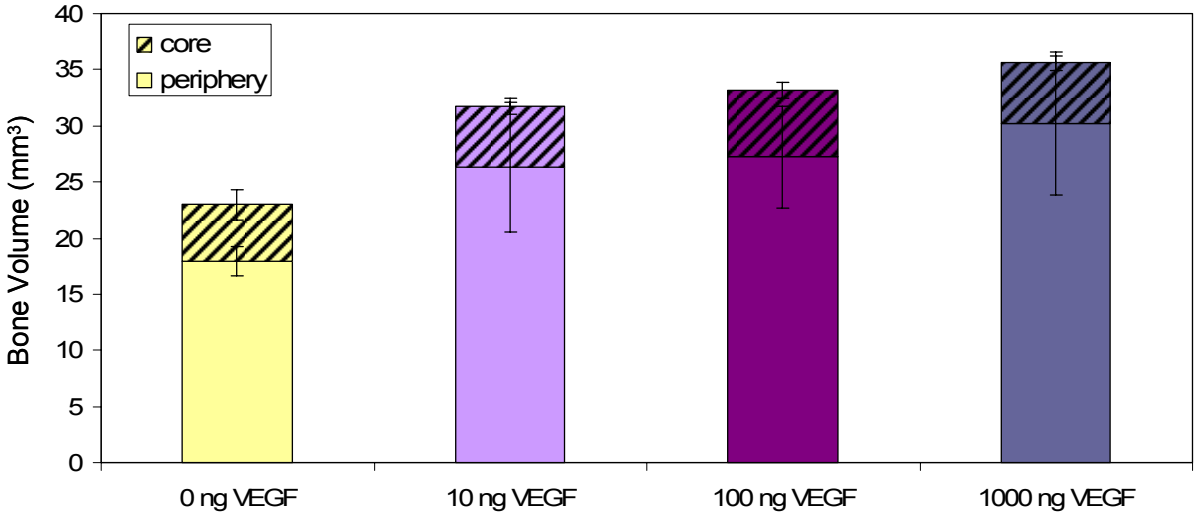

Figure 49: Bone volumes as determined using *in vitro post mortem* micro-CT at 12 weeks post-op ($4 \leq n \leq 7$). There were no significant differences for core or peripheral bone volumes.

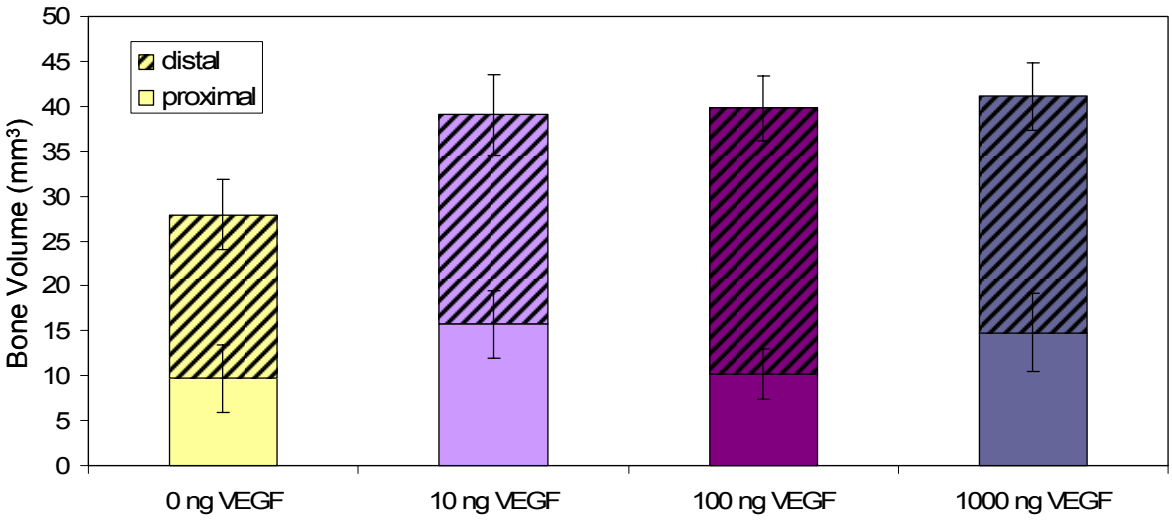

Figure 50: Bone volumes as determined using *in vitro post mortem* micro-CT at 12 weeks post-op ($4 \leq n \leq 7$)There were no significant differences for proximal or distal bone volumes.

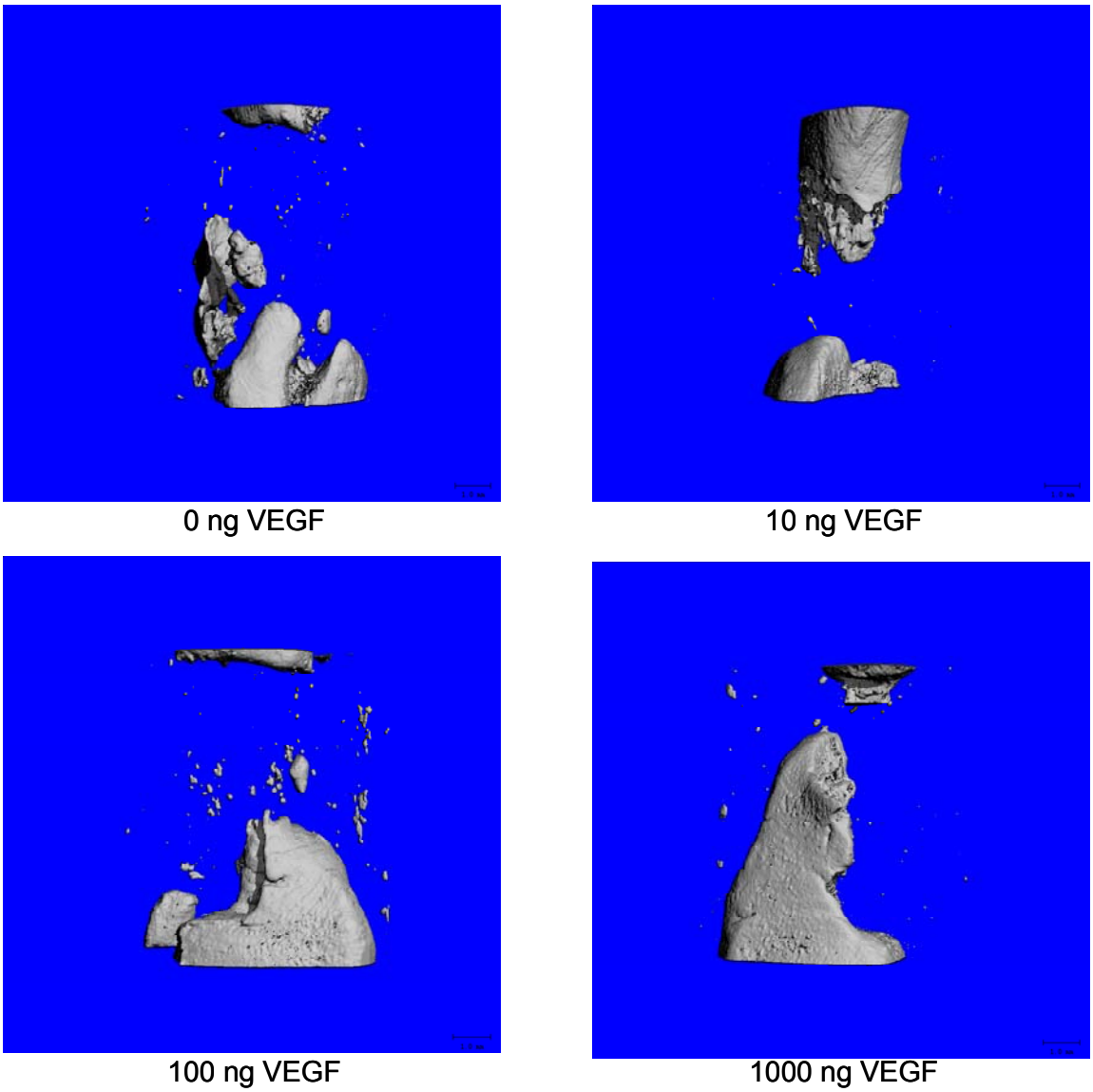

Figure 51: Micro-CT images of samples from *in vitro* scans at 12 weeks post-op.

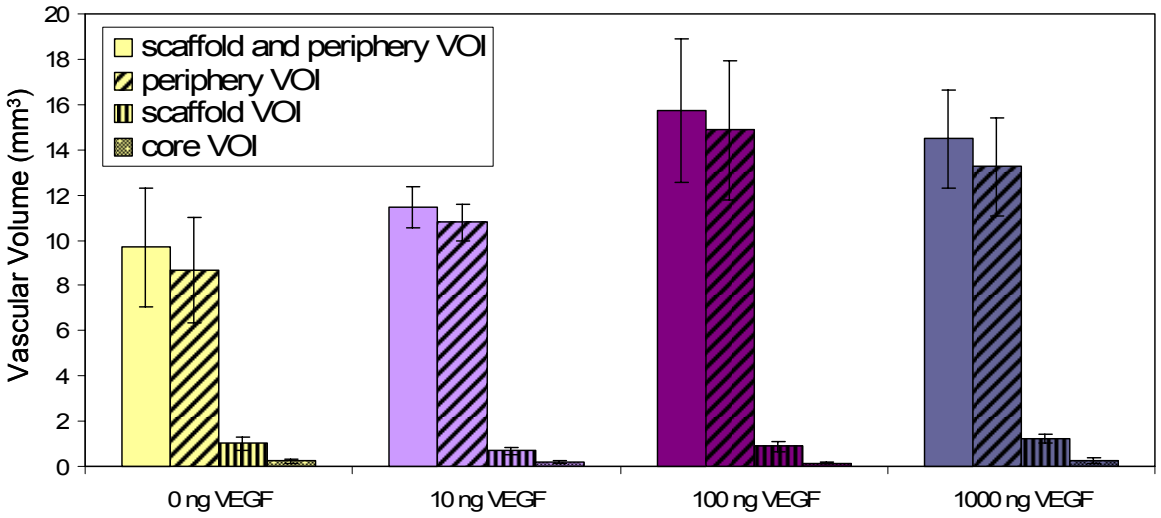

Figure 52: Vascular volumes as determined using contrast agent-enhanced micro-CT at 2 weeks post-op ($5 \leq n \leq 6$). There were no treatment differences in any of the VOIs assessed.

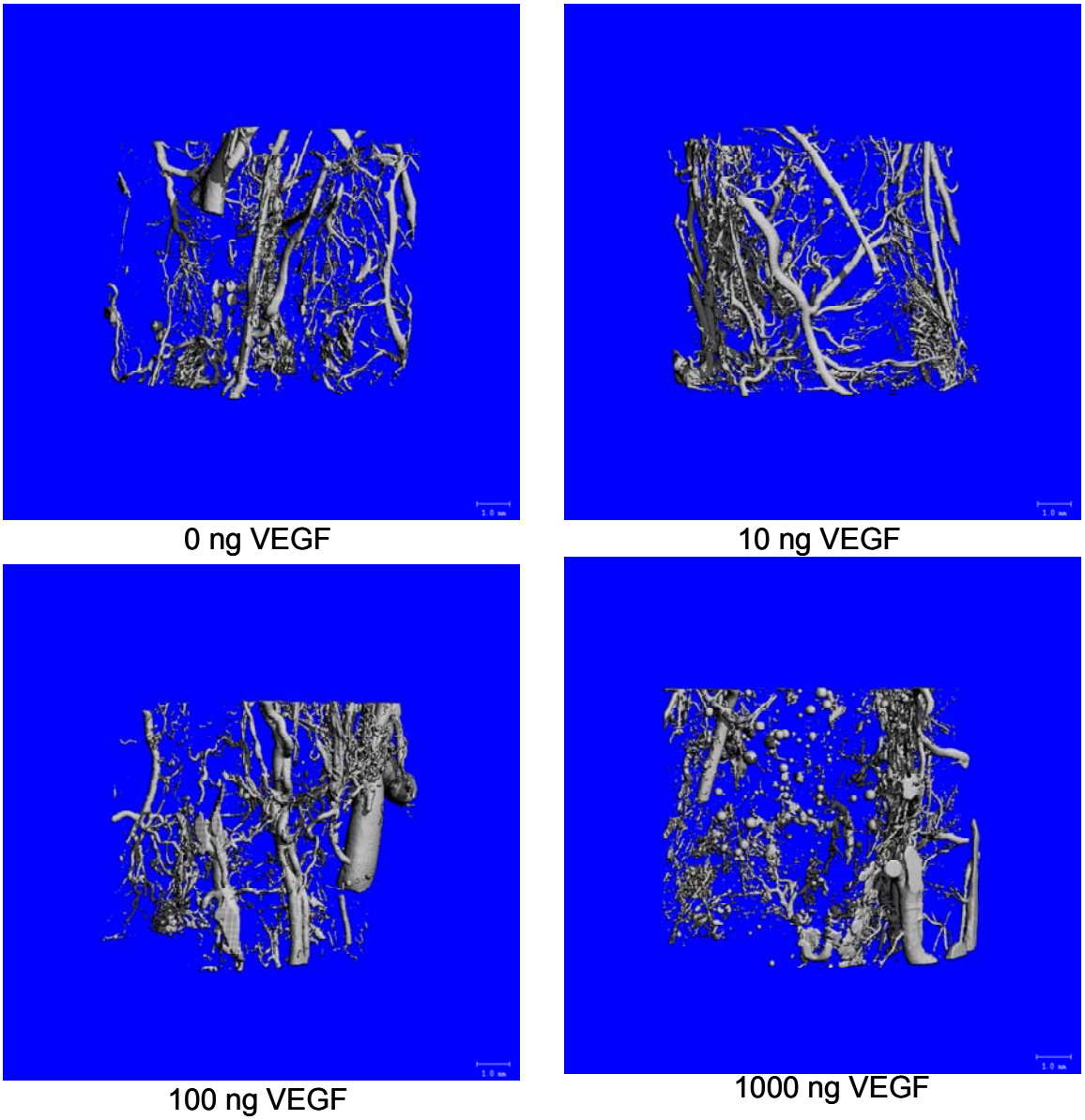

Figure 53: Micro-CT images of perfused and decalcified samples after two weeks of implantation *in vivo*.

Study 2: Effects of Scaffold Geometry and Composition on Bone Formation and Vascular Invasion

Altering the geometry of the PLDL scaffold (coring) or composition (addition of 10% TCP) did not significantly affect the formation of mineralized matrix within the central region of the defect, as determined by *in vivo* micro-CT (Figure 54). Likewise, *post mortem* assessment of the entire defect region (8 mm) did not reveal any differences in treatment regardless of the VOI selected (Figure 55, Figure 56, Figure 57). Micro-CT images mirrored the improved bridging rates seen with the addition of cored PLDL/TCP scaffolds to the defect and the similarities in bone volume between all treatment groups (Figure 58).

The effects of alginate on the ingrowth of vasculature into scaffolds delivering VEGF were assessed using contrast agent-enhanced micro-CT at 2 weeks post-op. Although there were no significant differences between treatment groups, there was an increase in vascular volume in both the total (scaffold and periphery) and peripheral VOIs (Figure 59, Figure 60).

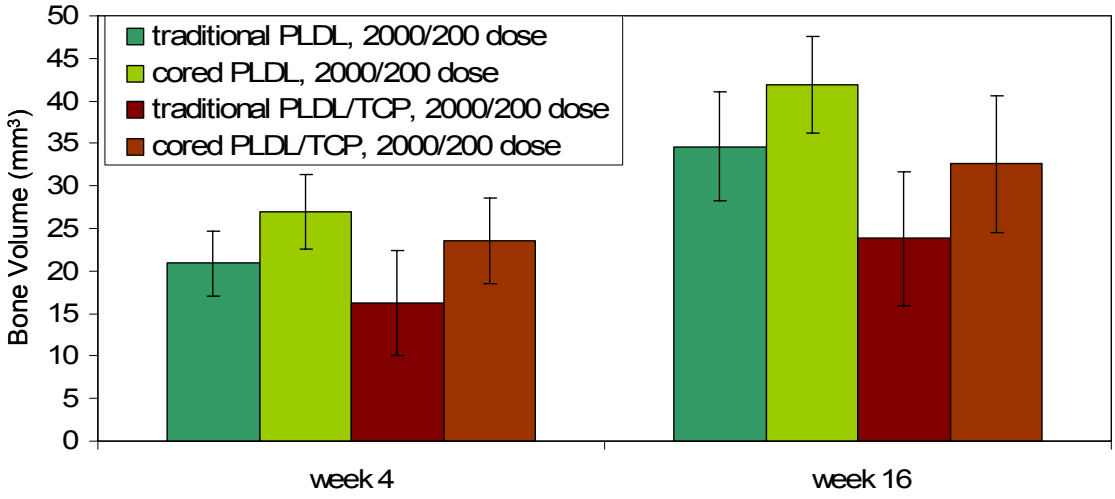

Figure 54: *In vivo* micro-CT data taken from scans at weeks 4 and 16 post-op ($8 \leq n \leq 16$). There were no significant differences between any of the treatment groups.

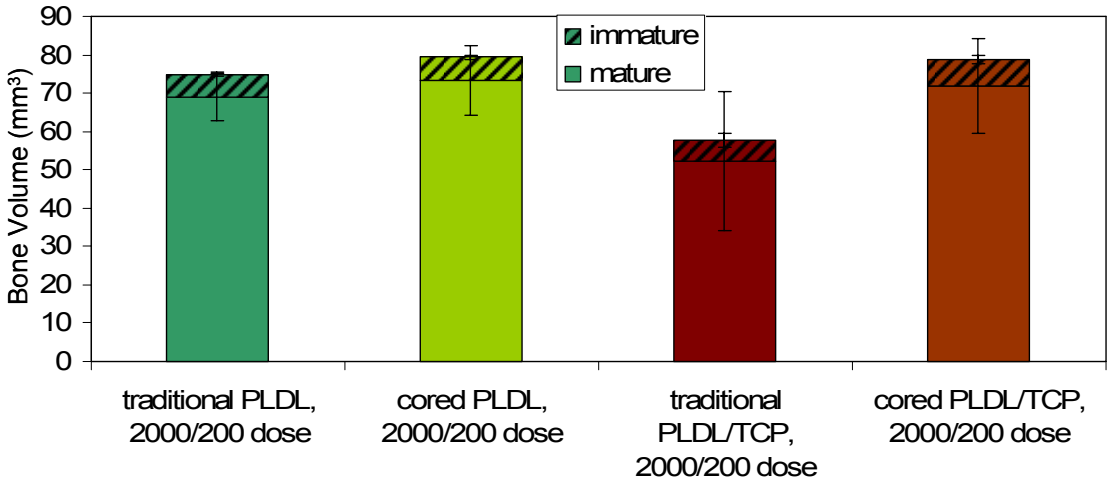

Figure 55: Data from *post mortem* micro-CT scans at 16 weeks post-op ($5 \leq n \leq 14$). There were no significant differences.

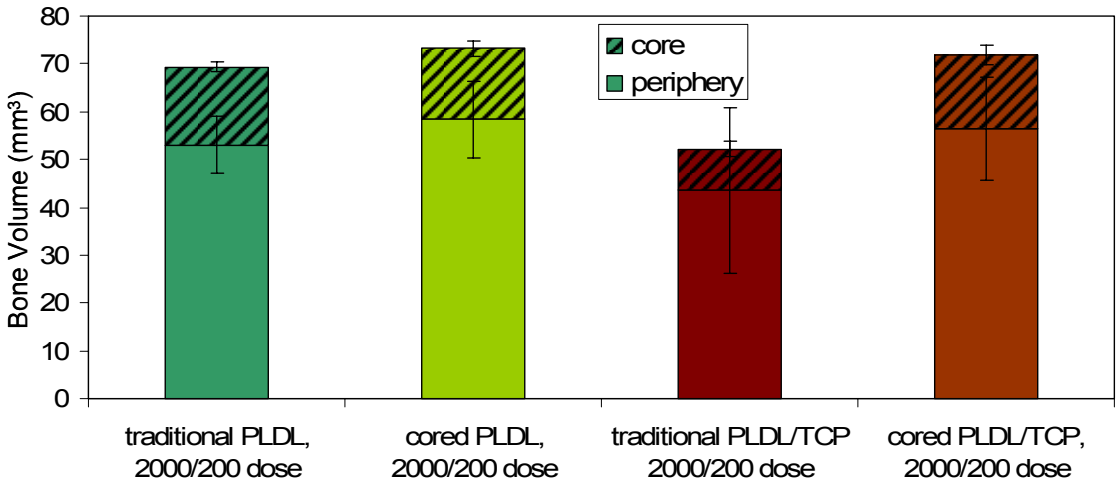

Figure 56: Spatial analysis of the *in vitro* micro-CT scans from 16 weeks post-op revealed no significant differences in the distribution of new bone between the treatment groups ($5 \leq n \leq 14$).

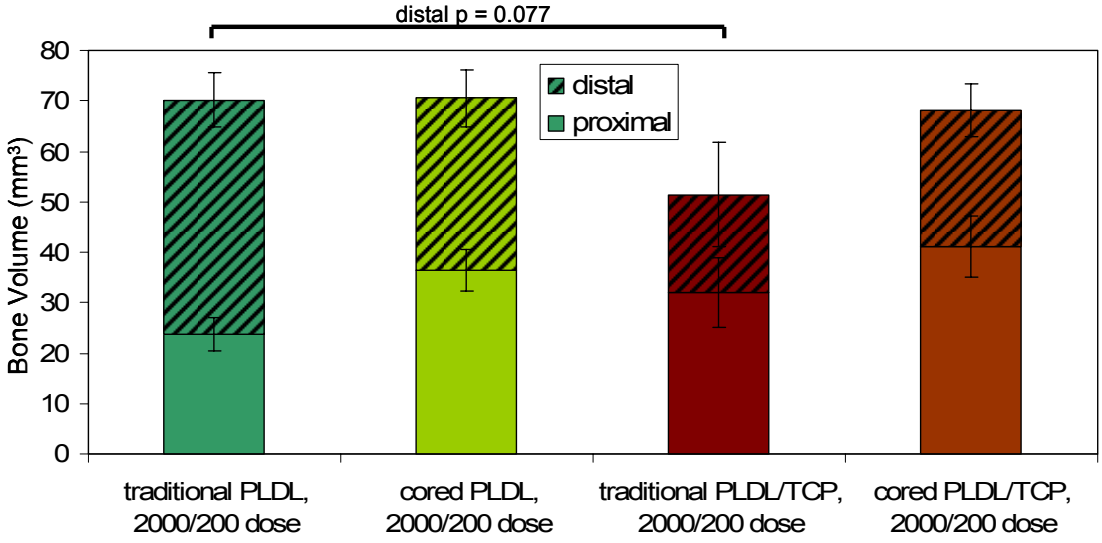

Figure 57: Distribution of the mineralized matrix between proximal and distal halves of the defect site. There were no significant differences ($5 \leq n \leq 14$).

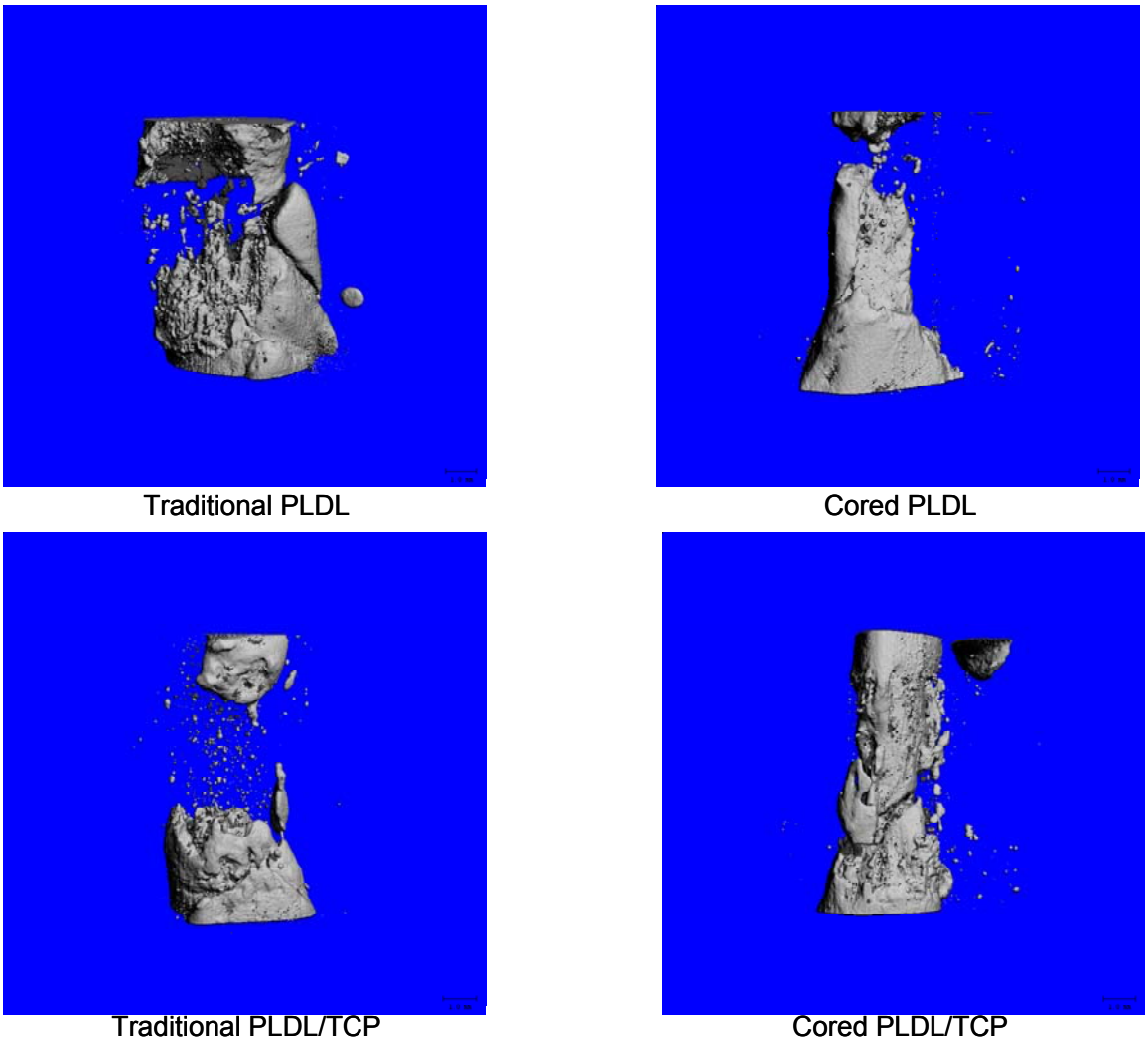

Figure 58: Micro-CT images of the samples at 16 weeks post-op. The images showed union rates that paralleled those seen in the 2-D digital X-ray analysis.

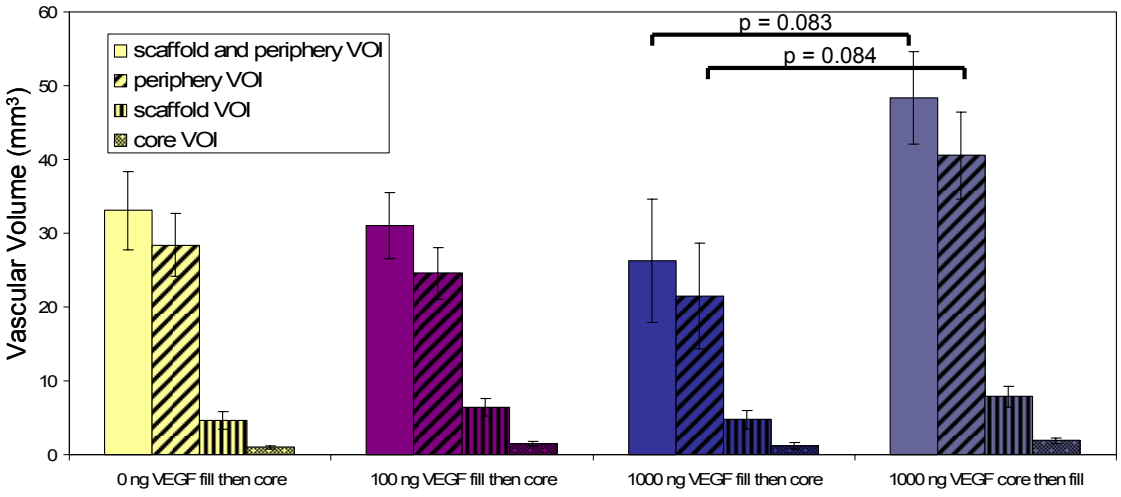

Figure 59: There were no significant differences between doses or growth factor loading regimes in terms of vascular ingrowth ($5 \leq n \leq 9$). There was an increased peripheral vascular volume in the 1000 ng core then fill group as compared to the same dose delivered by filling the scaffold and then removing a core.

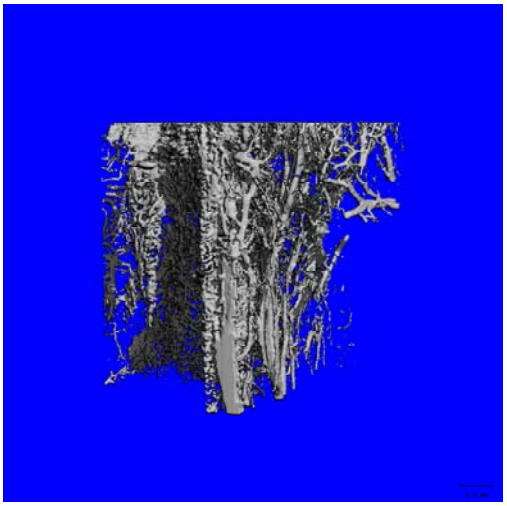

0 ng VEGF Fill then Core

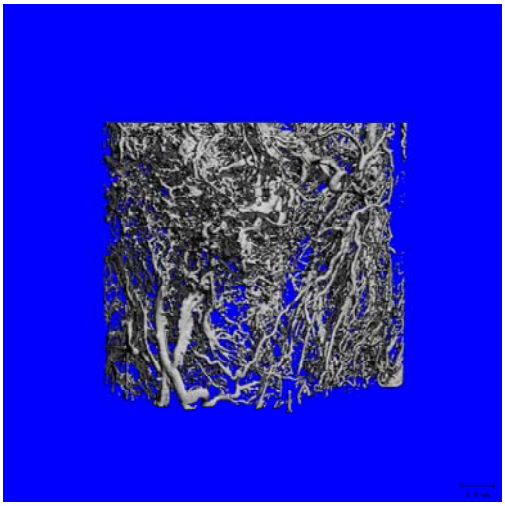

100 ng VEGF Fill then Core

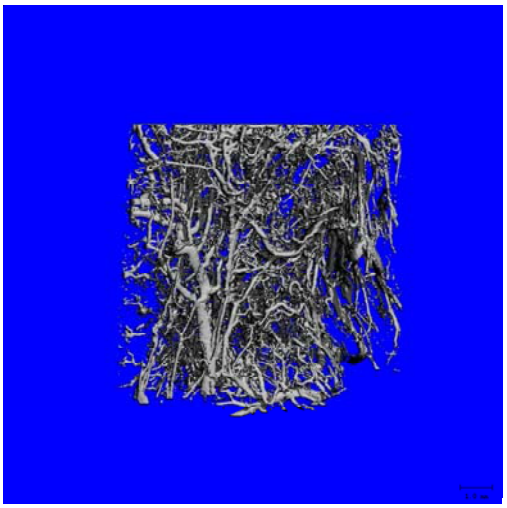

1000 ng VEGF Fill then Core

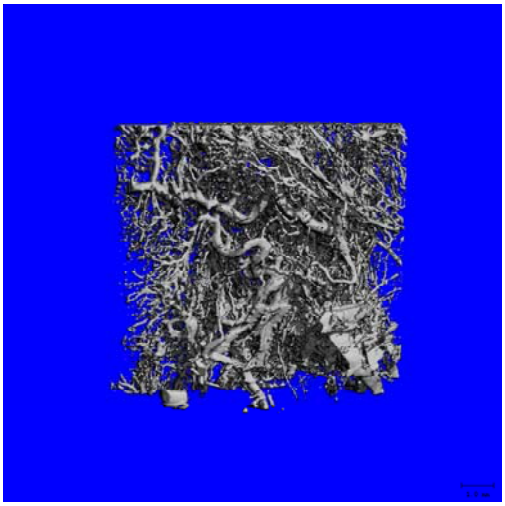

1000 ng VEGF Core then Fill

Figure 60: Micro-CT images of samples from the four treatment groups at 2 weeks post-op. No significant differences in vascularity were detectable.

Study 3: Addition of an Angiogenic Growth Factor to the Osteogenic Cocktail BMP-2/TGF-β3

Addition of 2000 ng BMP-2/200 ng TGF-β3 to the cored PLDL/TCP scaffolds significantly improved bone formation within the defects at 4 and 12 weeks post-op as assessed by *in vivo* micro-CT. Addition of VEGF – with or without BMP-2/TGF-β3 – had no effect on bone volume. The groups that received BMP-2/TGF-β3 had significantly elevated mature, immature, and total bone volumes as compared to the scaffold only and VEGF only treatment groups at 4 weeks post-op. The BMP-2/TGF-β3-receiving groups had elevated mature and total bone volume measurements at 12 weeks post-op as compared to the scaffold only and VEGF only treatment groups (Figure 61). The two groups with BMP-2/TGF-β3 incorporated into the scaffold also experienced significant increases in bone volume with time, while the scaffold only and VEGF only groups did not.

Post-mortem analysis of bone volume within the 8 mm defect revealed the same patterns (Figure 62). Bone volume in both the core and periphery of the scaffold was increased by the addition of BMP-2/TGF-β3, but not by addition of VEGF (Figure 63). Both distal and proximal bone volumes were elevated in the BMP-2/TGF-β3-treated groups as compared to delivery of a scaffold alone. The group that received all three growth factors (BMP-2/TGF-β3/VEGF) had elevated proximal and distal bone volumes as compared to delivery of VEGF alone as well. Co-delivery of only BMP-2 and TGF-β3 significantly increased distal bone volume as compared to VEGF alone (Figure 64).

Delivering VEGF alone or with BMP-2/TGF-β3 did not have an effect on revascularization of the defect site (Figure 65, Figure 66). Treatment was not a significant

factor in determining vascularity within any of the VOIs assessed (peripheral and scaffold, periphery, scaffold, or scaffold core).

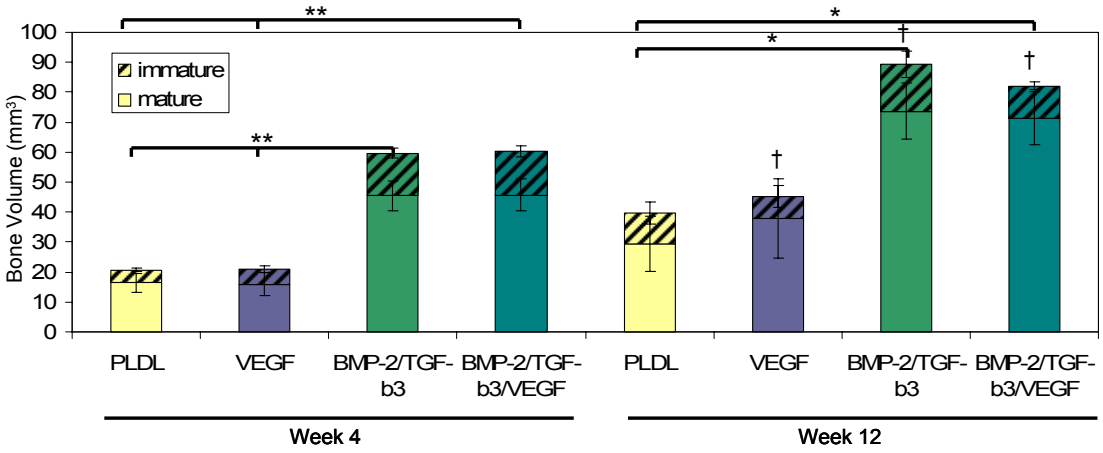

Figure 61: *In vivo* bone volumes determined using micro-CT at weeks 4 and 12 post-op ($5 \leq n \leq 12$). ** $p < 0.001$ for immature, mature, and total bone volumes. * $p < 0.05$ for mature and total bone volumes. † $p < 0.05$ for time. The addition of BMP-2/TGF-β3 significantly increased mature and immature bone volumes at 4 weeks over delivery of VEGF or a naked scaffold. At 12 weeks post-op, addition of BMP-2/TGF-β3 significantly increased mature and total bone volumes over delivery of a scaffold or VEGF alone. The VEGF, BMP-2/TGF-β3, and BMP-2/TGF-β3/VEGF groups all experienced a significant increase in bone volume between weeks 4 and 12.

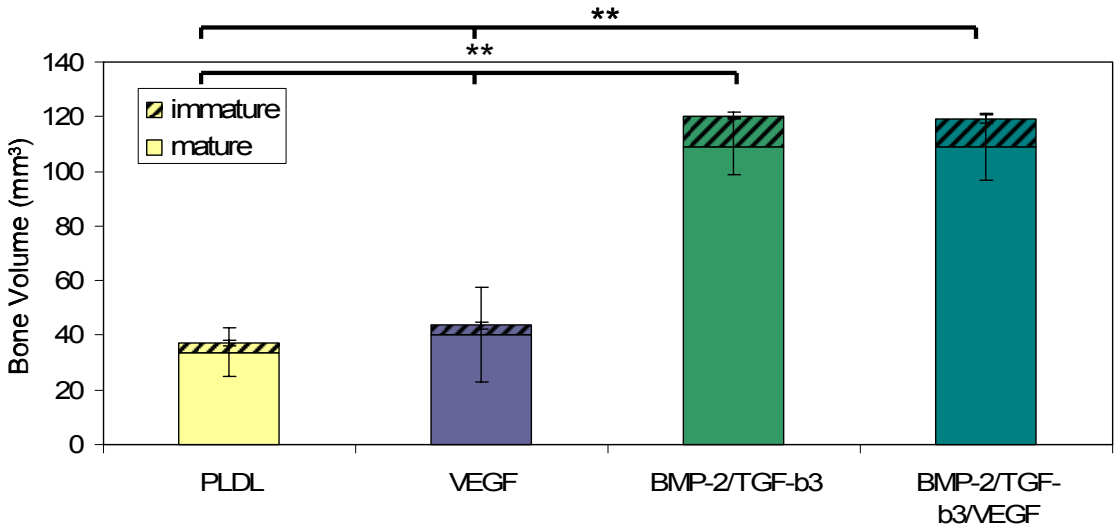

Figure 62: Bone volumes determined using *in vitro* micro-CT ($4 \leq n \leq 12$). ** $p < 0.030$ for immature, mature, and total bone volumes. The groups that received BMP-2/TGF-β3 in the treatment, with or without VEGF, demonstrated a significant increase in immature, mature, and total bone volumes over delivery of VEGF alone or a scaffold alone.

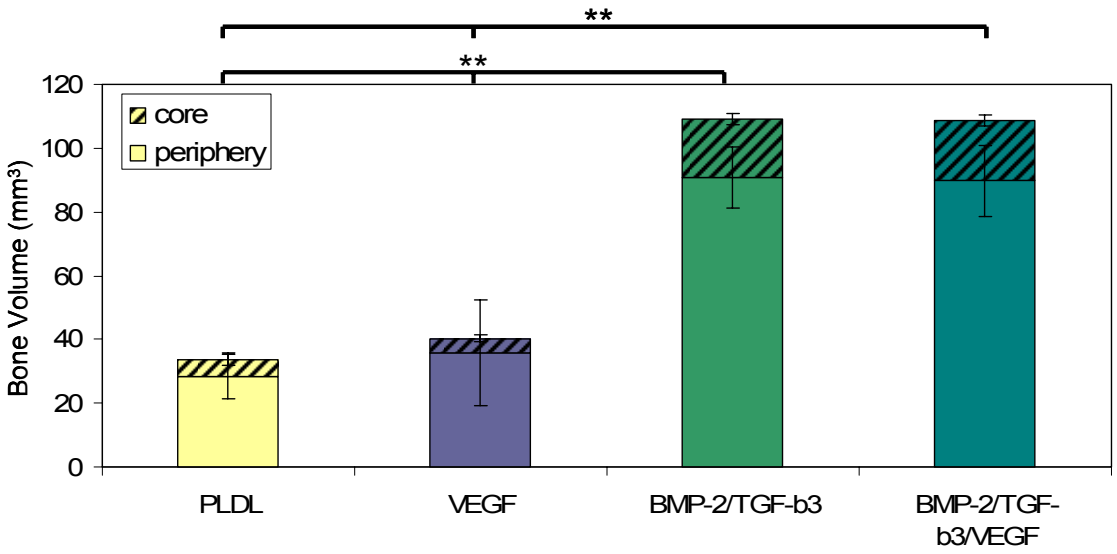

Figure 63: Core and peripheral VOIs were evaluated in the *in vitro* scans at 12 weeks post-op ($4 \leq n \leq 12$). ** denotes $p < 0.050$ for core and periphery VOIs. Co-delivery of BMP-2/TGF-β3 with or without VEGF significantly increased bone volumes in the core and peripheral regions over delivery of VEGF or a scaffold alone.

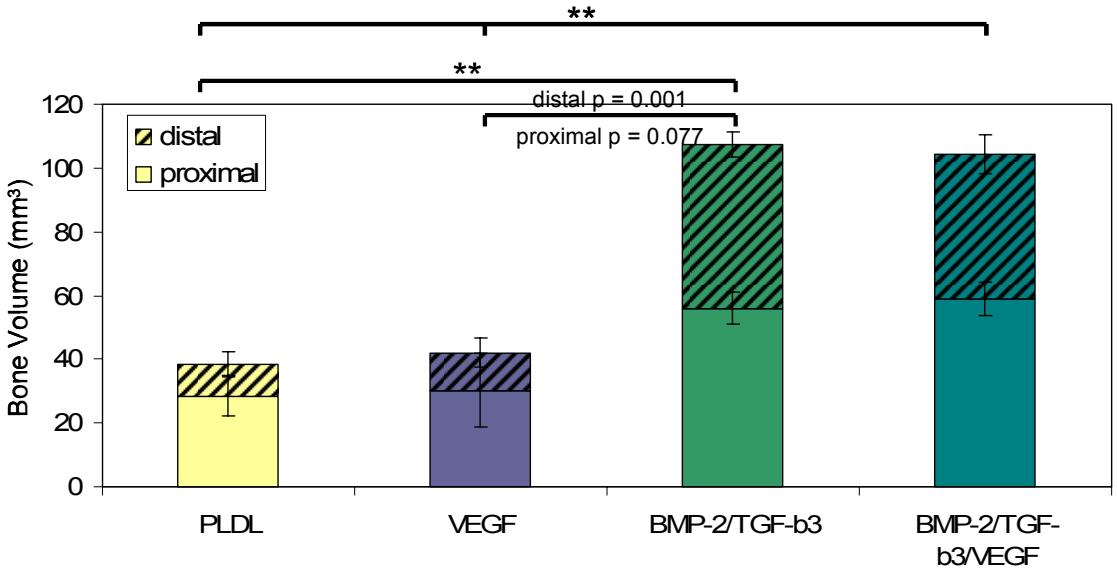

Figure 64: Proximal and distal halves of the 8 mm defect region were analyzed using *in vitro* micro-CT ($4 \leq n \leq 12$). ** denotes $p \leq 0.042$ for proximal and distal VOIs. Addition of BMP-2/TGF-β3 to the defects significantly increased bone volume in both the proximal and distal regions over delivery of a scaffold alone.

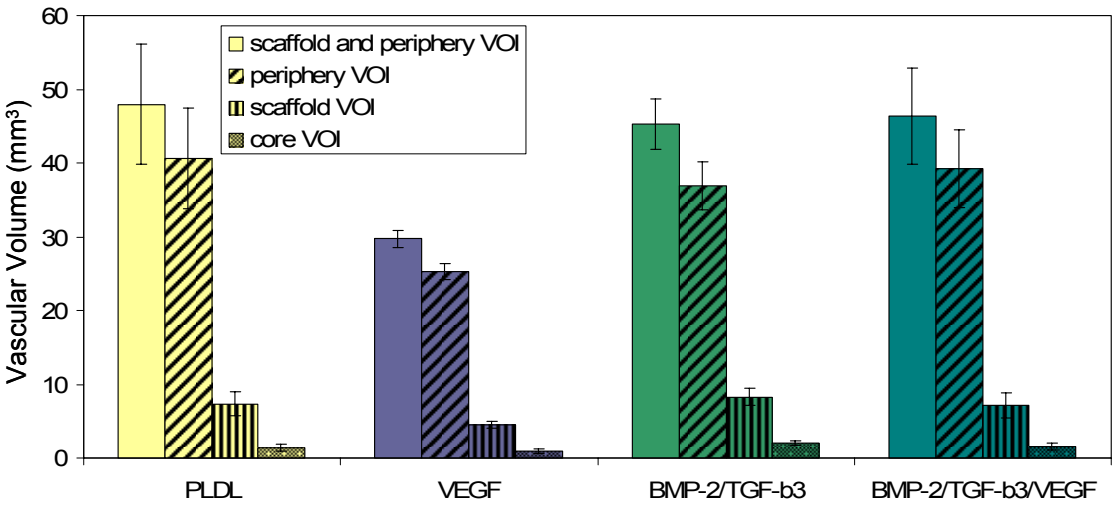

Figure 65: Vascular volumes quantified within the defect site at 2 weeks post-op (n = 8). Treatment was not a significant factor in determining the angiogenic response.

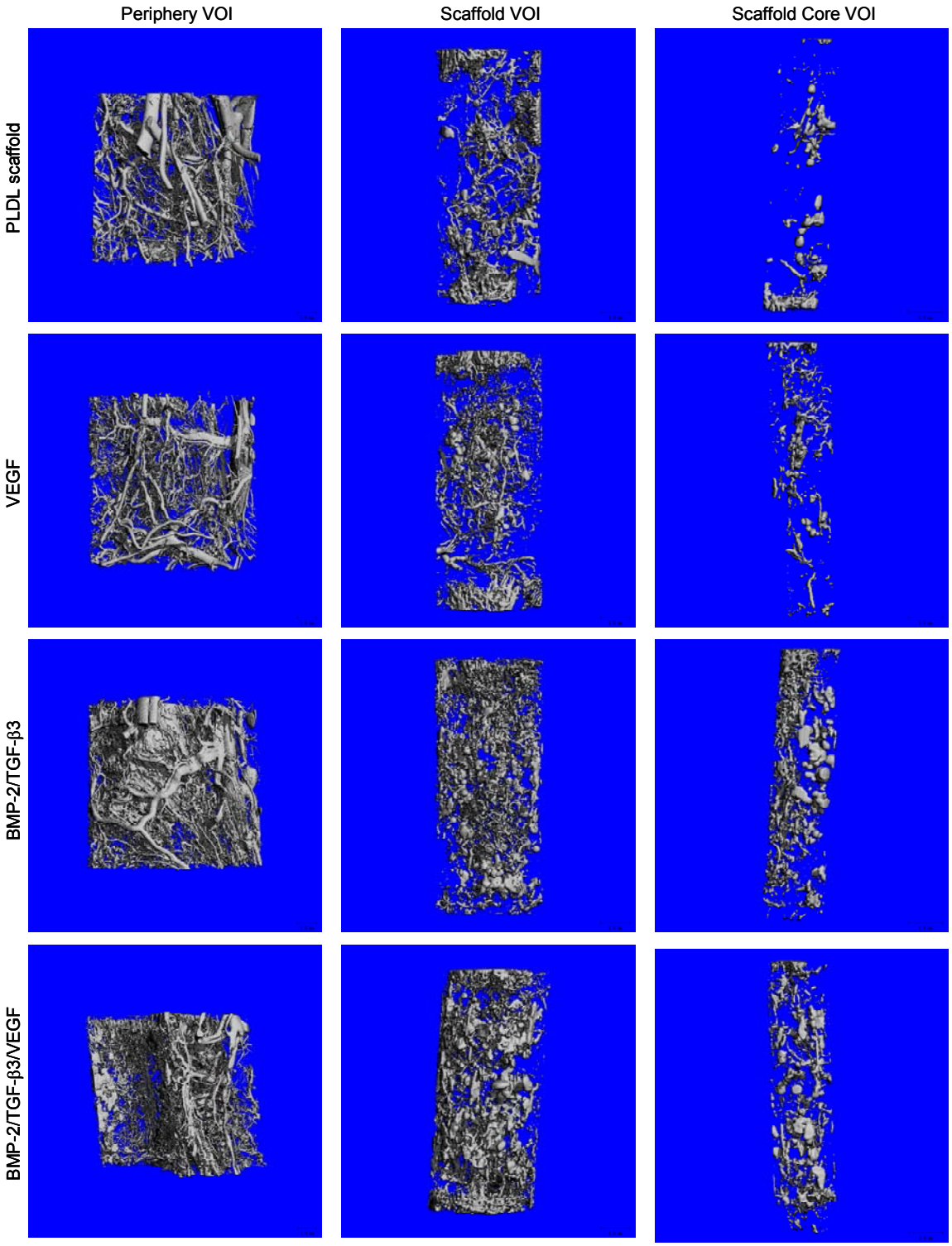

Figure 66: Micro-CT images of perfused, decalcified samples at 2 weeks post-op. No differences in vascularity were detectable.

5.4.5 Mechanical Testing

Study 1: Dose-Dependent Effects of VEGF Delivery on Bone and Vascular Structure Formation

The delivery of VEGF at any dose did not significantly impact mechanical properties. Stiffness and maximum torque were unaffected by delivery of VEGF (Figure 67, Figure 68). Work to maximum torque was similarly unaffected.

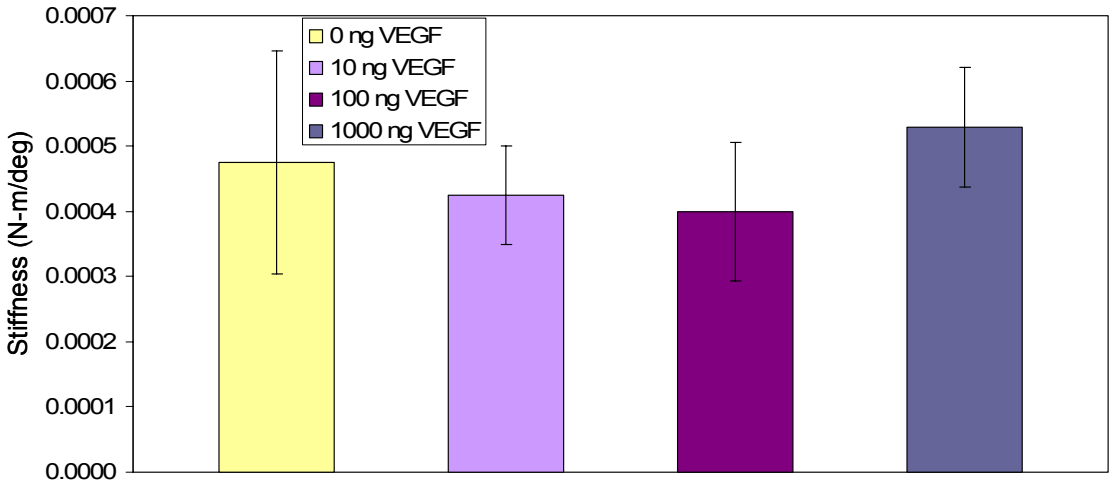

Figure 67: Stiffness measured at 12 weeks post-op ($4 \leq n \leq 7$). VEGF delivery had no effect on stiffness.

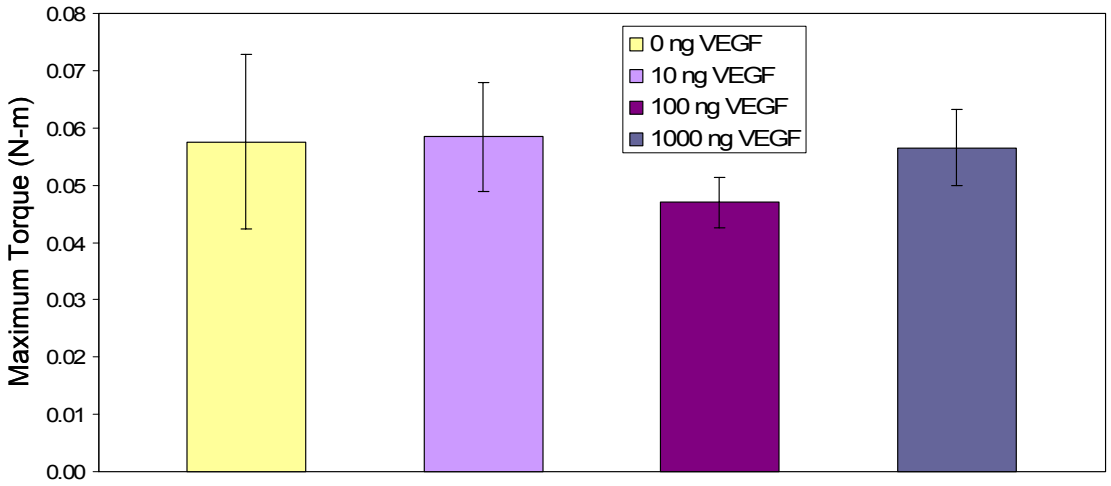

Figure 68: Maximum torque values at 12 weeks post-op ($4 \leq n \leq 7$). Delivery of VEGF at any dose did not impact maximum torque.

Study 2: Effects of Scaffold Geometry and Composition on Bone Formation and Vascular Invasion

Modification of the scaffold geometry (removal of a 1.5 mm longitudinal core) and composition (addition of 10% TCP) did not significantly impact stiffness or maximum torque (Figure 69, Figure 70).

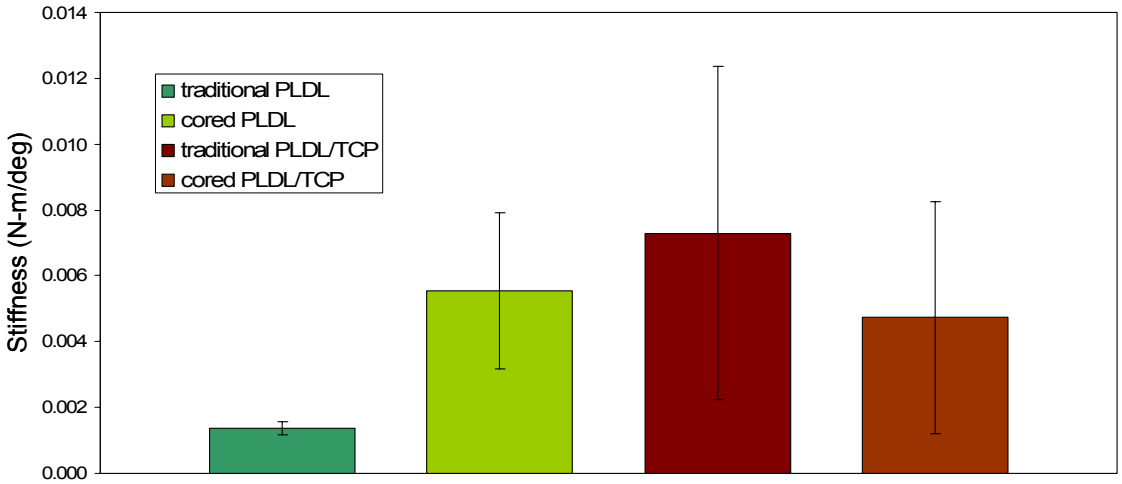

Figure 69: Stiffness was not significantly impacted by scaffold modification ($7 \leq n \leq 14$).

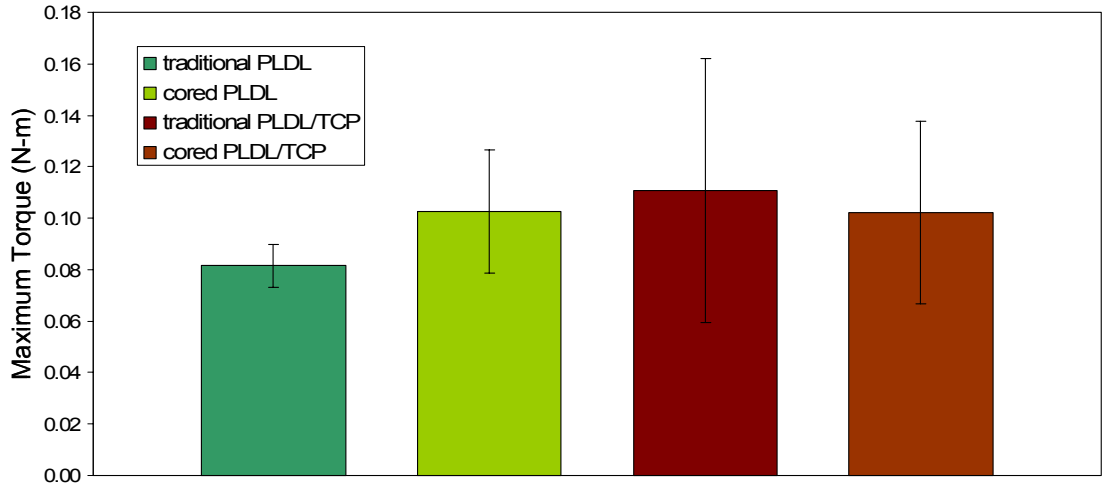

Figure 70: Maximum torque was not significantly impacted by scaffold modification ($7 \leq n \leq 14$).

Study 3: Addition of an Angiogenic Growth Factor to the Osteogenic Cocktail BMP-2/TGF-β3

Delivery of BMP-2/TGF-β3 significantly increased stiffness ($p = 0.004$). Taken individually, there were no significant differences between treatment groups, although treatment was a significant factor ($p = 0.004$) (Figure 71). Similarly, treatment was a significant factor in determining maximum torque ($p = 0.041$); delivery of BMP-2/TGF-β3 significantly increased maximum torque ($p = 0.004$) (Figure 72).

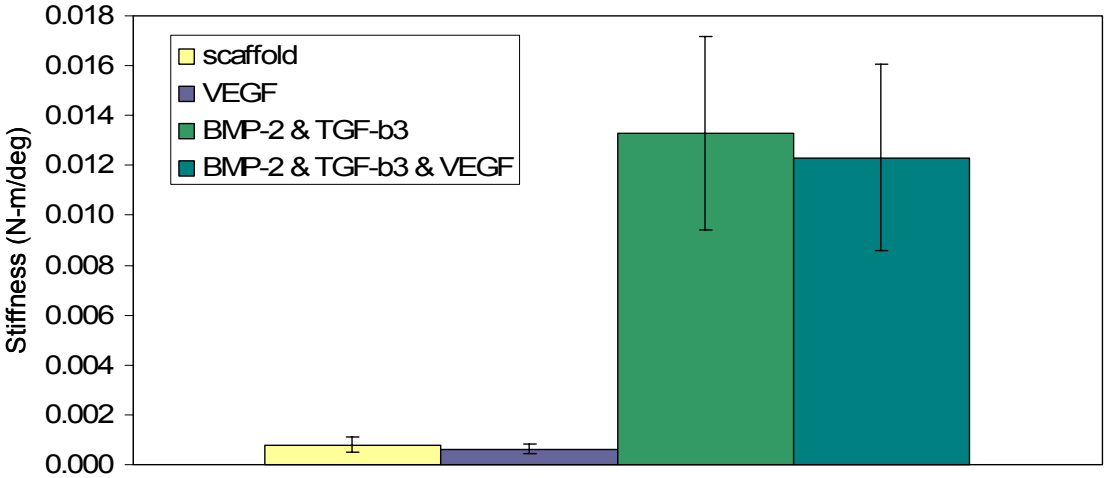

Figure 71: Stiffness measurements taken at 12 weeks post-op ($5 \leq n \leq 12$). Treatment was a significant factor ($p = 0.040$). Collectively, delivery of 2000 ng BMP-2/200 ng TGF-β3 significantly increased stiffness over defects that did not receive BMP-2/TGF-β3 ($p = 0.004$).

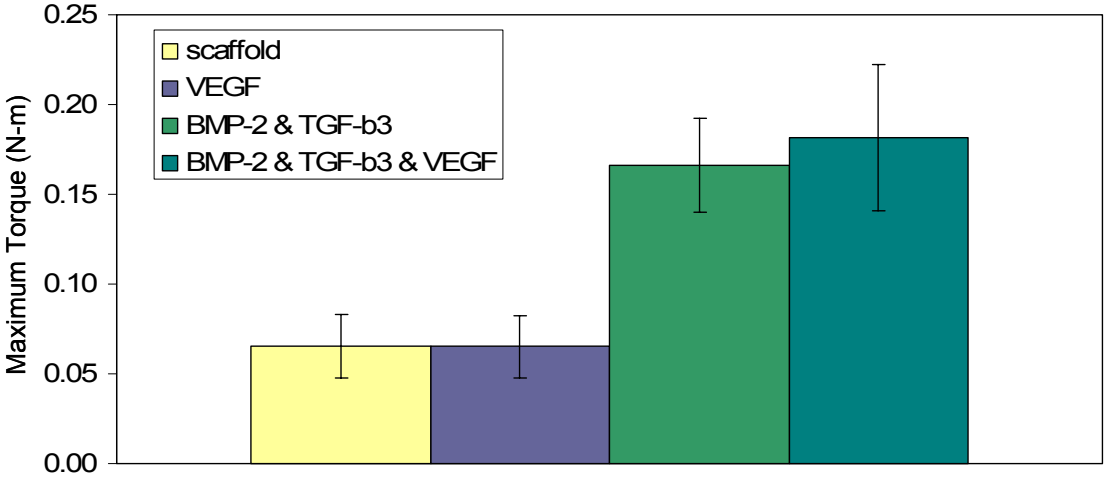

Figure 72: Maximum torque measured at 12 weeks post-op ($5 \leq n \leq 12$). Treatment was a significant factor ($p = 0.041$). Collectively, delivery of 2000 ng BMP-2/200 ng TGF-β3 significantly increased maximum torque over defects that did not receive BMP-2/TGF-β3 ($p = 0.004$).

5.4.6 Histology

Staining of samples with Masson's trichome and von Kossa methods revealed minimal ingrowth of mineralized tissue into the porosity of a traditional geometry PLDL/TCP construct augmented with 2000 ng BMP-2 and 200 ng TGF-β3 (Figure 73). Micro-CT analysis of this group also indicated a somewhat decreased bone volume as well. The cored PLDL/TCP growth factor augmented scaffold showed mineral deposition throughout the longitudinal macropores of the scaffold (Figure 74). Similarly, a representative cored PLDL/TCP scaffold augmented with BMP-2, TGF-β3, and VEGF demonstrated mineralized matrix formation throughout the scaffold pores (Figure 75). Higher magnification images of H&E stained sections showed that the mineralized tissue was cellular in nature. Multinucleated cells resembling osteoclasts were visible on the surfaces of the newly deposited bone (Figure 76). Cells with single nuclei were also apparent on the newly formed bone surfaces (Figure 77).

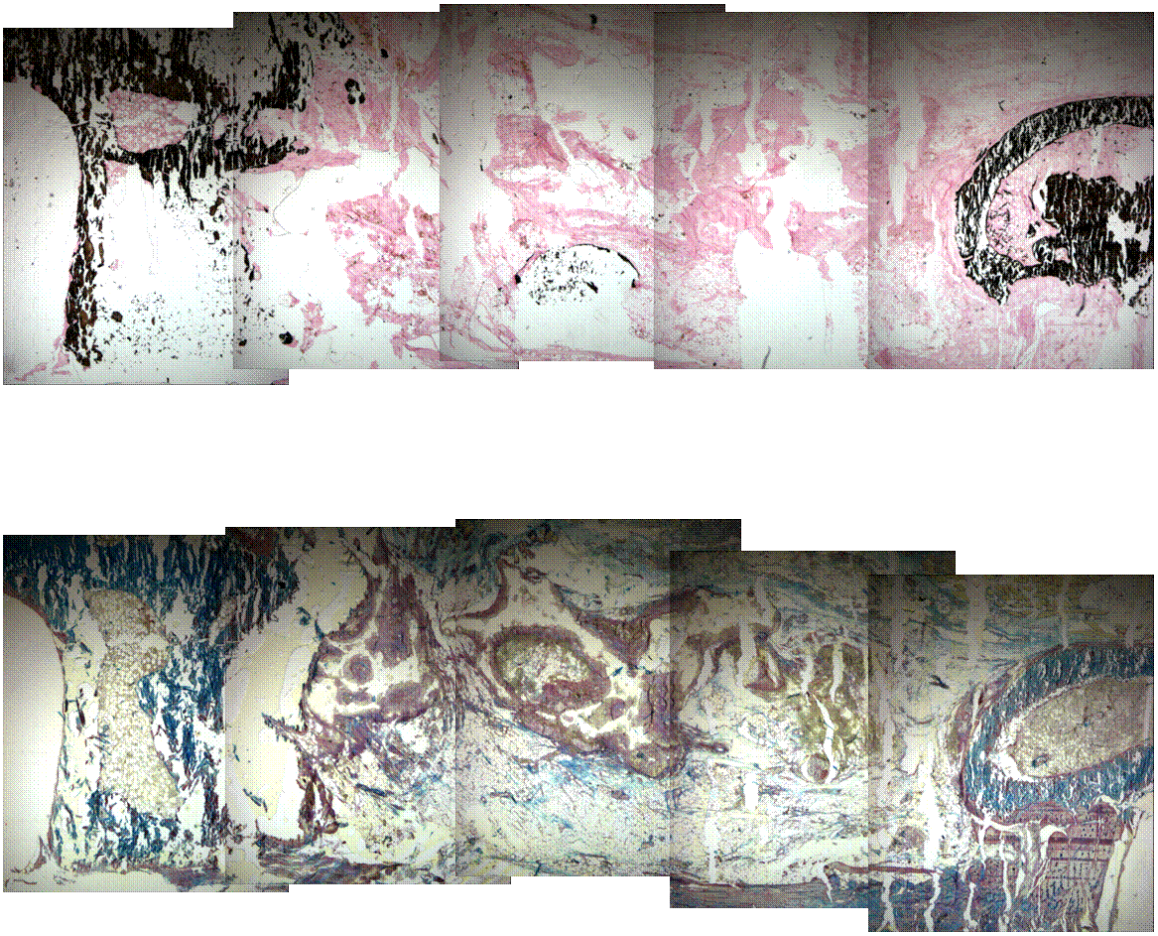

Figure 73: Histological sections taken from a sample treated with a traditional geometry PLDL/TCP construct augmented with 2000 ng BMP-2 and 200 ng TGF-β3. Consistent with micro-CT quantification of bone volumes, this sample shows little mineralized tissue invasion. Upper row, von Kossa staining; lower row, Masson's trichrome.

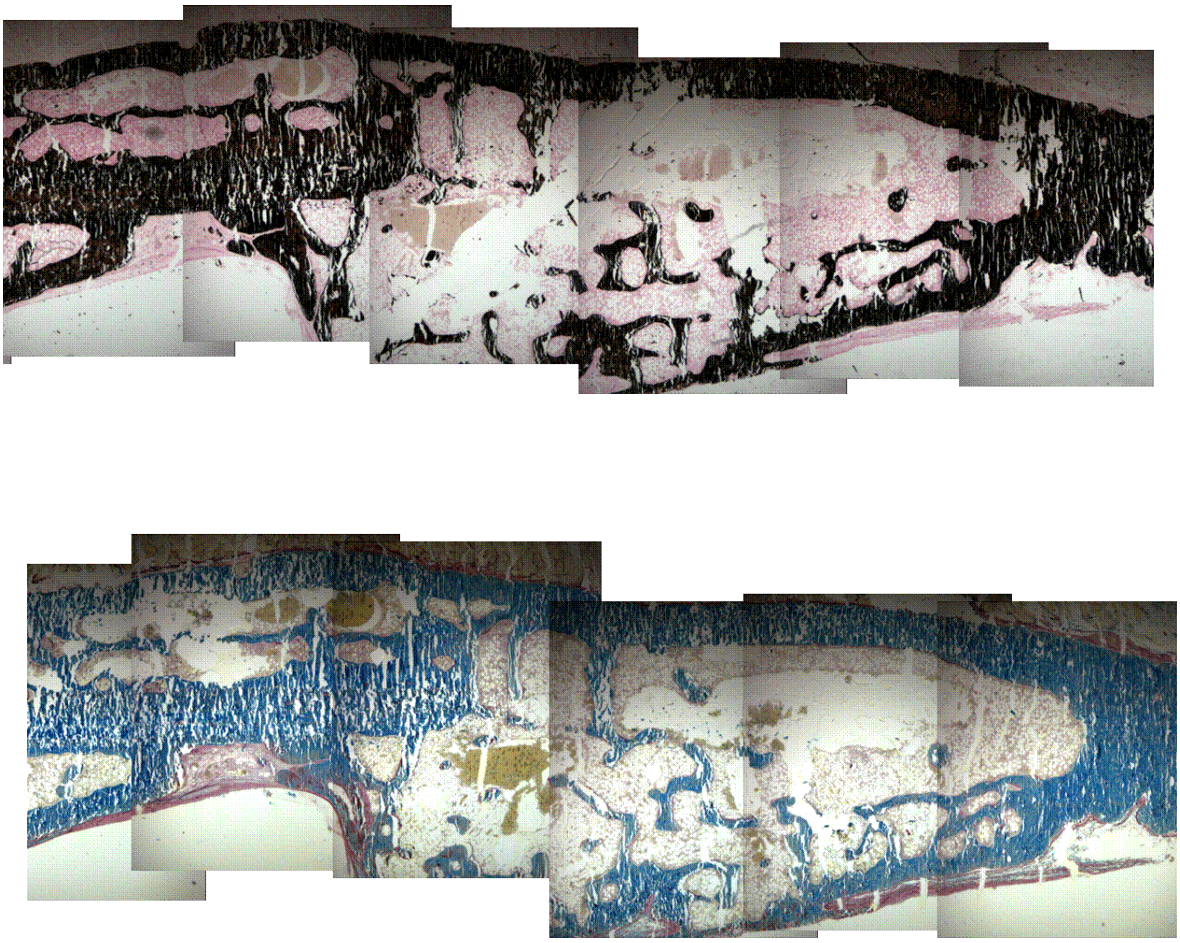

Figure 74: Histological sections taken from a sample treated with a cored PLDL/TCP construct augmented with 2000 ng BMP-2 and 200 ng TGF-β3. Consistent with micro-CT quantification of bone volumes, this sample shows invasion of mineralized tissue into the construct. Upper row, von Kossa staining; lower row, Masson's trichrome.

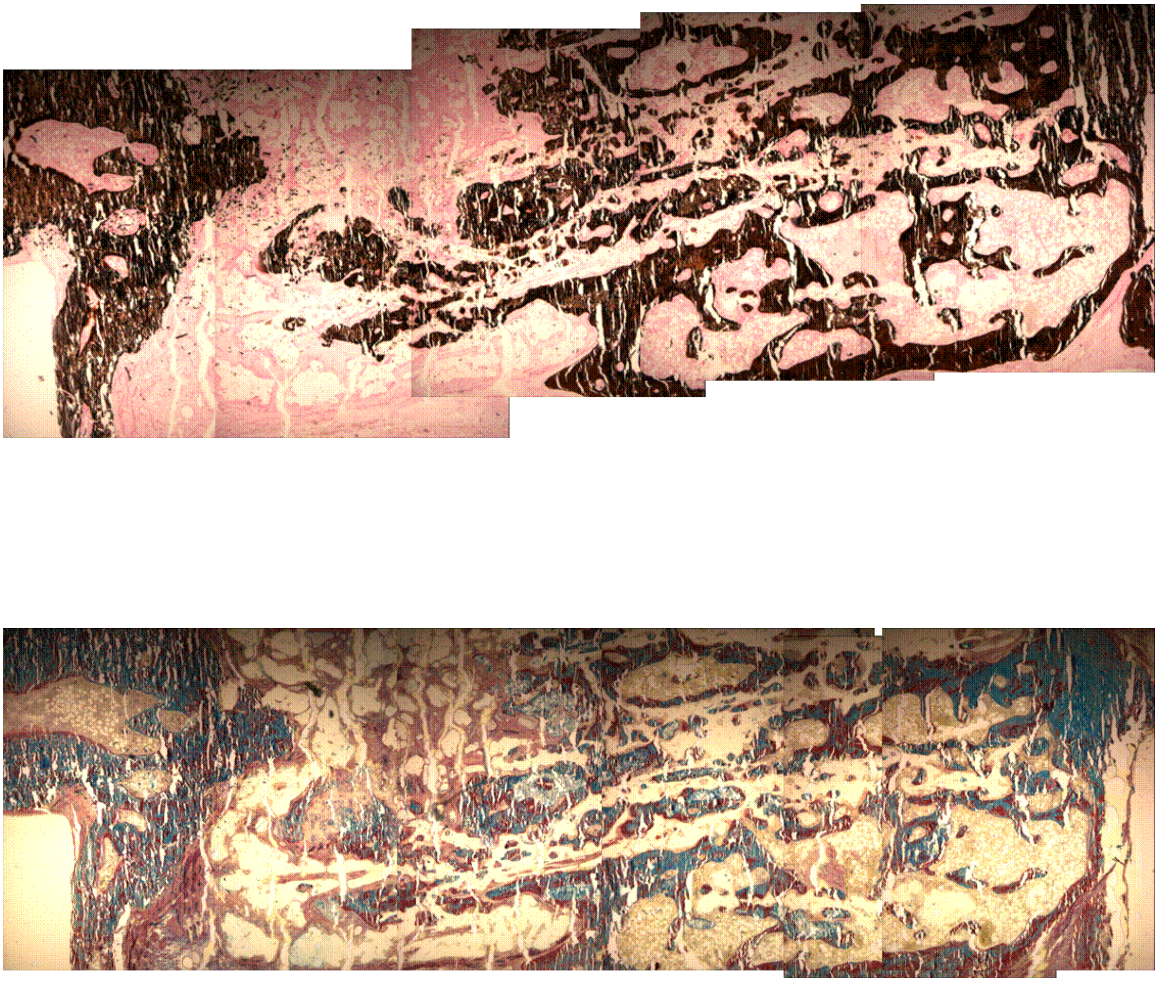

Figure 75: Histological sections taken from a sample treated with a cored PLDL/TCP construct augmented with 2000 ng BMP-2, 200 ng TGF-β3, and 1000 ng VEGF. Consistent with micro-CT quantification of bone volumes, this sample shows significant invasion of mineralized tissue into the construct. Upper row, von Kossa staining; lower row, Masson's trichrome.

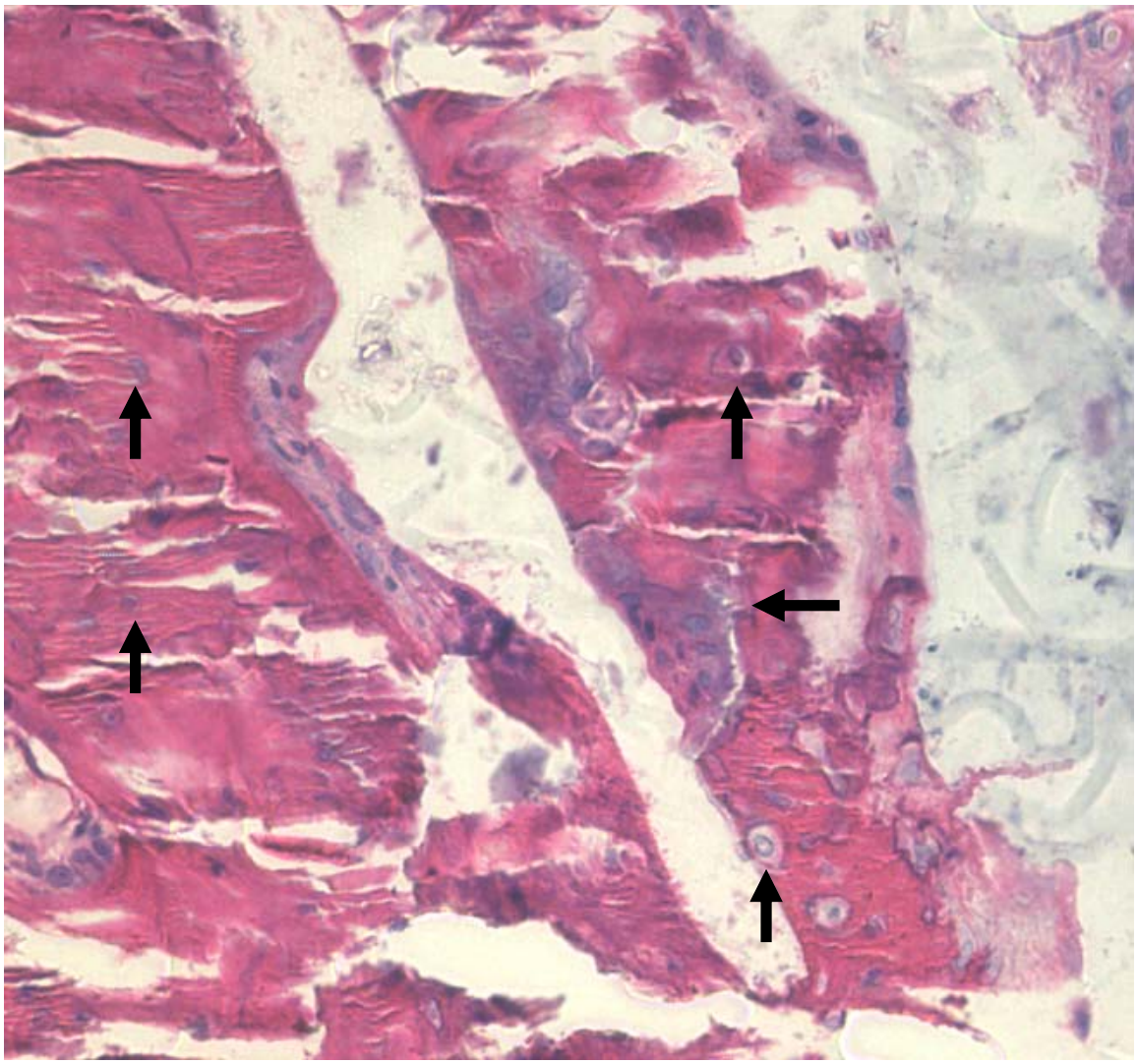

Figure 76: Histological sections stained with H&E indicate that the mineralized matrix formed in the tissue-engineered constructs is cellular in nature, and undergoing active remodeling. Up arrows indicate osteocytes embedded in the mineralized matrix. Sideways arrow indicates the presence of a multinucleated osteoclast.

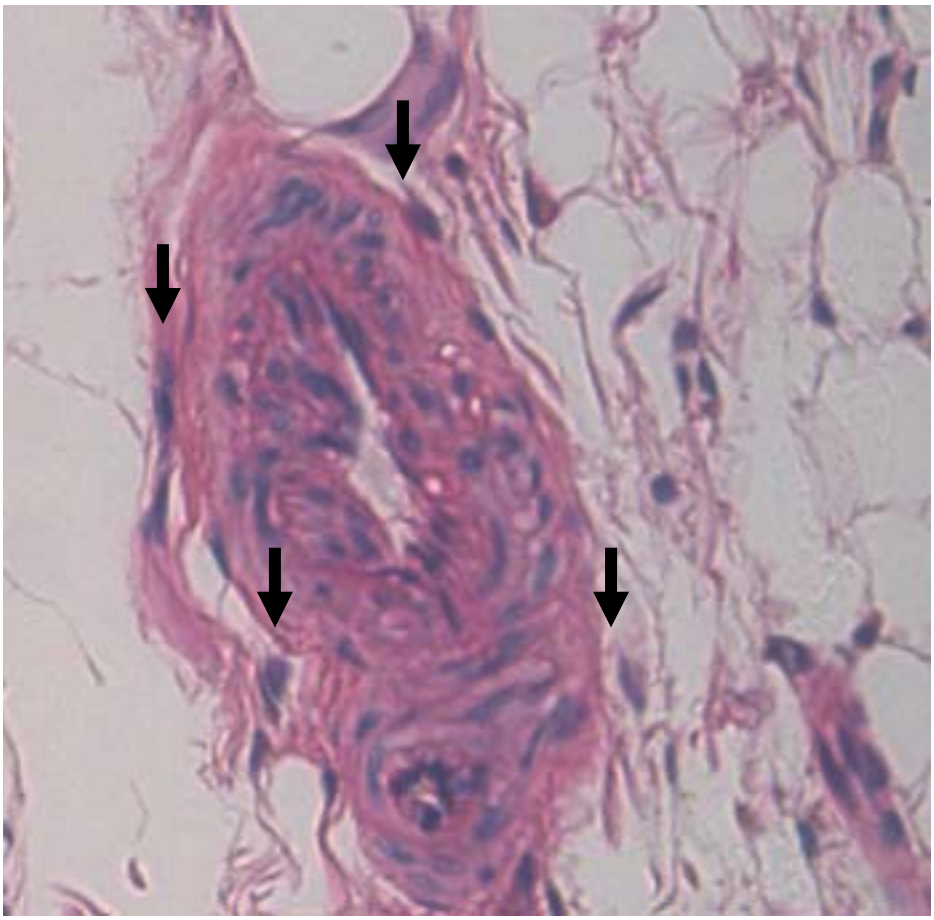

Figure 77: Histological sections stained with H&E indicate that the mineralized matrix formed in the tissue-engineered constructs is cellular in nature, and undergoing active remodeling. Down arrows indicate cells on the surface of the maturing mineralized matrix.

5.5 Discussion

Although the potency of VEGF as an angiogenic growth factor is well documented, its effects on bone formation are widely varied and may be highly dose-dependent [STREET 2002, ECKHARDT 2003]. Use of VEGF in a large segmental defect has only been investigated in one other study; a rabbit radial defect model was treated with 0-1000 μg of VEGF. Delivery of high dose VEGF did enhance the callus volume of these defects [STREET 2002]. Delivery of VEGF protein has also been reported to enhance bone formation in irradiated calvarial defects [KAIGLER 2006]. The studies presented here noted two things; delivery of VEGF at doses that may cause angiogenic responses in various *in vivo* models are ineffective at promoting new bone formation in this model, and elevation of early vascular structure development was not enhanced by the delivery method of VEGF used in this model. Delivery of as little as 10 ng/ml of VEGF has been shown to induce chemotaxis of osteoblastic cells [MAYR-WOHLFHART 2002]. VEGF concentrations in a standard rat tibial fracture model peak at 5 days post-fracture at a concentration of approximately 100 pg/ml [PUFE 2002]. The equivalent doses delivered in the studies here range from 1-10 μg/ml, well above the threshold of physiologic values. Application of 1.25 μg of VEGF to a 10 x 5 mm cranial defect in conjunction with demineralized bone matrix grafts enhanced bone regeneration over control samples [EMAD 2006]. Delivery of 20-50 μg VEGF per gram of alginate (50 ug/g equates to 36 ng VEGF per implant) to a subcutaneous model of angiogenesis resulted in a significant increase in the number of blood vessels formed [LEE 2003]. Implants used here contained 10-1000 ng VEGF each. Delivery of 2-4 μg of VEGF has been shown to induce extensive angiogenesis in an *in vivo* model as well [ELCIN 2001].

The dose-dependence of VEGF's effects on angiogenesis vary widely in reports [STREET 2002]. The quantity of growth factor actually delivered to these defects was significantly less than that which was intended. In a similar alginate system, VEGF release was reported to reach 40% of the growth factor incorporated by 21 days of *in vitro* incubation [SILVA 2007]. The release of only ~25% here suggests that perhaps the PLDL scaffold is binding up some of the growth factors as the alginate releases them, resulting in inefficient delivery of the intended dose. One other probable explanation for these results is that the dose of VEGF used in this model is simply too low to accelerate the bone repair process or further stimulate angiogenesis in the model. Clearly, based on the growth factor release kinetics, the dose of VEGF that was actually released is far lower than that which was intended to be delivered. Recently published studies indicate that the dose of VEGF required to enhance mineral formation in certain models may be around 3 μg [HUANG 2005, HAO 2007, KAIGLER 2006, STREET 2002]. The quantity of bioavailable growth factor may also be lower due to the complex signaling and activity that takes place in traumatic injury. Removal of a large section of tissue activates proteases, which may be degrading the growth factors as they are released from the implant. Sequestering the growth factors in the alginate may also prevent some percentage of the protein from being released in active form; it is possible that the growth factors are not in an active conformation or orientation when contained in the alginate.

It is, however, also possible that the animal's angiogenic response is already at its maximum capacity to respond due to the acute injury; this would leave no room for elevation of vascular structure development to improve. It is also possible that in such a small total defect size (8 mm), that revascularization is not the rate-limiting step. Without

delivery of VEGF, scaffolds become vascularized throughout. Work by Rai et al. indicates that there is a potential to enhance vascularity within the defect site at 3 weeks post-op in this model; delivery of platelet-rich plasma resulted in a trend towards elevated vascular volume at 3 weeks post-op as compared to delivery of a scaffold alone [RAI 2007]. The delivery of PRP was shown to enhance mineralization over delivery of a scaffold alone at 12 weeks, but not at 4 weeks post-op. The timing of VEGF release in the model system presented here may be suboptimal. Delivery at a later time point when the acute physiologic reactions have subsided may be more effective at generating an angiogenic response.

Alternatively, the alginate matrix may be binding the VEGF, inhibiting release of the protein into the surrounding tissue. Residual alginate matrix within the scaffold, as well as chains that have been freed from the matrix due to crosslink degradation, may be bound to VEGF, inhibiting detection of the molecule. Delivery of VEGF from an alginate matrix has been shown to enhance the bioactivity of the growth factor [SHERIDAN 2000]. Sustained release of VEGF has been shown to enhance angiogenesis over a longer period of time (8 weeks), while damping the initial response [ELCIN 2001]. If the release of VEGF is delayed in the PLDL/alginate system used here, it may be that the angiogenesis was quantified at a time point (2 weeks) too early to capture the physiologic response. Yet another possible explanation is that the VEGF is bound by the scaffold in an inactive form as the alginate degrades, resulting in delivery of a far lower dose of VEGF than was intended.

The *in vitro* experiment quantifying growth factor release from the scaffolds put the cumulative release of growth factors at about 25% of the quantity loaded, with the

majority of the release occurring over the first 2-5 days in culture. There are a variety of possible explanations for the fate of the remaining ~75% of growth factor. The simplest explanation is that the remainder of the growth factor is bound up in the residual alginate matrix. Because of the large osteogenic response seen with implantation of the BMP-2/TGF-β3-containing constructs, it is probable that the bound growth factor is released or exerts its effect as cells invade the construct. Another possibility is that the remainder of the growth factor is actually released from the matrix, but in denatured or inactive form. Although this may be the case, it might be unlikely; the delivery of low doses of BMP-2 in other segmental bone defect repair models does not stimulate osseous union [LEE]. Alternatively, the growth factors could be released still bound to the alginate fragments, or be binding to the PLDL scaffold itself as they are released from the alginate. If the growth factors are still bound to alginate fragments, they may be active, but unable to be detected by the antibodies used in the ELISAs as the alginate could be blocking the detection epitopes. The PLDL scaffolds were pre-coated with fibronectin prior to growth factor seeding. Although the stability of fibronectin may have occluded open binding sites for the growth factors, inhibiting their adhesion to the scaffold, fibronectin itself has been known to bind proteins.

It is difficult to determine how well the sustained delivery mechanism selected for use here correlates properly to the physiologic response to fracture repair. Expression of TGF-β3 typically peaks during the endochondral bone formation/periosteal response phase, and is sustained through primary bone formation during fracture healing. Histological evaluation of samples did not show evidence of endochondral bone formation, although a periosteal response to the injury was activated sometime during the

first four weeks *in vivo*. BMP-2 expression during fracture healing peaks in the early stages of injury and inflammation, with continued lower level expression throughout fracture healing [GERSTENFELD 2003]. It may be that the efficacy of BMP-2 in this model is due in part to early delivery of soluble active growth factor with sustained low-level delivery through later time points, somewhat paralleling the natural fracture healing response. VEGF expression during fracture healing is not as great in magnitude as that of BMP-2, but appears to be more active during the primary bone formation stage of fracture healing. This suggests that evaluating vasculature at a later time point may enable differences between treatment groups to be determined.

Scaffold architecture and composition plays an important role in the vitalization of the implant. This is apparent as the lack of porosity in allografts and many ceramic implants impedes tissue ingrowth. Although treatment differences between sample groups were not apparent in terms of bone volume or mechanical properties, the union rate of the cored PLDL/TCP constructs was higher than that of any other group. For this reason, the cored PLDL/TCP scaffolds were selected for investigation in the studies that followed. Despite the lack of significant differences between treatment groups in the study assessing the growth factor loading regimes, it should be noted that between studies 1 and 2, there was a 2-fold increase in the vascularity. This may be due to the removal of the core from the center of the scaffold (the perfusion and imaging techniques remained constant between the two studies). The addition of 10% TCP to the scaffold was done under the hypothesis that accelerating the scaffold degradation process *in vivo* such that it would more closely match the rate of bone ingrowth. The long residence time of the

scaffold in the host body, however, means that 12 weeks may be too short of a time period to determine the effects of adding a ceramic on degradation of the PLDL scaffold.

The addition of VEGF to the osteogenic growth factor cocktail of BMP-2/TGF-β3 had no beneficial effect on bone formation or vascular invasion. It has been previously reported that co-delivery of DNA encoding BMP-4 and VEGF enhances bone formation in a synergistic manner when delivered subcutaneously in the presence of bone marrow stromal cells [HUANG 2005]. Data presented in the work described here does not show an interactive effect with co-delivery of BMP-2 and VEGF protein. This may be due to the low doses of total protein used, the rate of growth factor release from the alginate matrix within the scaffold, or a combination of both factors. The work by Huang et al. describes the synergistic interaction between BMP-4 and VEGF gene delivery to occur only when BMSCs were co-delivered in the scaffold as well. The time required for osteoprogenitor cells to infiltrate the alginate-filled PLDL scaffolds may be such that the majority of the freely diffusible growth factor is gone by the time the cells populate the defect region. The remainder of the VEGF and BMP-2 protein, bound to the residual alginate and/or PLDL, could be sequestered in manner that prevents a single cell from interacting with both growth factors in the means necessary to induce a synergistic response.

The rate of delivery and mechanism of growth factor delivery may be critical to the success of the therapy. Scaffold geometry also plays an important role in enabling the invasion of vascular structures into the defect site, particularly within the bounds of the scaffold itself. Co-delivery of VEGF with BMP-2 and TGF-β3 provided no additional benefit over delivery of the two osteogenic growth factors alone in terms of

revascularization of the defect site or regeneration of functional bone. Delivery of VEGF at doses that may induce neovascularization in a variety of models was unsuccessful in elevating the angiogenesis over the innate, unaugmented response of the host body to creation of the defect. These doses of VEGF were also unsuccessful in promoting new bone formation. In the third study, however, it should be noted that the VEGF-treated defects did experience a significant increase in bone volume between weeks 4 and 12 post-op.

The co-delivery of 2000 ng BMP-2 and 200 ng TGF-β3 demonstrated continued bone formation over 12 weeks *in vivo* and resulted in significantly improved mechanical properties over groups that did not receive BMP-2/TGF-β3 as a treatment (VEGF only or scaffold only). The maximum torque of the BMP-2/TGF-β3-treated samples approached, and in some cases reached, that of intact age-matched femurs. Studies described in previous chapters met with similar success in terms of bone volume and rate of bony union, but had marginally less success in reaching intact femur mechanical properties. The third study done in the chapter presented here used a new batch of fixation plates that turned out to be structurally compromised; approximately 50% of the plates in the VEGF only and scaffold only treatment groups fractured between weeks 8 and 12 *in vivo*. This reduction in mechanical integrity of the fixation plates might have resulted in increased load-sharing with the scaffold in the defect site. In defects without BMP-2/TGF-β3, there was inadequate mineralized matrix invasion to support load. Defects that did receive BMP-2/TGF-β3 had adequate integration with the host bone and mineralization within the central region of the implant to support this load. The increase in bone volume could also be due to delivery of a more potent lot of growth factor.

In conclusion, addition of VEGF at any of the three purportedly angiogenic doses – 10 ng, 100 ng, and 1000 ng – did not improve mineralization or revascularization of the defect site over delivery of a PLDL scaffold alone. Although scaffold geometry did not affect the bone volume or mechanical properties for defects treated with BMP-2/TGF-β3-augmented PLDL scaffolds with cored geometries and/or 10% TCP added. The rate of bony union was higher, however, in the cored PLDL/TCP group. Based on this observation, the cored PLDL/TCP scaffold was selected for use in the remaining studies. The manner in which the growth factors were added and the longitudinal core of the scaffold removed did not significantly affect vascular volume, although there was a strong trend towards increased peripheral vascular volume in the group treated with 1000 ng VEGF delivered in PLDL/TCP scaffolds that were pre-cored and then loaded with growth factor-containing alginate. This observation, along with ease of use for the surgeon, prompted the use of pre-cored PLDL/TCP scaffolds for the triple growth factor study. Delivery of VEGF alone or with BMP-2/TGF-β3 did not significantly enhance mineralization or mechanical properties of the samples over co-delivery of only BMP-2 and TGF-β3. The VEGF-treated group did experience a significant increase in bone volume with time though, suggesting that controlled release of VEGF may enhance bone formation long-term (beyond the 12 week scope of these studies). The complex problem of the release of the BMP-2, TGF-β3, and VEGF from the scaffolds merits further investigation. The simplest explanation for the fate of the unreleased growth factors is that they are sequestered in the remaining alginate, and exert their bioactivity only when cellular invasion forces degradation of the alginate structure and the progenitor cells take up the bound growth factor.

CHAPTER 6

CONCLUSIONS AND FUTURE DIRECTIONS

6.1 Segmental Defect Model and Analysis Techniques

The development of a reproducible and robust critically-sized defect model described in Aim I was central to the work in this thesis. The hardware and techniques used to stabilize and create these defects improves upon that of other researchers in several ways. Firstly, the hardware enables stable fixation of the defects, limiting confounding factors such as micromotion. Micromotion in a defect site compromises the body's ability to heal and may make subcritically sized defects appear critical in nature. Stabilization of bone defects is critical to healing. Early experimentation with 5 mm defects (data not included in this thesis) revealed that 5 mm segmental defects were subcritical in size; they healed randomly and spontaneously in the absence of treatment. Attempts at defect fixation using the standard polyethylene block and four Kirshner wires method revealed gross instabilities in the defects. Many of the defects treated with this fixation technique collapsed over the duration of a 12 week study. The novel hardware developed here not only provides stability to the defect, but also serves as a guide for the surgeon. Two notches designed into the underside of the plate serve as guides for placement of the miniature oscillating saw, enabling the surgeon to reproducibly generate 8 mm long defects. The stainless steel anchor plates secure directly to the bone using four miniature screws, providing a solid base to which the polysulfone bridging plate is affixed. This polymer plate allows *in vivo* X-ray and micro-CT imaging of the defect site,

enabling the researcher to do longitudinal studies and thereby reducing the number of animals and variability within each study. Removal of the plate is easy and can be achieved without damaging the bone or repair tissue, as the polymer plate is affixed to the stainless steel anchor plates, not the bone itself. Facile removal of the bridging plate is critical to maintaining the integrity of the repair tissue for mechanical testing *post mortem*.

The image analysis techniques used in the work described here have been shown to match histomorphometric techniques for quantifying vasculature, and exceed conventional techniques in reproducibility [DUVALL 2004]. One aspect of the vascular perfusion/micro-CT method that would benefit from further analysis is the determination of the proper resolution at which samples should be scanned. A resolution of 20 μm was most reasonable in terms of the scan time and computational power required to analyze the data. Analysis of samples at a higher resolution (10 μm) does not significantly alter the vascular volume, but does impact other parameters such as connectivity (see Appendix A). The increase in image detail obtained with higher resolution comes at the cost of time, data storage capacity, and computational power. Another aspect of this imaging technique that would benefit from improvement is the contrast agent used. Use of the Microfil silicone-based contrast agent requires termination of the animal. If a high-contrast agent suitable for delivery *in vivo* that is also capable of being segmented from the bone could be developed, longitudinal studies of vascular development in defects would be possible.

It was hoped that by correlating mechanical properties with bone volume data through the studies presented here, a means of estimating stiffness and maximum torque

form *in vivo* or *in vitro* micro-CT scans would be developed. Several VOIs were analyzed in an attempt to establish this correlation – the central 4.5 mm long region of the defect, the entire defect (8 mm), the proximal half of the defect, and the distal half of the defect. Although statistically significant correlations between stiffness and all VOIs and maximum torque and all VOIs emerged, the R-squared value ranged form 41.6% to 65%. The distal, proximal, and central VOIs did not correlate with maximum torque or stiffness in an increasing linear manner for bone volumes of less than approximately 50 mm^3. Similarly, use of the entire 8 mm VOI did not result in a positive linear correlation for bone volumes of less than 100 mm^3. These findings indicate that there may be some critical bone volume that must be achieved before increases in maximum torque or stiffness occur. Further work into establishing this threshold value would be of interest in attempting to use *in vivo* scans to assess mechanical integrity of the defects.

6.2 Growth Factor Delivery and Release

The delivery mechanism for VEGF, BMP-2, and TGF-β3 used in these studies is simple in conception and implementation, but challenging to characterize. Based on findings in the literature and the data obtained from the *in vivo* studies here, it is clear that the alginate-filled PLDL scaffold results in controlled release of the growth factors over an 2-5 day period of time. *In vitro* characterization of the growth factor release kinetics indicated that only a quarter of the total protein delivered is freely diffusible from the scaffold in its active form. Studies investigating delivery of VEGF from an alginate hydrogel system have put the total release of growth factor at about 40% of the quantity incorporated into the alginate over 21 days *in vitro* [SILVA 2007]. Comparison of the

studies presented here and those in the literature suggest that remainder of this growth factor might be bound within the remaining alginate and PLDL scaffold, exerting its effect only as cells migrate through the construct. The ability of the implant to release bioactive factors to the host tissue may be critical to the success of the tissue-engineered treatment strategy. If the growth factor is delivered exclusively as a molecule tethered to the scaffold, there is no diffusible signal to the surrounding host cells that would potentitate cellular proliferation and/or migration to the implant site [RIZZI 2006, LUTOLF 2003]. On the other hand, if the growth factor is too readily diffusible, there is inadequate sustainment of the signal to achieve a substantial biological response unless a large quantity of bioactive agent is delivered [OHURA 1999, HONG 2000]. Further investigation of the growth factor release from the alginate-PLDL system could be accomplished by dissolving the residual alginate matrix as a means of releasing bound growth factor, although it is possible that the growth factors remain secured to the alginate polymer chains themselves. Radiolabeling the growth factors and tracing their release from the matrix would provide a more accurate description of the location of the growth factors with time. Engineering a well-controlled release strategy for growth factors is difficult. In most hydrogel and polymer systems, the microstructure of the delivery vehicle changes with time as the growth factor is released and the matrix of the delivery system degrades, gains water content, or becomes more porous. Use of controlled-release microspheres with varying degradation rates delivered in a stable hydrogel would be one option for controlling growth factor release in a minimally changing matrix.

6.3 Growth Factor Co-Delivery and Interactions

While co-delivery of BMP-2 and TGF-β3 significantly improved bone formation in a dose-dependent manner and improved the mechanical properties of the repair tissue over delivery of a scaffold alone, there was a marked absence of synergistic interaction. Co-delivery of physiologic doses of BMP-2 and TGF-β3 with BMSCs in an ectopic mouse model has been shown to produce a synergistic interaction that enhances osteogenesis by 6 weeks post-implantation [SIMMONS]. In the segmental defect model, delivery of the same physiologic dose of growth factor elicits no response above that seen with delivery of a scaffold alone. Co-delivery of the two growth factors at a dose one order of magnitude greater did, however, induce a significant increase in both early (4 weeks) and late (12 weeks) bone formation. The delicate balance of BMP-2 and TGF−β3 that produces the synergistic effect seen ectopically may be altered by scaling up the dosage in a linear manner, or by the presence of the growth factor milieu released by the resorption of the fracture haematoma, influencing the interactions between the proteins. The acute and traumatic nature of the segmental defect model may activate a significant early inflammatory response and produce active proteases within the injury site. This, combined with the many endogenous signaling molecules, may result in decreased or altered signaling as compared to the less acute subcutaneous model. Additionally, the segmental defect model used here relied on the proliferation and migration of endogenous osteoblastic cells to vitalize the implanted scaffold, whereas the subcutaneous study directly co-delivered the BMSCs with the growth factors. This delay in the presence of cells within the matrix may be partially responsible for the lack of a synergistic response,

as some of the freely diffusible growth factor had dissipated from the implant or lost its bioactivity by the time cells populated the scaffold.

Similarly, co-delivery of BMP-4 and VEGF in gene form has been shown to produce synergistic interactions in the presence of BMSCs in the murine subcutaneous implantation model [HUANG]. In the studies presented here, BMP-2 rather than BMP-4 was selected, and the BMP/VEGF combination was delivered in protein form. Because of this, one would not necessarily assume that a synergistic interaction between BMP-2 and VEGF would result, although it does make a reasonable hypothesis. Although the same potential explanations for the lack of positive interaction between the BMP-2 and VEGF as were delineated previously for the BMP-2/TGF-β3 system, there is also the strong possibility that not enough VEGF was released to interact properly with the BMP-2. Alginate is known to bind VEGF when used as a hydrogel delivery system, although this interaction has been reported to enhance the bioactivity of the protein when it is released [SILVA 2007].

One future direction for consideration if the growth factor delivery system is selected for further use would be the determination of growth factor interactions in a more controlled model, such as *in vitro* tissue culture or subcutaneous or intramuscular implantations. A model system with fewer confounding factors – here the complex microenvironment created by induction of a severe defect – could potentially make it easier to tease out interactions between the growth factors. However, this approach is limited in its relevancy; the initial motivation for the use of growth factor co-delivery in the critically sized segmental femur defect model came from the finding that BMP-2 and TGF−β3 interacted synergistically in the subcutaneous implantation model.

In most animal models of osteogenesis, the results of treatments are highly dependent on the type of scaffold used. It is possible that the PLDL scaffolds selected for use in these studies limited bone formation due to the small diameter of the macropores and relatively slow degradation rate. Use of a collagen sponge in this model would provide a means of assessing the effects of delivering slow vs. fast-degrading implants. It would also provide some comparison to the clinical BMP-2/ACS spinal fusion treatment. Another control group that is important in evaluating the efficacy of the growth factor treatment is the allograft. This is the clinical standard treatment, and direct comparison of the growth factor strategy tested here with the traditional allograft treatment would provide a measure to assess the potential advantages to using a tissue-engineered implant for functional bone repair.

The use of BMSCs or MSCs delivered with or without angiogenic and/or osteogenic growth factors is also an interesting direction for research to expand using the model system established here. Although the host's body provides adequate quantities of progenitor cells to regenerate the mineralized matrix and restore a certain level of mechanical integrity, augmentation of the implant with autogenous or syngeneic marrow progenitor cells may provide a means of accelerating the repair process. This approach has been widely investigated, but the survival of the delivered cells after implantation is sometimes compromised by the lack of a functional vascular supply to the defect site [KADIYALA, MARCACCI 2007]. Augmentation of a cellularized scaffold with bioactive factors that promote a rapid autogenous vascular and mineral deposition response could provide a means of maintaining the graft viability. In a similar vein of thought, modification of grafted cells to produce specific osteogenic genes has enhanced

the healing response [SAVARINO 2007, XIE 2007]. Although bone marrow progenitor cells have been the typical choice for these cell-based therapies, alternative cell sources have been investigated for use after genetic modification, including muscle-derived cells and fibroblasts [KREBSBACH 2000, PHILLIPS 2006, SHEN 2004]].

Regeneration of bone in a segmental defect model requires the presence of cells, a scaffold or delivery vehicle, and a bioactive agent (such as a protein or gene). There is an unknown critical balance that must be achieved between these three components. The response described in the previous chapters may be limited by the availability of host cells as well as the delivery mechanism chosen for the growth factors. Conversely, delivery of cells alone has been somewhat limited by the lack of a biological stimulus that invokes a host response that will promote development of a nutrient supply to the engrafted tissue.

6.4 Potential Modifications to the Model

The use of the critically-sized femoral defect model described in the previous chapters has been constrained to immediate treatment after creation of the defect. Clinically, this aspect of the model may be irrelevant. In treatment of bone trauma, the ability of the host body is frequently compromised due to a variety of factors, including delayed treatment, radiation, infection, chronic nonunion, and smoking. A research model that mimics these confounding factors inherent to clinical treatment could potentially provide the opportunity to evaluate the full potential of delivered cytokines to augment the healing process. Induced chronic infection in a rat segmental defect model has indicated that, in conjunction with antibiotic therapy, delivery of only high doses (200

μg) of BMP-7 can induce bony repair [CHEN 2006]. Similarly, irradiation of bony defects has been shown to compromise the body's ability to heal the defect. Radiation treatment provides a more relevant model for developing treatments for osteosarcoma. Patients who smoke tend to have longer bone healing times as well, although the reasons for this are not fully understood. Chronic nonunions may be more difficult to heal than an acute injury because the body's natural sequence of healing reactions may have senesced. Reactivating these inherent phases of healing, such as haematoma formation, angiogenesis, and cartilaginous callus formation, may prove difficult. All of these modifications to the segmental defect model would provide a scenario more relevant to certain clinical conditions and possibly a more challenging defect to heal.

6.5 Conclusions

In starting this work it was hypothesized that by exploiting growth factor interactions, osseous repair of segmental bone defects could be generated more quickly and with greater functionality than could be achieved by delivery of a single growth factor at the same dose. The data presented here does not support that hypothesis. Although a dose-dependent increase in bone formation and mechanical properties was seen with co-delivery of BMP-2 and TGF-β3, co-delivery of these growth factors at the higher dose did not provide significant benefit over delivery of BMP-2 alone. Addition of VEGF to the osteogenic combination of BMP-2 and TGF-β3 provided no benefit over delivery of these two factors alone.

The work presented here has established a revised and improved model for large bone defect repair and quantitatively analyzed the biological response to co-delivered

growth factor therapies in terms of angiogenesis, osteogenesis, and functionality of the repair tissue. The effects of scaffold geometry and composition on bone and vascular ingrowth were also investigated. Comparison of BMP-2 and TGF-β3 co-delivered at two doses indicated a positive dose-dependent response. The hypothesized benefit of adding TGF-β3 to BMP-2 was not supported. Altering the scaffold geometry by removing a 1.5 mm diameter core and composition by addition of 10% TCP improved the rate of bony union and enabled more extensive revascularization of the defect site than was achieved with un-cored scaffolds. Delivery of VEGF alone to the defect site had no impact on bone formation or vascular invasion. Addition of VEGF to the BMP-2/TGF-β3 osteogenic cocktail had no beneficial effect over co-delivery of the osteogenic growth factors alone. The groups that received VEGF, BMP-2/TGF-β3, or BMP-2/TGF-β3/VEGF demonstrated a significant increase in bone volume between weeks 4 and 12 post-op, suggesting possible sustained release of the growth factors. The sustained release hypothesis could be supported by the only partial release of the growth factors in an *in vitro* protein release kinetics study.

The acute injury caused by creating a critically-sized segmental defect activates a complex biological response beginning with haematoma formation and the angiogenic reaction. This immediate response is believed to be critical for inducing revascularization of the defect site. In many trauma situations, segmental defects are not immediately treated via surgical intervention. In these cases, delivery of VEGF might be more efficacious as the body's natural angiogenic response may have senesced, giving room for a pro-angiogenic cytokine to exert its influence.

This work sheds light on some of the critical factors for repair of large bone defects, motivates further investigation and modification of existing growth factor-based therapies, and opens the door for investigation of cellular-based tissue-engineered therapies in a robust osseous defect model. Further investigation into both combining growth factor and cell-based or growth factor and mechanically-oriented therapies would be interesting areas for further research.

APPENDIX A

EFFECTS OF VOXEL RESOLUTION ON MICRO-COMPUTED TOMOGRAPHY ANALYSIS OF PERFUSED RAT HINDLIMB VASCULATURE

The utility of micro-CT as a quantitative imaging tool is limited by two incompatible factors: time and resolution. A high-resolution image requires significantly more time to generate and analyze, as well as more storage space, than a medium- or low-resolution image does. In certain applications, however, the improved resolution of the image merits the use of more costly imaging. For the studies described here, a medium resolution of 20 μm was selected. This voxel size permitted timely analysis of a large quantity of specimens while still providing the capacity to detect quantitative differences in vasculature. A subset of perfused decalcified samples was analyzed at high resolution (voxel size of 10 μm) for purposes of comparison. The changes in quantitative parameters were generally consistent with what one would expect to occur by increasing the resolution of the image: connectivity and vessel number drastically increased, while the average vessel thickness and spacing decreased. Vascular volume experienced a moderate increase in switching to high resolution (Table 3). These changes in parameters suggest that at a higher resolution, the micro-CT imaging technique is better able to separate and detect small vascular structures that blended together or were undetectable at medium resolution.

Table 2: Micro-CT parameters obtained at high and medium resolution in the VOI containing only the implanted scaffold for perfused hindlimbs in the rat segmental defect model treated with VEGF.

SCAFFOLD VOI

Parameter	High Resolution Value	Medium Resolution Value	Mean Difference (H-M Res)	Standard Deviation	Average % Change
Vascular Volume (mm^3)	6.8321	5.6018	1.2304	1.2024	18.0086
Connectivity ($1/mm^3$)	26.1258	2.8766	23.2493	17.6091	88.9896
Vessel Number (1/mm)	3.5957	1.1505	2.4452	0.5231	68.0041
Vessel Thickness (mm)	0.1067	0.1338	-0.0271	0.0133	-25.3808
Vessel Spacing (mm)	0.2921	0.9051	-0.6130	-0.6256	-209.8919

Table 3: Micro-CT parameters obtained at high and medium resolution in the VOI containing only the core 2 mm of the implanted scaffold for perfused hindlimbs in the rat segmental defect model treated with VEGF.

SCAFFOLD CORE VOI

Parameter	High Resolution Value	Medium Resolution Value	Mean Difference (H-M Res)	Standard Deviation	Average % Change
Vascular Volume (mm^3)	1.6390	1.2096	0.4294	0.5388	26.1970
Connectivity ($1/mm^3$)	10.3973	2.8751	7.5222	7.2962	72.3474
Vessel Number (1/mm)	1.7938	1.2034	0.5905	0.2258	32.9154
Vessel Thickness (mm)	0.1336	0.1276	0.0060	0.0265	4.5219
Vessel Spacing (mm)	0.5905	0.8649	-0.2744	0.0929	-46.4641

Table 4: Micro-CT parameters obtained at high and medium resolution in the VOI containing the implanted scaffold and periphery for perfused hindlimbs in the rat segmental defect model treated with VEGF.

SCAFFOLD AND PERIPHERY VOI

Parameter	High Resolution Value	Medium Resolution Value	Mean Difference (H-M Res)	Standard Deviation	Average % Change
Vascular Volume (mm^3)	31.3566	28.5370	2.8197	2.9163	8.9923
Connectivity ($1/mm^3$)	12.7035	2.1735	10.5300	12.2348	82.8907
Vessel Number (1/mm)	3.5957	0.8917	2.7041	0.6473	75.2023
Vessel Thickness (mm)	0.1067	0.1513	-0.0446	0.0316	-41.8170
Vessel Spacing (mm)	0.2921	1.1457	-0.8536	0.1194	-292.2651

The pattern in relative change between parameters was slightly different for the scaffold core VOI. In this VOI, the vascular volume increased, connectivity, vessel number, and vessel thickness increased, and vessel spacing decreased by only about 50% with increasing resolution. The percent decrease in vessel spacing was dramatically less for the core VOI than for the scaffold or scaffold and periphery VOIs. This can be explained by the relatively sparse distribution of vascular structures within the core of the scaffold as compared to the abundance of vascular structures surrounding the scaffold.

The increase in resolution improved the ability of micro-CT to isolate vascular structures. One phenomenon that was not affected by the increase in resolution is the presence of mysterious “blobs” in the images (Figure 78). These rounded blob structures appeared in both medium- and high-resolution images. It is unclear if the structures are simply very dense beds of small capillaries that appear as a single globular structure due to the limited ability of the micro-CT to distinguish between extremely small structures, or if they are in fact pools of contrast agent that occur due to the inherent leakiness of immature vessels. If it were manageable to do histology on the perfused samples, it is theoretically possible that the blobs could be isolated and identified using histomorphometric techniques paired with immunostaining.

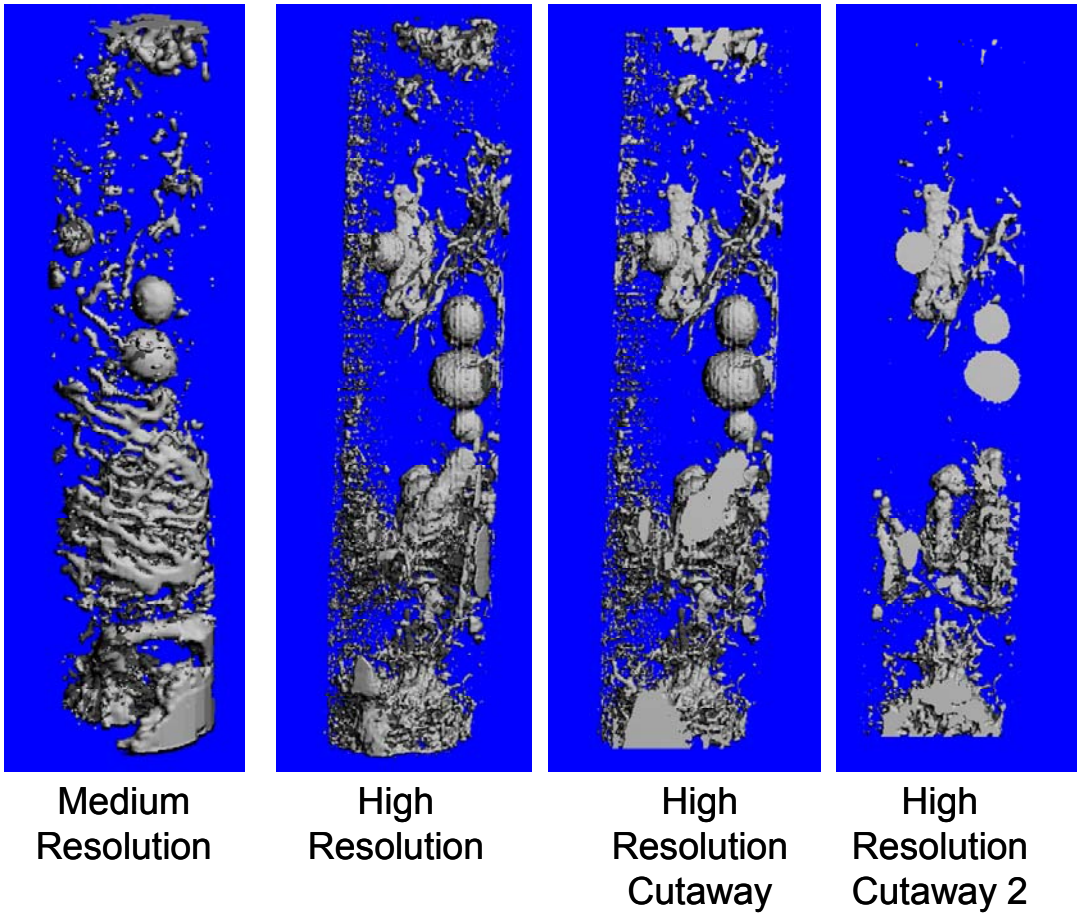

Figure 78: Micro-CT images of the same sample at medium and high resolutions. Note the presence of the apparently solid amorphous globular structures in both images.

APPENDIX B

FABRICATION OF POLY(L-LACTIDE-CO-D,L-LACTIDE) ORIENTED POLYMER SCAFFOLDS

Materials:

- Polymer (PLDL, PLGA, PTMC, P(TMC-L-DL), etc.) (PLDL = Resomer LR 706, Boehringer Ingelheim)
- Azodicarbonamide (Aldrich, cat # 123-77-3)
- α-Tricalcium phosphate, ground to a fine powder
- Media bottle, 100ml size
- 316 stainless steel wire (0.004" diameter stress relieved wire, California Fine Wire)
- Syringes -- 5ml and 1ml
- Syringe needles – ga sizes 22, 20, and 16 (grey, yellow, and purple respectively)
- Heat shrinkable tubing (1/8" – 3/16", GB electrical from Home Depot)
- Beakers
- Acetone (Aldrich)
- Hexanes (Aldrich)
- Peanut oil
- Scotch or autoclave tape
- Ruler

- Razor blades
- Biopsy punches (4mm diameter for rat seg gap scaffolds)
- Oven
- Long-handled hemostats.
- Resin reaction flask, power controller, heating mantle, heat/stir plate, thermometer setup in fume hood.

Procedure:

Polymer solution preparation

1. Combine dry polymer and azo compound powder in desired concentration in the media bottle

   30% azo = 5.6 g PLDL, 100 ml acetone, 2.4 g azo

   To make 10% TCP, add 1 g TCP to 100 ml PLDL/azo solution.
2. Add approximately 10x by weight acetone (density ~ 0.79 g/ml)
3. Allow the polymer to dissolve and reach a uniform solution. This step may take a few days, and may require addition of extra solvent or heat (37ºC water bath for a few minutes is ok).
4. Solution should be viscous but still flow and maintain a single phase.

Wire coating procedure

1. String up lengths of wire (10 to 15 feet long) across the room, securing the ends with tape.
2. Partially fill a 5 ml syringe with polymer solution.

3. Thread the wire into the 1 ml syringe (from the back so the wire tip comes out the small end of the syringe). If this is difficult, thread the wire through a sewing needle and bend the wire, then drop the needle through the syringe, or slightly bend the wire to eliminate its natural curvature.
4. Thread the end of the wire through the 22 ga syringe needle, attach the needle to the syringe, and retape the wire to the wall or shelf.
5. With the 1 ml syringe tilted slightly upwards, inject the solution from the 5 ml syringe into the 1 ml syringe.
6. Pull the 1 ml syringe along the wire slowly so that a coating of solution is deposited on the wire. Remove any blobs of polymer solution with the tip of the 5 ml syringe (or your finger) carefully.
7. To begin the next wire, either rethread the wire on a new syringe or needle or rethread the ones you used for the first wire.
8. You only coat once with the 22 ga needle.
9. Allow this coating to dry for approximately 30 minutes, or until dry to the touch.
10. Repeat this coating step twice more on each wire using the 20 ga needles. Allow these coats to dry 2 hours each or until dry to the touch.
11. Repeat this coating four times with the 16 ga needle. For these coatings, you may need to refill the 1 ml applicator syringe with solution from the 5 ml syringe as you move along the wire. To do this, drip a little solution at a time in the applicator syringe as you continue to pull it along the wire. This allows the wire motion to carry the solution to the tip without producing backpressure and making too much of a mess. Allow these coats to dry 2 hours or overnight.

12. The next day, cut the wires into 8 cm lengths using a ruler and a razor blade.

Preparing scaffold equipment

1. Turn the oven on and heat to 125ºC.
2. Resin reaction flask should sit on the heating mantle, which should sit on top of a stir plate. The heating mantle is controlled with a power controller. A thermometer should be clamped and suspended in the flask.
3. Fill the flask ~half way with peanut oil. Remember – oil expands when it is heated. Make sure the thermometer tip is in the oil and you can read the graduations.
4. Turn the stir bar on
5. Turn the power controller that controls the heating mantle on. It should be set at the 82 rating so that the oil heats quickly without overheating. The maintenance of proper temperature will also depend on the flow rate of the fume hood. It will take about 45-60 minutes to heat to 260ºC.
6. Fill the 250 ml beaker with water and place it near the stir plate.

Heat treating the coated wires

1. Count out wires to bundle them. This can be done one of two ways:
    a. Either by weighing out 10 wires, and subtracting 65.5 mg (for the bare wire) to determine how much polymer coating per meter of wire there is. Then calculate the polymer coating mass per 1 wire. Divide 424.4 mg by the mass of polymer per one wire (mg/wire) to get the number of wires

you need – this produces the scaffold size that Angela used to test the mechanical properties. This typically enbds up being 55-65 wires.

   b. Usually, i bundle 110 wires together, and measure them out by counting the number of wires. This provides a large enough diameter scaffold to punch out 4 mm scaffolds later.

2. Pile the wires together and push them into the heat shrink tubing. You may have to cut the tubing.
3. Pull out one wire on each end longer than the others – this will give you something to hold on to while frying the scaffolds.
4. Place the heat shrink bundles in the oven on a piece of foil for 25 minutes at 125ºC.
5. Remove the bundles from the oven and cut in half using wire cutters.
6. Unsheath the heat shrink tubing using a razor blade. The individual coated wires should not be clearly distinguishable at this time.

Azodicarbonamide decomposition

1. Verify that the peanut oil is at 260ºC.
2. Clamp onto the one wire that's sticking out of the uncut end of the coated wire bundle with the long-handled hemostats.
3. Quickly dip the sample into the peanut oil such that it is completely covered.
4. Gas will begin to escape the structure.
5. When the gas effervescence stops (20-30 seconds), quickly remove the sample and submerge it in a beaker full of water to quench it. Sometimes the wires will

start to separate from each other during the procedure. If this occurs, you may lose your sample, so remove it quickly before full decomposition and quench in water. I find that for bundles of 110 wires, the scaffolds puff up and are on the verge of coming apart when the effervescence ceases.

6. Repeat for the second half of the fused scaffolds.

Final steps

1. Blot the fried scaffolds with a paper towel.
2. Dip the fried scaffolds in hexane to remove any excess oil. You should be able to see the oil perfuse out of the pores.
3. Remove the wires with hemostats. Hold on to any wires you can find without damaging the ends and pull along the long axis of the scaffold. The wires should come out with a little resistance.
4. Cut the scaffolds to size. The diameter can be sized using a biopsy punch.
5. Wash the scaffolds again in new hexane to remove any remaining oil.
6. Soak the scaffolds in water for a few hours to ensure any degradation products are leached out (the degradation compounds are water soluble).

Sterilization

1. Wash the scaffolds in 70% ethanol, then DI water, three times each, ending with a water wash. I usually do this by putting all of the scaffolds into a 50 ml conical and shaking them with the liquid. Then place them (using forceps) into eppendorf tubes and allow them to dry with the lids open overnight. Then close the tubes and

number the scaffolds (best = 1, worst = highest #), place 2 scaffolds per sterilization pouch, and place in a box to be shipped to the γ-irradiation facility.

2. The dose for sterilization is 25 kGy (or 2.5 Mrad) at a standard dose rate. This takes about 4 hours to do. Ask for a dose confirmation sheet for the scaffolds.

APPENDIX C

RAT SEGMENTAL DEFECT SURGERY PROTOCOL

1.1 Supplies

Autoclave on trays, duplicate for two-table setup

Tray 1

- surgery drill
- surgery saw
- saw hex tool
- jacobs chuck attachment and chuck keys
- # 65 uncoated drill bits (1 per rat + extra = _____)
- 5.5 x 12 x 0.4 mm micro oscillator saw blade (1 per rat + extra = _____)

Tray 2 (double this for 2 table surgeries)

- scalpel handles (2)
- hemostats (2 curved mosquito)
- needle holders/suture cutters (2)
- small sharp scissors (1)
- blunt scissors to cut drapes (1)
- pickups (brown-adson forceps) (2)

- small pointed forceps (2 curved, 2 straight)
- hex wrench for bone clamp (1)
- russian forceps (2)
- wound clip applicator (1)
- wound clip remover (1)
- retractors (3)
- plate and bone holding clamp (1)
- miniature screws, #00-90, ¼" length (eight per animal + extra = _____)
- miniature screws, #000-120, 3/32" length (eight per animal + extra = _____)
- bone plate assemblies, 1 polysulfone and 2 steel components per animal = _____ps & _____ss)
- small screw drivers – 2 of each size, larger and smaller tips (4)

Tray 3

- sterile surgery towels for draping over animal and on table

Ethylene oxide- or gas plasma-sterilized materials

- ioban film (1 small size per table)

Gamma-irradiation sterilized materials

- polymer scaffolds for implantation (quantity = _____)

Autoclave separately in pouches

- sterile bowls (2) (double for 2 table surgeries)
- blunt square-ended bovie tips (2)

- ❑ white bovie cords (2)
- ❑ hoses for surgery drill (2) and surgery saw (1)
- ❑ extra wound clips
- ❑ surgery lamp handles (2 sets)

Other materials

- ❑ 4-0 vicryl suture (1 per rat = _____)
- ❑ #10 scalpel blades (2 per rat + extra = _____)
- ❑ sterile 4x4 gauze (1 package per rat = _____)
- ❑ small sterile drapes (at least one package of 2 per rat, + extra = _____)
- ❑ half-drapes for surgery table (1 per table = _____)
- ❑ table drape for table with tools (1 per table)
- ❑ surgical gowns for each sterile person
- ❑ sterile gloves (one pair per person per rat)
- ❑ glass bead sterilizer (1 per table)
- ❑ sterile water for rinsing tools, and sterile water for irrigation (in bottle, 500 ml per table)
- ❑ sterile needles for irrigation (gavage or 16g, 1 per table = _____)
- ❑ sterile 10 ml syringes for irrigation (1 per table= _____)
- ❑ extra nitrogen tank for second power saw

Procedure

- Turn on glass bead sterilizer

- Prewarm the surgery table and cover with a drape.
- Clip hair from around the entire leg and hip area on the dorsal and ventral sides, including the lower abdomen (above where the rat's waist would be if it had one) and down to the ankles.
- Sterilize the entire shaved area, including the foot (the foot cannot be completely sterilized).
- Transfer the rat to the surgery table, insert the rat's nose into the nose cone, and elevate the feet so that they do not contact the tail. Secure the rat to the table with Ioban or a loop of suture running over the animal's incisors and through the isoflurane face mask.
- Holding the ankles with forceps, wrap Ioban around the animal's feet. Cut a hole into the sterile drape for each foot and pull the feet through the hole. Or alternately arrange drapes around the leg to leave only one leg at a time exposed.
- Place another sterile drape over the nonsterile areas of the rat's torso and anesthesia nose cone.
- Assemble the plate components on the instrument table. Secure the blade into the oscillating saw. Prepare the drill as well.
- Make a long incision from the knee to above the hip on the *anterior* side of the femur. Retract the skin away.
- Using blunt dissection, separate the quadriceps muscles on the *anterior* side of the femur, *slightly* lateral of the femur midline (at the first lateral muscle bundle). There should be a visible split in the muscle bundles that can serve as a guide. be

careful to avoid the femoral artery and the large cutaneous vein to the medial side of the quadriceps.

- Loosen and retract the soft tissues from around the femur. Muscle tissue must be separated from the defect area to allow the plate & bone holding clamp to grip around the femur.
- Place the fixation plate on the anterior side of the femur and hold in place with the plate & bone holding clamp. Drill through the bone using the screw holes on the plate as a guide. Start on the distal end and insert a threaded screw. Then place a proximal screw in the same manner.
- Place the remaining two screws.
- Using the oscillating saw, cut through the middle section of the diaphysis as indicated by the notches on the fixation plate, removing the central 8 mm of the femur. These cuts should be made perpendicular to the long axis of the femur and parallel to each other. Cool the site while cutting by irrigating with sterile water. Flush out the site after cutting to remove any debris and resdiual bone chips.
- If a scaffold is being placed, press-fit it into the defect site using a lateral approach. If necessary, snip off excess lengths on the screws.
- Close the soft tissues with 4-0 vicryl suture.
- Close the skin incision using 4-0 vicryl suture and then apply wound clips.
- Paint new-skin mixed with finely ground metronidazol over the incisions to discourage the animals from chewing on the sutures.
- Remove the Ioban from the animal's feet and body, and cradle the rat in a dark washcloth until it begins to move and regains sternal recumbency.

- Administer analgesics (buprenorphine) and return the animal to its cage. Begin observations. An Elizabethan collar may be placed if necessary to prevent the animal from chewing at its incisions. If possible, however, this should be avoided as the collar causes the animal additional stress.

- Observations: each animal must be observed daily for ambulation.

  typical notes on ambulation:

  1) the animal is walking normally.

  2) the animal is weight-bearing on the operated leg(s), but lame.

  3) the animal is not bearing weight on the operated leg(s).

  4) the animal is dragging the operated leg(s).

  If an animal is not bearing weight on the operated leg(s), or is dragging the operated leg(s) for three consecutive days, consult the staff veterinarian. The protocol calls for the animal to be euthanized in such a scenario.

APPENDIX D

RAT VASCULAR PERFUSION PROTOCOL

Materials:

- 0.9% normal saline
- 1000 u/ml heparin
- Microfil MV-122 (yellow color lead chromate compound) (http://www.flowtech-inc.com)
- 10% neutral buffered formalin
- properly labeled waste bottles for formalin waste
- 1 pair small surgical scissors, 1 pair large scissors, 2 hemostats, 1 small curved pair of forceps
- 22 gage (blue) 1" long catheters
- needles
- pipettes and pipette aid
- 1ml and 20ml syringes
- peristaltic pump set at 15 ml/min flowrate
- luer lock connectors as needed
- diapers/chucks/absorbent plastic-backed workbench pads
- 50 ml conicals for storage of femurs
- gauze and cotton swabs

Scale-up is based on 2 ml blood/25 g mouse, assumes rats have a blood volume of ~64 ml/kg

Procedure:

Prepare solutions

- 0.9% normal saline (~450 ml/rat)

  9 g sodium chloride

  1000 ml DI water

- contrast agent (make 18 ml/rat)

  do not add catalyst until immediately before perfusing animal

  mix 5% catalyst, 95% MV (yellow) compound:

  do not add diluent

  do not heat MV compound

- 10% neutral buffered formalin (~300 ml/rat)

Perfusion

1. Set up the peristaltic pump, check the flow, and bleed all air out of the line using the saline solution. You may have to start flow by siphoning the saline through the tubing using a syringe.
2. Induce anesthesia at 5% isoflurane in an induction chamber.
3. Switch animal over to the face mask at 2% isoflurane.

4. Check for pedal withdrawal reflex using the toe pinch. When this reflex is not seen, the animal has reached a deep surgical plane and the procedure can begin.
5. Using scissors, cut through the skin on the lower abdomen above the junction of the legs with the body. Then elevate the muscle tissue and cut through the muscle wall, exposing the internal organs.
6. Move the internal organs aside and out of the abdominal cavity (to the animal's left).
7. Locate the abdominal aorta and inferior vena cava by feeling for a pulse. The aorta is the smaller vessel to the animal's left side. The vena cava is the larger, darker vessel to the right side.
8. Using a cotton swab, carefully rub away the fatty tissue covering the aorta and vena cava.
9. Clamp off one of the renal veins if you can see it (on the animal's left side, running towards the vena cava).
10. Tunnel under the aorta and vena cava using a pair of curved forceps. Then spread the tips of the forceps and route a pair of curved hemostats through the tunnel. Do not clamp down yet with the hemostats.
11. Place a 22g (blue) 1" long catheter into the abdominal aorta going towards the hindlimbs. The aorta is the smaller, whitish-looking vessel that is left of the animal's midline. The insertion point should be just above the point where the animal's left renal vein joins the vena cava. The catheter should be inserted with the needle bevel facing up. When the catheter is placed correctly, blood will be drawn up into the hub of the catheter.

12. Administer 250 units (0.25 ml of 1000u/ml) heparin through the catheter and allow it to circulate for approximately one minute.
13. Clamp down across the vena cava and aorta with the curved hemostats.
14. Verify that the catheter has not descended down one of the branches of the aorta that lead to the legs. The bifurcation point is located just below the junction of the renal veins with the inferior vena cava. If the catheter has moved preferentially down one branch, back it out until the end is above the branching point.
15. Attach the tubing from the peristaltic pump.
16. Cut a vent in the vena cava to allow fluid to exit
17. Optional step -- tie the catheter in place using a single loop of suture.
18. Start the pump and deliver saline.
19. Carefully expose and examine the femoral arteries and veins to see if the blood is clearing out.
20. When ~200 ml of saline has been delivered, move the animal to 5% isoflurane and cut the diaphragm and aortic arch to euthanize the animal.
21. After the animal is dead and ~300 ml of saline has been delivered, switch off the pump and move the tubing to the formalin reservoir.
22. Perfuse the animal with approximately 300 ml of formalin, until the feet and tail become stiff. The limbs may appear to dance as the formalin moves through. Hold the legs in an outstretched position while the fixing step occurs.
23. Stop the pump and rinse through the vasculature again with ~100 ml saline.
24. Stop the pump and place a diaper under the animal.
25. Prepare the Microfil (17.1 ml contrast agent, 0.9 ml catalyst).

26. Using a syringe connected to the catheter hub, deliver 15 mls of Microfil into the vasculature. You should see the femoral veins and arteries fill with yellow, and the feet should yellow as well.
27. Allow the Microfil to polymerize for about an hour.
28. Remove the hindlimbs and store in formalin for at least two weeks to fix the tissue.

REFERENCES

Andreshak JL, Rabin SI, Patwardhan AG, and Wezeman FH. Tibial segmental defect repair: chondrogenesis and biomechanical strength modulated by basic fibroblast growth factor. The Anatomical Record 1997:248:198-204.

Arosarena OA, Falk A, Malmgren L, Bookman L, Allen MJ, Schoonkmaker J, Tatum S, and Kellman R. Defect repair in the rat mandible with bone morphogenic proteins and marrow cells. Archives of Facial and Plastic Surgery 2003:5:103-108.

Asahara T, Takahashi T, Masuda H, Kalka C, Chen D, Iwaguro H, Inai Y, Silver M, and Isner JM. VEGF contributes to postnatal neovascularization by mobilizing bone marrow-derived endothelial progenitor cells. The European Molecular Biology Organization Journal 1999:18:3964-3972.

Attias N, and Lindsey R. Management of large segmental tibial defects using a cylindrical mesh cage. Clinical Orthopaedics and Related Research 2006:450:259-266.

Awad HA, Zhang X, Reynolds DG, Guldberg RE, O'Keefe RJ, and Schwarz EM. Recent advances in gene delivery for structural bone allografts: a review. Tissue Engineering 2007: epub ahead of press April.

Baldik Y, Talu U, Altinel L, Bilge H, Demiryont M, and Aykac-Toker G. Bone healing regulated by nitric oxide. Clinical Orthopaedics and Related Research 2002:404:343-352.

Baltzer AWA, Lattermann C, Whalen JD, Wooley P, Weiss K, Grimm M, Ghivizzani SC, Robbins PD, and Evans CH. Genetic enhancement of fracture repair: healing of an experimental segmental defect by adenoviral transfer of the BMP-2 gene. Gene Therapy 2000:7:734-739.

Baltzer AWA and Lieberman JR. Regional gene therapy to enhance bone repair. Gene Therapy 2004:11:344-350.

Barou G, Mekraldi S, Vico L, Boivin G, Alexandre C, and Lafage-Proust MH. Relationships between trabecular bone remodeling and bone vascularization: a quantitative study. Bone 2002:30:604-612.

Bensaid W, Oudina K, Viateau V, Potier E, Bousson V, Blanchat C, Sedel L, Guillemin G, and Petite H. De novo reconstruction of functional bone by tissue engineering in the metatarsal sheep model. Tissue Engineering 2005:11:814-824.

Betz OB, Betz VM, Nazarian A, Egermann M, Gerstenfeld LC, Einhorn TA, Vrahas MS, Bouxsein ML, and Evans CH. Delayed administration of adenoviral BMP-2 vector improves the formation of bone in osseous defects. Gene Therapy 2007: epub ahead of press 26 April.

Betz OB, Betz VM, Nazarian A, Pilapil CG, Vrahas MS, Bouxsein ML, Gerstenfeld LC, Einhorn TA, and Evans CH. Journal of Bone and Joint Surgery 2006:88A:355-365.

Borrelli J, Prickett WD, Ricci WM. Treatment and nonunions and osseous defects with bone graft and calcium sulfate. Clinical Orthopaedics and Related Research 2003:411:245-254.

Bouletreau PJ, Warren SM, Spector JA, Peled Zm, Gererets RP, Greenwald JA, and Longaker MT. Hypoxia and VEGF up-regulate BMP-2 mRNA and protein expression in microvascular endothelial cells: implications for fracture repair. Plastic and Reconstructive Surgery 2002:109:2384-2397.

Bostrom M, Lane JM, Tomin E, Browne M, Berberian W, Turek T, Smith J, Wozney J, and Schildhauer T. Use of bone morphogenetic protein-2 in the rabbit ulnar nonunion model. Clinical Orthopaedics and Related Research 1996:327:272-282.

Braun Ch. Autogenously vascularised bone allografts. Archives of Orthopaedic and Trauma Surgery 1992:111:250-254.

Bruder SP, Jaiswal N, Ricalton NS et al. Mesenchymal stem cells in osteobiology and applied bone regeneration. Clinical Orthopaedics and Related Research 1998:355S:S247-S256.

Bruder SP, Kraus KH, Goldberg VM et al. The effect of implants loaded with autologous mesenchymal stem cells on the healing of canine segmental bone defects. Journal of Bone and Joint Surgery 1998:80-A;985-996.

Bruder SP, Kurth AA, Shea M et al. Bone regeneration by implantation of purified, culture-expanded human mesenchymal stem cells. Journal of Orthopaedic Research 1998:16:155-162.

Burkus, JK, Gornet MF, Dickman CA, and Zdeblick TA. Anterior lumbar interbody fusion using rhBMP-2 with tapered interbody cages. Journal of Spinal Disorders & Techniques 2002:15:337-349.

Buschmann I, Heil M, Jost M, and Schaper W. Influence of inflammatory cytokines on arteriogenesis. Microcirculation 2003:10:371-379.

Byers BA, Guldberg RE, Hutmacher DW, and Garcia AJ. Effects of Runx2 genetic engineering and *in vitro* maturation of tissue-engineered constructs on the repair of critical size bone defects. Journal of Biomedical Materials Research A 2006:76:646-655.

Carano RAD, Filvaroff EH. Angiogenesis and bone repair. Drug Discovery Today 2003:8:980-989.

Carlevaro MF, Cermelli S, Cancedda R, Cancedda FD. Vascular endothelial growth factor (VEGF) in cartilage neovascularization and chondrocytes differentiation: auto-paracrine role during endochondral bone formation. Journal of Cell Science 2000:113:59-69.

Carmeliat P. Mechanisms of angiogenesis and arteriogenesis. Nature Medicine 2000:6:389-395.

Case ND, Duty AO, Ratcliffe A et al. Bone formation on tissue-engineered cartilage constructs in vivo: effects of chondrocyte viability and mechanical loading. Tissue Engineering 2003:9:587-596.

Chakkalakal DA, Strates BS, Garvin KL et al. Demineralized bone matrix as a biological scaffold for bone repair. Tissue Engineering 2001:7:161-177.

Chakkalakal DA, Strates BS, Mashoof AA et al. Repair of segmental bone defects in the rat: an experimental model of human fracture healing. Bone 1999:25:321-332.

Chang SC-N, Chuang H, Chen Y-R, Yang L-C, Chen J-K, Mardini S, Chung H-Y, Lu Y-L, Ma W-C, and Lou J. Cranial repair using BMP-2 gene engineered bone marrow stromal cells. Journal of Surgical Research 2004:119:85-91.

Chen X, Kidder LS, Lew WD. Osteogenic protein-1 induced bone formation in an infected segmental defect in the rat femur. Journal of Orthopaedic Research 2002:20:142-150.

Chen X, Schmidt AH, Tsukayama DT, Bourgeault CA, and Lew WD. Recombinant human osteogenic protein-1 induces bone formation in a chronically infected, internally stabilized segmental defect in the rat femur. Journal of Bone and Joint Surgery 2006:88A:1510-1523.

Chu T-MG, Warden SJ, Turner CH, and Stewart RL. Segmental bone regeneration using a load-bearing biodegradable carrier of bone morphogenetic protein-2. Biomaterials 2007:28:459-467.

Costa C, Soares R, and Schmitt F. Angiogenesis: now and then. Acta Pathologica, Microbiologia, et Immunologica Scandinavica 2004:112:402-412.

Deckers MML, Karperien M, van der Bent C et al. Expression of vascular endothelial growth factors and their receptors during osteoblast differentiation. Endocrinology 2000:141:1667-1674.

Deckers MML, van Bezooijen RL, van der Horst G et al. Bone morphogenetic proteins stimulate angiogenesis through osteoblast-derived vascular endothelial growth factor A. Endocrinology 2002:143:154-1553.

Dudziak ME, Saadeh PB, Mehrara BJ et al. The effects of ionizing radiation on osteoblast-like cells *in vitro*. Plastic and Reconstructive Surgery 2000:106:1049-1061.

Duvall CL, Taylor RW, Weiss D, Guldberg RE. Quantitative microcomputed tomography analysis of collateral vessel development after ischemic injury. American Journal of Physiology. Heart and Circulatory Physiology 2004:287:H302-H310.

Dvorak HF. Vascular permeability factor/vascular endothelial growth factor: a critical cytokine in tumor angiogenesis and a potential target for diagnosis and therapy. Journal of Clinical Oncology 2002:20:4368-4380.

Eckardt H, Bundgaard KG, Christensen KS, Lind M, Hansen ES, and Hvid I. Effects of locally applied vascular endothelial growth factor (VEGF) and VEGF-inhibitor to

the rabbit tibia during distraction osteogenesis. Journal of Orthopaedic Research 2003:21:335-340.

Egermann M, Baltzer AW, Adamaszek S, Evans C, Robbins P, Schneider E, and Lill CA. Direct adenoviral transfer of bone morphogenetic protein-2 cDNA enhances fracture healing in osteoporotic sheep. Human Gene Therapy 2006:17:507-517.

Egermann M, Schneider E, Evans CH, and Baltzer AW. The potential of gene therapy for fracture healing in osteoporosis. Osteoporosis International 2005:16:S120-S128.

Einhorn TA and Lane JM. Expression of bone morphogenetic proteins in fracture healing. Clinical Orthopaedics and Related Research 1998:355S:S116-S123.

Elcin YM, Dixit V, and Gitnick G. Extensive in vivo angiogenesis following controlled release ofhuman vascular endothelial cell growth factor: implications for tissue engineering and wound healing. Artificial Organs 2001:25:558-565.

Emad B, Sherif E-M, Basma GM, Wong RWK, Bendeus M, and Rabie ABM. Vascular endothelial growth factor augments the healing of demineralized bone matrix grafts. International Journal of Surgery 2006:4:160-166.

Endo M, Kuroda S, Kondo H, Maruoka Y, Ohya K, and Kasugai S. Bone regeneration by modified gene-activated matrix: Tissue Engineering 2006:12:489-497.

Enneking WF, Campanacci DA. Retrieved human allografts: a clinicopathological study. Journal of Bone and Joint Research 2001:83-A:971-986.

Erol B, Kusumi K, Lou J, and Dormans JP. Etiology of congenital scoliosis. The University of Pennsylvania Orthopaedic Journal 2002:15:37-42.

Feighan JE, Davy D, Prewett AB, Stevenson S. Induction of bone by a demineralized bone matrix gel: a study in a rat femoral defect model. Journal of Orthopaedic Research 1995:13:881-891.

Fergusen C, Alpern E, Miclau T, and Helms JA. Does adult fracture repair recapitulate embryonic skeletal formation? Mechanisms of Development 1999:87:57-66.

Ferrara N. Role of vascular endothelial growth factor in regulation of physiological angiogenesis. American Journal of Physiology, Cell Physiology 2001:280:C1358-C1366.

Frost HM. Bone "mass" and the "mechanostat": a propostal. The Anatomical Record 1987:219:1-9.

Gebhardt MC, Flugstad DI, Springfield DS, and Mankin HU. The use of bone allografts for limb salvage in high-grade extremity osteosarcoma. Clinical Orthopaedics and Related Research 1991:270:169-180.

Gerber H-P, Vu T, Ryan AM et al. VEGF couples hypertrophic cartilage remodeling, ossification and angiogenesis during endochondral bone formation. Nature Medicine 1999:5:623-628.

Gerstenfeld LC, Cullinane DM, Barnes GL, Graves DT, and Einhorn TA. Fracture healing as a post-natal development process: molecular, spatial, and temporal aspects of its regulation. Journal of Cellular Biochemistry 2003:88:873-884.

Giardino R, Aldini NN, Fini M, Tanzi MC, Fare S, Draghi L, Carpi A, Nicolini A, and Giavaresi G. Bioabsorbable scaffold for in situ bone regeneration. Biomedicine and Pharmacotherapy 2006:60:386-392.

Glowacki J, Einhorn T, Lane J. Angiogenesis in fracture repair. Clinical Orthopaedics and Related Research 1998:355S:W82-S89.

Gogolewski S, Pineda L, and Busing CM. Bone regeneration in segmental defects with resorbable polymeric membranes: IV. Does the polymer chemical composition affect the healing process? Biomaterials 2000:21:2513-2520.

Gomez G, Korkiakoski S, Gonzalez M-M, Lansman S, Ella V, Salo T, Kellomaki M, Ashammakhi N, and Arnaud E. Effect of FGF and polylactide scaffolds on calvarial bone healing with growth factor on biodegradable polymer scaffolds. The Journal of Craniofacial Surgery 2006:17:935-942.

Gu F, Amsden B, and Neufeld R. Sustained delivery of vascular endothelial growth factor with alginate beads. Journal of Controlled Release 2004:96:463-472.

Guldberg RE, Ballock RT, Boyan BD et al. Analyzing bone, blood vessels, and biomaterials with microcomputed tomography. IEEE Engineering in Medicine and Biology Magazine 2003:22:77-83.

Guldberg RE, Caldwell NJ, Guo XE et al. Mechanical stimulation of tissue repair in the hydraulic bone chamber. Journal of Bone and Mineral Research1997:12:1295-1302.

Hao X, Silva EA, Mansson-Broberg A, Grinnemo K-H, Siddiqui AJ, Dellgren G, Wardell E, Brodin LA, Mooney DJ, and Sylven C. Angiogenic effects of sequential release of VEGF-A_{165} and PDGF-BB with alginate hydrogels after myocardial infarction. Cardiovascular Research 2007: epub ahead of press 6 April.

Hokugo A, Ozeki M, Kawakami O, Sugimoto K, Mushimoto K, Morita S, and Tabata Y. Augmented bone regeneration activity of platelet-rich plasma by biodegradable gelatin hydrogel. Tissue Engineering 2005:11:1224-1233.

Hollinger JO, Kleinschmidt JC. The critical size defect as an experimental model to test bone repair materials. The Journal of Craniofacial Surgery 1990:1:60-68.

Hong L, Tabata Y, Miyamoto S, Yamamoto M, Yamada K, Hashimoto N, and Ikada Y. Bone regeneration at rabbit skull defects treated with transforming growth factor-β1 incorporated into hydrogels with different levels of biodegradability. Journal of Neurosurgery 2000:923:315-325.

Huang Y-C, Kaigler D, Rice KG, Krebsbach PH, and Mooney DJ. Combined angiogenic and osteogenic factor delivery enhances bone marrow stromal cell-driven bone regeneration. Journal of Bone and Mineral Research 2005:20:848-857.

Huang Y-C, Simmons C, Kaigler D, Rice KG, and Mooney DJ. Bone regeneration in a rat cranial defect with delivery of PEI-condensed plasmid DNA encoding for bone morphogenetic protein-4 (BMP-4). Gene Therapy 2005:12:418-426.

Hunt TR, Schwappach JR, and Clarke AH. Healing of a segmental defect in the rat femur with use of an extract from a cultured human osteosarcoma cell-line (saos-2); a preliminary report. Journal of Bone and Joint Surgery 1996:78A:41-48.

Isobe M, Yamazaki Y, Mori M, Amagasa T. Bone regeneration produced in rat femur defects by polymer capsules containing recombinant human bone morphogenetic protein-2. Journal of Oral and Maxillofacial Surgery 1999:57:695-698.

Ito H, Koefoed M, Tiyapatanaputi P et al. Remodeling of cortical bone allografts mediated by adherent rAAV-RANKL and VEGF gene therapy. Nature Medicine 2005:11:291-297.

Itoh T, Mochizuki M, Nishimura R, matsunaga S, Kadosawa T, Kokubo S, Yokota S, and Sasaki N. Repair of ulnar segmental defect b y recombinant human bone morphogenetic protein-2 in dogs. Journal of Veterinary Medical Science 1998:60:451-458.

Ito H, Koefoed M, Tiyapatanaputi P, Gromov K, Goater JJ, Carmouche J, Zhang X, Rubery PT, Rabinowitz, Samulski RJ, Nakamura T, Soballe K, O'Keefe RJ, Boyce BF, and Schwarz EM. Remodeling of cortical bone allografts mediated by adherent rAAV-RANL and VEGF gene therapy. Nature Medicine 2005:11:291-297.

Jones AL, Bucholz RW, Bosse MJ, Mirza SK, Lyon TR, Webb LX, Pollak AN, Golden JD, and Valentin-Opran A. Recombinant human BMP-2 and allograft compared with autogenous bone graft for reconstruction of diaphyseal tibial fractures with cortical defects. Journal of Bone and Joint Surgery 2006:88A:1431-1441.

Kadiyala S, Jaiswal N, and Bruder SP. Culture-expanded, bone marrow-derived mesenchymal stem cells can regenerate a critical-sized segmental bone defect. Tissue Engineering 1997:3:173-185.

Kaigler D, Wang Z, Horger K, Mooney DJ, and Krebsbach PH. VEGF scaffolds enhance angiogenesis and bone regeneration in irradiated osseous defects. Journal of Bone and Mineral Research 2006:21:735-744.

Kasper FK, Young S, Tanahashi K, Barry MA, Tabata Y, Jansen JA, and Mikos AG. Evaluation of bone regeneration by DNA release from composites of oligo(poly(ethylene glycol) fumarate) and cationized gelatin microspheres in a critical-sized calvarial defect. Journal of Biomedical Materials Research A 2006:78A:335-342.

Katsube K, Bishop AT, Simari RD, Yla-Herttuala S, and Friedrich PF. Vascular endothelial growth factor (VEGF) gene transfer enhances surgical revascularization of necrotic bone. Journal of Orthopaedic Research 2005:23:469-474.

Kim J, Kim IS, Cho TH, Lee KB, Hwang SJ, Tae G, Noh I, Lee SH, Park Y, and Sun K. Bone regeneration using hyaluronic acid-based hydrogel with bone

morphogenetic protein-2 and human mesenchymal stem cells. Biomaterials 2007:28:1830-1837.

Kinniard T, Stabile E, Burnett MS, Lee CW, Barr S, Fuchs S, and Epstein SE. Marrow-derived stromal cells express genes encoding a broad spectrum of arteriogenic cytokines and promote in vitro and in vivo arteriogenesis through paracrine mechanisms. Circulation Research 2004:94:678-685.

Koefoed M, Ito H, Gromov K et al. Biological effects of rAAV-caAlk2 coating on structural allograft healing. Molecular Therapies 2005:12:212-218.

Kokubo S, Fujimoto R, Yokota S, Fukushima S, Nozaki K, Takahashi K, and Miyata K. Bone regeneration by recombinant human bone morphogenetic protein-2 and a novel biodegradable carrier in a rabbit ulnar defect model. Biomaterials 2003:24:1643-1651.

Komaki H, Tanaka T, Chazono M, and Kikuchi T. Repair of segmental bone defects in rabbit tibiae using a complex of β-tricalcium phosphate, type I collagen, and fibroblast growth factor-2. Biomaterials 2006:27:5118-5126.

Kraus KH, Kadiyala S, Wotton H, Kurth A, SHea M, Hannan M, Hayes WC, Kirker-Head MA, Bruder S. Critically-sized osteo-periosteal femoral defects: a dog model. Journal of Investigative Surgery 1999:12:115-124.

Krebsbach PH, Gu Keni, Franceschi RT, and Rutherford RB. Gene therapy-directed osteogenesis: BMP-7-transduced human fibroblasts form bone in vivo. Human Gene Therapy 2000:11:1201-1210.

Kretlow JD and Mikos AG. Review: mineralization of synthetic polymer scaffolds for bone tissue engineering. Tissue Engineering 2007:13:927-938.

Kurz H. Physiology of angiogenesis. Journal of Neuro-Oncology 2000:50:17-35.

Langenfeld EM and Langenfeld J. Bone morphogenetic protein-2 stimulates angiogenesis in developing tumors. Molecular Cancer Research 2004:2:141-149.

Lee KW, Yoon JJ, Lee JH, Kim SY, Jung HJ, Kim SJ, Joh JW, Lee HH, Lee DS, and Lee SK. Sustained release of vascular endothelial growth factor from calcium-induced

alginate hydrogels reinforced by heparin and chitosan. Transplantation Proceedings 2004:36:2464-2465.

Lee KY, Peters MC, and Mooney DJ. Comparison of vascular endothelial growth factor and basic fibroblast growth factor on angiogenesis in SCID mice. Journal of Controlled Release 2003:87:49-56.

Lee SC, Shea M, Battle MA et al. Healing of large segmental defects in rat femurs is aided by RhBMP-2 in PLGA matrix. Journal of Biomedical Materials Research 1994:28:1149-1156.

Li JZ, Hankins GR, Kao C, Li H, Kammauff J, Helm GA. Osteogenesis in rats induced by a novel recombinant helper-dependent bone morphogenetic protein-9 (BMP-9) adenovirus. The Journal of Gene Medicine 2003:5:748-756.

Lieberman JR, Daluiski A, Stevenson S et al. The effect of regional gene therapy with bone morphogenetic protein-2-producing bone-marrow cells on the repair of segmental femoral defects in rats. Journal of Bone and Joint Surgery 1999:81-A:905-917.

Lienau J, Schell H, Duda GN, Seebeck P, Muchow S, and Bail HJ. Initial vascularization and tissue differentiation are influenced by fixation stability. Journal of Orthopaedic Research 2005:23:639-645.

Lin ASP, Barrows TH, Cartmell SH, Guldberg RE. Microarchitectural and mechanical characterization of oriented porous polymer scaffolds. Biomaterials 2003:24:481-489.

Lisignoli G, Fini M, Giavaresi G, Aldini NN, Toneguzzi S, and Fachini A. Osteogenesis of large segmental radius defects enhanced by basic fibroblast growth factor activated bone marrow stromal cells grown on non-woven hyaluronic acid-based polymer scaffold. Biomaterials 2002:23:1043-1051.

Livingston Arinzeh T, Peter SJ, Archambault MS, van den Bos C, Gordon S, Kraus K, Smith A, and Kadiyala S. Allogeneic mesenchymal stem cells regenerate bone in a critical-sized canine segmental defect. Journal of Bone and Joint Surgery 2003:85A:1927-1935.

Lucarelli E, Fini M, Beccheroni A et al. Stromal stem cells and platelet-rich plasma improve bone allograft integration. Clinical Orthopaedics and Related Research 2005:435:62-68.

Lutolf MP, Weber FE, Schmoekel HG, Schense JC, Kohler T, Muller R, and Hubbell JA. Repair of bone defects using synthetic mimetics of collagenous extracellular matrices. Nature Biotechnology 2003:21:513-518.

Maes C, Carmeliet P, Moermans K, Stockmans I, Smets N, Bouillon R, Carmeliet G. Impaired angiogenesis nad endochondral bone formation in mice lacking the vascular endothelial growth factor isoforms $VEGF_{164}$ and $VEGF_{188}$. Mechanisms of Development 2002:111:61-73.

Maissen O, Eckhardt C, Gogolewski S, Glatt M, Arvinte T, Steiner A, Rahn B, and Schlegel U. Mechanical and radiological assessment of the influence of rhTGF-β3 on bone regeneration in a segmental defect in the ovine tibia: pilot study. Journal of Orthopaedic Research 2006: 24:1670-1678.

Marcacci M, Kon E, Moukhachev V, Lavroukov A, Kutepov S, Quatro R, Mastrogiacomo M, and Cancedda R. Stem cells associated with macroporous bioceramics for long bone repair: 6- to 7-year outcome of a pilot clinical study. Tissue Engineering 2007:13:947-955.

Marrony S, Bassilana F, Seuwen K, and Keller H. Bone morphogenetic protein 2 induces placental growth factor in mesenchymal stem cells. Bone 2003:33:426-433.

Mayer H, Bertram H, Lindenmaier W, Korff T, Weber H, and Weich H. Vascular endothelial growth factor (VEGF-A) expression in human mesenchymal stem cells: autocrine and paracrine role in osteoblastic and endothelial differentiation. Journal of Cellular Biochemistry 2005:95:827-839.

Mayr-Wolfhart U, Waltenberger J, Hausser H et al. Vascular endothelial growth factor stimulates chemotactic migration of primary human osteoblasts. Bone 2002:30:472-477.

McColl BK, Stacker SA, Achen MG. Molecular regulation of the VEGF family – inducers of angiogenesis and lymphangiogenesis. Acta Pathologica, Microbiologia, et Immunologica Scandinavica 2004:112:463-480.

Mukhopadhyay D, Zeng H, and Bhattacharya R. Complexity in the vascular permeability/vascular endothelial growth factor (VPF/VEGF)-receptors signaling. Molecular and Cellular Biochemistry 2004:264:51-61.

Nakagawa M, Kaneda T, Arakawa T, Morita S, Sato T, Yomada T, Hanada K, Kumegawa M, and Hakeda Y. Vascular endothelial growth factor (VEGF) directly enhances osteoclastic bone resorption and survival of mature osteoclasts. Federation of European Biochemical Societies Letters 2000:473:161-164.

Neufeld G, Cohen T, Gengrinovitch S, and Poltorak Z. Vascular endothelial growth factor (VEGF) and its receptors. The Federation of American Societies for Experimental Biology Journal 1999:13:9-22.

Niedzwiedzki T, Dabrowski Z, Miszta H, and Pwlikowski M. Bone healing after bone marrow stromal cell transplantation to the bone defect. Biomaterials 1993:14:115-121.

Nottebaert M, Lane JM, John A et al. Omental angiogenic lipid fraction and bone repair: an experimental study in the rat. Journal of Orthopaedic Research 1989:7:157-169.

Oakes DA, Lee CC, Lieberman JR. An evaluation of human demineralized bone matrices in a rat femoral defect model. Clinical Orthopaedics and Related Research 2003:413:281-290.

Oest ME, Dupont KM, Kong HJ, Mooney DJ, and Guldberg RE. Quantitative assessment of scaffold and growth factor-mediated repair of critically-sized defects. Journal of Orthopaedic Research 2007: epub ahead of press 5 April.

Ohura K, Hamanishi C, Tanaka S, Matsuda N. Healing of segmental bone defects in rats induced by a β-TCP-MCPM cement combined with rhBMP-2. Journal of Biomedical Materials Research 1999:44:168-175.

Peled E, Boss J, Bejar J, Zinman C, Seliktar D. A novel poly(ethylene glycol)-fibrinogen hydrogel for tibial segmental defect repair in a rat model. Journal of Biomedical Materials Research A 2007:80:874-884.

Peterson B, Zhang J, Iglesias R, Kabo M, Hedrick M, Benhaim P, and Lieberman JR. Healing of critically sized femoral defects, using genetically modified

mesenchymal stem cells from adipose tissue. Tissue Engineering 2005:11:120-129.

Phillips JE, Hutmacher DW, Guldberg RE, and García AJ. Mineralization capacity of Runx2/Cbfa1-genetically engineered fibroblasts is scaffold dependent. Biomaterials 2006:27:5535-5545.

Pufe T, Wildemann B, Peterson W, Mentlein R, Raschke M, and Schmidmaier G. Quantitative measurement of the splice variants 120 and 164 of the angiogenic peptide vascular endothelial growth factor in the time flow of fracture healing: a study in the rat. Cell and Tissue Research 2002:309:387-392.

Rabbany SY, Heissig B, Hattori K, and Rafii S. Molecular pathways regulating mobilization of marrow-derived stem cells for tissue revascularization. Trends in Molecular Medicine 2003:9:109-117.

Rai B, Oest ME, Dupont KM, Ho KH, Teoh SH, and Guldberg RE. Combination of platelet-rich plasma with polycaprolactone-tricalcium phosphate scaffolds for segmental bone defect repair. Journal of Biomedical Materials Research A 2007:81:888-899.

Ramoshebi LN and Ripamonti U. Osteogenic protein-1, a bone morphogenetic protein, induces angiogenesis in the chick chorioallantoic membrane and synergizes with basic fibroblast growth factor and transforming growth factor-β1. The Anatomical Record 2000:259:97-107.

Reddi AH. Initiation of fracture repair by bone morphogenetic proteins. Clinical Orthopaedics and Related Research 1998:355S:S66-S72.

Riley EH, Lane JM, Urist MR, Lyons KM, and Lieberman JR. Bone morphogenetic protein-2: biology and applications. Clinical Orthopaedics and Related Research 1996:324:39-46.

Rizzi SC, Ehrbar M, Halstenberg S, Raeber GP, Schmoekel HG, Hagenmuller H, Muller R, Weber FE, and Hubbell JA. Recombinant protein-co-PEG networks as cell-adhesive and proteolytically degradable hydrogel matrixes. Part II: biofunctional characteristics. Biomacromolecules 2006:7:3019-3029.

Rohner D, Hutmacher DW, Cheng TK, Oberholzer M, and Hammer B. In vivo efficacy of bone-marrow-coated polycaprolactone scaffolds for the reconstruction of

orbital defects in the pig. Journal of Biomedical Materials Research B Applied Biomaterials 2003:66:574-580.

Roldan JC, Jepsen S, Miller J, Feitag S, Rueger DC, Acil Y, and Terheyden H. Bone formation in the presence of platelet-rich plasma vs. bone morphogenetic protein-7. Bone 2004:34:80-90.

Saadeh PB, Khosla RK, Mehrara BJ, Steinbrech DS, McCormick SA, DeVore DP, and Longaker MT. Repair of a critical size defect in the rat mandible using allogenic type I collagen. The Journal of Craniofacial Surgery 2001:12:573-579.

Saadeh PB, Mehrara BJ, Steinbrech DS et al. Mechanisms of fibroblast growth factor-2 modulation of vascular endothelial growth factor expression by osteoblastic cells. Endocrinology 2000:141:2075-2083.

Saadeh PB, Mehrara BJ, Steinbrech DS, Dudziak ME, Greenwald JA, Luchs JS, Spector JA, Ueno H, Gittes GK, and Longaker MT. Transforming growth factor-β1 modulates the expression of vascular endothelial growth factor by osteoblasts. American Journal of Physiology 1999:277:C628-C637.

Sakata Y, Ueno T, Kagawa T, Kanou M, Fujii T, Yamachika E, and Sugahara T. Osteogenic potential of culture human periosteum-derived cells – a pilot study of human cell transplantation into a rat calvarial defect model. Journal of Cranio-Maxillofacial Surgery 2006:34:461-465.

Savarino L, Baldini N, Greco M, Capitani O, Pinna S, Valentini S, Lombardo B, Esposito MT, Pastore L, Ambrosio L, batytista S, Causa F, Zeppetelli S, Guarino V, and Netti PA. The performance of poly-ε-caprolactone scaffolds in a rabbit femur model with and without autologous stromal cells and BMP4. Biomaterials 2007:28:3101-3109.

Schantz J-T, Hutmacher DW, Lam CXF, Brinkmann M, Wong KM, Lim TC, Chou N, Guldberg RE, and Teoh SH. Repair of calvarial defects with customised tissue-engineered bone grafts II. Evaluation of cellular efficiency and efficacy in vivo. Tissue Engineering 2003:9:S127-S139.

Schmitt JM, Hwang K, Winn SR, and Hollinger JO. Bone morphogenetic proteins: an update on basic biology and clinical relevance. Journal of Orthopaedic Research 1999:17:269-278.

Schmoekel HG, Weber FE, Schense JC, Gratz KW, Schawalder P, and Hubbell JA. Biotechnology and Bioengineering 2005:89:253-262.

Shah AV, and Jathal BS. Evaluation of freeze-dried dura mater allograft as a cololagen based barrier (an experimental animal study). Cell and Tissue Banking 2003:4:133-139.

Sheller MR, Crowther RS, Kinney JH, Yang J, Di Jorio S, Breunig T, Carney DH, and Ryaby JT. Repair of rabbit segmental defects with the thrombin peptide, TP508. Journal of Orthopaedic Research 2004:22:1094-1099.

Shen H-C, Peng H, Usas A, Gearhart B, Fu FH, Huard J. Structural and functional healing of critical-size segmental bone defects by transduced muscle-derived cells expressing BMP-4. The Journal of Gene Medicine 2004:6:984-991.

Sheridan MH, Shea LD, Peters MC, and Mooney DJ. Bioabsorable polymer scaffolds for tissue engineering capable of sustained growth factor delivery. Journal of Controlled Release 2000:64:91-102.

Silva EA, and Mooney DJ. Spatiotemporal control of vascular endothelial growth factor delivery from injectable hydrogels enhances angiogenesis. Journal of Thrombosis and Haemostasis 2007:5:590-598.

Simmons CA, Alsberg E, Hsiong S et al. Dual growth factor delivery and controlled scaffold degradation enhance in vivo bone formation by transplanted bone marrow stromal cells. Bone 2004:35:562-569.

Spector JA, Luch JS, Mehrara BJ, Greenwald JA, Smith LP, and Longaker MT. Expression of bone morphogenetic proteins during membranous bone healing. Plastic and Reconstructive Surgery 2001:107:124-134.

Spector JA, Mehrara BJ, Greenwald JA, Saadeh PB, Steinbrech DS, Bouletreau PJ, Smith LP, and Lonaker MT. Osteoblast expression of vascular endothelial growth factor is modulated byt eh extracellular microenvironment. American Journal of Physiology Cell Physiology 2000:280:C72-C80.

Srouji S, Rachmiel A, Blumenfeld I, and Livne E. Mandibular defect repair by TGF-β and IGF-1 released from a biodegradable osteoconductive hydrogel. Journal of Cranio-Maxillofacial Surgery 2005:33:79-84.

Stevenson S, Cunningham N, Toth J et al. The effect of osteogenin (a bone morphogenic protein) on the formation of bone in orthotopic segmental defects in rats. Journal of Bone and Joint Surgery 1994:76-A:1676-1687.

Stevenson S, Li XQ, Davy DT, Klein L, and Goldberg VM. Critical biological determinants of incorporation of non-vascularized cortical bone grafts. Quantification of a complex process and structure. Journal of Bone and Joint Surgery 1997:79A:1-16.

Street J, Bao M, deGuzman L et al. Vascular endothelial growth factor stimulates bone repair by promoting angiogenesis and bone turnover. Proceedings of the National Academy of Sciences of the United States of America 2002:99:9656-9661.

Swift ME, Kleinman HK, DiPietro LA. Impaired wound repair and delayed angiogenesis in aged mice. Laboratory Investigation 1999:79:1479-1497.

Swiontkowski MF, Aro HT, Donell S, Esterhai JL, Goulet J, Jones A, Kregor PJ, NMordsletten L, Paiement G, and Patel A. Recombinant human bone morphogenetic protein-2 in open tibial fractures. Journal of Bone and Joint Surgery 2006:88A:1258-1265.

Tarkka T, Sipola A, Jamsa T, Soini Y, Yla-Herttuala S, Tuukkanen J, and Hautala T. Adenoviral VEGF-A gene transfer induces angiogenesis and promotes bone formation in healing osseous tissues. The Journal of Gene Medicine 2003:5:560-566.

Tombran-Tink J, and Barnstable CJ. Osteoblasts and osteoclasts express PEDF, VEGF-A isoforms, and VEGF receptors: possible mediators of angiogenesis and matrix remodeling in bone. Biochemical and Biophysical Research communications 2004:316:573-579.

Tsuchida H, Hashimoto J, Crawford E, Manske P, and Lou J. Engineered allogeneic mesenchymal stem cells repair femoral segmental defect in rats. Journal of Orthopaedic Research 2001:21:44-53.

Tsuji K, Bandyopadhyay A, Harfe BD, Cox K, Kakar S, Gerstenfeld L, Einhorn T, Tabin CJ, and Rosen V. BMP2 activity, although dispensable for bone formation, is required for the initiation of fracture healing. Nature Genetics 2006:28:1424-1429.

Tuominen T, Jamsa T, Tuukkanen J, Marttinen A, Lindholm TS, and Jalovaara P. Bovine bone implant with bovine bone morphogenetic protein in healing a canine ulnar defect. International Orthopaedics 2001: 25:5-8.

Tuominen T, Jamsa T, Tuukkanen J, Nieminen P, Linholm TC, Linholm TS, and Jalovaara P. Native bovine bone morphogenetic protein improves the potential of biocoral to heal segmental canine ulnar defects. International Orthopaedics 2000:24:289-294.

Umeda H, Kanemaru S-I, Yamashita M, Kishimoto M, Tamura Y, Nakamura T, Omori K, Hirano S, and Ito J. Bone regeneration of canine skull using bone marrow-derived stromal cells and β-tricalcium phosphate. The Laryngoscope 2007:epub ahead of press 24 April.

Viateau V, Guillemin G, Bousson V, Oudina K, Hannouche D, Sedel L, Logeart-Avramoglou D, and Petite H. Long-bone critical-size defects treated with tissue-engineered grafts: a study on sheep. Journal of Orthopaedic Research 2007: epub ahead of press, 22 February.

Villars F, Bordenave L, bareille R, and Amedee J. Effect of human endothelial cells on human bone marrow stromal cell phenotype: role of VEGF? Journal of Cellular Biochemistry 2000:79:672-685.

Werntz JR, Lane JM, Burstein AH et al. Qualitative and quantitative analysis of orthotopic bone regeneration by marrow. Journal of Orthopaedic Research 1996:14:85-93.

Wheeler DL, Enneking WF. Allograft bone decreases in strength *in vivo* over time. Clinical Orthopaedics and Related Research 2005:435:36-42.

Wozney JM and Rosen V. Bone morphogenetic protein and bone morphogenetic protein gene family in bone formation and repair. Clinical Orthopaedics and Related Research 1998:346:26-37.

Xie C, Reynolds D, Awad H, Rubery PT, Pelled G, Gazit D, Guldberg RE, Schwarz EM, O'Keefe RJ, and Zhang X. Structural bone allograft combined with genetically engineered mesenchymal stem cells as a novel platform for bone tissue engineering. Tissue Engineering 2007:13:435-445.

Xie K, Wei D, Shi Q, and Huang S. Constitutive and inducible expression and regulation of vascular endothelial growth factor. Cytokine and Growth Factor Reviews: 2004:15:297-324.

Yamamato M, Tabata Y, Hong L, Miyamoto S, Hashimoto N, and Ikada Y. Bone regeneration by transforming growth factor β1 released from a biodegradable hydrogel. Journal of Controlled Release 2000:64:133-142.

Yamamoto M, Takahashi Y, and Tabat Y. Enhanced bone regeneration at a segmental bone defect by controlled release of bone morphogenetic protein-2 from a biodegradable hydrogel. Tissue Engineering 2006:12:1305-1311.

Yao Z, Lafage-Proust M, Plouet J, Bloomfeld S, Alexandre C, and Vico L. Increase of both angiogenesis and bone mass in response to exercise depends on VEGF. Journal of Bone and Mineral Research 2004:19:1471-1480.

Yasko AW, Lane JM, Fellinger EJ et al. The healing of segmental bone defects, induced by recombinant human bone morphogenetic protein (rhBMP-2). Journal of Bone and Joint Surgery 1992:74-A:659-670.

Yu Y, Yang J-L, Chapman-Sheath PJ, and Walsh WR. TGF-β, BMPs, and their signal transducing mediators, smads, in rat fracture healing. Journal of Biomedical Materials Research 2002:60:392-397.

Zabka AG, Pluhar GE, Edwards III RB, Manley PA, Hyashi K, Heiner JP, Kalscheur VL, Seeherman HJ, and Markel MD. Journal of Orthopaedic Research 2001:19:318-327.

Zein I, Hutmacher DW, Tan KC, and Teoh SH. Fused deposition modeling of novel scaffold architectures for tissue engineering applications. Biomaterials 2002:23:1169-1185.

Ziegelhoefer T, Fernandez B, Kostin S, Heil M, Voswinckel R, Helish A, and Schaper W. Bone marrow-derived cells do not incorporate into the adult growing vasculature. Circulation Research 2004:94:230-238.

VITA

MEGAN ELIZABETH OEST

Megan was born to her parents, Jane and Allen, in Portland, Oregon on July 15, 1979. Megan was preceded by her dear cousins Kirin and Amara. Three years later, she was joined by her beloved sister, Julie. She attended Lakeridge High School and earned varsity letters in golf and forensics, ranked in the state in both areas. In 1997, Megan moved to Corvallis, Oregon to attend Oregon State University. During her tenure at OSU, Megan also raced for the Oregon State Varsity Women's Crew team. She lettered in this sport and was ranked in the Pac-10 conference, earning the Student Athlete of the Year award from OSU in 2001. Graduating in 2001 with a B.S. in bioengineering, she moved across the continent to Georgia Institute of Technology where she undertook work to complete a Ph.D. in bioengineering. During her six years at Georgia Tech, Megan was awarded a National Science Foundation Graduate Fellowship and Georgia Tech President's Fellowship. Megan has also joined the RAINN (Rape, Abuse, and Incest National Network) speaker's bureau and actively works to spread awareness about sexual and domestic violence.